BNL 50769

PROCEEDINGS OF THE HEAVY ION FUSION WORKSHOP

HELD AT
BROOKHAVEN NATIONAL LABORATORY
UPTON, NEW YORK

OCTOBER 17-21, 1977

BROOKHAVEN NATIONAL LABORATORY
ASSOCIATED UNIVERSITIES, INC.
UPTON, NEW YORK 11973

DISCLAIMER

BNL 50769
UC-21
(Inertial Confinement Fusion – TID-4500)

PROCEEDINGS OF THE HEAVY ION FUSION WORKSHOP

HELD AT
BROOKHAVEN NATIONAL LABORATORY
UPTON, NEW YORK

OCTOBER 17-21, 1977

Editor:
Lyle W. Smith

ACCELERATOR DEPARTMENT

BROOKHAVEN NATIONAL LABORATORY

ASSOCIATED UNIVERSITIES, INC.

UNDER CONTRACT NO. EY-76-C-02-0016 WITH THE

UNITED STATES DEPARTMENT OF ENERGY

NOTICE

Printed in the United States of America
Available from
National Technical Information Service
U.S. Department of Commerce
5285 Port Royal Road
Springfield, VA 22161
Price: Printed Copy $8.00; Microfiche $3.00

February 1978 840 copies

ACKNOWLEDGMENTS

We wish to express our sincere thanks to the members of the organizing committee and the working group leaders. Each of them accepted and competently undertook major responsibilities. We are greatly indebted to all of the participants, who worked hard for long hours in applying their knowledge and skills to the task of the study and in writing their results, which appear in this report. We speak for every participant in thanking many others for their help in preparation before, during and after this Workshop; we wish we could name them all. We thank Joan Depken, Jeannette Thiede and Florence Warren for their skillful assistance in typing these Proceedings. Finally, we are most grateful to the Proceedings Secretary, Lillian Kouchinsky, who met all our requests, both reasonable and unreasonable, with cheerful efficiency.

L.W. Smith
Editor

THIS PAGE

WAS INTENTIONALLY

LEFT BLANK

CONTENTS

I. INTRODUCTION

Following the ERDA Summer Study of Heavy Ions for Inertial Fusion (LBL-5534) an Ad Hoc Heavy Ion Fusion Coordinating Committee was formed. Its first meeting, 24 March 1977, was attended by R. Bangerter (LLL), D. Berley (NSF), M. Cooper (ERDA/ASGA), D. Keefe (LBL), R. Martin (ANL), A. Maschke (BNL), D. Sutter (ERDA/HEP) and L. Teng (FNAL). It was generally agreed that a one-week workshop would be useful in about six months. BNL was suggested as a site. At the time, the feeling was that this workshop would focus on parameters appropriate to an accelerator/target experiment. At a meeting of the HIF 10 man working group in June, at ERDA Headquarters, Les Levine suggested that there be no classified discussions at the workshop. Because the principal purpose of the workshop was to be accelerator design, and since a number of our European colleagues were planning to attend, this suggestion was unanimously approved. At this same meeting, the acronym HIDE (Heavy Ion Demonstration Experiment) was introduced. At the time, the suggested parameters were 25 kJ of 5 GeV heavy ions, (U, say) delivered in about 1 ns (15 TW). Fifty million dollars was mentioned as a ball-part cost. Subsequent discussion indicated that since much of the cost of the facility was related to the very low energy portion, it would not cost much more to go to 100 kJ and 50 TW.

The first meeting of the Workshop Organizing Committee met at BNL on 18 August 1977. In attendance were A. Maschke (BNL), R. Martin (ANL), L. Teng (FNAL), L. Smith (LBL) (for D. Keefe), W. Herrmannsfeldt (SLAC), D. Tidman (U. Maryland), R. Bangerter (LLL) and D. Sutter (DOE). L. Levine and T. Godlove (NRL) were unable to participate. The two principal goals of the workshop were established to be 1) keep workers in the field abreast of developments and 2) define a variety of HIDE concepts that can then be studied in more detail during the following year. The general structure of the workshop was outlined, and A. Maschke was designated as Workshop Chairman. The Workshop itself was organized into working groups, each with a chairman, and are listed here.

Working Groups (Chairman)

1. Atomic/Molecular
   (R. Poe, U. C. Riverside)
2. Plasma and Neutralization Effects
   (D. Tidman, U. Maryland)
3. Reactor
   (J. Maniscalco, LLL)
4. Ion Sources/Preaccelerators
   (E. Parker, ANL/D. Clark, LBL)
5. Low β Linacs
   (R. Kustom, ANL/J. Staples, LBL)
6. High Current Beam Transport
   (L. Smith, LBL)
7. Vacuum Systems
   (H. Halama, BNL)
8. Systems/Cost
   (P. Grand, BNL)

HIDE Working Groups

Induction Linac
(F. Mills, FNAL/B. Richter, SLAC)

Synchrotrons
(M. Barton, BNL)

RF Linac/Accumulators
(D. Young, FNAL)

A final meeting of the Organizing Committee and Working Group Chairman was held on the Sunday afternoon preceding the Workshop. Burt Richter suggested that the HIDE goals should be upgraded to that which might be satisfactory for a power plant scenario. As a result, the HIDE parameters were taken to be 1 MJ and 100 TW. The problem of determining what a first step should be was not addressed at this stage. During the course of the Workshop the idea developed of building a low β linac and accumulator (energy around 1 GeV) which would serve as injector into a section of induction linac. This would test the basic features of all three of the HIDE scenarios, prior to a commitment to a full scale HIDE.

II. OVERVIEW

Three different types of accelerator systems were studied as candidates for a power plant ignition system. These were the Induction Linac, the RF Linac/Accumulators, and the Synchrotron/Storage Ring systems. Technically feasible solutions were outlined for all three, with various scenarios involving differing amounts of "uncertainty" factor. None of the scenarios involved technical problems that could not be overcome by increasing the cost of the system.

Consider the Induction Linac scenario. A technically conservative, albeit expensive, solution to the "ion source" problem, which requires 10's of amperes for several microseconds, is to use an rf linac and accumulator. A more attractive solution is under study at LBL involving direct extraction and drift tube acceleration of such beams. Since a system like this has not been built and operated, a relatively high uncertainty factor is associated with both its cost and performance. The other area of the Induction Linac scenario which merits a high uncertainty factor is the cost. The largest induction linacs built to date have been only a few megavolts. What will happen to the cost as one scales to systems hundred of times larger has not yet been exhibited.

The Linac/Accumulator scenario involves a different class of uncertainty factors. For instance, the body of data on the cost of linac cavities and rf systems is quite extensive. Although the linear accelerator under consideration is an order of magnitude longer than any similar one now in existence, it is doubtful that a dramatic reduction in cost/MV will be achieved. A principal uncertainty in the Linac/Accumulator scenario is the satisfactory preservation of the ion source brightness through the early stages of acceleration. Typical uncertainties are an order of a factor of two. Doubling the number of accumulators would compensate this. Another area of uncertainty, not related to the first, involves filling the horizontal and vertical acceptances of the accumulator rings without substantial losses of beam. Here again, the uncertainty is an order of a factor of two between what is anticipated versus what is assured. The relatively short time that the beam resides in the accumulator makes this scenario relatively insensitive to uncertainty in beam-gas and beam-beam cross sections.

The Synchrotron or Synchrotron/Storage Ring scenario has its principal uncertainty factors in the area of vacuum and beam-beam cross section uncertainties. The vacuum requirements have been met for storage rings, but not in a rapid cycling synchrotron. On the other hand, synchrotron magnet and rf technology is very highly developed, and reliable cost and component performance estimates can be made. Since the synchrotron relies on an rf linac for its injector, it shares this technology with the other scenarios. Because synchrotrons tend to be cheaper/volt than linacs, scenarios with multiple synchrotrons in parallel are likely to be favored. The linac injector will typically have no trouble filling more than one synchrotron. Intensity related vacuum breakdown, and beam-beam scattering losses, if they turn out to be bothersome, are all alleviated by adding more synchrotrons.

In sketching out the three accelerator scenarios, no account was taken of the possibility that space-charge neutralization might be used to enhance the performance of the various schemes. Any advances made in this area would introduce substantial improvements in all of the scenarios.

A. W. Maschke

III. Reviews of Current Laboratory Programs

1. BNL HEAVY ION FUSION PROGRAM

A. W. Maschke

INTRODUCTION

A principal attraction of Heavy Ion Fusion is that existing accelerator technology and theory is sufficiently advanced to allow one to commence the design of a machine capable of igniting thermonuclear explosions. There are, however, a number of features which are not found in existing accelerators built for other purposes. The main thrust of the BNL Heavy Ion Fusion program has been to explore these features.

LONGITUDINAL BUNCHING

In a conventional accelerator the bunch length has not been of much concern. For fusion application, we want to bunch the beam as tightly as possible. There are a number of questions that arise:

1. If the bunching occurs rapidly, can we tolerate space charge forces in excess of the conventional space charge limit? Tests done with 200 MeV protons circulating in the BNL AGS indicated that we could obtain space charge tune shifts in excess of an integer. This confirms results in computer simulations that indicate tune shifts on the order of $\upsilon/2$ should be allowed in a transient condition.

2. What sort of bunching factors might one be able to obtain in a circular machine? Typical accelerators operate with bunching factors of about 10. By bunching factor we mean the distance between bunches divided by the length of the bunch. Experiments were done with 6 GeV protons on a flat top of the AGS magnet cycle, in order to obtain as large a bunching factor as possible. We were able to measure a bunch length (FWHM) of $\leq$ 3 ns, at a 220 ns separation. If all twelve beams were combined, this represents a power in excess of 1 TW. The bunch length measurements were limited by the bandwidth of our detection system. We anticipate better results will be obtained when the present deficiencies have been corrected.

VERY LOW VELOCITY ACCELERATION

Conventional heavy ion accelerators have not required high currents. Consequently, we have cocommenced the construction of a short ($\frac{1}{2}$ meter), high current low β linac to accelerate Xe^{1+} from 750 keV to 1.1 MeV. We have already operated the duoplasmatron source with Xenon, and obtained currents in the 5-10 mA range. The dominant species was Xe^{+1}, at an energy of 750 keV. A surplus rf transmitter, obtained from LBL, has been modified to provide power at 16.6 MHz for the strucuture. The velocity, of 0.0036, makes this the lowest β structure ever built. Operation is expected in November. A feature of the design is the easily removable drift tube assemblies. The internal features can be modified without major cavity alterations. The focusing is done externally by a pulsed triplet.

SPACE CHARGE NEUTRALIZATION

Existing accelerators all operate on the principle that space charge forces are unneutralized. However, for the Heavy Ion Fusion program, considerable advantage could be obtained if space charge forces could be reduced or eliminated. Three places are of special concern:

1. Transport to the final focus,
2. longitudinal compression, and
3. accumulation in a circular ring.

The BNL neutralizing studies are directed toward a theoretical and experimental understanding of these phenomena, so that one will be able to incorporate the advantages of neutralization into future HIF accelerator designs.

2. ARGONNE HEAVY ION FUSION PROGRAM

R. L. Martin

SUMMARY

The experimental part of Argonne's heavy ion fusion program is directed toward demonstrating the first, and in many ways most difficult, section of a viable accelerator facility for heavy ion fusion. This includes a high current, high brightness, singly charged xenon source, a dc preaccelerator at the highest practical voltage, and a low beta linac of special design. The latter would demonstrate rf capture with its attendant inefficiencies and accelerate ions to a velocity acceptable to more conventional rf linac structures such as the π-3π Wideroe. The initial goals of this program are for a source current of 100 mA of Xe^{+1}, a preaccelerator voltage of 1.5 MV, and less than 50% loss in rf capture into the low beta linac. If reliable operation of such a system is demonstrated, we believe that one of the major uncertainties in the heavy ion fusion concept will have been overcome.

Beyond this initial program, we have proposed that a linear accelerator with a voltage gain up to 200 MV as a minimum should be constructed and would form the initial stage of an operational heavy ion fusion facility irrespective of what type of acceleration to high energies (synchrotron, conventional rf linac, or linear induction accelerator) were employed beyond this point. In order to maximize beam current in any desired charge state, the source should produce singly charged ions with stripping to the desired charge state at the appropriate energy. Such a procedure is consistent with the Argonne program.

An experimental program with heavy ion beams as they become available at Argonne is planned to investigate space charge limited transport, neutralization, and vacuum questions.

Conceptual design studies and systems analysis continue. The program's current emphasis is on rapid cycling synchrotrons.

ION SOURCES AND COLUMNS

A high brightness Xe^{+1} ion source was delivered to Argonne in September by Hughes Research Laboratories. The source uses a low voltage Penning ion discharge and has a single aperture Pierce extraction electrode configuration. It delivers a beam of 2.5 mA of Xe^{+1} at 80 keV in a very narrow beam. The source is being mounted on a test stand for beam experiments on transmission of space charge limited beams, neutralization, and studies on vacuum effects.

The source was also tested at Hughes for production of a Bi^{+} beam and can also produce an Hg^{+} beam. The use of Hg^{+1} appears feasible with sufficient case; the practical use of Bi^{+1} appears extremely difficult.

Hughes Research Laboratories is presently scaling this source to a current of 100 mA at a constant current density of 15 mA/cm^2. This work is being carried out in collaboration with a high gradient column design at ANL for 1.5 MV voltage in the preaccelerator. The high current source and column should be available for installation into the Dynamitron by late spring of next year. Success with this source and column in the preaccelerator will stimulate efforts to achieve even higher voltages.

DYNAMITRON

A 4 MV Dynamitron dc accelerator was obtained from the Goddard Space Flight Center in Maryland. The accelerator has been installed at Argonne; and voltage tests, both dc and pulsed, to 2.5 MV have been carried out successfully. The Dynamitron is now being disassembled for modification of its final configuration. The latter includes an extension of 3 ft to the pressure vessel and installation of a quick opening flange. The flange is on the opposite end to the normal flange and provides rapid access to the source and column which will be mounted to accelerate to the opposite direction from the rectifier stack. This procedure allows a large aperture, high gradient column design not constrained by the rectifier stack. Additional modifications to the Dynamitron include replacement of the rectifier tubes (~ 100) with solid state rectifiers, recoupling the rectifiers for full wave rectification, strengthening of the coupling between the dees and the rectifier ring, and enlargement of the source terminal. As a full wave rectifier configuration, the maximum voltage will be 2 MV, beyond which the system has already been tested, and will have double the current carrying capacity. Tests indicate that the latter should exceed 50 mA and with some further modifications to the rf power supply may prove adequate for the 100 mA currents desired. If such modifications should prove too extensive, a Radiation Dynamics, Inc. oscillator capable of the required power is already available.

The modifications to the Dynamitron should be complete in January so that testing can resume. The high current xenon source and high gradient column are expected to be available in late spring of 1978.

LOW BETA LINAC

An rf linac to accelerate the Xe^{+1} beam above the 1.5 MV of the Dynamitron is being designed. The design is dominated by the need for strong quadrupoles to contain the high ion current at this relatively low voltage. Two low power models of 12.5 MHz cavities have been completed and tested. These include a 1/4 wavelength folded line resonator and a spiral resonator. The mechanical stability of the latter was inadequate. The properties of the folded line resonator were quite satisfactory. However, construction cost estimates from vendors were considered too high so

that we are presently studying modifications that would reduce the cost.

Two other types of rf cavities are being investigated. These are the capacitively loaded coaxial line and the lumped inductor. Modelling and testing at high power will be carried out. After settling on an optimum design for the cavities of the low beta linac, as many complete cavities (with rf power for acceleration) will be constructed as our funding will allow.

CONCEPTUAL DESIGN STUDIES

Studies directed toward accelerator configurations for 100 KJ systems have shown that the initial goals for pellet experiments with lower beam energies have introduced some new problems not inherent in higher power systems. These are a result of the assumption of smaller pellet size, requiring faster beam deposition and lower ion energy. Problems of longitudinal beam compression are thus more severe, and beam transport problems at the lower ion energies indicate the need for more beams than for higher power systems rather than fewer. In addition, 1 MJ systems utilizing rapid cycling synchrotrons may prove economically competitive with the lower energy systems.

For the above reasons, Argonne's program has concentrated most recently on rapid cycling synchrotrons for the ion beam fusion program. Activities include studies of the influence of B on the bunching factor, longitudinal bunching requirements, and on magnets for rapid cycling synchrotrons. On the latter, a particularly attractive design is one employing two separate apertures with ac magnetic fields switching between the two. Both are linked by a dc biasing magnetic field. If ac coupling to the dc coil can be eliminated, the latter could be made superconducting. A model of this magnet is being tested to determine its properties.

3. LAWRENCE BERKELEY

D. Keefe

The LBL directorate in 1976 made available discretionary funds to allow preliminary planning efforts to get under way in this promising new area. Direct ERDA funding started late in March of 1977. Part of the earlier efforts included preparation of a study proposal "Heavy-Ion Fusion-Proposal for a Program at Lawrence Berkeley Laboratory, (September, 1976)" which included not just the topics later funded and reported on here, but also proposed activities in other areas such as ion-ion and ion-gas interactions, ion-matter energy loss, cryogenic acceleration systems, etc., all of which will have bearing on the design of an ultimate system.

In choosing the present direction of our research and development program we tried first to single out those features that presented essentially new problems in accelerator design as opposed to those that we felt more comfortable about handling in a straightforward way. Among the latter are repetition rate, power conversion efficiency, creation of megajoule beams, and experience in engineering, estimating, meeting construction schedules, operating with high availability and having adequate control systems for the large scale igniter system that will be required. At least some of these features will present new challenges to other proposed igniter technologies e.g., lasers, REBs, ion diodes. The essentially novel problems facing the accelerator scientist we identified as the need for (a) large charge per pulse (or high current) and (b) high beam-power on target. The required currents are one to two orders of magnitude beyond our present experience for heavy ions, and the power much more than that; the power in particular presents a new (but visible) frontier because accelerators for experiments usually seek to provide the lowest possible power for users.

We have been addressing these problems on three fronts:

1) An intensive theoretical program was launched to try to understand the conditions for safe propagation of intense beam currents in focussing systems, such as continuous and interrupted solenoid lens systems, and quadrupole strong-focussing systems. Analytic methods have led to significant advances in understanding of the new problems; with computational techniques a large amount of new information has been generated on space-charge-dominated transport phenomena; also, at this time a new LBL particle numerical simulation code is almost ready to give new results. In the last few months a rewarding exchange has taken place with a group at the Naval Research Laboratory, who have adapted existing numerical simulation codes there to study this problem.

2) Because the Bevalac is an operating heavy ion linac and synchrotron facility with an ongoing R & D effort and in expectation of imminent upgrading to bring it up to a uranium-ion capability, it was a natural choice to make an addition to these activities to examine low-β rf accelerating structures and ion sources suitable for HIF. These studies have shown that the requirements for an rf injector for HIDE are just a short step away from those now being designed for the SuperHilac third injector which is soon to be constructed. The multi-aperture ion-source work has progressed to the point of demonstrating currents of heavy ions suitable for HIDE, but not yet for a power plant.

3) An experimental program on intense beam propagation was clearly of high priority. Experiments scaled in particle mass, for example, electron table-top devices, even proton models, were rejected because of the large extrapolation factors in favor of proceeding directly to heavy ions. While multi-ampere beams of gaseous ions, e.g., Xe, have been produced at LBL with CTR sources, we have chosen for the moment to construct a large aperture contact-ionization source of Cs^{+1} which should be free of troublesome gas-load problems. A drift tube system employing pulse-power units is planned to accelerate a beam of about one ampere to 2-3 MV (total charge $\approx 2\mu C$). A quadrupole transport system of some 24 magnets (12 periods) will be installed to study transport characteristics (such as emittance degradation). We have arranged to borrow much of the required equipment but have started to install the added power supply facilities needed to supply the electrical requirements. Other experiments to take place in the future will involve instability studies, beam bunching and neutralization.

We have benefitted by interaction with visiting scientists from other laboratories -- D. Tidman (University of Maryland) spent two months here, I. Hofmann (Max Planck Institute for Plasma Physics, Garching) will be with us for a year and W. Herrmannsfeldt (SLAC) is participating in the program on a 50% basis. In addition, V. K. Neil (LLL) and R. Cooper (LASL) are participating in the theoretical studies.

A workshop on Low-β High Intensity Accelerating Structures was held at LBL on June 1-3, 1977.

4. THE LAWRENCE LIVERMORE LABORATORY PROGRAM IN HEAVY ION FUSION

R. Bangerter

The Lawrence Livermore Laboratory is involved in three areas of research in heavy ion fusion:

1. Target design.
2. Combustion chamber design.
3. Ion beam propagation studies in the combustion chamber environment.

Through the laser fusion program, the Laboratory is also involved in all other aspects of inertial confinement fusion, such as target fabrication, diagnostics, and systems studies.

There have been two significant developments in target design since the 1976 Summer Study. The first is the evolution of new target designs with low power and energy requirements. These new designs increase our confidence that beam powers of $\sim$ 100 TW and beam energies of $\sim$ 1 MJ are sufficient to drive a fusion reactor.

The second development is the design of targets having calculated energy gains of 500-1000. For a given input energy a high gain relaxes the requirements on target fabrication costs, accelerator efficiency and repetition rate.

Several combustion chamber designs are being investigated. The most promising is the "lithium waterfall" approach. In this approach a thick ($\geq$ 50 cm) liquid lithium waterfall protects the chamber wall from neutrons, x-rays, blast and pellet debris while also serving as a breeding blanket for tritium.

The beam transport group at Livermore has extensive experimental and theoretical experience in the propagation of intense electron beams. The computer programs for electron beam propagation are being modified to calculate ion beam propagation. Preliminary results indicate that stable propagation of ion beams over distances of the order of 10 m (the probable radius of a combustion chamber) are possible at pressures $\sim$ 1 Torr. Some earlier calculations indicated much lower pressures were required. These low pressures would have excluded the lithium waterfall combustion chamber design.

In case combustion chamber pressures $\leq 10^{-3}$ Torr are required, we are studying the possibility of replacing the liquid lithium waterfall with a wall of small falling balls made of a lithium containing ceramic. We are also studying other fluid wall materials such as graphite. In addition to providing low chamber pressures, gas cooled ceramic or graphite systems may prove more environmentally acceptable than liquid lithium systems.

IV. HIDE Working Groups:

A. SYNCHROTRON BASED SYSTEM

1. SUMMARY

Mark Q. Barton

The one week duration of the Workshop proved far short of the time necessary to develop a detailed ion source to target scenario for a demonstration facility. Nonetheless, the Workshop proved useful for establishing constraints and for raising questions about the viability or cost effectiveness of this approach.

A point of discussion early in the week concerned the number of beams on target. Cost estimation schemes, particularly at Argonne, have indicated the desirability of a very large number (perhaps 100) of beams. There was, however, in the group, a sizable contingent who found this large number objectionable. Their reasons are traced to the following arguments:

1. The large number, in fact, may not be technically feasible.
2. Detailed designs of the transport systems for such beams have not been done. When they are completed, they may show that the assumptions in cost estimation arguments may have to be modified and a lower number of beams will result.
3. It may be that target people will impose, in the future, an upper limit as well as a lower limit on the acceptable number of beams on target.

There is no compelling reason to believe that any of these arguments are true. Nonetheless, there was a sufficiently strong intuitive feeling by enough people in the group to steer the discussion towards a system with a small number of beams. Certainly these questions should be addressed directly before any significant effort is spent on any system contingent on a large number of beams.

Once the decision was made to concentrate on a small number of beams, the transmittable power per beam line restricts the options to:

1. highest energy consistent with suitable range
2. highest feasible atomic number
3. lowest possible charge state.

Unfortunately all these constraints point to high cost. For example, a ring of about 100 m radius with 1 Tesla fields could hold 1 MJ of 4^+ bismuth (A = 209) ions of 35 GeV each. With modest bunching, and eight extraction points, this ring could provide 160 TW for a total 1 MJ. Each beam would be near its limit at 20 TW. Any reduction in energy, atomic number or increase in charge state makes it impossible to transport the required power to target in eight or fewer beams.

Even though such a ring could contain the requisite stored energy, (without bunching) it could not be used as a synchrotron. This is a result of space charge constraints very similar to what occurs in the beam transport. If one injects into this ring at a lower energy than 35 GeV, the space charge limit is exceeded at injection. The only possible resolutions are to:

1. use a lower charge state
2. use another ring which is rapidly cycled to fill this ring
3. use several simultaneously pulsed synchrotrons to fill the big ring.

These arguments are based on the very simple space charge limit

$$N = \frac{2\pi\Delta\nu}{Br_p}\left(\frac{A}{2}\right)\epsilon_n\,(\beta\gamma^2)$$

where N is the number of stored particles, $\Delta\nu$ is the acceptable betatron oscillation tune shift usually taken as 0.2 - 0.25, B the rf bunching factor, r_p is the classical radius of the proton, A the atomic weight of the ion and q its charge state, $\pi\epsilon_n$ is the normalized emittance as determined by the target and we have assumed 20π mm mrad. β and γ are the usual relativistic factors. If we multiply the number of particles N, by the energy per particle, we can determine how many megajoules can be stored. In Table IV-A-1/1, we show some simple results of this formula for charge states 1, 2 and 4 for an atomic number of about 200 (gold, bismuth, mercury, etc.) at 35 GeV. The first column gives the energy that can be stored in a full energy ring. The second column gives the energy that can be stored at 35 GeV in a ring used as a synchrotron so that N is space

charge limited at an injection energy of 2 GeV. Except for q = 1, the entries in this column fall short of the 1 MJ requirement and the final column shows the number of synchrotron or rapid cycles to develop the full 1 MJ. It was noted, incidentally, that the rapid cycling synchrotron may be even further limited. The rapid cycling automatically implies an unfavorable bunching factor which further limits the number of particles which can be stored.

TABLE IV-A-1/1. Implications of Space Charge Limits.

35 GeV IONS AT A ~ 200
BUNCHING FACTOR = 2
$\Delta\nu = 0.25$
$E_n = 20 \times 10^{-6}$ mrad

CHARGE STATE	STORED ENERGY 35 GeV	STORED ENERGY 2→35 GeV	NUMBER OF ACCELERATION CYCLES REQUIRED
1	> 8 MJ	~ 1 MJ	1
2	~ 2 MJ	~ 0.12 MJ	~ 8
4	~ 0.5 MJ	~ 0.033	~ 30

From this table we see that one clear scenario would use a single synchrotron ring designed for charge state 1. This ring fits all space charge criteria, etc. but other details were not examined. It looks surprisingly like the synchrotron option developed by Teng at the Berkeley study a year ago.

Another option might be to use eight independent synchrotrons each operating in charge state 2. This has the additional advantage that one of the rings capable of storing ~ 100 kJ could be built as a preliminary experiment.

A number of areas were explicitly identified as needing further work. These are described below:

1. Cross sections for ion-ion charge exchange scattering and beam-gas stripping reactions. There were some discussions about these subjects during the Workshop although no new calculations were done as part of this group effort.

   It is clear that a synchrotron with its relatively slow acceleration process is much more sensitive to these effects than linear accelerators of either the rf or induction types. Even with optimistic guesses as to cross sections, vacuum requirements may be as low as 10^{-11} Torr and acceleration and storage times should be limited to a fraction of a second. Clearly these cross sections must be experimentally determined and their implications explicitly folded into any design which is seriously considered.

2. Instabilities. A variety of coherent instabilities has plagued circular accelerators. Intuitively, one might expect heavy ion machines of the type of interest here to be relatively free of these problems. Nonetheless, rings designed for heavy ion fusion should be carefully examined in this respect.

3. Linac performance. The single ring could be filled with a linac current of 50 mA in a normalized emittance of 2π mm mrad. Even this performance may be difficult. If an even brighter beam could be obtained, it might simplify some aspects of the problem.

4. Bunching. A very cursory study was done of the bunching problem. This problem is common to all scenarios but it is attractive to consider the synchrotron itself as a bunching device. With rf voltages, of some tens of MV per turn, this is indeed feasible. Clearly, more work is needed in this area.

5. Costs. It was not possible to develop any scenario sufficiently to start cost estimates. A rough idea of the scope of the scenario described above can be made by comparison with well-known machines. For example, the ring would be about three times as large as the AGS at BNL, with a vacuum system like the ISR at CERN. A linac about 2.5 times as large as the LAMPF machine would serve as injector. An rf system comparable to the one for PEP at SLAC would be needed for bunching the beam. The total cost is clearly going to be large. Hopefully, some ingenious developments will come along to reduce costs.

6. Intermediate steps. If, indeed, a charge state of one is required, there is no obvious way that a reduced scope (e.g., 100 kJ) device could be built as an intermediate step towards a full scale facility. With a multiple ring scenario, one could build a fraction of the rings. Even this step has the disadvantage that the linac, which represent a sizable fraction of the cost, would have to be built full scale. Perhaps intermediate money would be better spent exploring some of the outstanding technological questions.

2. ARGUMENTS FOR LOW q IN 1MJ SYNCHROTRON

Ch. Leemann

INTRODUCTION

Some general arguments favoring low q/A are outlined and the specific example of a T = 35 GeV, M = 209, q=1 synchrotron is discussed.

CONSIDERATIONS ON MAXIMUM DELIVERABLE ENERGY

In prescribed normalized emittance $E_n = \pi\varepsilon_n$:

$$W \leq \frac{\delta\nu}{r_p}\,\varepsilon_n\beta\gamma^2\;\; 2\pi B\left(\frac{A}{q}\right)^2\;\; m_p c^2\left(\gamma_f - 1\right) \qquad (1)$$

based on keeping $\delta\nu \leq 0.25$ at all times (corresponding β,γ) except during final bunching.

If ε_n is expressed by the pellet radius using a simple geometric argument:

$$\varepsilon_n \leq \frac{R\cdot r}{L}\;\beta_f\gamma_f\,,\quad r=\left[\frac{W\,\Omega}{\pi E\lambda}\right]^{\frac{1}{2}}\,,\quad E \simeq 20\ \text{MJ/g},\ \lambda \text{ range},$$

beam overlap, $\Omega < 0.5$, we obtain

$$W = \left(\frac{\delta\nu}{ro}\right)^2\frac{R^2}{L^2}\frac{4\Omega}{E\lambda}\beta_f^2\;\;\gamma_f^2\left(\gamma_f - 1\right)^2\beta^2\gamma^4\pi B^2\left(\frac{A}{q}\right)^4 m_p^2 c^4 \qquad (2)$$

If the final focusing is limited by the last quadrupoles (assume fixed B_o) then R is no longer a free parameter but $R\ (q) = \frac{q}{A}\cdot R\ (1)$ and we obtain again $W \propto \left(\frac{A}{q}\right)^2$ (3)

(a) This indicates that care has to be exercized in how the problem is defined since the power of (A/q) can be changed by that.

(b) It should be noted that the bunching factor B in Eqs. (1), (2) cannot be arbitrarily chosen but depends on the rise time of the magnetic field and most importantly the longitudinal emittance.

If at a given injection energy and charge state Eq. (1) cannot be satisfied, multiple synchrotron pulses or parallel systems must be used. Tune shift considerations also determine the number of accumulator rings.

Consider two extreme cases:

(a) Stack N_p synchrotron pulses in accumulator ring in betatron phase space:

X & Y plane, no dilution

then

$$\varepsilon_{synch} = N_p^{-\frac{1}{2}}\,\varepsilon_f$$

$$W_{tot} = W_{p_i}\cdot N_p \propto N_p\,\frac{\varepsilon_f}{N_p^{\frac{1}{2}}} = N_p^{\frac{1}{2}}\,\varepsilon_f$$

So multiple plusing gains (ideally) as $N_p^{\frac{1}{2}}$.
Now there are two points weakening this argument:

(I) There will be dilution in the stacking process.

(II) The higher repetition rate required will reduce B and therefore reduce the available W/pulse.

(b) Instead of stacking consider parallel systems:

N accumulator rings each receiving one synchrotron pulse from one or more (up to N) synchrotrons.

Then the transverse emittance in accumulator rings and synchrotrons is the same, the total longitudinal emittance is $N\cdot\varepsilon_{synch}$. Whether this is tolerable or not depends on the momentum spread tolerable at the target and the longitudinal emittance.

In the present context 1 MJ in $\varepsilon_n = 2.10^{-5}$m with mass 209 at 35 GeV was assumed, $\frac{\delta p}{p}$ at target was left relatively unspecified (0.5 to 1.10^{-3}).

Fig. IV-A-2/1 plots the normalized emittance for different charge states compatible with 1 MJ in 1 pulse with $\Delta\nu = 0.25$ and B = 0.25 (arbitrarily) vs. injection energy.

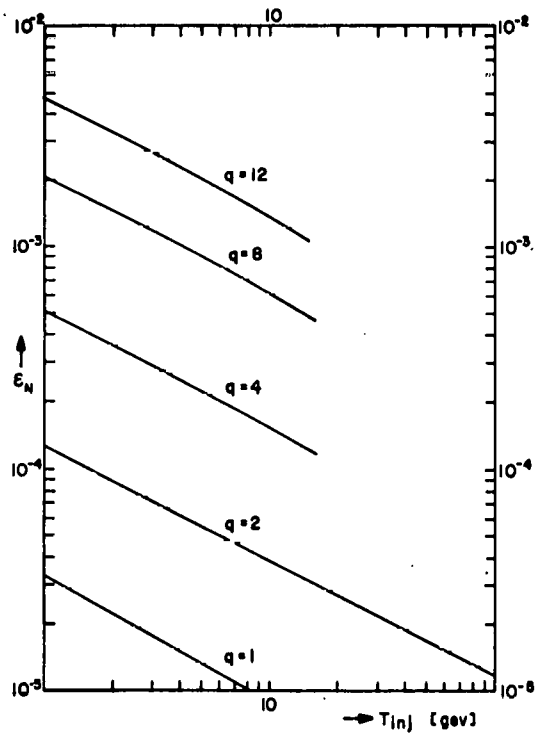

Fig. IV-A-2/1. Normalized emittance vs. injection energy.

We conclude $T_{inj,min}$ for 1 pulse is for q=1 and 2:

q	$T_{inj,min}$
1	2.4 GeV
2	36 GeV > T_f

These numbers are subject to some variations depending on the actually applicable bunching factor B. They indicate, however, that with the assumed values of ϵ_n and T_f a single synchrotron pulse of $\sim$ 1 MJ is possible only for q=1.

If several synchrotron pulses are accumulated we must also ensure that tune shifts in the accumulator ring(s) remain acceptable during the fitting procedure. The corresponding upper limits on W are tabulated in Table IV-A-2/1.

Table IV-A-2/1. Stored energy in accumulator rings.

$\Delta\nu = 0.25$, $\epsilon_v = 2.10^{-5}$m, B = 0.5

Q	T = 35 GeV (present case, low Z target)	T = 20 GeV (high Z target)
1	$9 \cdot 10^6$ J	$3.6 \cdot 10^6$ J
2	$2.25 \cdot 10^6$ J	$0.9 \cdot 10^6$ J
4	$5.63 \cdot 10^5$ J	$0.2 \cdot 10^6$ J

So at T=35 GeV 2 rings are required for q = 4, at T = 20 GeV 5 rings are required for q = 4, and q = 2 is marginal for 1 ring only.

These considerations lead one to concentrate on a concept based on a q = 1, single pulse synchrotron injected at $T_{inj} \cong 2$ GeV.

3. CONSIDERATIONS ON THE USE OF SYNCHROTRONS FOR THE HEAVY ION FUSION PROJECT

A. G. Ruggiero

I. The scheme which makes use of "Synchrotrons" for the Heavy Ion Fusion Project is schematically shown in Fig. IV-A-3/1.

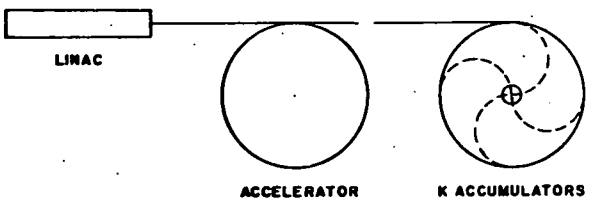

Fig. IV-A-3/1. Schematic of Synchrotron Based System.

A linac is delivering an average electric current I_L of heavy ions of charge state Z and atomic mass A. The kinetic energy is T_L and the normalized emittance ε_L (on both planes). A number of pulses, m, are injected in an accelerator, $\sqrt{m}$ of them horizontally and $\sqrt{m}$ vertically. Assuming a factor 2 for dilution, the emittance at injection is

$$\varepsilon_A = 2\sqrt{m}\,\varepsilon_L \quad \text{(normalized)}$$

(again on both planes), and the average current

$$I_i = mI_L .$$

This beam is then accelerated to a final kinetic energy T extracted and transferred to one of the κ accumulators. This operation is repeated p times for each accumulator, again $\sqrt{p}$ times on the horizontal plane and $\sqrt{p}$ times on the vertical plane. If we take also here a factor 2 for dilution, the final emittance would be

$$\varepsilon = 4\sqrt{mp}\,\varepsilon_L \quad \text{(normalized)}.$$

Denoting with β_I and β_F the velocity factors at injection and extraction, the final average current in each accumulator is

$$I = mp\,\frac{\beta_F}{\beta_i}\,I_L .$$

Each accumulator has h bunches, for a total number of κh beams which have to be extracted and sent to the target at the center of the accumulators. Figure IV-A-3/1 shows the case of h = 4. For each curved line shown toward the center, there are κ transport lines on top of each other and each carrying one bunch. Before the extraction, all the bunches are furtherly compressed to get a final peak current I.

Because we want to use the largest bending field possible, we impose that the accumulators and the accelerator have the same average radius, R.

The total number of particles on the target is

$$N = \kappa\frac{2\pi R}{Ze\beta c}\,I.$$

The total beam energy is then

$$W = eNT$$

and the power

$$P = h\kappa TI/eZ.$$

During the beam acceleration and accumulation one wants to make sure the space charge tune shift $\Delta\nu$ does not exceed at any time a reasonable limit.

The tune shift is given by

$$\Delta\nu = \frac{Zr_p}{A}\,\frac{I_p}{ec}\,\frac{R}{\varepsilon/\pi}\,\frac{1}{(\beta\gamma)^2}$$

where I_p is the peak current, ε the normalized emittance and $\beta\gamma$ the relativistic factor at a given time during acceleration or accumulation, and

$$r_p = 1.5347\times10^{-18}\ \text{m}.$$

Also the maximum power that can be transported down a beam line is given by

$$P_{max} = 2.5\times10^{3}\left(\frac{A}{Z}\right)^{4/3}\left(\frac{\varepsilon}{\pi}\right)^{2/3}(\beta\gamma)^{5/3}(\gamma-1)^{2/3}B_Q\ \text{TW}$$

where ε is again the normalized emittance in πm-rad units and B_Q is the field at the edge of the quadrupoles in the transport line given in Tesla units.

Finally, denoting with B the average field in the accelerator and accumulator

$$R = 3.1\frac{A\beta\gamma}{ZB}\ \text{meters}$$

where B is given in Tesla units.

II. For the exercise in this paper we shall consider acceleration of ions of Bismuth (A = 209) from T_L = 2 GeV up to T = 35 GeV. For the design of an experimental project we shall take also

$$W = 1\text{MJ and } T = 160\ \text{TW}.$$

We shall nevertheless keep the charge state Z as a free parameter. Also we set reasonably

$$B = 10\ \text{kG and } B_Q = 10\ \text{kG}.$$

This will immediately give

$$R = \frac{406\ m}{Z} .$$

Also from considerations on the target size and on the focusing capability of the last section of the transport line, we take for the final normalized emittance

$$\epsilon = 10\pi \text{ mm-mrad.}$$

The relevant kinematic parameters are shown in Table IV-A-3/1.

Table IV-A-3/1. Kinematic Parameters (A=209).

T =	2 GeV	35 GeV
β	0.1422	0.5306
γ	1.0103	1.1798
$B\gamma$	0.1437	0.626
$(\beta\gamma)^{5/3}$	0.0394	0.4581
$\gamma-1$	0.0103	0.1798

and

$$A^{5/3} = 1240.3.$$

From the same target considerations we also take a final momentum spread

$$\Delta p/p = 10^{-2} .$$

Which is small enough to eventually avoid the aberration effects of the transport lines. Since the final bunch length is 6 ns, we have then for the invariant longitudinal bunch area

$$S = 3.88 \text{ eV·s (per bunch).}$$

From all these assumptions we derive

$$N = 1.8\times10^{14} \text{ (total number of ions)}$$

$$\boxed{P_{max} = 119 Z^{-4/3} \text{TW}} \qquad \text{(at 35GeV)}$$

and, if we take a space charge limit of $\Delta\nu = 0.2$,

$$\boxed{I_p = 12.6\ A} \qquad \text{(at 35 GeV)} .$$

III. Let us first give a look at one single accumulator. Let b ($\geq$1) be the bunching factor (before final compression), then

$$I_p = bI.$$

The revolution period is

$$\boxed{T_s = \frac{16\ \mu s}{Z}} .$$

Then, if N_r is the number of particles per ring,

$$eN_r = \frac{2.0\times10^{-4}}{bZ^2}$$

and the beam energy per ring is

$$W_r = \frac{7\ MJ}{bZ^2} .$$

The number $\varkappa$ of accumulators is then given by the ratio W/W_r. The minimum number of accumulators versus z and other parameters are shown in Table IV-A-3/2.

Table IV-A-3/2. Accumulator Parameters vs. Z.

Z	R	P_{max}	T_s	b	$\varkappa$
1	406 m	119 TW	16 μs	7	1
2	203	47	8.	1.75	1
3	135.3	27	5.3	1.56	2
4	101.5	19	4.	1.31	3
5	81.2	14	3.2	1.12	4
6	67.7	11	2.7	1.17	6
7	58	9	2.3	1.00	7
8	50.7	7	2.0	1.09	10

The required number of accumulators increases with Z. For large Z, the beam is transferred to the accumulators essentially debunched (b=1). Only <u>one</u> accumulator is required for Z=1 and Z=2, but with Z=1 there is the advantage that it is possible to transfer the beam already tightly bunched. Observe that the accelerator radius R decreases with Z. For Z>8, the ring becomes too small for accommodation of the transport lines and the reactor in the center. Observe also the large amount of power that can be transported for low values of Z.

IV. We assume that the final compression is rapid enough so that, though the space-charge limit $\Delta\nu$= 0.2 is exceeded, nevertheless the beam survives. If n = hk is the total number of bunches on the target and $\hat{I}$ is the final peak current, we have

$$\boxed{\hat{I} = \frac{eZ\mathcal{P}}{nT} = 4.57\frac{Z}{n}kA}$$

The extra bunching factor required is then

$$\hat{I}/I_p = 363Z/n$$

One should observe that this compression factor is over and above that shown in column (b) of Table IV-A-3/2. An overall bunching of 100 should be possible; a factor 10-20 could be obtained with a standard RF system and another factor 5-10 with a more exotic scheme. For the same number of beams, the required overall bunching ($b\hat{I}/Ip$) decreases with Z until b becomes unphysically smaller than unity, and then increases again with Z. For instance take n = 12. Then the overall bunching is 7x30 for Z=1 and 1.75x30x2 for Z=2. The latter case seems to be a better choice.

In Table IV-A-3/3 we show the overall bunching and the product of the number of rings per their size versus Z for n=24.

Table IV-A-3/3. Overall Bunching and Orbit Length vs. Z (n=24).

Z	B	$\hat{I}/I_p$	$b\hat{I}/I_p$	κR	κ
1	7	15	105	406 m	1
2	1.75	30	53	203	1
3	1.56	45	70	271	2
4	1.31	60	79	304	3
5	1.12	75	84	325	4
6	1.17	90	105	406	6
7	1.00	105	105	406	7
8	1.09	120	131	507	10

The total orbit length does not change much with Z, and obviously large Z would represent a better choice because, though the number of accumulators increases, their size decreases and they would overall be less expensive because they could share the same tunnel and utilities. In addition the overall required bunching does not really change very much with Z. These considerations would then lead toward a choice of large Z. On the other hand, there is a limit on the transport power P_{max} (see Table IV-A-3/2) which would suggest a smaller Z unless one increases the number beams, which would be more expensive, but by how much we do not yet know.

V. Let us now look at the accelerator. Let us consider the lower energy end (T=2 GeV). We could let our feelings lead us and argue that if we found a workable solution for low energy, then it should be all right for any other larger energy.

The normalized emittance is

$$\epsilon_A = \frac{\epsilon}{2\sqrt{p}} \text{ (normalized)}$$

and the average current is

$$I_A = \frac{\beta_i}{\beta} \frac{I}{P} .$$

Let b_i be the bunching factor at injection.

As that in the accumulator, b, the peak current at injection is

$$\hat{I}_A = \frac{\beta_i}{\beta} \frac{b_i}{b} \frac{I_p}{p} .$$

Where I_p is the peak current in the accumulators before final compression.

The space-charge tune shift is now

$$\Delta\nu = \left\{ \frac{Zr_p}{A} \frac{I_p}{ec} \frac{R}{\epsilon/\pi} \frac{1}{(\beta\gamma)^2} \right\} \frac{2}{\sqrt{p}} \frac{\beta_i}{\beta} \frac{b_i}{b} \frac{(\beta\gamma)^2}{(\beta_i\gamma_1)^2} .$$

This is then converted to the following condition for being at the space-charge limit,

$$b_i = 0.1\, b\sqrt{p}.$$

Assuming a minimum $b_i = 2$, the required number of turns $\sqrt{p}$ (per plane), the emittance ϵ_A and the average current I_A are shown in Table IV-A-3/4.

Table IV-A-3/4. Injection Parameters for the Accelerator (b_i=2).

Z	b	$\sqrt{p}$	ϵ_A	I_A
1	7	3	0.167 π cm-mrad	53.6 mA
2	1.75	12	0.042	13.4
3	1.56	13	0.038	12.8
4	1.31	15	0.033	11.5
5	1.12	18	0.028	9.3
6	1.17	17	0.029	10.0
7	1.00	20	0.025	8.4
8	1.09	18	0.028	9.6

The numbers in this Table suggest that one-turn injection from the linac to the accelerator is adequate. The emittances and currents shown are those that have to be delivered from the linac. The brightness of the beam (I/ϵ^2) increases by a factor 5 from Z=1 to Z=2 and more slowly for larger Z. The values for Z=1 can likely be achieved, but there is some concern for those at larger Z.

Some special considerations are required for the case Z=1. If we take p=1 and we drop the factor 2 for dilution, we obtain an initial bunching factor of 1.4 that is small but likely still manageable. Thus for Z=1 the total required number of particles $N = 1.8 \times 10^{14}$ could be injected, accelerated and stored in one single machine. In this case one also needs multi-turn injection from the linac, 3 turns horizontally and 3 turns vertically. The linac parameters are the same of those specified in Table IV-A-3/4. For Z>1 there are no other choices than those shown in Table IV-A-3/4.

At this point, one may draw a temporary conclusion. The case Z=1 seems to be more advantageous because the entire process can be accomplished in a single machine. Of course, the choice of Z also affects the linac. For a given voltage, it is certainly better to accelerate ions with larger charge. But the amount of these ions down at the source is strongly limited. It seems better to accelerate ions with Z=1 to at least some intermediate energy and then produce more heavily charged ions by stripping. This would make overall linac length shorter and save some money. If the economic saving is not adequate, the choice Z=1 seems to be the most advantageous so far.

VI. The accumulators and the accelerator have different requirements. The magnet aperture is larger in the accumulators which, on the other hand, are dc machines. A lattice with reasonable focusing (β_{max} = 20 m, η_{max} = 30 m) is certainly possible. To contain an emittance of 16π mm-mrad at 35 GeV and a momentum spread of 1%, a physical aperture of 10 cm should be adequate. The accelerators have more modest requirements for aperture since they have to accommodate the emittance shown in Table IV-A-3/4 and smaller beam momentum spreads. On the other hand, they are to be pulsed at a reasonably high rate.

A special case is again Z=1 if one wants to make use of one single machine. The magnet aperture has now to be large enough to accept an emittance of 70π mm-mrad at injection and a momentun spread of 1% (during bunch compression) at full energy. It appears that a physical aperture of 10 cm should again be adequate, but now the magnets are cycled at high repetition rate.

VII. It remains now to check whether the schemes outlined above could be matched to a reasonably accelerating rf cycle.

Let us define the bunching factor as the ratio of the rf bucket full height to the beam height when fully debunched

$$b \equiv \frac{\pi\sqrt{2}}{4}\frac{Y}{\alpha}$$

where Y and α are parameters related to the bucket height and area. This definition applies for completely full buckets with area equal to the bunch area S.

$$S = 8\frac{\alpha}{f_A}\sqrt{\frac{Z\,V\,AE_o\gamma^3}{3\pi^3 h}}$$

where f_A is the accelerating voltage for β=1 and E_o=(0.938 GeV) is the rest energy of a proton. We are also assuming that the number of bunches is equal to the harmonic number h. We have

$$b < b_{max}$$

where

$$b_{max} = \sigma\frac{AeT\kappa_c\gamma^2}{Z^2 r_p W}\beta\sqrt{p}\,\Delta\nu$$

is the maximum bunching allowed by the space charge tune shift $\Delta\nu$. Here σ=1 for multiturn injection ($p \geq 2$) and σ=2 for single-turn injection (p=1).

Inserting numbers,

$$\frac{Y}{\alpha} < 4.8\,\sigma\frac{\kappa}{Z^2}\sqrt{p}\,\beta\gamma^2 = f_z\,\beta\gamma^2.$$

The quantity f_z is given in Table IV-A-3/5 for various values of Z. The number of accumulators k and the number of turns p are taken from Tables IV-A-3/2 and IV-A-3/4.

If we take a total number of bunches around 24, since the number of accumulators k is determined, we have then the number h of bunches per ring. This number is also shown in Table IV-A-3/5 together with f_A.

Table IV-A-3/5. RF Parameters for the Accelerator.

Z	f_Z	k	h	f_A	V_o
*1	9.6	1	24	2.82 MHZ	14.3 kV
1	14.4	1	24	2.82	14.3
22	14.4	1	24	5.64	28.6
3	13.9	2	12	4.23	5.4
4	13.5	3	8	3.76	2.1
5	13.8	4	6	3.53	1.1
6	13.6	6	4	2.82	0.4
7	13.7	7	4	3.29	0.5
8	13.5	10	3	2.82	0.22

*No accumulator

Observe that the accelerating frequency is already quite low (a fraction of MHz at injection). It could be increased only at the cost of increasing the number of bunches by filling only part of the rf buckets.

All the cases shown in Table IV-A-3/5, except the first one, have a relatively easy acceleration cycle. To speed up the acceleration, the rf voltages and phases are programmed so that the beam is bunched at the limit of space-charge. This corresponds to b=2 at injection and b=10 at the top energy. The rf phase φ_s increases from a minimum of 18° at injection to 75° at extraction. At the end of the acceleration, the beam would be transferred rapidly to the accumulator and allowed to debunch. This operation will keep the beam in the accumulators always below the space charge limit.

In Fig. IV-A-3/2 we have plotted Y/α vs. $\beta\gamma^2$

as well as vs. φ_s. We have calculated and show in the same figure φ_s vs. $\beta\gamma^2$. This curve is independent of the charge state Z but does not apply to the case Z=1 with no accumulator. This case, as one can see from Table IV-A-3/5, is not easily fitted by a reasonable rf program in the low energy range.

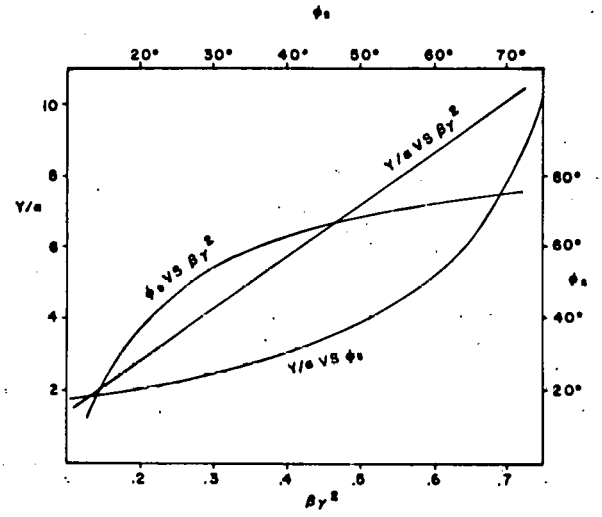

Fig. IV-A-3/2. Y/α vs. $\beta\gamma^2$ and φ_s.

The rf voltage, V, is calculated once the rf phase φ_s is known by requiring that the bucket area and bunch area are equal

$$V = \frac{S^2 f_A^2 h\pi^3}{32Z\alpha^2 AE_o\gamma^3} = \frac{74.9\ hf_A^2}{Z\alpha^2\gamma^3}$$

(f_A in MHz, V in Volts) .

The total voltage per turn Vo required in the limit of γ=1 and α=1 is also shown in Table IV-A-3/5. The voltage toward the end of the acceleration (φ_s=75°) is 5.5×10^3 times larger for all cases. The final required voltage V_f per turn and the fraction, g, of the machine occupied by rf cavities, based on an optimistic estimated 50 kV/m gradient are shown in Table IV-A-3/6. The only obviously reasonable cases are those with Z≥4.

The time, τ, required for acceleration is also shown in Table IV-A-3/6. It is rather large and increases with Z. The actual time required for filling the κ accumulators each p times is κp times τ, and is unfortunately large compared to the beam lifetime due to charge exchange.

Table IV-A-3/6. Final Voltage, RF Occupancy and Acceleration Time.

Z	V_f	g	τ
*1	79 MV	62%	2.3 sec
1	79	62	2.3
2	158	248	0.6
3	30	71	2.1
4	12	38	3.9
5	6	24	6.0
6	2.2	10	13.8
7	2.8	15	9.5
8	1.2	8	18.9

*No accumulator

The acceleration time can be considerably reduced by increasing the initial rf voltage, but then the bunching factor also increases.

CONCLUSIONS

These considerations, of course, cannot really be conclusive. They require a better evaluation and analysis at much lower pace than that at which they were drawn during the five-day Workshop. Honestly, we cannot answer yet either way whether synchrotrons can be used to accelerate heavy ion beams for the pellet fusion.

It seems to us that there are no real limitations on the transverse plane. But the design of an adequate accelerating cycle is rather tight if the acceleration has to be conducted at a reasonable rate. This, of course, should be confronted with the question of the beam lifetime that has not been taken into account here. A second problem that has not been taken into consideration in this note is the final beam compression.

Overall, we believe that the synchrotron presents an attractive solution because of its low cost and size. Nevertheless, we are still far away from reaching a conclusion on a possible set of parameters.

Another important fact that emerged from our study is that the choice of the charge state A is influenced by conflicting requirements. It is not yet obvious to us which value of Z would be the most convenient one.

4. BUNCHING FACTOR IN TRANSVERSE SPACE CHARGE CALCULATIONS

T. K. Khoe

In a strong focusing synchrotron the momentum compaction factor is small compared to unity. Hence the transverse beam dimensions are mainly determined by the betatron amplitudes. On the other hand, the longitudinal particle distribution depends upon the phase motion. In the expression for the transverse space charge limit, the bunching factor B_f is the ratio between average and maximum linear charge density. The maximum linear charge density is proportional to the beam bucket height. The mean linear charge density is proportional to beam bucket area averaged over 2π. Thus,

$$B_f = \frac{\text{beam bucket area}}{2\pi \text{ full bucket height}}$$

It is not difficult to show that for a chosen longitudinal beam emittance the maximum value of B_f is obtained when the rf buckets fit tightly around the bunches. The bunching factor can then be written in the form

$$B_f = \frac{2\sqrt{2}}{\pi} \frac{\alpha(\Gamma)}{Y(\Gamma)} \qquad (1)$$

where $\Gamma = \sin \phi_s$. The quantities $\alpha(\Gamma)$ and $Y(\Gamma)$ are tabulated in a CERN report.[1] The ratio α/Y is equal to $1/2\sqrt{2}$ for $\Gamma = 0$ and decreases to zero for $\Gamma = 1$. Substituting $V = 2\pi R \rho \dot{B}/\Gamma$ and $\beta = \Omega R/c$ in the bucket area expression [2]

$$A_b = \left[\frac{h q V E}{2\pi |\eta|}\right]^{1/2} \alpha(\Gamma) \frac{16\beta}{h^2 \Omega},$$

and solving for $\frac{\alpha}{\Gamma^{1/2}}$ one obtains

$$\frac{\alpha}{\Gamma^{1/2}} = \frac{A_b h^{3/2} c}{16 R^{3/2}} \left[\frac{|\eta|}{q \rho \dot{B} E}\right]^{1/2}. \qquad (2)$$

Table IV-A-4/1. $\alpha/\Gamma^{1/2}$ and B_f as a function of Γ.

Γ	$\alpha/\Gamma^{1/2}$	B_f
0.50	0.4715	0.36
0.55	0.3891	0.34
0.60	0.3177	0.32
0.65	0.2553	0.29
0.70	0.2007	0.27
0.75	0.1527	0.24
0.80	0.1108	0.22
0.85	0.0743	0.19
0.90	0.0431	0.15

It turns out that B_f as a function of $\alpha/\Gamma^{1/2}$ can be written in the form

$$B_f = 0.5 \, (\alpha/\Gamma^{1/2})^{\,0.385}.$$

The right hand side of Equation (2) is determined by the chosen values of beam bucket area, harmonic number, mean synchrotron radius, magnet radius, magnet cycling time and the transition energy. In a fast cycling synchrotron the magnetic field varies with time as

$$B = \frac{B_2 + B_1}{2} - \frac{B_2 - B_1}{2} \cos 2\pi f t,$$

where B_1 and B_2 are the field values at injection and ejection, and f is the repetition frequency. The transverse space charge limit is determined by chosen values of the normalized emittance and the minimum value of $\gamma^2 \beta B_f$. In the early acceleration period B_f decreases much faster than the increase of $\gamma^2\beta$ and the transverse space charge limit occurs at $t > 0$.

EXAMPLE

Particle atomic weight and charge state:
$A = 209$, $q = 4$
Injection energy $T_1 = 2$ GeV
Maximum energy $T_2 = 35$ GeV
Repetition frequency $f = 10$ Hz
Maximum field $B_2 = 1$ T
$q B_2 \rho = 406.14$ T-m, $\rho = 101.535$ m
$R = 135$ m, $B_1 = 0.2296$ T
$\eta = \frac{1}{\gamma^2} - \frac{1}{\gamma_t^2} \approx \frac{1}{\gamma^2}$, $A_b = 0.05$ ev - sec
$h = 100$; $\dot{B} = (B_2 - B_1)\pi f \sin 2\pi ft = 24.2 \sin 20\pi t$ T/sec
$E = \gamma A mc^2 = 194.6 \gamma$ GeV

Substituting these parameters in Equation (2), one finds

$$\frac{\alpha}{\Gamma^{1/2}} = \frac{0.01367}{\gamma^{3/2} (\sin 20\pi t)^{1/2}}$$

Table IV-A-4/2 gives γ, β $\alpha/\Gamma^{1/2}$, B_f and $\gamma^2\beta B_f$ as a function of t. The transverse space charge limit occurs 6 msec into the acceleration period, when $\gamma^2 \beta B_f = 0.01875$. Assuming $\gamma \beta \epsilon_v = \gamma \beta \epsilon_h = 2 \times 10^{-5}$ m-rad and $\Delta \upsilon_v = 0.25$ one finds

$$N_{inc} = \frac{A}{q^2} \pi (\epsilon_v \gamma\beta) \left(1 + \sqrt{\frac{\epsilon_h}{\epsilon_v}}\right) \gamma^2 \beta B_f \Delta \upsilon_v$$

$$= 4.8 \times 10^{12}.$$

Table IV-A-4/2. γ, $\beta\gamma/\Gamma^{1/2}$, B_f and $\gamma^2 \beta B_f$ as a function of t.

t(msec)	γ	β	$\alpha/\Gamma^{1/2}$	B_f	$\gamma^2\beta B_f$
0	1.01028	0.1423		2π	0.092
2	1.01055	0.1441	0.038	0.142	0.021
4	1.01138	0.1496	0.027	0.124	0.019
6	1.01283	0.1586	0.022	0.115	0.01875
8	1.0150	0.1710	0.019	0.109	0.0192

References

1. CERN/MPS-SI/Int. DL/70/4, April 23, 1970, Appendix D.
2. See reference 1 page 31.

HIDE working groups :

B. RF LINAC BASED SYSTEM - -

1. SUMMARY

D. E. Young

INTRODUCTION

The task of this group* during the Workshop was to develop consistent designs for rf-linac heavy-ion accelerator fusion systems that meet the target requirements of 1 MJ of beam energy delivered in a pulse that builds up in about 20 nsec to a rate of 100 TW for 6 nsec, with a specific energy deposition of 20 MJ per gm in a target pellet. It was also suggested that a scaled-down version of these parameters with the same energy deposition but at a lesser beam energy of 100 KJ, building up to a power level of 50 TW be considered which would serve as a Heavy Ion Demonstration Experiment (HIDE). Shortage of time during the workshop prevented the development of a set of consistent parameters that meet these requirements exactly, but the results are useful for a first iteration and for drawing conclusions relative to an rf linac based accelerator system.

Compared with other systems considered for heavy-ion fusion, an rf linac has some advantages among which are:

(i) It makes use of a very well-known technology.

(ii) It has modular construction, so that modules are reproducible, expandable, and can be tested in sections.

(iii) It has rapid acceleration which is important if the beam lifetime is limited by internal collisions to a short time.

(iv) The average intensity can be raised easily by increasing the pulse length consistent with the longitudinal emittance requirement.

(v) It has greater capability than many other systems; an rf linac could, for example, fire more than one boiler by running at a higher repetition rate.

(vi) It has easy (not to say inevitable) extraction.

On the other side of the coin, there are disadvantages, which include:

(i) An rf linac necessarily operates at a reduced current for a longer pulse length so that an accumulator ring with associated transport lines is required to give the required current amplification over the nsec pulse length.

(ii) Although the work of our group did not include cost estimating and there are no firm cost data, it appears that an rf linac may possibly be a high-cost system compared with synchrotron systems.

In our design work, we have not considered space-charge neutralization in the linac, the accumulator, or the final transport. If it is possible to make use of neutralization, this would have a profound effect on the design of any heavy-ion fusion system.

OVERVIEW OF THE SYSTEMS

Systems have been considered for several different ions in order to explore some possible limits of linac design. These cases are:

(i) Xe^{+3} ions at 7.4 GeV - Case 7.4.

(ii) $(A = 200)^{+1}$ ions at 20 GeV - Case 21.

(iii) (A = 200) ions stripped to a +3 charge state during acceleration to 20 GeV - Case 23.

(iv) Xe^{+3} ions at 2.2 GeV - Case 2.2. This is a 0.1 MJ case thought of as a HIDE experiment.

All these cases make use of a 1 MV or higher Cockcroft-Walton pre-injector followed by acceleration in Wideröe structures through the low-beta region, then by acceleration in Alvarez structures for the remainder of the way. At full energies, there are one or more accumulator rings and associated rf and transport equipment to form a short pulse and to direct it to the pellet target.

---

* R. Arnold, D. Boehne, F. Cole, C. Curtis, H. Grunder, J. Keane, J. Staples, J. Stoval, D. Swenson and D. Young

The linac system achieve current multiplication by "funnel" loading of individual rf bunches into the buckets of succeeding linacs of double frequency (see Fig. IV-B-1/1). Thus, for example, eight ion sources and linacs of frequency f fill all the buckets of four linacs of frequency 2f, which in turn fill all the buckets of two linacs of frequency 4f, which in turn fill all the buckets of one linac of frequency 8f. It is possible, of course, to extend this doubling pattern even further and that is done in the A = 200 cases we shall discuss here.

A fast deflection system is required to combine the two separate beams in the lower frequency linac tanks into the single beam in the higher frequency linac tank. The hardware for doing this did not seem to be beyond current practice.[1] It was, however, recognized that some emittance dilution might result in this process and this has been considered in the emittance values used in the study (Table IV-B-1/4).

The accelerated beam is stored by betatron stacking in one or more accumulator rings. The number of rings is chosen to keep the stored beam within space charge and emittance limits in the ring. The beam is then bunched in longitudinal space and compressed to give current amplification. The separate beam bunches are extracted at multiple extraction points and transported to the target possibly with further pulse shaping and intensity amplification.

The system parameters are summarized in Table IV-B-1/1 below.

Table IV-B-1/1. System Parameters.

Case	7.4	21	23	2.2
Particle	Xe^{+3}	200^{A+1}	200^{A+3}	Xe^{+3}
Final Energy (GeV)	7.4	20	20	2.2
Injector Voltage (MV)	1	1.8	1.8	1
Final Linac Current (mA)	240	400	400	120
No. of Linac Tank Types	4	5	7	3
Linac Orbit Length (km)	1.5	12	4.1	0.4
Total Linac Tank Length (km)	2.05	18.52	7.05	0.5
No. of Accumulator Rings	12	1	3	12
No. of Extraction Points per Ring	8	10	10	8

LINAC SYSTEMS

In a linac with constant field strength E_0 and phase angle ϕ_s, the phase width of a bunch varies as $(\beta\gamma)^{-3/4}$. When the phase width has damped by a factor C, it is possible to increase the linac frequency by a factor C without losing particles. The only values of C seriously considered in the workshop were C = 2 and C = 3. It is believed that it is more economical to change frequencies as often as possible, because the linac tanks themselves and all rf equipment become smaller. No serious study of the optimal value of C has been made. The value C = 2 was chosen for use here. This value corresponds to a $\beta\gamma$-ratio of 2.52 and the ratios employed in the workshop have been between 2.8 and 3.0. Linac parameters are listed in Table IV-B-1/2 below for the four cases studied.

TABLE IV-B-1/2. Linac Parameters.

A. Case 7.4 (1 MV Pre-Injector, β_{out} = .0069)

Tank	1	2	3	4
Tank Type	Wideröe (π-3π)	Wideröe (π-3π)	Alvarez (2π)	Alvarez (2π)
Length(m)	16.7	46	267	1200
Frequency (MHz)	15	30	60	120
β_{out}	0.0194	0.0546	0.153	0.327
T_{out}(GeV)	0.024	0.19	1.51	7.40
I_{out}(emA)	30	60	120	240
Focusing	FODO	FODO	FFDD	FFDD
Aperture Radius (cm)	3	2.2	1.1	0.8
Avg. Acceleration Field (MV/M)	.42	1.2	1.65	1.65
No. of Gaps	64	125	500	2000

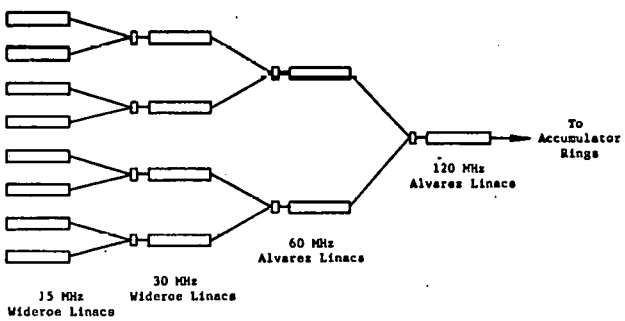

Fig. IV-B-1/1. "Funnel" Loading of a Linac From Lower Frequency Linacs.

D. Case 2.2

This case is the same as the first three stages of Case 7.4 with a slightly lengthened Alvarez tank.

Table IV-B-1/2. Linac Parameters. (Continued)

B. Case 21 (1.8 MV Pre-Injector, β_{out} = .00438)

Tank	1	2	3	4	5
Tank Type	Wideröe (π-3π)	Wideröe (π-3π)	Wideröe (π-3π)	Alvarez (2π)	Alvarez (2π)
Length (m)	32	77	600	3670	7650
Frequency (MHz)	5	10	20	40	80
β_{out}	0.0124	0.0348	0.0978	0.2662	0.428
T_{out} (GeV)	0.014	0.114	0.904	7.022	20.0
I_{out}(emA)	25	50	100	200	400
Focusing	FODO	FODO	FODO	FFDD	FFFDDD
Aperture Radius (cm)	4	2.8	2.0	1	1.4
Avg. Acceleration Field (MV/m)	0.39	1.3	1.3	1.7	1.7
No. of Gaps	64	110	600	2700	5900

C. Case 23 (1.8 MV Pre-Injector, β_{out} = .00438)
Strip to +3 after first Wideröe tank.

Tank	1	2	3	4	5	6	7
Tank Type	Wideröe (π-3π)	Wideröe (π-3π)	Wideröe (π-3π)	Wideröe (π-3π)	Wideröe (π-3π)	Alvarez (2π)	Alvarez (2π)
Length (m)	32	12.5	25.8	56	153	1600	2200
Frequency (MHz)	5	10	10	20	20	40	80
β_{out}	.0124	.020	.035	.06	.099	.267	.428
T_{out}(GeV)	.014	.038	.115	.338	.926	7.07	20
I_{out}(emA)	25	50	50	100	100	200	400
Focusing	FODO	FODO	FODO	FODO	FODO	FFDO	FFDO
Aperture Radius (cm)	4	4	2	3	1.8	3	2
Avg. Acceleration Field (MV/m)	.39	.61	1.0	1.3	1.3	1.3	2
No. of Gaps	64	26	32	80	130	1200	1500

Case 7.4 requires 60 emA of Xe^{+3} from the pre-injector. It was considered difficult to achieve this intensity directly from the ion source, but stripping a higher current of Xe^{+1} (at β = .011) appeared to be a good possibility for achieving this current. (See section V-D these proceedings)

In these designs the beam intensities are well below the space-charge limited values in all tanks. Only at the entrance to the first Wideröe tank does the margin of safety become small.

ACCUMULATOR RINGS

The number of accumulator rings is given in Table IV-B-1/1. We have estimated their overall size by assuming an average bending field of 1 T, corresponding in our minds to a maximum field of 2 T, except in Cases 2.2, where we have simply used the ring from Case 7.4. Some parameters are given in Table IV-B-1/3.

We have assumed in every case an aperture sufficient to contain the transverse emittance required at the target, an unnormalized emittance* of 2.5 cm-mrad. This will give apertures of the order of 10 cm.

PERFORMANCE ESTIMATES

a. Emittance*. The linacs discussed in the Workshop are beyond the performance of those now in operation and we have had to make use of estimated

* Transverse emittance as used in this report is defined by $\epsilon = \frac{\text{area}}{\pi}$ (unnormalized) and $\epsilon_n = \beta\gamma \frac{\text{area}}{\pi}$ (normalized) and is considered to apply to approximately 90% of the beam current.

emittance values through the acceleration and accumulation cycle. We have done this on two bases: the first, Case a, an estimate of what could be expected with the present state of the art and the second, Case b, containing improvements one might reasonably hope to achieve. These are summarized in Table IV-B-1/4.

Table IV-B-1/3. Accumulator-Ring Parameters.

Case	7.4	21	23	2.2
	Xe^{+3}	200^{A+1}	200^{A+3}	Xe^{+3}
Number of Rings	12	1	3	12
Energy (GeV)	7.4	20	20	2.2
β	0.326	0.428	0.428	0.186
γ	1.06	1.11	1.11	1.02
p (GeV/c)	44.1	89.0	89.0	23.8
$B\rho$ (T-m)	49.0	297	98.8	26.5
$\langle B \rangle$ (T)	0.980	0.988	0.988	0.530
R (m)	50	300	100	50
f_{rev} (MHz)	0.312	0.0681	0.204	0.178
τ_{rev} (μsec)	3.21	14.7	4.89	5.62

Table IV-B-1/4. Estimated Normalized Emittances (all in cm-mrad).

	Case a	Case b
Source	0.02	0.02
Low β (Wideröe) Linac	0.1	0.08
End of Linac	0.2	0.12

One may hope to achieve even larger brightness results by means of development, but we felt it unwise to base our designs on any figures less conservative than those in Table IV-B-1/4.

The ring emittances are all assumed to be 2.5 cm-mrad (unnormalized). Then, Table IV-B-1/5 shows the relations between linac and ring emittances in the cases studied.

Table IV-B-1/5 Emittance Limits

Case	7.4		21		23		2.2	
Emittance Case	a	b	a	b	a	b	a	b
ϵ_{linac} (unnorm) (cm-mrad)	0.579	0.347	0.422	0.253	0.422	0.253	1.05	0.63
ϵ_{ring} (cm-mrad)	2.5	2.5	2.5	2.5	2.5	2.5	2.5	2.5
$\epsilon_{ring}/\epsilon_{linac}$	4.3	7.2	5.9	9.9	5.9	9.9	2.4	4.0
n = Max No. of Turns*	16	49	36	100	36	100	4	16
I_i Linac Current (emA)	240	240	400	400	400	400	240	240
Max Current = nI_L (eA)	3.8	11.8	14.4	40	14.4	40	1.0	3.8
Max Number N_ϵ	$0.3\cdot10^{14}$	$0.8\cdot10^{14}$	$1.3\cdot10^{15}$	$3.6\cdot10^{15}$	$4.4\cdot10^{14}$	$1.2\cdot10^{15}$	$1.1\cdot10^{13}$	$4.2\cdot10^{13}$

*Assuming no emittance dilution in the process of multiturn injection.

b. Space-Charge Limits: We calculate the space-charge limited number of particles from

$$N_{sc} = \frac{2\pi mc^2 \Delta\nu \epsilon_n \beta\gamma^2}{(qe)^2}$$

where qe is the ion charge. We take $\Delta\nu = 1/4$ and take no account of a bunching factor. The results are shown in Table IV-B-1/6.

Table IV-B-1/6. Space-Charge Limits.

Case	7.4	21	23	2.2
N_{sc}	$4.9\cdot10^{13}$	$1.3\cdot10^{15}$	$1.4\cdot10^{14}$	$1.4\cdot10^{13}$

SYSTEM GOALS

On the other hand, we can calculate the number of particles needed in one accumulator ring from the relation

$$N_R Tm = W$$

Table IV-B-1/7. Required System Performance.

Case	7.4	21	23	2.2
W (MJ)	1	1	1	0.1
m	12	1	3	12
N_R	$0.7\cdot10^{14}$	$3.1\cdot10^{14}$	$1.0\cdot10^{14}$	$0.2\cdot10^{14}$
Required Linac Pulse Length (msec)	1.68	0.12	0.36	0.45

We see by comparison of Tables IV-B-1/5, 6 and 7 that every system can meet the required performance although close to the space-charge limits, but that the Xenon systems 7.4 and 2.2 require the less conservative emittance assumptions to reach required performance within the emittance limits. The emittance limit of the Xenon systems could be raised, of course, by going to higher final energy (at larger cost).

LONGITUDINAL EMITTANCE

It is assumed that the total momentum spread of the beam on the target pellet must be kept within 2% from considerations of the final focusing. This corresponds to the energy spread shown in Table IV-B-1/8 for the four cases studied. We also give the longitudinal emittance ϵ_L, assuming a total pulse length $\Delta\tau = 12$ nsec and the accumulator energy spread $\Delta E_A = \epsilon_L/\tau_{rev}$.

If we assume that all stacking in the accumulator rings is in betatron phase space and that there is no dilution of longitudinal emittance, the energy spreads ΔE_A are also the output energy spreads of the linac. The values of ΔE_A given in Table IV-B-1/8 seem feasible with present rf linac technology.

Table IV-B-1/8. Energy Spread and Emittance.

Case	7.4	21	23	2.2
$\frac{\Delta p}{p}$ (assumed) (±)	0.02	0.02	0.02	0.02
$\frac{\Delta T}{T}$	0.0388	0.0381	0.0381	0.0397
ΔT (GeV)	0.287	0.762	0.762	0.087
$\epsilon_L = \Delta T \Delta\tau$ (eV-sec)	3.44	9.14	9.14	1.04
ΔE_A (MeV)	1.07	0.62	1.87	0.19

CURRENT AMPLIFICATION

The current amplification and the final bunching required can be calculated from the linac pulse length τ_L given in Table IV-B-1/7 and the requirement that the final beam pulse be of fixed length τ_F. We take this fixed length to be 20 nsec. The total current amplification K is then τ_L/τ_F. The final bunching B_F required is reduced from the total by factors of the number of rings m, number of extraction points p, and n, the number of turns injected to reach N_R. We give the results of these calculations in Table IV-B-1/9.

Table IV-B-1/9. Amplification and Bunching Factors*.

Case	7.4	21	23	2.2
K	$8.4\cdot10^4$	$6.3\cdot10^3$	$1.8\cdot10^4$	$2.2\cdot10^4$
m	12	1	3	12
P	8	10	10	8
n	44	8.4	8.4	16
B_F	20	75	75	14

*Based on 1 MJ delivered over 20 nsec; i.e. 10 nsec leader and 10 nsec main pulse at the 100 TW level.

Bunching factors B_F of this magnitude are felt to be possible. Recent experiments on the AGS have achieved factors in excess of 70.[2] It is also possible to build an induction buncher so that this bunching can be done in the transport lines to the target.[3]

FINAL TRANSPORT

We have calculated only the final quadrupole, believing it to be the most critical. We assume 4.5-T pole-tip fields and a 25-cm radial aperture for a quadrupole 10 m from a target of emittance 2.5 cm-mrad. Table IV-B-1/10 gives the calculated quadrupole lengths ℓ_Q.

Table IV-B-1/10. Final Beam Transport Quadrupole Lengths.

Case	7.4	21	23	2.2
ℓ_Q (m)	0.38	2.46	0.82	0.21

These are not unreasonable quadrupole lengths and show that the final transport is feasible.

There is a maximum power that can be transmitted by a transport line.[4,5] We calculate the power transmitted in our five cases and show the results in Table IV-B-1/11. We also show the power needed per transport line; i.e., 100 TW/mp for the 100 TW cases and 50 TW/mp for the HIDE case.

Table IV-B-1/11. Transport Power Limits (TW).*

Case	7.4	21	23	2.2
Transport Limit	4.0	186	43	.51
Power Needed	1.04	10	3	0.52

* Calculations based on quadrupole pole-tip field of 4 T and an acceptance of 2.5 cm-mrad.

CONCLUSION

An rf linac accelerator system with accumulator(s) has been described to meet the target requirements for ion beam fusion using a conservative extrapolation of the current state-of-the art.

No optimization of the design has been done although clearly there are many trade-offs that might be possible, i.e., a higher ion charge state reduces the length of the linac at the expense of more accumulator rings and transport systems to the target. The system which accelerates Xenon in a plus 3 charge state has a linac of reasonable length, but the necessity of not exceeding emittance limits dictated by the target and reactor design (and to a lesser extent space-charge limits) require 12 accumulators each with eight transport lines. For reasons of cost and complexity this might not be the best solution. It should be pointed out, however, that progress on obtaining smaller emittance beams (or alternately transporting larger emittance beams) and/or transporting partially neutralized beams can greatly reduce the number of transport lines and make the Xe^{+3} design more attractive. The Xe^{+3} system could be scaled down for a Heavy Ion Demonstration Experiment. Because of these reservations, we conclude that the confidence level is certainly higher for the A = 200 system, particularly for the +1 charge-state, than for the Xenon systems.

References

1. "RF Deflectors for combining Two Linac Beams", (In Section E of this report).
2. G. Danby, E. Gill, J. Keane, and A. W. Maschke, "Preliminary Results of 200 MeV Bunching Experiments", BNL 50643 (March 1, 1977) also: BNL Heavy Ion Fusion Program Review (Section III of these Proceedings).
3. See Workshop Summary
4. G. Lambertson, L. J. Laslett, L. Smith, "Transport of Intense Ion Beams" (Report LBL-5552), IEEE Trans. Nucl. Science, June 1977, p. 993.
5. Report on High Current Beam Transport (Section V-F of these Proceedings).

HIDE working groups:

C. INDUCTION LINAC BASED SYSTEM

1. SUMMARY

B. Richter, A. Faltens, W. B. Herrmannsfeldt, K. Johnsen, D. Judd, D. Keefe, E. Lofgren, F. Mills, V. K. Neil, and S. Penner

INTRODUCTION

The objective of all of the accelerator working groups at this meeting has been to develop a system design showing how a particular kind of accelerator can deliver 1 megajoule of energy to a fusion target at peak powers of 100 terawatts. These energy and peak power requirements correspond to the "moderate confidence" case given by the target designers for an ion fusion driver which can give a targe gain of several hundred. Since this is a first attempt at such a systems study, we have not attempted to optimize parameters but rather to show an existence proof for such a machine. Therefore, the choices of accelerator energy, ion charge state, number of beams, etc., have been made more by "feel" than by any sophisticated economic analysis.

One of the most difficult constraints to meet in any accelerator design is that imposed by transverse space charge effects. While the induction linac (a single pass machine) can tolerate larger space charge forces than are allowable in synchrotrons or storage rings, the problem is still formidable. For a given power on target, space charge forces are reduced by increasing the beam energy and by increasing the number of beams on the target. However, we feel that beam transport for large numbers of beams is both complex and expensive and we have, therefore, restricted ourselves in this example to the simplest of all cases--that of two beams. We have also chosen to use a maximum energy consistent with the pellet design--26 GeV in each of two beams with an assumed focal spot size of 1 mm radius. (Ion kinetic energy limitations are discussed more fully in a paper by R. Bangerter in these Proceedings.)

In the rest of this report we outline the main accelerator design and the system to be used for pulse compression. Ion source requirements and pre-accelerator requirements are also discussed. Several of the items treated here are treated more fully in individual reports in these Proceedings.

THE MAIN ACCELERATOR

An induction linac consists of a collection of accelerating modules interspersed with focusing lenses. The accelerating modules are, in essence, transformers with the ion beam serving as the secondary of the transformer. The material used for the transformer cores and the practical maximum attainable voltage gradients depend on the pulse length. Typical voltage gradients versus pulse length are give below.

Pulse Length (μsec)	Voltage Gradient (MV/m)
8	0.1
1	0.5
0.5	1.0
0.15	2.0

The core material used for these accelerating modules is usually iron for pulse lengths greater than ½ microsecond, and ferrite for pulse lengths for less than ½ microsecond. The efficiency for each accelerating module increase with decreasing pulse length so it is advantageous to run the accelerator with a pulse length as short as possible. The estimated efficiency for the accelerating systems described below is about 10 to 20 percent for acceleration through the kinetic energy range from 1 to 26 GeV.

Space charge forces determine the peak current which can be transported in an induction lin linac with a given maximum pole-tip field in the focusing lenses. The Maschke equation gives the peak transportable power as

$$P = 2.4 \times 10^3 \left(\frac{A}{Z}\right)^{4/3} (\beta\gamma)^{5/3} (\varepsilon_n B)^{2/3} (\gamma - 1) \quad (1)$$

where P is the peak transportable power in terawatts; A and Z are the atomic number and charge state of the ion, respectively; β is the ion velocity of light; γ is the ratio of the total ion energy to its rest energy; ε_n is the normalized transverse emittance in meter radians and B is the maximum focusing field in Tesla. The constant in front of Equation (1) has had some time dependence and the value used here is the current, generally agreed upon value. In what follows we assume uranium as the ion species to be accelerated, but by this we mean any ion species with an atomic number of around 200.

Figure IV-C-1/1 shows the maximum transportable particle current (not the electrical current) and the minimum pulse length versus ion kinetic energy

in an induction linac delivering 1 megajoule at a kinetic energy of 26 gigavolts. We have assumed a maximum focusing field of 1.1 Tesla and a normalized emittance of 2 x 10^{-5} meter radians. The two cases shown in the figure are for ion charged states of 1 and 3.

With Z = 1 the peak power at the end of the accelerator can be as high as 100 terawatts. The beam need only be split into two (which can be done by splitting the beam in transverse phase space) and the two 50 terawatt beams can then be transported to the target with the same kind of 1 T pole-tip field focusing lenses used on the main accelerator. The transport system will require a modest voltage gradient to balance the longitudinal space charge forces which tend to spread the beam along its direction of motion. The beam pulse length can be less than 0.15 microseconds at all kinetic energies above 1 GeV allowing the use of the maximum accelerating gradient. However, this part of the accelerator will be quite long requiring approximately 13 kilometers to raise the ion energy from 1 to 26 gigavolts.

For charge state three, the minimum pulse length out of the accelerator is 40 nsec corresponding to a peak power of 25 terawatts. For this case we again split the beam and use a transport system whose final focusing elements have a maximum pole-tip field of 3 Tesla which allows a peak power of up to 50 terawatts in each beam. The pulse compression system is described in the next section. An accelerating gradient of 1 megavolt per meter can be used from 1 to 5 gigavolts and a gradient of 2 megavolts per meter from 5 to 26 gigavolts. The total required accelerator length is thus 4.8 kilometers. While the transport system for this Z = 3 case is more complicated than that for the Z = 1 case, the reduced length for the main accelerator clearly reduces the cost of the accelerator by a very large amount. Cost optimization will certainly require considerable more study.

PULSE COMPRESSION

In addition to the transverse space charge effects summarized in Equation (1), there exist longitudinal space charge forces whereby the longitudinal component of the field generated by the particles in the accelerator beam tends to debunch that beam. These effects are usually not significant in the main accelerator where they can easily be compensated by adjusting the accelerating field. However, they can be very important in the final beam transport, especially when the accelerator output pulse must be further compressed as in the Z = 3 case described above.

Judd (in this section of these Proceedings) has studied this problem and analyzed the effect of these longitudinal space charge forces on the maximum pulse compression (hence, peak power) which can be achieved in a given beam. The procedure used is illustrated schematically in Figure IV-C-1/2a,b,c. Figure IV-C-1/2a shows the bunch longitudinal charge distribution assumed for simplicity to be parabolic. Figure IV-C-1/2b shows the space charge field produced by this charge distribution--a linear ramp for the assumed parabolic charge distribution. Figure IV-C-1/2c illustrates the compression process wherein a large compressive field is applied and the length of the compressive ramp is decreased as the pulse length decreases.

Under these conditions the equation of motion for the bunch length L is of the form

$$\frac{d^2L}{dt^2} = -K_1 + \frac{K_2}{L} \quad . \qquad (2)$$

The behavior of the bunch length versus time is illustrated in Figure IV-C-1/3. The dashed curve shows bunch length versus time in the absence of space charge effects. The solid curve illustrates the effect of longitudinal space charge. There is a minimum pulse length L_{min} whose value is related to the initial pulse length L_0, the maximum amplitude of the compressing field ΔE, and the total charge in the bunch, Q. The equation for the maximum compression factor is

$$\frac{L_0}{L_{min}} = \frac{10^{-5}\gamma^2 \Delta E}{Q} L_0^2 \qquad (3)$$

where ΔE is in megavolts per meter, L_0 is in meters, and Q is in coulombs.

For the Z = 3 example given in the previous section, the maximum compression factor is 10 assuming ΔE = 2 MV per meter and L_0 corresponding to a 40 nsec pulse duration at the beginning of the compression. The distance the bunch would travel in reaching its maximum compression is given by

$$D = \beta \left(\frac{\gamma^3 M_0 c^2 L_0}{eZ\Delta E}\right)^{\frac{1}{2}} \qquad (4)$$

where $M_0 c^2$ is the rest energy of the ion. For our Z = 3 case, this distance corresponds to 250 meters. Since the maximum pulse compression factor is considerably larger than the factor of 4 required to reach the 100 terawatts power level in the fusion target, there is no problem from longitudinal space charge effects for our example.

ION SOURCE AND PREACCELERATOR

We have not examined the injection problem in any detail in our working group. It is clear from Figure IV-C-1/1 that an induction linac could best be fed by a high peak current gun capable of delivering a particle current of about 50 amps in a few microseconds at a kinetic energy on the order of 100 MeV. Such a high current source is being studied at LBL. Progress is being made, and since the development of such a source would considerably simplify injection into a induction

linac, this research should be continued.

Low current sources with intensities on the order of 100 milliamps do exist. As an alternative injection system, Kjell Johnsen has examined the possibility of using a conventional ion source and linac with an accumulator ring as an injector into an induction linac. As an example, a one gigavolt, 100 milliamp, charge 1 ion beam is assumed to be injected into a 20 meter radius accumulator ring. The parameters of the accumulator ring are given in Table IV-C-1/1. The ring uses superconducting bending magnets with field of about 5 T, but with an average bending field of only 3.5 T to allow space for focusing elements, rf equipment, and injection and ejection apparatus. Note that though the magnets are superconducting, the range of a 1 gigavolt heavy ion is sufficiently short so that it is easy to shield cryogenic elements from particles lost from the beam. Eighty-three turns are assumed to be stacked in the ring to convert the injected current of 100 milliamps to a circulating current of 8.5 amperes with a circulation period of 4.2 microseconds.

Three alternate schemes have been considered for transfer into the induction linac. In the first, the beam is ejected in a single turn giving a 4.2 microsecond pulse into the induction linac. This pulse can be rapidly compressed with a ramped accelerating field in the linac to get the pulse length down to that required for efficient acceleration.

The second alternative is to bunch the beam adiabatically in the ring in order to reduce the bunch length by a factor of 2, making for a more efficient bunching and acceleration process in the early states of the induction linac. This adiabatic bunching requires a modest rf voltage per turn at a frequency of about 250 KHz. The bunching process takes a few milliseconds to complete which may give problems with intrabeam charge exchange scattering or beam-gas interactions.

The third method is designed also to compress the beam within the accumulator ring but to do this in a rapid fashion circumventing possible problems with charge exchange scattering or beam-gas interactions. This method involves the sudden turn-on of an rf system giving 50 to 100 kilovolts per turn at about 250 KHz. In roughly 300 microseconds (1/6th of a phase oscillation period) the beam will have shrunk to a 2 microsecond pulse length and then may be fast ejected into the induction linac where it will continue to shrink until the induction linac fields halt the shrinkage.

The first or third method seems most promising as alternatives to the high current injector.

CONCLUSIONS

The induction linac does seem capable of delivering the required 1 megajoule of energy at peak powers of about 100 terawatts. The required components for the main accelerator exist in the laboratory. The ion source and preaccelerator technologies are not so well developed. The best injector for an induction linac is the high current gun which could deliver currents of tens of amperes into an induction accelerator at an energy of around 100 MeV. Such sources are under study. The alternative of a conventional low current ion source and rf accelerator (also used in other acceleration schemes such as synchrotrons or full energy accumulators) also seems usable for the induction linac, but as indicated in reports of other working groups is by no means easy.

Considerable work needs to be done on component technology before any reliable cost estimates and economic optimizations can be made.

Table IV-C-1/1. Accumulator Ring Parameters.

Bending Field	5 T
Average Field	3.5 T
Betatron Tune	≈ 3
Orbit Period	4.2 μsec
Normalized Emittance	$2\pi \times 10^{-5}$ mrad
Aperture	± 6 cm
Injected Turns	83

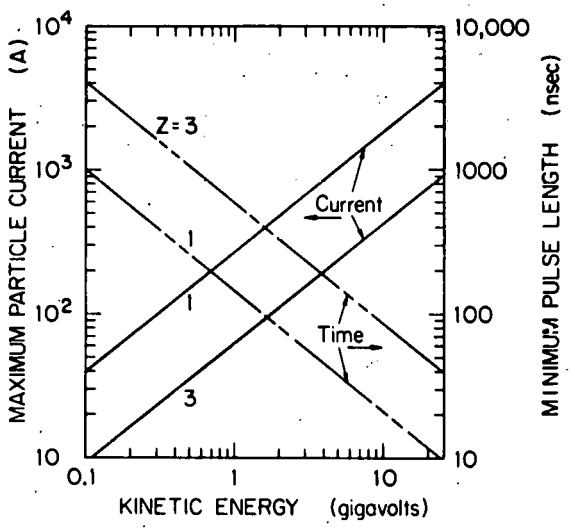

Fig. IV-C-1/1. Maximum particle current (left axis) and minimum beam pulse length (right axis) vs. kinetic energy for a beam of uranium ions delivering a total energy of 1 megajoule at 26 gigavolts. The maximum focusing field assumed is 1.1 T.

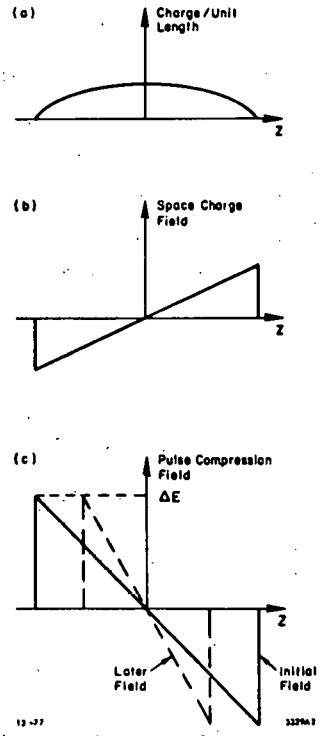

Fig. IV-C-1/2. Schematic of the pulse compressing system. 2a shows the assumed parabolic charge distribution vs. distance along the bunch. 2b shows the space charge debunching field for the charge distribution of 2a. 2c shows the pulse compression field at t = 0 (heavy line) and at some later time (dashed line).

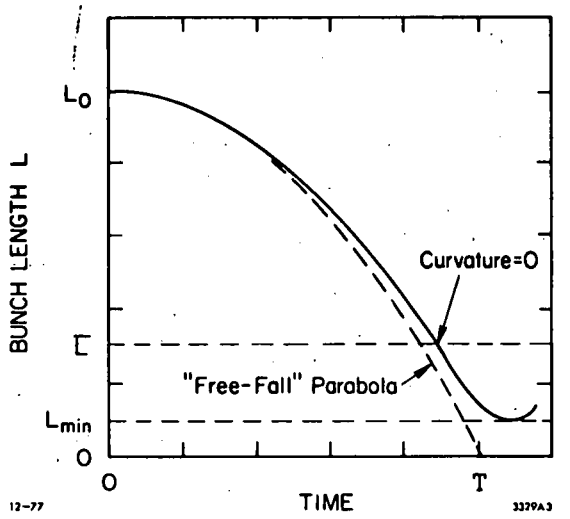

Fig. IV-C-1/3. Pulse length vs. time in the absence of space charge (dashed line) and in the presence of space charge (solid line). The curve with space charge is drawn for a maximum pulse compression factor of 10. The point $\bar{L}$ is the geometric mean of L_0 and L_{min}.

2. QUASI-STATIC DRIFT-TUBE ACCELERATING STRUCTURES FOR LOW-SPEED HEAVY IONS

A. Faltens and D. Keefe

INTRODUCTION

One of the major problems in the application of a linear induction accelerator to Heavy Ion Fusion has been that of finding a suitable injector which could deliver of the order of 100A for a few μsec within a normalized emittance of $\epsilon_N = 2 \times 10^{-5}$ radian-meters. At last year's HIF Summer Study, magnetically-insulated diodes and reflex triodes appeared to offer some promise, as they have delivered ion currents (protons) of hundreds of kiloamperes for ~ 0.1 μsec at an energy of about 1 MeV. It soon became clear, however, that such currents could not be transported without neutralization, and that further acceleration would be difficult with neutralization. In the past year the transport problem has been greatly clarified, and it seems that the desired 100A U^{+1} could be transported only at energies above ~ 70 MeV with 4 T superconducting magnets, and above 250 MeV with 1.1 T normal magnets. There is, of course, no sharp boundary in pulse length below which induction units do not work; rather, they become increasingly inefficient as the pulse duration increases and the beam current decreases; so it becomes desirable to look for alternative means of acceleration at the very low energy end of the accelerator. The pulsed drift-tube accelerating structure described in this paper is one such alternative.

A pulsed drift-tube accelerating structure is shown in Fig. IV-C-2/1. Its gross characteristics are almost the opposite of those of induction units, in that its usefulness is limited almost entirely to low velocity ions and relatively long pulse duration. The accelerator is quasi-static in the sense that for slowly-varying voltages applied to the drift-tubes, all particles at a given axial position experience essentially the same voltage gain regardless of radius. The voltage of the drift-tube is switched when all of the beam bunch is within it, so that the beam moves as if going through a series of d.c. accelerating gaps. In contrast to an rf linac there is essentially no synchrotron oscillation motion nor instantaneous energy spread induced in the beam, although either or both may be intentionally generated if desired. The drift-tubes are driven by pulse-power modulator circuitry in a non-resonant mode which allows pulse shaping as desired.

INJECTOR NEEDS FOR HIDE AND BEYOND:

A possible approach to designing a 100 kJ Heavy Ion Demonstration Experiment (HIDE) as part of the heavy-ion fusion program has recently been suggested by Richter.[1] In this approach one would consider first how to provide for a 1 MJ, 100 TW facility (parameters that are close to what is needed for a pilot power-plant) and then forego the major accelerating device required therein; reducing the particle kinetic energy by a factor of ten thus leads to a 100 kJ experiment with the capability of later expansion to the 1 MJ case. One much-discussed scenario for HIDE involves acceleration by means of rf linacs of about 100 particle micro-coulombs to an ion kinetic energy, $T \approx 1$ GeV, accumulation and modest bunching in a small storage ring to a final pulse length of $\tau \approx 2$ μsec, and finally injection into an induction linac section in which the beam is accelerated and strongly bunched. An apparent attraction of this scenario is that one gains experience in the use of rf and pulsed non-resonant systems and models the behavior of an intense ion beam in a circular machine. Later upgrading to the 1 MJ, 100 TW capability would be accomplished by adding either a linac (rf or induction) or a synchrotron to raise the kinetic energy by an order of magnitude.

If the upgrade is visualized to take place by building a large induction linac, then injection of relatively few amperes at an energy as high as $qV_i \approx 1$ GeV, while viable, is not well-matched to the intrinsic properties of this type of machine (here q is the ion charge state, and V_i the beam "voltage"). It is the purpose of this report to discuss an alternative type of injector system, also based upon pulse-power technology, which is better matched to the induction linac properties. If we adhere to the arbitrarily-chosen value of 2 μsec for the injected pulse-length required, τ_i, then a pulsed drift-tube structure with a total voltage in the 50-100 MV range could deliver the appropriate injection current of 50-75 amps. We shall discuss several design features and design strategies for this system. It is not clear whether such an injector has application to other accelerator systems apart from the induction linac.

In discussing representative numerical examples we shall use parameters appropriate to the 1 MJ, 100 TW upgraded HIDE case (see Table IV-C-2/1).

In what follows we shall concentrate on explaining the general concept and discussing realistic physical and technical limitations imposed by the availability of voltage sources, electrical switches, pulse rise-times, etc. and by the need to avoid electrical resonances in the intended non-resonant structures. These limitations are stringent in some regards, and can demand use of certain strategies (e.g. parallel accelerators with later stacking) to achieve the design goals; some such strategies will be outlined.

To simplify the discussion we avoid certain design issues that must be faced and demonstrated to have good solutions. For example, we assume (a) that a pulsed (10 - 100 μsec) high-voltage (2 MV) source with an anode area of 100-1000 cm^2 can deliver a current ^1I_o in the 1 to 5 ampere range with a suitable emittance; (b) we do not specify the transport system through the first few drift-tubes, say to the 5 - 10 MV point, and assume quadrupole transport from there on; and (c) the best strategy for obtaining charge state q = 4, should that be the most desirable, is not specified.

Any one of these points requires very careful study in itself; for instance, during the early stages of rapid acceleration the transport system will be different from the usual quadrupole lattice case and the transport system may require some grid focussing (of the type designed by Herrmannsfeldt[3], followed by electrostatic quadrupoles and/or solenoids. This will be discussed in detail in another report.[4] Careful design and experimental demonstration are needed to show that the appropriate emittance can be achieved and preserved.

Table IV-C-2/1. HIDE-Upgrade (1 MJ, 100 TW) Parameters.

Charge State	q =	1	4
Final Voltage	V_f	10 GV	6.5 GV
Final Kinetic Energy	T_f	10 GeV	26 GeV
Number of Beams		2	2
Target radius	r	2 mm	1 mm
Current per Beam**	I_f	5 kA	7.7 kA
Charge (electrical)	$^1[I\tau]$	100 μC	
Charge (electrical)	$^4[I\tau]$		155 μC
Pulse Length at injection	τ_i	2 μsec	2.1 μsec
Current at at injection†	I_i	50 amps	75 amps
Injection Voltage	V_i	115 MV	80 MV
Injection Kinetic Energy	T_i	115 MeV	320 MeV

* Assumes A = 238 and a specific energy in a gold shell of 20 MJ/gm.

** Assumes pole tip field in final transport system can be 4 T and the magnets occupy 50% of the space. The normalized emittance is taken to be $\pi\epsilon_N = 2\pi \times 10^{-5}$ radian meters. The Laslett "figure-of-merit" is taken to be 0.93.[2]

† Assumes pole tip field of 1 T (and 50% occupancy factor) at injection point. If a pole tip field of 3 T is assumed then I_i can be doubled and the injector voltage decreased to less than half.

CONCEPT AND STRATEGIES

General Concept: The idea of accelerating a bunch of charged particles through a drift-tube and changing the voltage while they are electrically hidden inside is an old one; the unusual features under discussion here simply involve the physical scale and the freedom to employ arbitrary pulse shapes. The drift-tubes needed are visualized to have a bore radius A ~0.1 - 0.5 m, a typical length, D ~10 - 20 m, and an applied high-voltage pulse (∓ 1 MV) from a pulse power source (to be discussed later). The total number of drift-tubes required is on the order of fifty. A variety of systems using such elements is shown schematically in Fig. IV-C-2/1. A long sausage-shaped bunch of charged particles is drawn from a gridded multi-aperture source (pulsed to + 1 MV) into the initial drift tube (D_o meters long) which first is pulsed to - 1 MV, and later, when the bunch is hidden within, is pulsed in reverse to + 1 MV, to provide another increment of q MeV in energy upon exit. Referring to Fig. IV-C-2/1A it is seen that the same technique can be repeated in later drift-tubes, each of which has comparable length and similar voltages, but which can have decreasing aperture as the particle energy increases and the matched beam size decreases.

Depending on how one chooses the voltage pulse shapes three possibilities can be distinguished:

(i) All drift-tubes have flat-topped voltages applied: In this case the front particle of bunch gains energy before the last particle. Thus, the spatial length of the bunch grows in time in proportion to the bunch speed. Successive drift-tubes would need to be increased in length in similar proportion and very soon the needed structures would become unacceptably long. This case corresponds to $D \propto \sqrt{V}$ and the current, I = constant.

(ii) As soon as convenient, e.g. between the first and second drift-tubes, a specially shaped voltage pulse is applied across and inter-drift-tube-gap; thereafter all gaps have flat-topped voltage pulses: If the shaping-pulse rises from zero at the time of passage of the front particle to full value as the last particle crosses the gap a tilt of the momentum ellipse is created such that the spatial length of the bunch remains a constant even under acceleration by constant voltage at every succeeding gap. Thus the drift-tubes can be kept (roughly) constant in length with savings in the overall length of the injector. In this case D = Constant, and the current increases along the structures as $I \propto \sqrt{V}$.

(iii) Following a shaping pulse of the type described, successive gaps provide not a flat-topped voltage pulse, but one that has a modest positive ramp: The momentum ellipse is therefore provided with a further small tilt at each accelerating gap, the bunch length in space becomes progressively shorter and the beam current increases faster than $\sqrt{V}$. From consideration of the transverse space-charge limit in a quadrupole system[5] it can be shown that, in principle, the bunch length L can be compressed as fast as $L \propto (V)^{-1/3}$ and still remain within the space charge-limit. The drift-tube lengths can be made shorter as the acceleration proceeds, but for practical reasons (see below) cannot be shortened in proportion to L.

The instantaneous energy spread created by the time-changing fields in the gap, $\Delta T(r) \approx -\frac{qer^2}{4c^2}\frac{d^2V}{dt^2}$, is negligible for the time-rates of

change contemplated.

In what follows we adopt a gap-voltage history as described under (iii) above.

ARRANGEMENT OF SUITABLE COMPONENTS: STRATEGIES

A numerical example best illustrates the range of possibilities that may have to be catered for. From Table IV-C-2/1 and assuming a 2 MV source, we see that the initial bunch length needed if (for q = 1) ${}^1L_o = \frac{130}{{}^1I_o}$ m where ${}^1I_o$ is the current at the source. (If an adequate current, denoted by ${}^4I_o$, of charge state q = 4 could be drawn from a source, which is unlikely, then the initial bunch length would be ${}^4L_o = 390/{}^4I_o$. Instead, the most likely strategy for obtaining charge state +4 is to extract some 190 μC of charge state +1 from the source, accelerate the bunch to about 10 MeV and pass it through a stripper to obtain the desired 155 μC of charge state +4 ions. The initial bunch length in this case would be ${}^4L_o = 250/{}^1I_o$ meters.) If a source current, ${}^1I_o$, of 5 amps can be obtained then D_o ($\simeq L_o$) would be 26 m and close enough to the desirable range (10 - 20 m) to allow the single-pass system shown in Fig. IV-C-2/1A to be used. If, on the other hand, the current from the source were as low as ${}^1I_o$ = 1 amp then the drift-tube length implied, 130 m, is out of the question and some partitioning of the beam and/or structure into, say, six pieces is needed. The very long structure is undesirable because of its low acceleration rate and low electrical efficiency, and care must be taken to switch voltages sufficiently slowly to avoid exciting the electrical-line resonances or damp them if excited.

The number of segments required thus is probably in the range of one to six, depending on where in the expected 1 - 5 amp range the achieved current value falls, and some strategies for segmenting and recombining the beam, therefore, merit discussion. On paper an attractive possibility is illustrated in Fig. IV-C-2/1B which shows how multiple pulsing of the drift-tubes would allow a train of pulses (just two shown) to be accelerated. Each pulse is separated by a drift-tube length from its neighbor. At the end of the injector the final drift-tubes are required to accelerate differentially the successive pulses with respect to each other so that they come together after a drift space. At that point (within the induction linac) the differential speeds can be removed by suitable pulsing of a number of cavities and a single long-bunch character restored. The drift length for recombination can be occupied by induction linac modules which can continue to provide energy to the particles as the bunches drift together. Note that in the example shown the voltage gradient (MV/m) of the structure is double that of a single pulse system. Practically, a small number of multiple pulses is realizable, but the system becomes increasingly difficult as the number is increased much beyond two.

Because the pulsed drift-tube structure is intrinsically a low gradient one (~0.1 MV/m) the length and cost of the transport magnets (assumed dc superconducting) becomes of large concern. A scheme for utilizing a few drift-tubes over and over again by recirculating the bunch has been examined as a possibility (Fig. IV-C-2/1C). Low-field pulsed bending magnets are used to direct the bunch through a number of long drift-tubes surrounded by fixed-field quadrupole lenses. It was found possible to select a fixed-field focussing system such that beam motion was stable despite the changing energy and changing space-charge forces for an interesting number of revolutions (≥20).[8] A recirculator would require injection at about T = 10 MeV but, thereafter, could provide enough energy to be followed immediately by an induction linac. This system, unfortunately, requires multiple pulsing of the drift-tubes with a variety of voltage wave-forms.

Figure IV-C-2/1D illustrates probably the most straightforward approach in which a number of drift-tube injectors are used in parallel and, at appropriate voltages determined by the space charge limits, the beam segments are stacked in transverse phase space. In principle, the four beams illustrated can be recombined with an emittance growth of only a factor of two in each plane; in practice, the strong space charge forces will probably cause some dilution. Recombination in longitudinal phase-space by drifting the bunches together, analogously to the scheme shown in Fig. IV-C-2/1B, is a possible option if desired. A useful property of the system shown, in which common modulators are used for each stage, is that all particles observe the same accelerating voltage history and undesirable effects due to power source fluctuations are minimized.

INFLUENCE OF THE EXISTING STATE OF COMPONENT TECHNOLOGY ON DRIFT-TUBE STRUCTURE DESIGN.

General Considerations: The output voltage wave-form from a 1 MV pulse-power bi-polar modulator will have the general features displayed in Fig. IV-C-2/2. The rise-time is irrelevant and is followed by a time, τ_{SW} which is the time required to change polarity before the voltage again becomes suitable for acceleration and, finally, a fall time which is irrelevant. Allowing for electric field penetration at both the drift-tube ends for a distance of roughly the bore radius, we note that the length is given by

$$D = 2a + L + v\tau_{SW}.$$

The first term is small (≤ 1 m), the second can, by suitable ramping, be made to decrease with total voltage at a rate $L \propto L_o V^{-1/3}$, while the last term increases as $\sqrt{V}$ and is directly proportional to the switching time. The relative contributions of the different terms can be seen from Fig. IV-C-2/3 for cases with q = 1 and q = 4 and for two different switching times, τ_{SW} = 0.3 μsec and 3 μsec. It is assumed that the initial bunch length, L_o, is 20 m so that the first few drift-tubes will be somewhat longer than the desired

upper range of 20m, and that this length is appropriate for V = 3 MV for q = 1 (T = 3 MeV) and q = 4 (T = 12 MeV). It is clear from the figure that the compactness of the structure depends strongly on the switching time achievable. At a high enough ion-velocity, v, possibly beyond the range of interest, to abandon bipolar-pulsing and retreat to a unipolar pulse with a rise-time $\tau \approx 0.1$ μsec can, paradoxically, lead to a higher-gradient structure.

VOLTAGE SOURCES AND SWITCHES: It is obvious that, for a given structure and transport system, one should apply the highest voltage which the structure will tolerate. It is also necessary to do so in order to keep the average accelerating field, $< E_z > = 2/D$ MV/m, high compared to the longitudinal self-fields of the bunch, $E_{zq} = -\frac{30}{\beta}(1 + 2 \ln \frac{a}{b}) \frac{dI}{dz}$. The availability of reliable electrical components and switches places strong limitations on possible modulator choices. For example, we have assumed the use of reliable pulse power technology at the 1 MV level, but it needs to be verified that trustworthy insulators at suitable cost will be available; if not, the voltage choice may have to be decreased somewhat, at the expense of average gradient. As examples, we discuss four cases for modulator choices:

(i) An approach suitable for the early drift-tubes is illustrated in Fig. IV-C-2/4A; it involves a low-voltage (20-100 kV) lumped pulsed forming network (PFN) switched by means of thyratron to the primary of a step-up pulse transformer that delivers 1 MV at the secondary output. A particular example design is shown in some detail in Fig. IV-C-2/5. The parameters under consideration in this case do not exactly match those derived from Table IV-C-2/1, but are not very different. The drift-tube is 12 m long, the beam current is 1-5 amps, and the total energy delivered to the beam is a few tens of joules. Note that in this system the stored energy in the pulse-line need only be a few kilojoules and about 80% of this energy can be recovered and restored in the line. It can be seen from Fig. IV-C-2/3 that the utility of this approach is probably confined, for the examples considered, to the first 30 MV or so of the q = 1 case.

(ii) The next choice of modulator to be considered is represented in Fig. IV-C-2/4B. The unipolar Marx can have a rise-time of 0.1 μsec and a similar crow-bar time, and could be pulsed either while the bunch enters or exits from the drift-tube. Modest ramping of the pulse or more subtle pulse-shaping can be achieved by low-voltage pulse-forming networks applied to the lowest decks of the Marx. This approach does not lend itself readily to energy recovery; at the few kilojoule level, however, this is probably not an important consideration.

(iii) An attractive choice for a modulator, illustrated in Fig. IV-C-2/4C, is a combination of two Marx generators with opposite polarities. Since the rise-time is not important in this case the first generator can power the load through a large resistor R_1. When it becomes time to switch polarity the first generator is crow-barred and the second one activated through a series output spark-gap, and most of the open-circuit voltage is developed on the drift-tube load if the resistance R_1 is adequately large. The RC-limited switching time, τ_{SW}, will be of order 0.3 μsec in which case its influence on the drift-tube length is not important (see Fig. IV-C-2/3).

(iv) A combination of Marx generators with suitable de-coupling resistors (see Fig. IV-C-2/4D) can be arranged to provide multiple pulses to a single drift-tube. A system for the two bipolar pulses illustrated requires that $R_1 \gg R_2 \gg R_3 \gg R_4$ and it is obvious that extension to a significantly greater number of pulses rapidly become unreasonable.

In previous publications [7,8] we have drawn attention to the special attraction of using pulse-power technology, in the form of the induction linac, for the acceleration of high-current beams, because of the capability of obtaining very high peak-power from an inherently low average-power source. Analogous arguments can be seen to hold for the pulsed drift-tube low-velocity structure discussed in this paper. Each drift-tube is used to supply only about 200 joules to the beam, but at a power level that varies from some 5 MW at the beginning of the injector to a healthy 100 MW at the end. The installed averaged power capability needed for acceleration alone should be significantly less than 1 MW.

At the same time we have adverted to the limitations imposed by the present state of development of this technology, particularly the narrow range of switches available.[7,8] The strategies outlined earlier indicate that credible ways of circumventing these limitations can be constructed, but more elegant and less costly solutions would be possible if there were a wider variety of switches to choose from. For example, existence of a fast-opening switch would immediately allow a multiple-pulsing capability to an arbitrary degree (c.f. the system illustrated in Fig. IV-C-2/4D. Spark-gap switches provide a relatively low-cost method of switching at the 1 MV level, have satisfactory rise-time and jitter, and at the power values relevant to the present application can offer high reliability. Intrinsically, however, they have a long recovery time (>1 msec) and have to be regarded as one-shot devices on the time-scale of beam manipulation that concerns us here. Thyratrons, significantly more expensive (although cost on the scale of an injector which needs rather few elements is probably unimportant), have the attraction of a shorter dead-time, 10 μsec or less, which is tantalizingly close to multiple-pulse exploitation in the earliest stages of a pulsed drift-tube accelerator. They are at present limited, however, to voltages of less than 200 kV and if used in combination with pulse-transformers to reach the 1 MV domain seem to have application only in the earliest stages of acceleration. The limitation which enters through the transformer is not due to the switch, but the need for voltage transformation. There are interesting new

PULSED QUASISTATIC DRIFT TUBE INJECTOR
(SOME EXAMPLE CONFIGURATIONS)

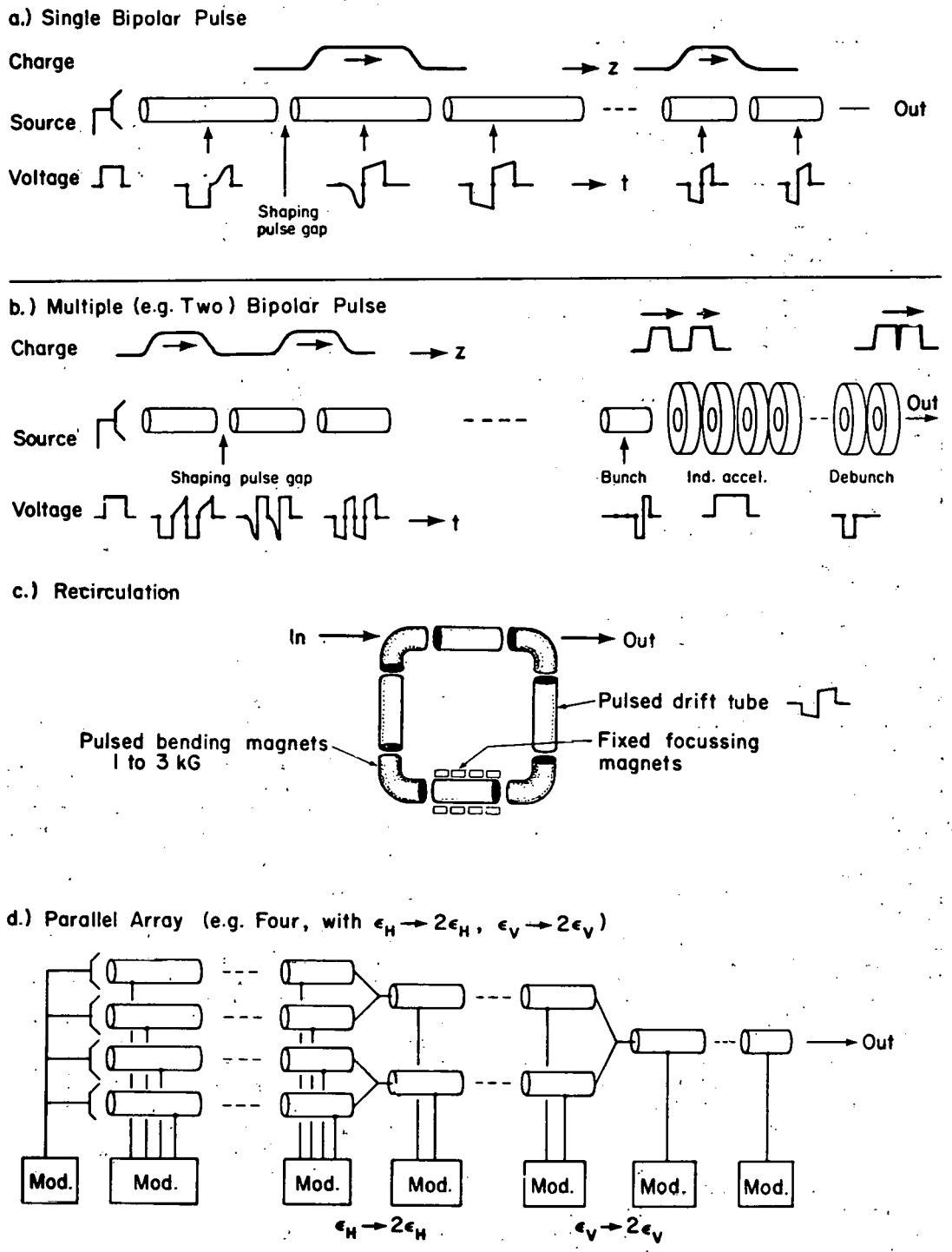

Fig. IV-C-2/1. Some possible arrangements of components in a pulsed drift-tube structure: (A) In-line arrangement of drift-tube to each of which is applied a single bipolar pulse (for explanation of pulse shaping see text); (B) In-line arrangement where two pulses, in this example, are successively applied; The gradient (MV/m) is twice that of the former example; (C) Re-circulation through multiply-pulsed drift-tubes by means of pulsed bending magnets; (D) Inversely branched lay-out in which pulse stacking takes place (transverse stacking only, shown).

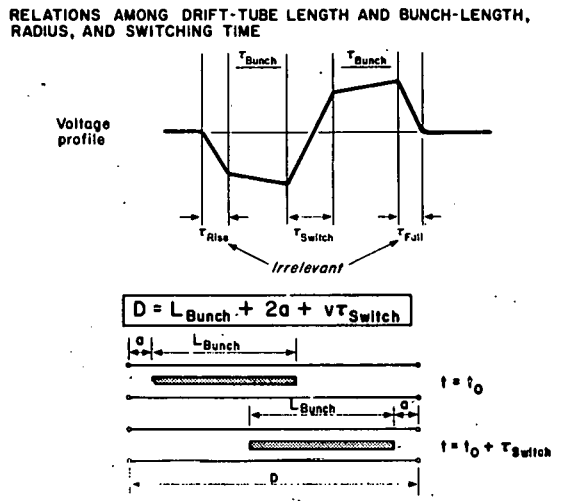

Fig. IV-C-2/2. Illustration of how the switching-time, τ_{SW} affects the drift-tube length.

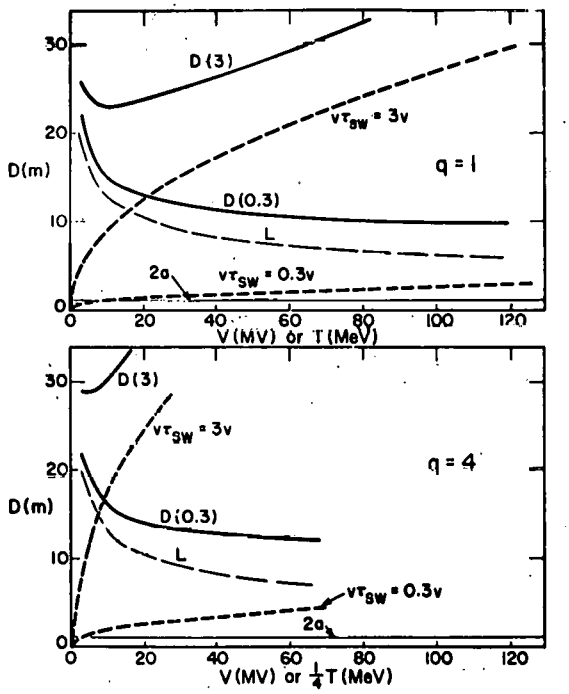

Fig. IV-C-2/3. The relative contribution of various parameters to the drift-tube length, D, as the beam voltage (V(=T/q) varies: (A) for q = 1 (B) for q = 4. Two values for τ_{SW} = 3 μsec and 0.3 μsec are indicated.

developments in vacuum-tube switch technology stimulated by the need for high-power series-regulator switches for neutral-beam sources for the Tokamak programs.[9] Such tubes could approach the 10-100 MW pulse-power requirements with a switching-time that is negligible on the time-scale of present concern. The voltage capability of these tubes will be in the 150-200 kV range so that pulse transformer characteristics would still impose certain limitations. While we have not explored here the possible gains to be derived from the use of such switches their potential application should be examined further, especially in multiple pulsing of short drift-tubes without the use of pulse transformers.

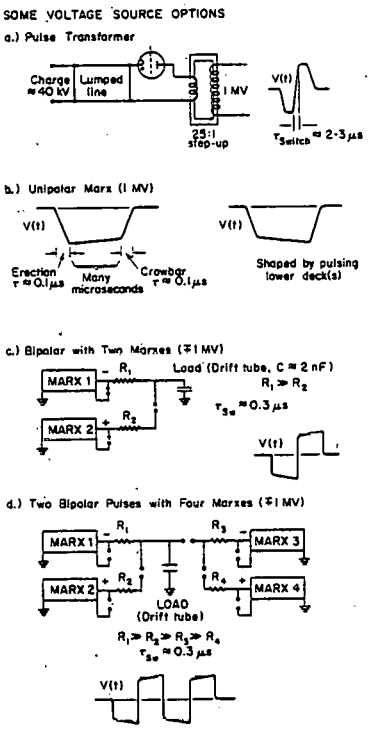

Fig. IV-C-2/4. Some pulse modulator choices: (A) Thyratron and pulse-transformer. (B) Unipolar Marx generator, (C) Bipolar Marx generator combination, (D) Double pulsing (Bipolar) Marx Generator Combination. The natural RC droop of the Marx pulse can be removed and a positive ramp created by pulsing the lower decks.

CONCLUSIONS

The major attractions of the pulsed drift-tubes are that they are non-resonant structures and that they appear suitable for accelerating a very high current bunch at low energies. The mechanical tolerances of the non-resonant structure are very loose and the cost per meter should be low; the cost of the transport system is expected to be the major cost. The pulse power modulators used to drive the drift-tubes are inexpensive compared to rf sources with equivalent peak-power. The longitudinal emittance of the beam emerging from the structure could be extremely low.

ACKNOWLEDGEMENTS

We are particularly grateful to Dr. W. B. Herrmannsfeldt for his many valuable contributions to the drift-tube accelerator concept, and we thank our colleagues, G. Lambertson, L. J. Laslett, and L. Smith for their criticisms and discussions.

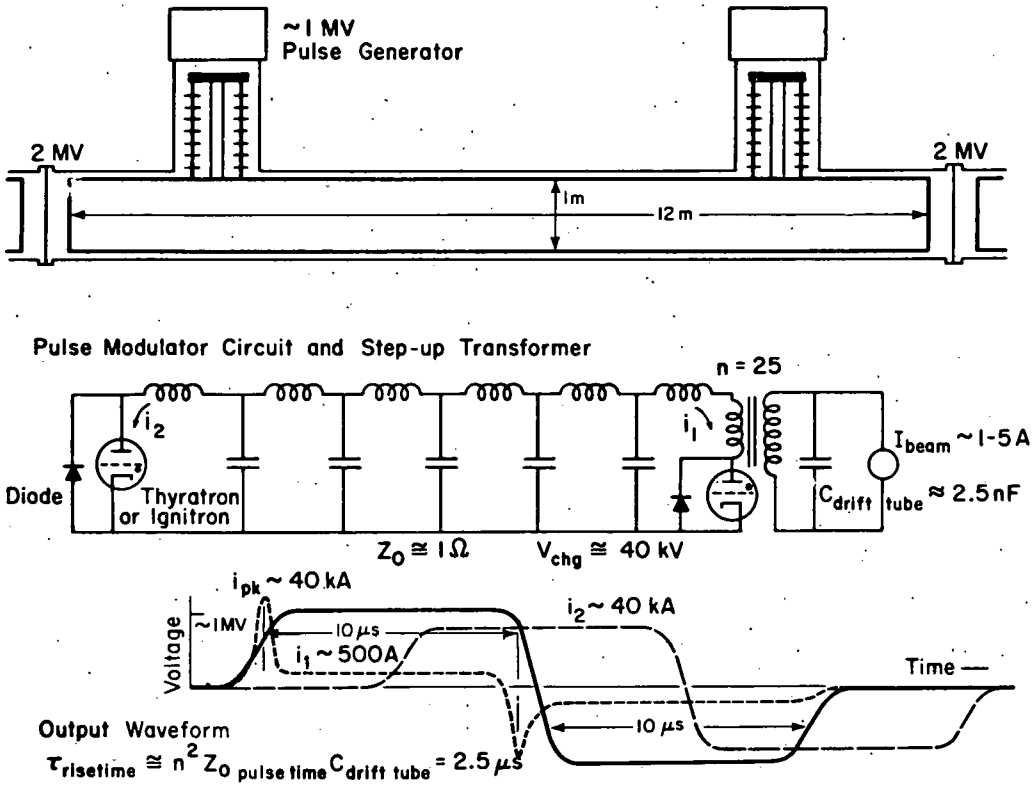

Fig. IV-C-2/5. Example drift-tube and circuit to illustrate the approach outlined in Fig. IV-C-2/4A.

References

1. B. Richter et. al.: Preceeding paper in these Proceedings.
2. L. J. Laslett: Report in these Proceedings.
3. W. B. Hermannsfeldt: Unpublished calculations using the E-GUN computer code: see SLAC Report.
4. W. B. Hermannsfeldt, et. al., to be published.
5. See, for example: G. R. Lambertson L. J. Laslett, and L. Smith, IEEE Trans. NS-24 993 (1977).
6. L. J. Laslett, and D. Keefe: Unpublished (Nov. 1976).
7. A. Faltens, and D. Keefe: LBL-6453; to be published in Proc. Xth Int. Conf. on High-Energy Accelerators. (Serpukhov, July 1977).
8. A. Faltens, D. Keefe, and D. L. Judd: LBL-6768; to be published in Proc. 2nd Int. Top. Conf. on High-Power Electron and Ion Beam Research and Technology (Cornell, October 1977).
9. Eimac Type X2209 and RCA Type A 3012 preliminary data.

3. ESTIMATES OF POST-ACCELERATION LONGITUDINAL BUNCH COMPRESSION

David L. Judd

INTRODUCTION

The target requirement for the use of pulses of high-energy heavy ions as igniters of inertial-fusion pellet targets which is least familiar in present accelerator technology is that of delivering a few magajoules of energy within a few nanoseconds. Spot size and energy deposition requirements indicate that ions with $A > 100$ should have a kinetic energy of order 10-50 GeV; this calls for $\sim 10^{15}$ ions with a total charge $Q \sim 2 \times 10^{-4}$ q Coulomb (ion charge = qe) to arrive at the target together in N_b bunches, each of length $L = \beta ct \sim$ 1-2 meter. The longitudinal self-field within such a bunch has a maximum value on the order of 5 to 10 times $Q/(4\pi\epsilon_o N_b L^2)$, which has the order of magnitude 10 (q/N_b) MV/m. Such fields are far above those available for equilibrium longitudinal containment from known synchrotron or storage ring rf systems, even for q = 1, unless an unrealistically large number N_b of bunches is contemplated. Therefore, it seems very probable (as has been emphasized by Maschke) that transient longitudinal "implosion" of the bunches just before their arrival at the target will be required.

Our purpose here is to obtain approximate estimates of the parametric dependences of attainable final implosive bunch compressions in forms allowing comparisons among different processes. We make several simplifying assumptions whose quantitative validity will require more detailed calculations to assess. However, the conclusions obtained should provide useful guides even though the numerical coefficients are uncertain at present.

We assume that transverse containment of a bunch within a radius much less than its length is provided by means not specified here, and that transverse and longitudinal motions of ions within a bunch may be regarded as uncoupled. Within a bunch we take the effective longitudinal self-field to be given by

$$E_z^{sc} \simeq -(gqe/\gamma^2)(\partial\lambda/\partial z) \qquad \text{(cgs)}$$

with λ the number of ions per unit length, z the distance measured from the bunch center, and g a geometrical factor of order unity [see L. Smith, LBL-5543, p. 77, eq. (1)]. The factor γ^{-2} accounts for partial cancellation of electric by magnetic self-force. If $\lambda(z)$ is parabolic (proportional to $1 - (2z/L)^2$)

$$E^{sc} \simeq (6gQ/\gamma^2 L^2)(2z/L),$$

with Q the total charge in the bunch. We adopt this model, setting $6g = k$ and recognizing that its value will depend on the form of $\lambda(z)$ as well as beam bunch radius and beam pipe properties. For numerical estimates here we will take $k \sim 10$, hoping that this introduces some conservatism.

If an equal but opposite mean (i.e., path-averaged) external linearly ramped electric field with average value zero is applied, with sawtooth ramp amplitude

$$\overline{\Delta E} = kQ/(\gamma L)^2 ,$$

it is possible for all the ions in the bunch to be in equilibrium at rest in the bunch frame with constant bunch length L given by

$$L^{-2}\,(\overline{\Delta E}) = kQ/(\gamma^2 \cdot \overline{\Delta E})$$

provided there is no longitudinal velocity dispersion. In our picture the post-acceleration bunch compression operation begins at t = 0 with the bunch in such an equilibrium state at initial length L_i. (In some actual systems the acceleration and compression operations may overlap; we neglect this possibility here and separate them for convenience. Further on we will introduce an initial ordered velocity "tilt" in longitudinal (z,p_z) phase space and a "thermal" longitudinal velocity distribution.)

In applying our results we will have two different types of system in mind. One of these consists of an induction linac as the main accelerator. We picture a single bunch emerging from it with bunch length L_i in the equilibrium condition just described. The bunch then passes through a compressor section consisting of a drift line containing pulsed-gap elements similar to those in the linac except that they produce large electric fields ramped linearly in time (sawtooth) with average value zero. (Such a bunch may be split into two parts, to be brought to the target separately, either before or during the post-acceleration compression, and the drift lines may contain bending magnets as well as the pulsed-gap system and transverse focusing magnets; these matters will not be considered here.)

The second type of system consists of a number n of dc-magnet accumulator or storage rings which receive beams by multi-turn injection from a synchrotron or rf linac which provides the main acceleration. Within each ring the resulting beam may initially fill the entire circumference. We will assume that after filling the beam is gently collected into h bunches in each ring by slowly turning on an rf accelerating system at the hth harmonic of the ring circulation frequency until within each rf cycle a bunch extends over the roughly linear portion of the sinusoidal accelerating wave, its central particle crossing the gaps at the stable time of zero field. In this condition somewhat less than half the ring circumferences will be occupied by the bunches, and each will be in the equilibrium state described above. It is envisioned that in such systems the implosion process to be described below starts and continues within the rings until the bunch lengths have decreased to a given value,

at which time the h bunches are extracted from each ring into h transport lines. (Here again the collection and implosion processes may overlap in actual designs, but we separate them for convenience.) We will also consider including in these transport lines sawtooth pulsed-gap supplementary compressor systems like those described above as being downstream from an induction linac.

IMPLOSIVE COMPRESSION

Our somewhat idealized implosive compression operation is started at t = 0 by suddenly applying a large linearly-ramped external longitudinal electric field whose initial (path-averaged) strength is

$$E^{ext}(z) \simeq - \Delta E_o (2z/L_i) \quad \text{for} \quad |z| < \tfrac{1}{2}L_i \quad .$$

We define a dimensionless bunch length $\rho = L(t)/L_i$; it is the reciprocal longitudinal compression factor. At later times the applied sawtooth amplitude and slope are defined in terms of L(t) and $\epsilon(\rho)$ by

$$E^{ext}(z,L) \simeq - \epsilon(\rho) \Delta E_o \ (2z/L) \quad \text{for} \ |z| < \tfrac{1}{2}L;$$

here $\epsilon(\rho)$ is a dimensionless function having initial value unity, whose different variations serve to define the several compression regimes to be described below.

The equation of motion of an ion is

$$(\gamma^3 M) \ d^2z/dt^2 = qe(E^{ext} + E^{sc}) =$$

$$qe \left[-\epsilon(\rho) \ \Delta E_o + kQ/(\gamma L)^2 \right] \ (2z/L) \quad ,$$

where $\gamma^3 M$ is the "relativistic longitudinal mass" of an ion of mass $M = Am_p$. Applying this equation to ions at the bunch ends where $|z| = \tfrac{1}{2}L$, we obtain the "envelope equation":

$$d^2L/dt^2 = - \left[2qe \ \Delta E_o / \gamma^3 M \right] \epsilon(\rho) + \left[2kqeQ/\gamma^5 ML^2 \right] \quad .$$

Now we adopt a dimensionless time τ defined by $\tau = t/T$, with

$$T^2 = (\gamma^3 ML_i)/ \ (4qe \ \Delta E_o) \qquad (cgs) \quad .$$

Dividing by L_i, the equation of motion in these units is

$$d^2\rho/d\tau^2 = - \frac{1}{2} \left[\epsilon(\rho) - \frac{R}{\rho^2} \right]$$

where R is a dimensionless parameter given by

$$R = (kQ)/ \ (\gamma^2 L_i^2 \ \Delta E_o) \quad (cgs) =$$

$$(kQ)/ \ (4\pi\epsilon_o \gamma^2 L_i^2 \ \Delta E_o) \qquad (MKS)$$

and $(4\pi\epsilon_o)^{-1} = 9 \times 10^9$. The "energy integral" of this equation is found by multiplying by $d\rho/d\tau$ and integrating; with out initial condition $d\rho/d\tau = 0$ at $\rho = 1$, it is

$$(d\rho/d\tau)^2 = \int_\rho^1 \epsilon(x) \ dx - \frac{1 - \rho}{\rho} \ R \ .$$

For any given $\epsilon(\rho)$ we may find $\rho(\tau)$ from this equation by another integration. (An additional term, representing the effect of a "thermal" or random velocity spread, or, equivalently, that of a non-zero longitudinal emittance, will be added to these equations in a later section, where its significance is discussed.)

SPECIFICATION OF AN IMPLOSION PROCEDURE BY $\epsilon(\rho)$

In a pulsed-gap line the applied sawtooth ramp amplitude may be maintained constant at the value ΔE_o throughout the compression, for times at least as short as 10 nanoseconds, while its slope increases inversely with bunch length; this corresponds to $\epsilon(\rho) = 1$ for $\rho \leq 1$. If the beam continues to drift past the end of this system before attaining its minimum length, this corresponds to

$$\epsilon(\rho) = \begin{cases} 1 & \rho_T < \rho < 1 \\ 0 & \rho < \rho_T \end{cases}$$

with ρ_T the dimensionless bunch length at the transition point where the compressor field ends.

For a ring rf system it is advantageous to use the largest available accelerating voltage amplitude throughout that part of the compression process which occurs within the ring. The slope of the quasi-linear part of this sinusoidal wave, which is the analog of the sawtooth pulse in the linear system, will therefore be constant during this compression; the amplitude of the part occupied by a bunch will therefore be directly proportional to its length. (We do not consider here the theoretical possibility of rapidly adding a number of higher harmonics to the waveform so as to change its slope during compression, because the total number of turns involved will be found to be relatively small; in addition, the electronic complications seem out of proportion to the possible gain.) This condition corresponds to

$$\epsilon(\rho) = \rho \quad \text{for} \quad \rho_T < \rho < 1$$

with ρ_T the dimensionless bunch length at the time of extraction from the ring. If these bunches pass through a pulsed-gap compressor line after extraction from a ring,

$$\epsilon(\rho) = \epsilon_L \quad \text{for} \quad \rho_2 < \rho < \rho_1$$

with ρ_1, ρ_2 the dimensionless bunch lengths on entry and departure from this line and ϵ_L the ratio

that of the quasi-linear part of the rf field amplitude in the ring at t = 0, denoted by ΔE_o.

CONTINUOUS PULSED-GAP COMPRESSION

As a first example of the use of the general results we set up $\epsilon(\rho) = 1$. Then

$$(d\rho/d\tau)^2 = \frac{(1-\rho)(\rho - R)}{\rho}$$

The bunch compresses like a nonlinear spring, whose restoring force varies as L^{-2}, when subjected to a constant compressive force. The spring reaches a momentary fully compressed state of rest at $\rho = R$, after which it would rebound reversibly were the bunch not then to arrive at the target. Its minimum length is

$$L_{min} = RL_i = (kQ)/(\gamma^2 L_i \Delta E_o) \quad ;$$

by writing this in the form

$$L_{min} L_i = (kQ)/(\gamma^2 \Delta E_o) = \left[\bar{L}(\Delta E_o)\right]^2$$

we see that the equilibrium bunch length, about which L oscillates between the extremes L_i and L_{min}, is the geometric mean of the extremes.

The remaining integral which yields the function $\tau(\rho)$ is an elliptic integral;

$$\tau(\rho) = \int_\rho^1 x(1-x)^{-1}(x-R)^{-1} \tfrac{1}{2}\, dx = 2E(\phi,k)$$

with E the standard elliptic integral $\int_0^\phi (1-k^2 \sin^2\theta)^{\frac{1}{2}}\, d\theta$. Its parameters are given by

$$\sin^2\phi = (1-\rho)/(1-R) \quad , \quad k^2 = 1 - R.$$

The total time to maximum compression is given by the complete elliptic integral:

$$\tau\ (R) = 2E(k).$$

For k near to unity (R << 1, corresponding to a large compression factor) E is insensitive to the value of R; $1 < E < 1.1$ for $0 < R < 0.1$ Therefore the bunch travels a distance

$$s = \beta c\tau(R)\ T \simeq \beta \left[(\gamma^3 Mc^2 L_i)/(qe\Delta E_o)\right]^{\frac{1}{2}}$$

during compression from L_i to L_{min}.

It is not necessary to be familiar with the properties of the elliptic integral to understand the physics of the process. For small R most of the compression occurs in the "free-fall" regime, in which E^{sc} (and therefore R) may be neglected;

$$d\rho/d\tau \simeq -(1-\rho)^{\frac{1}{2}},$$

and $\rho_{approx} = 1 - \tfrac{1}{4}\tau^2$, analogous to $h = h_o - \tfrac{1}{2}gt^2$ for free fall under gravity. In the final stage of compression the term in R must be included, as shown in Fig. V-G-2/1 (drawn for R = 0.1) in which $\rho(\tau)$, the approximate parabola ρ_{approx}, and the slope $d\rho/d\tau$ are plotted against τ. The sign of the curvature of $\rho(\tau)$ reverses at $\rho = R^{\frac{1}{2}} = \bar{L}/L_i$ at the time of maximum slope; the maximum slope is given by

$$|d\rho/d\tau|_{max} = 1 - R^{\frac{1}{2}}$$

The slope $d\rho/d\tau$ is of interest because it represents an ordered linear velocity tilt in longitudinal phase space; the front and back ends of the bunch have velocities (relative to a central particle) $\Delta v = \pm (dL/dt) \lesssim 0$ whose magnitudes are given by

$$|\Delta v/c| = \tfrac{1}{2}(L_i/cT)\ (d\rho/d\tau) =$$

$$|d\rho/d\tau|\ \ (qe\Delta E_o L_i)/(\gamma^3 Mc^2)^{\frac{1}{2}}\ .$$

The ordered momentum spread associated with this velocity spread is

$$\Delta p/p = \Delta(\beta\gamma)/\beta\gamma = (\gamma^2/\beta)(\Delta v/c) =$$

$$\pm\beta^{-1}|d\rho/d\tau| \left[(\gamma\, qe\, \Delta E_o\, L_i)/(Mc^2)\right]^{\frac{1}{2}}.$$

These results are valid in any self-consistent units; e.g., $e\,\Delta E_o$ in MeV/m, L_i in m, Mc^2 in MeV.

Should the compressive process cease when $\rho = \rho_T > \rho_{min}$, the subsequent behavior is given by

$$(d\rho/d\tau)^2 = (d\rho/d\tau)^2|_\rho = \rho_T - R\left[\frac{(1-\rho)}{\rho} - \frac{(1-\rho_T)}{\rho_T}\right]$$

$$= 1 - (\rho_T - R) - R/\rho\ .$$

The minimum value of ρ under these new conditions, denoted by ρ^*, is

$$\rho^* = R/\left[1 - (\rho_T - R)\right] > \rho_{min}$$

showing that the final compression attained is reduced by the factor $1 - (\rho_T - R)$ owing to early termination of the applied force. The time of drift between ρ_T and ρ^* is given by an elementary integral;

$$\tau(\rho^*) - \tau(\rho_T) =$$

$$R^{-\frac{1}{2}}\rho^{*3/2}\left[x^{\frac{1}{2}}(x-1)^{\frac{1}{2}} + \ell n\left\{(x-1)^{\frac{1}{2}} + x^{\frac{1}{2}}\right\}\right]$$

with $x = \rho_T/\rho^*$. For accurate work $\tau(\rho_T)$ must be found by evaluating the incomplete elliptic integral, but it is evident from Fig. V-G-2/1 that for small R the total time to the minimum will not change much if ρ_T is close to R.

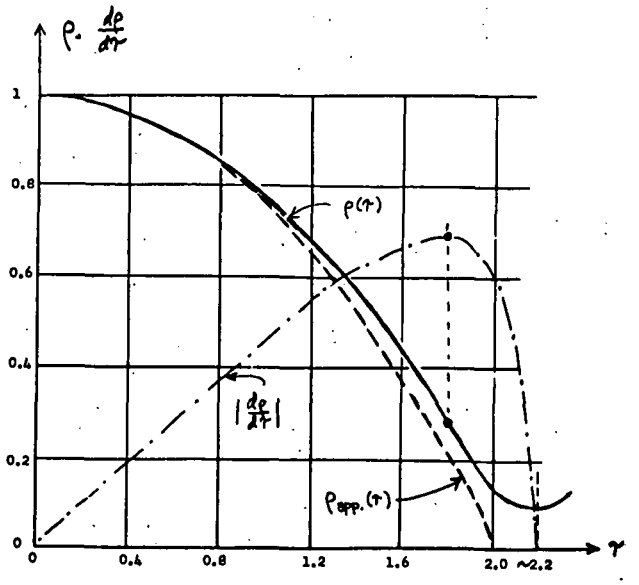

Fig. V-G-2/1. $(d\rho/d\tau)^2 = (1-\rho)(\rho - R)/\rho$; $(d\rho_{app.}/d\tau)^2 = (1-\rho)$; $\rho_{app.}(\tau) = 1 - \frac{1}{4}\tau^2$
Drawn for R = 0.1

INCLUSION OF INITIAL ORDERED LINEAR VELOCITY "TILT"

If some amount of inward drift has been induced by systems upstream of the point at which our implosive compression is assumed to begin, we may approximate it by altering the initial conditions so that

$$dL/dt\big|_{t=0} = -\Delta v_o(2z/L_i)$$

rather than zero as assumed above. Of course this is equivalent to starting farther down the curve of $\rho(\tau)$ such that of Fig. V-G-2/1; however, the dimensionless variables ρ and τ and the dimensionless parameter R have been defined in terms of the bunch length L_i rather than the value L_o of L at the back-extrapolated point where $d\rho/d\tau = 0$. Therefore, it is convenient to indicate the modifications needed to accomodate the new initial condition and the connection between scalings of these quantities based on L_i and on L_o.

We start by labeling parameters based on initial bunch length L_i by subscripts i:

$$\tau_i = t/T_i \ , \quad T_i^2 = \left[(\gamma^3 M)/(4qe\Delta E_o)\right] L_i \ ,$$

$$\rho_i(\tau_i) = L(\tau_i)/L_i \ , \quad R_i = \left[(kQ)/(\gamma^2\Delta E_o)\right] L_i^{-2} .$$

Next we define a new dimensionless parameter Q_i;

$$Q_i = (T_i/L_i)^2(\Delta v_o)^2 \ .$$

Then

$$(d\rho_i/d\tau_i)^2 = \left[(1-\rho_i)(\rho_i - R_i)/\rho_i\right] + Q_i \ ,$$

$$\tau_i(\rho) = \int_\rho^1 \left[\frac{x}{(1-x)(x-R_i) + Q_i x}\right]^{\frac{1}{2}} dx \ ,$$

$$(d\rho_i/d\tau_i)^2\big|_{max} = (1 - R_i^{\frac{1}{2}})^2 + Q_i \ , \text{ and}$$

$$\rho i_{min} = \tfrac{1}{2}(1 + R_i + Q_i) - \left[\tfrac{1}{2}(1 = R_i + Q_i)2 - R_i\right]^{\frac{1}{2}} .$$

This last relation is well approximated by

$$\rho_{i_{min}} \simeq R_i(1 - \tfrac{1}{2}Q_i)$$

if R_i and Q_i are both small with respect to unity. It is seen that the final compression attained is slightly greater than before, because of the "head start" represented by Q_i.

Parameters based on the back-extrapolated bunch length L_o corresponding to $d\rho/d\tau = 0$ are labeled by subscripts zero:

$$\tau_o = t/T_o \ , \quad T_o^2 = \left[(\gamma^3 M)/(4qe\Delta E_o)\right] L_o = T_i^2 L_o/L_i ,$$

$$\rho_o(\tau_o) = L(\tau_o)/L_o \ , \quad R_o = \left[(kQ)/(\gamma^2\Delta E_o)\right] L_o^{-2}$$

$$= R_i(L_i/L_o)^2 \ .$$

The parameter Q_o is zero by definition. Because we are here regarding the quantities labeled by i as known, the connections require only the determination of L_o, or equivalently of the ratio $L_i/L_o = \rho_{oc}$, the reciprocal compression associated with the back-extrapolated interval. The connection is made by observing that both formalisms must yield the same minimum bunch length;

$$L_{min} = \rho_{i_{min}} L_i = R_o L_o = \rho_{oc}^2 R_i L_o = \rho_{oc} R_i L_i \ .$$

Thus

$$\rho_{oc} = \rho_{i_{min}}/R_i$$

and for small R_i and Q_i

$$\rho_{oc} \simeq 1 - \tfrac{1}{2}Q_i$$

The connection is now complete and the solution is given by

$$\tau_o(\rho_o) = \int_{\rho_o}^{\rho_{oc}} \left[\frac{x}{(1-x)(x-R_o)}\right]^{\frac{1}{2}} dx = \int_{\rho_o}^{1} - \int_{\rho_{oc}}^{1}$$

$$= 2\left[E(\phi_\rho, k_o) - E(\phi_{oc}, k_o)\right] ,$$

in which the time origin of τ_o has been adjusted to agree with that of τ_i.

COMPRESSION IN A RING

For $\epsilon(\rho) = \rho$ we have $(d\rho/d\tau)^2 = \frac{1}{2}(1 - \rho^2)$

$$-R(1 - \rho)/\rho = (1 - \rho)\ \tfrac{1}{2}(1 + \rho) - R/\rho \quad ,$$

from which $\rho_{min} = \frac{1}{2}\left[(1 + 8R)^{\frac{1}{2}} - 1\right] \simeq 2R/(1 + 2R)$; $|d\rho/d\tau| = \min$ at $\rho = R^{1/3}$. For sufficiently small R we have $\rho_{min} \simeq 2R$, showing that the linearly decreasing compressive force results in only about half as much compression for the same values of Q, L_i, and ΔE_o provided that the process goes to completion within the ring. If a bunch is extracted at $\rho = \rho_T$ and then allowed to drift freely together, we have during this drift

$$(d\rho/d\tau)^2 = (d\rho/d\tau)^2|_{\rho=\rho_T} - R\left[(1 - \rho/\rho - (1 - \rho_T)/\rho_T\right]$$

$$= \tfrac{1}{2}(1 - \rho_T^2) - R(1 - \rho)/\rho \ ;$$

The new minimum value ρ^* of ρ under these conditions is

$$\rho^* = 2R/\left[1 - (\rho_T^2 - 2R)\right] > \rho_{min} \ ,$$

so that the compression attained is again reduced owing to early termination of compression; here, however, this loss is less than in the pulsed-gap line because the final stage of uninterrupted compression is very ineffective due to the linear decrease of effective force with L.

As for the pulsed-gap line, for small R almost all of the compression will occur before space charge repulsion plays a role; in this region

$$(d\rho/d\tau)^2 \simeq \tfrac{1}{2}(1 - \rho^2),$$

so that

$$\rho(\tau) \simeq \cos(\tau/2^{\frac{1}{2}})$$

and the minimum value of ρ , for uninterrupted compression, will occur near to the time

$$\tau = \pi/2^{\frac{1}{2}} \simeq 2.2$$

so that the total path length to this minimum is of the same order of magnitude as for the pulsed-gap line for the same Q, L_i, and ΔE_o although the bunch will be about twice as long.

Because the approximate cosine solution becomes inaccurate only near full compression, it should be adequate in many cases for the period up to the time of extraction of a bunch from a ring.

A COMPOSITE SYSTEM

Here compression in the range $1 > \rho > \rho_T$ occurs inside a ring, with $\epsilon(\rho) = \rho$, followed by extraction and further compression in a line with $\epsilon(\rho) = \epsilon_L$ = constant for $\rho_T > \rho$. After extraction,

$$(d\rho/d\tau)^2 = (d\rho/d\tau)^2|_{\rho=\rho_T} - (\rho - \rho_T)\epsilon_L$$

$$- R\left[(1 - \rho)/\rho - (1 - \rho_T)/\rho_T\right]$$

$$= \tfrac{1}{2}(1 - \rho_T^2) - (\rho - \rho_T)\epsilon_L - R(1 - \rho)/\rho$$

The minimum value of ρ is given by

$$\rho_{min} = (B/\epsilon_L)\left[1 - (1 - B^{-2}R\epsilon_L)^{\frac{1}{2}}\right]$$

with $$B = \tfrac{1}{2}\left[\tfrac{1}{2}(1 - \rho_T^2) + \rho_T\epsilon_L + R\right] .$$

There are several limiting cases of this result, but the most important one appears to be that in which the middle term in B dominates. This is because the pulsed-gap technology allows ramp height ΔE_o to be very much larger than in ring rf systems, so that $\epsilon_L >> 1$, and also because the value of ρ_T attainable in a ring is probably not very small. In this limit we have

$$\rho_{min} \simeq \tfrac{1}{2}\,\rho_T\left\{1 - \left[1 - (4R/\rho_T^2\epsilon_L)\right]^{\frac{1}{2}}\right\} \simeq R/(\rho_T\epsilon_L).$$

The compression factor obtainable from the line alone is ϵ_L/R , differing from R^{-1} because the definition of R is based on the ring's ΔE_o which is ϵ_L times smaller than that in the line. The limiting result above shows that this compression is reduced by the factor ρ_T owing to use of a lesser compressive force within the ring until ρ has diminished from unity to ρ_T.

COMPARISON OF A PULSED-GAP LINE WITH n RINGS USING FIRST HARMONIC

We start by making order-of-magnitude estimates of the requirements on an induction linac system. A bunch emerging from it should have a pulse length $\lesssim$ 200 nanosecond to allow use of ferrite-loaded modules along much of its length, but not very much less than this value so as to avoid expending an appreciable fraction of the available volt-seconds for longitudinal containment during acceleration. Therefore we use $L_i \sim 30$ m, appropriate for $\beta = v/c \sim \frac{1}{2}$. A pulsed-gap compressor line can supply sawtooth ramps of path-averaged field amplitude $\geq$ 1 MV/m with pulse times from 200 nsec down to 10 nsec or shorter. Let us assume that we wish to amply supply the pellet target needs by delivering $\sim$ 10 MJ in $\sim$ 10 nsec, using ions with $A \sim 200$ having kinetic energy 20 GeV. Then $\beta \sim 0.45$, $\gamma^2 \sim 5/4$, and $\sim 3 \times 10^{15}$ ions are needed, having total charge $\sim 5 \times 10^{-4}$ Coul if they are in the singly ionized state q = 1. The final bunch length $L_{min} = \beta c\Delta t$ is then $\sim 4/3$ m. The required value of ΔE_o is then

$$\Delta E_o \sim (k/4\pi\epsilon_o)(Q/\gamma^2 L_i L_{min}) =$$

$$\frac{10 \times 9 \times 10^9 \times 5 \times 10^{-4}}{(5/4) \times 30 \times (4/3)} \ \text{eV/m} \sim 1 \ \text{MV/m},$$

the value given above. Note that this expression is proportional to $\beta^{-3}\gamma^{-2}(q/A)$ times the beam power at the target.

For the rings we assume that L_i is a fraction F of a ring circumference C; F ~ 1/3 for the quasi-linear part of a sinusoidal accelerating field. We set $C\Delta E_o = \Delta V$, the number of volts per turn experienced by ions at the bunch ends at t = 0. Ejection from the ring occurs after compression by a factor ρ_T^{-1}, and we take R << 1 for the ring, as will be the case for a strong rf system. Then the minimum bunch length after subsequent drift, but without supplementary pulsed-line compression, will be

$$L_{min}^{ring} \sim 2(1 - \rho_T^2)^{-1}(k/4\pi\epsilon_o)(Q/n)/[\gamma^2 F\Delta V]$$

while that from the pulsed-gap compressor is

$$L_{min}^{line} \sim (k/4\pi\epsilon_o)Q/[\gamma^2 L_i \Delta E_o] .$$

Equating these expressions, we may solve for the number n of rings required to produce the same final pulse length, obtaining

$$n \sim 2(1 - \rho_T^2)^{-1} L_i\Delta E_o/[F\Delta V] .$$

Using $\rho_T < 1/3$, F ~ 1/3, L_i = 30 m and ΔE_o = 1 MV/m for the linac,

$$n \sim \frac{180}{\Delta V \ (MV/turn)} .$$

It seems clear that the compression factor available from a pulsed-gap line can be reproduced by rings only by using a large number of them or by filling much of their circumferences with truly heroic rf systems having a voltage per turn far beyond present experience.

COMPARISON OF RINGS WITH DIFFERENT HARMONICS h

Consider two ring systems, each with the same number n of rings, one with harmonic number h = 1 and the other with harmonic h. For the first,

$$L_{min}^{(1)} = 2K(Q/n)/[\gamma^2 FC\Delta E_o^{(1)}(1 - \rho_T^2)]$$

with the bunch in each ring having charge Q/n and initial length L_i = FC as above. In the second system there are h bunches in each ring with each bunch having charge Q/nh and initial length L_i = FC/h. Therefore

$$L_{min}^{(h)} = 2k(Q/nh)/[\gamma^2(FC/h) \ \Delta E_o^{(h)}(1 - \rho_T^2)] .$$

It is at once apparent that the explicit h-dependence cancels. The factor F measures only the fraction of the wave that is quasi-linear and will be the same for both, and there is no reason for ρ_T to differ. Therefore the minimum attainable bunch lengths are the same except for technological factors affecting the frequency dependence of the maximum attainable voltage per turn. Although these factors favor larger h, the gain is made at the cost of increasing the number of beam lines, final focusing magnets, and beam spots on the target by a factor h, giving a more complex and unwieldy system. In addition, the total distance traversed by each bunch is

$$s = \beta c\tau T \ , \text{ with } \beta\tau \sim 1$$

as shown above. It is reasonable to assume that the fraction of this distance traversed outside the ring after extraction is about the same for any h; i.e., ρ_T does not depend on h. With $T^2 \propto L_i \propto h^{-1}$, the external drift line length per bunch is $\propto h^{-\frac{1}{2}}$ and the total length of all drift lines is proportional to $h^{\frac{1}{2}}$.

Accumulator rings appear to be essential for systems using a synchrotron or rf linac as the main accelerator. From the estimates and calculations above it also appears essential to provide pulsed-gap compressor lines following bunch extraction. To minimize the total length of these lines a small number of separately extracted bunches is desirable. The optimization of such composite longitudinal compression systems is a complex problem whose solutions will depend on many cost and other factors that are not yet available.

MODIFICATIONS DUE TO NON-ZERO LONGITUDINAL EMITTANCE

Lloyd Smith has given an envelope equation [LBL-5543, p. 79, eq.(12')] which includes the effect of finite longitudinal emittance. In the study of post-acceleration bunch compression we may take β and γ as constants. If in his equation we replace $E_o\alpha$ by $\Delta E_o/(\frac{1}{2}L)$, z_m by $\frac{1}{2}L$, and ds by $\beta c\ dt$, and multiply by $2\beta c^2/\gamma^3$ we obtain

$$d^2L/dt^2 = -[2qe\Delta E_o/\gamma^3 M]\epsilon(\rho)+[2kqeQ/\gamma^5 ML^2]+$$
$$[(4c\epsilon)^2/\gamma^6 L^3]$$

which is the same as our envelope equation in Section 2 above except for the last term added on the right side. Here Smith's ϵ is the same as the usual normalized (ϵ_ℓ/π) as defined, for example, by Teng (LBL-5543, p. 13).

The physical basis of this added term is easy to understand. It represents the pressure against confining walls of a one-dimensional ideal gas, whose adiabatic equation is pV^γ=constant with the specific heats ratio γ equal to 3 in one dimension where volume V is the length L. Thus this force varies as L^{-3}.

If we define another dimensionless parameter S by

$$S = 4(c\epsilon)^2 M/(\gamma^3 qe\Delta E_o L_i^3)$$

the equation of motion in our dimensionless variables becomes

$$d^2\rho/d\tau^2 = -\tfrac{1}{2}[\varepsilon(\rho) - \frac{R}{\rho^2} - 2\frac{S}{\rho^3}]$$

and the first integral, with $d\rho/d\tau = 0$ at $\rho = 1$, is

$$(d\rho/d\tau)^2 = \int_\rho^1 \varepsilon(x)\, dx + R(1 - \rho^{-1}) + S(1 - \rho^{-2}).$$

Confining our attention to $\varepsilon(\rho) = 1$,

$$(d\rho/d\tau)^2 = (1 - \rho)[\rho^2 - (R + S)\rho - S]/\rho^2$$

The roots of the quadratic factor are

$$\rho_{min} = \tfrac{1}{2}(R + S) + [\tfrac{1}{4}(R + S)^2 + S]^{\frac{1}{2}}$$

and an unphysical negative root in which the sign of the square root is reversed. The simplest approximation to this result is that when $4S/R^2 \ll 1$, which turns out to be valid for some parameter choices bur not for others; in this limit the roots are $\rho_{min} \simeq R + S$ and $\rho \simeq - S/R$. It is a general property that $S/R \ll 1$, so that $(d\rho/d\tau)^2 \simeq (1-\rho) \times [\rho-(R + S)]/\rho$; the attainable compression is slightly reduced by the presence of the longitudinal emittance. In the opposite extreme $4S/R^2 \gg 1$ and the roots approach $\pm S^{\frac{1}{2}}$ so that the attainable compression is dominated by the emittance effect rather than the longitudinal self-field of the bunch. This compression is generally by a large factor because S is generally less than $\sim 10^{-3}$ and can be much smaller for values of A/q and ε on the low sides of the ranges being considered. This emittance-dominated regime is associated with large ion kinetic energy, strong compressive field, low charge state, and a large number of bunches, all of which favor large compression (small R) in the absence of emittance. Not all of the parametric dependences are obvious at first sight: $Q \to Q/N_b = qeN/N_b$; $N = W/E_k$ with W the total energy delivered; $\varepsilon < \tfrac{1}{2}\beta\gamma L_{min}(r_s/R_p)$ with L_{min} the final bunch length, r_s a spot radius on target, and R_p the beam port radius (see L. Teng, LBL-5543, p. 13); and $r_s^2 = W/\pi N_b \varepsilon_d \rho\ell$ with ε_d the mean energy deposited per unit mass and $\rho\ell$ the ion range in mass per unit area. From these relations

$$\frac{4S}{R^2} < \left(\frac{4\beta^2\gamma^3}{\pi k^2}\right)\left(\frac{A}{q}\right)^3 N_b \left(\frac{L_{min}}{R_p}\right)^2 \left(\frac{E_k}{\varepsilon_d R r_p L_i}\right)\left(\frac{\Delta E_o}{e/L_i^2}\right)\left(\frac{E_k}{W}\right)$$

$$\frac{S}{R} < \left(\frac{\beta^2\gamma^2}{\pi k}\right)\left(\frac{A}{q^2}\right)\left(\frac{L_{min}}{R_p}\right)^2 \left(\frac{E_k}{\varepsilon_d R r_p L_i}\right)$$

$$S < \left(\frac{\beta^2}{\pi\gamma}\right)\left(\frac{A}{q}\right)\frac{1}{N_b}\left(\frac{L_{min}}{R_p}\right)^2 \left(\frac{E_k}{\varepsilon_d R r_p L_i}\right)\left(\frac{e/L_i}{\Delta E_o}\right)^2\left(\frac{W}{E_k}\right)$$

in cgs units. Note that S/R is independent of W, N_b, and ΔE_o; because $E_k/\rho\ell$ is larger for larger A but otherwise insensitive and ε_d lies within a narrow range it is easy to show that S/R cannot exceed a few percent.

For the parameters in Section 8 we find $4S/R^2 \sim 1.6$, $\sim 1.7 \times 10^{-4}$, and $R \sim 0.02$, assuming $N_b = 2$ and $L_{min}/R_p = 3$. Changing to $q = 3$ gives $4S/R^2 \sim 0.06$, $S \sim 6 \times 10^{-5}$, and $R \sim 0.06$. However, for $q = 1$, $W = 1$ MJ, and $E_k = 40$ GeV with the other parameters the same we find $4S/R^2 \sim 50$, and $S \sim 4 \times 10^{-5}$; the estimated reciprocal compression $S^{\frac{1}{2}}$ is $\sim 6 \times 10^{-3}$.

CONCLUSION

This report is an account of work in progress it represents only the beginning of a continuing study of longitudinal compression. Although some numerical evaluations have been made, the results obtained at the time of the Brookhaven Workshop are not sufficiently representative or comprehensive to warrant inclusion here.

It is important to note that the ordered end-to-end velocity differences within a bunch during implosive compressions are far too great to meet the requirement $\Delta p/p < r_s/R_p$ arising from chromatic aberration at the final focusing magnet except very near the position of minimum bunch length where the bunch's self-field is rapidly braking these motions toward a stop. The tolerances required to allow this process to succeed will require careful study.

I learned during the Workshop that Dr. T. K. Khoe, in unpublished notes at the Argonne National Laboratory earlier this year, has given similar consideration to some of the problems treated here.

V. Technical Working Groups

A. ATOMIC AND MOLECULAR PHYSICS

1. SUMMARY

Robert T. Poe

INTRODUCTION

The atomic/molecular physics group has accomplished a number of objectives. These include a critical review of ongoing projects, the exploration and identification of new problems and areas of concern, a broad overview of the status and goals in atomic/molecular physics. Finally there results in, for the participants, a sense of coordinated plan toward a common objective.

ATOMIC/MOLECULAR PHYSICS IN ACCELERATORS AND STORAGE RINGS

For heavy ion beam transport (high β) in accelerator and storage rings, there are two broad classes of atomic/molecular scattering processes that affect the beam lifetime, the beam quality and the beam intensity. In subsequent discussions, we shall use the symbol A^{n+} for a general heavy ion, where A denotes its nuclear species and n denotes the charge state of the ion.

Beam-Background Gas Collisions: The loss of heavy ion beams due to collisions with atoms/molecules of the background gas, resulting in a changing of the charge state of the ion, determines the vacuum requirement in the accelerator and storage rings. This type of stripping process is represented, for example, by the following ionization process.

$$A^{n+} + N_2 \rightarrow A^{(n+1)+} + e^- + N_2$$

Since the heavy ion will be in BeV energy range in the laboratory frame, this type of charge stripping is a high energy ($\beta = \overline{c} \gg 0.1$) collision process where Born Approximation, should be valid. Within the framework of the Born Approximation, the cross section σ for the process is given as

$$\sigma = \frac{8\pi a_o^2 \alpha^2}{\beta^2} [I]$$

$$8\pi a_o^2 \alpha^2 = 3.75 \times 10^{-20} \text{ cm}^2$$

and where [I] is a (nearly) constant collision strength.

Calculations have been performed in the past year by Gillespie, Kim and Cheng[1] for Li^+, Cs^+, An^+ and Hg^{n+} with H_2, C, N, and O. This is discussed in a workshop report in this section by Cheng, Das, Kim and Raffenetti.

For this workshop, Gillespie (See this section) has examined two important questions in connection with their Born calculation. First, the systematics of the cross section are examined both with respect to the dependence on nuclear species A and the dependence on ion charge state n. Second, since the Born calculations were carried out with closure approximations (i.e., sum rule), cross section values contain both the ionization cross section, which does contribute to the ion beam loss, and the excitation cross section, which does not contribute to the ion beam loss. A study is made on the relative importance of these two cross sections in the special case of hydrogenic ions from He^+ to Zn^{29+}, and it was concluded that the sum rule approach will not overestimate the electron loss cross sections by more than a factor of 2.

Beam-background gas collisions are of importance in the reactor chamber which we shall discuss later.

Charge Changing Collisions Between Ions: Charge changing collisions within the pulse of heavy ions represents a serious problem in the ion beam intensity considerations independent of the vacuum requirement. It also represents a serious problem of atomic physics. Few relevant data exist in literature, either theoretical or experimental. In the collision the average relative energy between ions within the pulse is about 0.5 keV/nucleon, a low energy where theory becomes difficult. In this workshop we reviewed the progress in the study of one charge changing process, the ion-ion charge transfer process; and we explored a new process, the direct ionization process, that may prove to be equally important.

(i) Ion-Ion Charge Transfer Process: Ion-Ion charge transfer process of the type

$$A^{n+} + A^{n+} \rightarrow A^{(n+1)+} + A^{(n-1)+}$$

was identified in the last HIF workshop[2]. Theoretical study of this important process has just began at ANL (Kim), and University of Nebraska (Macek) and the University of California, Riverside (Poe). Through discussions at this Workshop a picture of the charge transfer process emerges. At low energies, charge transfer cross section will increase with energy since it is dominated by the energy available to the charge transfer. At higher energies, the charge transfer cross section decreases because it is inhibited by the associated momentum transfer factor. In the theoretical approaches being pursued there is considerable question as to whether molecular wave functions or atomic type wave functions are more convenient. From physics consideration both have their merits. Both approaches are now being pursued. A status report of the ANL group's progress was presented (See this section).

(ii) Direct Ionization Process: Discussions on the importance of the direct ionization process as a beam-loss mechanism in ion-ion collisions was initiated by Macek (U. Nebraska) at this workshop. An example of this type of process is illustrated

$$A^{n+} + A^{n+} \rightarrow A^{(n+1)+} + e^{-} + A^{n+}$$

The direct electron ejection may originate from either inner or outer atomic shells. For heavy ions, the ejection process may not be dominated simply by Coulomb interactions but perhaps more likely by the effect of the Pauli principle. That is, as two heavy ions become close to each other, the exclusion principle between electrons will drive electronic orbitals to higher levels. As ions recede from each other, the electronic levels will be such that inner shell vacancies will be created. This type of process is sometimes referred to as Pauli Excitation. For heavy ion systems, the dominant process that follows is the Auger process, the radiationless deexcitation of electrons from a higher level accomplished by the ejection of another electron.

Both the ion-ion charge transfer process and the ion-ion direct ionization process (particularly the outer shell ionization) represent a prominant gap in the understanding of ion-ion collisions and represent, because of its many-electron nature, a most difficult theoretical challenge. It is the consensus of the atomic/molecular physics groups in this HIF workshop that the initiation of experimental work on ion-ion collision is highly desirable if not imperative.

ATOMIC/MOLECULAR PHYSICS IN GAS FILLED REACTORS

A new area of exploration generated by this workshop is the need of atomic/molecular physics in connection with the heavy ion beam transport in the fusion reaction chamber. Interactions with the Plasma physics group, in particular with D. Tidman (U. Maryland) and S. Yu (LLL), was most fruitful. It is clear from these interactions that atomic/molecular physics and data plays an important role as the input in the reactor chamber studies. The general design parameter of focusing an intense ion beam over 10 meter chamber radius onto a target 1 mm in diameter places severe conditions on the beam and on the Plasma generated in the gas filled reactor chamber.

For the ion beam inside the reactor chamber, one is interested in knowing the effective charge Z_{eff} of the ion as it is a function of propagation toward the target. Here the charge stripping process for ions comes from its interaction with atom/molecule gas at high energies. For the neutralization process that may help to reduce the self-pinch effect of the intense ion beam, one requires the knowledge of the electric conductivity, the plasma density, and the plasma temperature in the surrounding gas. This fundamentally requires the information of energy spectra $f(\varepsilon)$ of low energy electrons in the medium, which are in turn produced by

- Secondary electron energy spectra from the ionization of background gas by fast heavy ions.
- Secondary electron energy spectra from the ionization of background gas by slow electrons ($\lesssim$50 eV).
- Excitation cross sections for background gas by slow electrons
- Multiple ionization cross sections of heavy ions by background gas.
- Photoionization processes.

A paper by S. Yu is presented in this workshop section. A considerable amount of data for these atomic processes are available in literature. They are essential to a realistic modeling of plasma problems in the reactor chamber.

Finally, the problem of ion generation was discussed. This topic is being pursued by Barnett of ORNL.

References

1. "Born Cross Sections for Ion Atom Collisions" C. H. Gillespie, Y. K. Kim, and K. T. Cheng. Submitted to Phys. Rev. A.

2. K. K. Kim, Proceedings to the ERDA Summer Study of Heavy Ions for Inertial Fusion, 1976. LBL 5543.

2. ATOMIC CROSS SECTIONS FOR HEAVY-ION FUSION

K. T. Cheng, G. Das, Y.-K. Kim
and R. C. Raffenetti

LIMITS OF ION-ION COLLISION CROSS SECTIONS

Orders of magnitude estimates can be made on upper and lower limits to charge-changing cross sections for ion-ion collisions in a storage ring. The upper limit is set by charge transfer between ions, and the lower limit by ionization of inner-shell electrons.

In Figure V-A-2/1 we present our preliminary data on the molecular potential calculations for the Cs^+ ion. At large internuclear separation, R, the interaction between two Cs^+ ions is basically Coulomb repulsion, e^2/R. As R decreases, the interaction potential rises faster (i.e., becomes more repulsive) than the Coulomb potential. According to our calculations based on a pseudo-potential method[1], the interaction potential becomes very repulsive at $R \approx 4a_0$, where a_0 is the Bohr radius (0.529Å). Although we do not have the details of the upper potential curve for Cs^{++}-Cs^0 system yet, it is clear from Figure 1 that the upper curve for the charge transferred system will cross the lower Cs^+-Cs^+ curve near $R_x = 4a_0$. Furthermore, we note that the diameter of a Cs^+ ion is $4.2a_0$. This implies that R_x is the distance at which the valence shells of the ions touch each other.

A simple estimate of the maximum charge transfer cross section, σ_{max}, can be made from R_x:

$$\sigma_{max} \approx \tfrac{1}{2}\pi R_x^2, \qquad (1)$$

where

$$R_x = 2\,(r)_{valence} \qquad (2)$$

The factor ½ in Eq. (1) comes from the average probability for charge transfer.[2] The ion-ion collision energy at which the cross section reaches a maximum can be estimated only after we have details of the upper potential curve near R_x. In Table V-A-2/1 we listed $(r)_{valence}$ of various ions and corresponding σ_{max}.

At the HIF Workshop, Macek pointed out that the lower limit of the ion-ion collision cross section is set by ionization of inner-shell electrons. The inner-shell electrons are promoted to highly excited molecular orbitals when the inner shells of the ions penetrate each other, and the electrons are subsequently ionized as the ions separate after the collision. An estimate of the inner-shell ionization cross section is obtained from the radius of the core orbital with its principal quantum number reduced by one from that of the valence orbital[3], i.e.,

$$\sigma_{min} \approx \pi\,(\langle r\rangle_{core})^2. \qquad (3)$$

Values of $\langle r\rangle_{core}$ and corresponding σ_{min} for some ions are listed in Table V-A-2/1 also. The values of $\langle r\rangle$ were calculated from the relativistic Hartree-Fock wavefunctions.[4]

COLLISION OF IONS WITH BACKGROUND GASES

In collaboration with G. H. Gillespie (Physical Dynamics, Inc., La Jolla), we calculated a number of cross sections for collisions of Li^+, Cs^+, Au^+, and Hg^{n+} (n=2 ~ 52) with H_2, C, N, and O at high β (=v/c), based on the Born approximation.[5] The details are presented in Table V-A-2/2. These cross sections are upper limits to those for ionization of ions by the background gas. The Born cross sections are expected to be good to ~ 50% or better at high β (~ 0.2 and up), and thus sufficient for estimating vacuum requirements for storage rings and high-β portion of accelerators. Note in Table V-A-2/2 that the cross section decreases by an order of magnitude only when the Hg ion is stripped almost 50 times. At ANL, computer programs are now ready to calculate cross sections for any combination of ions and target gas for high-energy collisions. The cross sections should be reliable to ~ 50% or better.

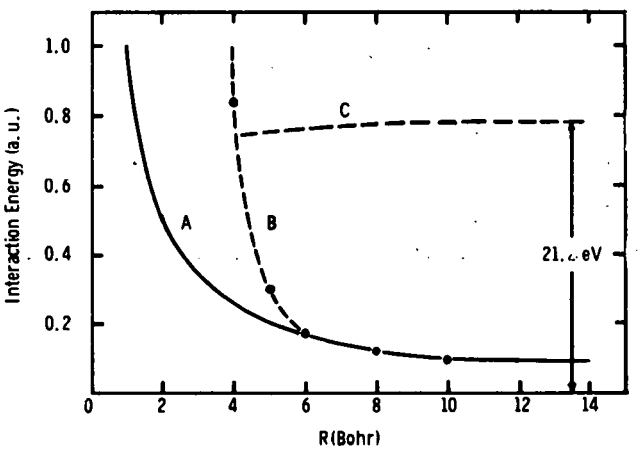

Fig. V-A-2/1. Potential curves for two Cs^+ ions. The ordinate is the interaction energy and the abscissa is the internuclear distance, both in atomic units. Curve A represents the Coulomb repulsion and Curve B shows our calculation for the repulsive ($^1\Sigma^+$) state of the $(Cs^+)_2$ molecule. Curve C is not based on reliable calculations, but it only indicates the relative position of the curve for the charge-transferred systems Cs^{++}-Cs^0. Curve C must lie 21.2 eV above Curve B at large R, but details at smaller R have not been calculated yet.

Table V-A-2/2. Born cross sections for total inelastic scattering of ions by background gases.[a]

$$\sigma_{in} = A\beta^{-2} + B\beta^{-4}$$

Ion	Target	A ($\AA^2$)	B ($\AA^2$)
Cs^+	H_2	7.46×10^{-3}	-5.4×10^{-5}
	N_2	9.34×10^{-2}	-2.1×10^{-4}
	O_2	1.04×10^{-1}	-1.9×10^{-4}
	CO	9.11×10^{-2}	-2.0×10^{-4}
Au^+	H_2	8.08×10^{-3}	-1.2×10^{-4}
	N_2	1.05×10^{-1}	-4.2×10^{-4}
	O_2	1.18×10^{-1}	-3.9×10^{-4}
	CO	1.02×10^{-1}	-4.2×10^{-4}
Hg^{2+}	N_2	9.71×10^{-2}	-2.4×10^{-4}
Hg^{20+}	N_2	3.68×10^{-2}	-2.4×10^{-4}
Hg^{34+}	N_2	2.24×10^{-2}	-1.1×10^{-4}
Hg^{52+}	N_2	6.04×10^{-3}	-1.0×10^{-4}

[a] Based on Ref. 5.

Table V-A-2/1. Limits of ion-ion collision cross sections based on the orbital sizes. See Eqs. (1) - (3) for notations. $\langle r \rangle$ in atomic units and σ in $\AA^2$.

Ion	$\langle r \rangle_{valence}$	σ_{max}	$\langle r \rangle_{core}$	σ_{min}
Cs^+	2.11	7.8	0.84	0.62
Au^+	1.58	4.4	0.50	0.22
Hg^{2+}	1.45	3.7	0.48	0.20
Hg^{5+}	1.31	3.0	0.48	0.20
Hg^{10+}	1.14	2.3	0.48	0.20
Hg^{20+}	0.46	0.4	0.17	0.03
U^I	3.88	26	0.90	0.71
U^{6+}	1.68	5.0	0.88	0.68
U^{20+}	0.78	1.1	0.35	0.11

References

* Work performed under the auspices of the U.S. Department of Energy.

1. G. Das and A. C. Wahl, J. Chem. Phys. 64, 4672 (1976).
2. See, for instance, R. E. Olson, F. T. Smith, and E. Bauer, Appl. Opt. 10, 1848 (1971).
3. B. Fastrup and G. Hermann, Phys. Rev. A 3, 1955 (1971).
4. J. P. Desclaux, Comput. Phys. Commun. 9, 31 (1975).
5. G. H. Gillespie, Y.-K. Kim, and K. T. Cheng, Born cross sections for ion-atom collisions, submitted to Phys. Rev. A.

3. STATUS OF HIGH-VELOCITY ATOMIC CROSS SECTION THEORY

George H. Gillespie

INTRODUCTION

Since the summer study last year[1], a number of specific calculations of atomic collision cross sections have been carried out in collaboration with Y.-K. Kim and K. T. Cheng of Argonne.[2] The goal of that work has been to provide some quantitative results for at least a few high-velocity cross sections relevant to the establishment of vacuum requirements. In addition to the work described in Ref. 2, there have also been some further calculations of a more exploratory nature, for the purpose of developing a clearer picture of the overall scheme of things. Particular questions which have been examined concern the charge state dependence of the cross sections, dependence of the cross sections on atomic number for a given net charge of the ion, and the relative contributions of excitation and ionization (electron-loss) processes to the total sum rule cross sections calculated in the approach used for these high-velocity problems. This note is an effort to tie some of these results together and, at the least, to collect them in one place.

The questions posed above all have a direct bearing on the vacuum problem. They are also important when one considers the role of such cross sections in the beam transport through a high-density gas region, such as may occur in the reaction chamber. While it will become clear that the answers are at present incomplete, there is enough information available that some definitive statements can be made.

NOTATION

A detailed discussion of the underlying theoretical treatment of the Born approximation cross sections will be avoided, there are sufficient references available on the methods used (Refs. 1 and 2, and additional references cited therein). There have been enough changes in notation, however, that some definitions are required. A particular cross section may be written as

$$\sigma \equiv 8\pi a_0^2 \frac{\alpha^2}{\beta^2} [I] , \qquad (1)$$

where

$$8\pi a_0^2 \alpha^2 = 3.75 \times 10^{-20} \text{ cm}^2 , \qquad (2)$$

and $\beta = v/c$. The parameter $[I]$ appearing in (1) will be referred to as the collision strength. At high velocities it is essentially independent of the energy (with at most a logarithmic dependence). Results are either expressed in terms of σ, $\beta^2\sigma$, or the collision strength, one being readily interchanged for the other via Eqs. (1-2). Various subscripts are used with the collision strength to define particular processes. They are used as ordered pairs generally, the first subscript referring to a process of the incident ion, the second for a process relevant to the target atom or molecule. Most are self-explanatory [ion=ionization; ex=excitation; el=elastic, i.e., the electronic final state is the same as the initial state; in=inelastic, i.e., the electronic final state is different from the initial state, which means either ionization or excitation has occurred].

UPPER BOUNDS ON ELECTRON STRIPPING CROSS SECTIONS FOR SINGLY CHARGED IONS

Figure V-A-3/1 provides a plot of the total excitation plus ionization cross sections for singly charged ions incident on H_2 or N_2 gases. The graph shows these as a function of the atomic number of the ion $[Z_N^{(1)}]$. The cross sections provide upper bounds to the stripping cross sections for any singly charged ion. The open circles give the results for explicit calculations[3] for the ions indicated; the solid lines are simply smooth curves drawn through them which should be useful for interpolation. For a given target gas, the cross sections generally rise in proportion to the atomic number $[Z_N^{(1)}]$, for $Z_N^{(1)} \leq 40$. This is expected since these cross sections are proportional to the number of electrons in the ion $[Z_e^{(1)}]$ and this differs only by one from the atomic number. This scaling was briefly discussed in last year's summer study but it is clear now that it breaks down for very heavy ions. For $Z_N^{(1)} > 50$, all of the cross sections for a particular target are the same within a factor of 1.3 or so, and are significantly below a linear extrapolation of the results for lighter ions. This simply reflects the fact that the geometrical size of these ions no longer increases substantially with atomic number. Some effects arising from the shell structure are also expected, but further calculations are required to assess this quantitatively.

HOW MUCH OF THE UPPER BOUND CROSS SECTION ARISES FROM EXCITATION?

This question arises because one is interested here in the charge changing cross sections, [i.e., at high velocity, the electron-loss cross sections], whereas the sum rule cross sections include excitation to any of several discrete bound states which do not result in any change in the ion's charge. One would like to know just how far above the electron stripping cross section does the calculated upper bound lie.

A precise answer to this question for a complex many-electron ion requires considerably more effort than has been expended in obtaining the upper bound cross sections. Nevertheless, this question can be answered within the context of a special class of ions, namely those consisting of only one electron. In this case the direct ionization contribution, and the discrete excitation to bound states, may be calculated separately. While conclusions based on an examination of one-electron-ion cross sections must be prefaced with some

caution, the results of such a study are not totally irrelevant. The relative contributions of excitation and ionization (i.e., electron-loss) to the total cross section is expected to depend largely on the binding energy of the last electron. The weaker the binding, the larger the relative contribution of ionization to the total cross sections. Furthermore, ions with similar binding energies, although differing in other respects, can be expected to have similar relative contributions to excitation and ionization.

Tables V-A-3/1 and V-A-3/2 give results for several one-electron ions for the collision strengths for either excitation ($I_{ex,el} + I_{ex,in}$) or ionization ($I_{ion,el} + I_{ion,in}$), as well as the sum of these two contributions ($I_{in,el} + I_{in,in}$) which determines the total upper bound cross sections.[4] (The actual cross sections may be obtained by substituting in (1) these collision strengths.) Targets considered are H_2 (Table V-A-3/1) and atomic N (Table V-A-3/2). In addition the percentages of the totals which are due to either excitation or ionization are shown in parentheses following each of the corresponding collision strengths.

Two points readily emerge upon examining percentages given in these tables. For the (relatively) weakly bound ion He^+, the total sum rule cross sections for either target are clearly dominated by the electron loss contributions (70-80%). As one goes to increased electron binding, this percentage does decrease, but even for the case of the 29 times ionized Zn ion, the electron loss contribution still exceeds 40% of the calculated sum rule cross section. These results suggest that, unless one is interested in the vacuum requirements for ions which are more than about 10 times ionized, cross sections calculated using the sum rule approach will not overestimate the electron loss cross sections by more than a factor of 2.

DEPENDENCE OF CROSS SECTIONS ON ION CHARGE STATE

In collaboration with Y.-K. Kim and K. T. Cheng some calculations of cross section parameters have been carried out for Hg ions in selected charge states. Table V-A-3/3 gives results for the collision strengths for five different Hg ions incident on atomic nitrogen. The upper bounds on the electron stripping cross sections are given

Table V-A-3/1. Contributions of Excitation and Ionization to Sum Rule Cross Sections for One-Electron Ions Incident on H_2.

$Z_N^{(1)}$	(Ion)	Excitation $I_{ex,el}+I_{ex,in}$	(%)	Ionization $I_{ion,el}+I_{ion,in}$	(%)	Total $I_{in,el}+I_{in,in}$
2	(He^+)	.229	(30.6)	.521	(69.4)	.751
4	(Be^{3+})	.129	(39.9)	.194	(60.1)	.322
6	(C^{6+})	.0820	(44.6)	.102	(55.4)	.184
8	(O^{7+})	.0573	(47.5)	.0632	(52.5)	.121
10	(Ne^{9+})	.0425	(49.5)	.0433	(50.5)	.0857
12	(Mg^{11+})	.0329	(51.0)	.0316	(49.0)	.0645
14	(Si^{13+})	.0263	(52.2)	.0242	(47.8)	.0505
16	(S^{15+})	.0216	(57.9)	.0191	(42.1)	.0455
18	(Ar^{17+})	.0181	(53.8)	.0155	(46.2)	.0336
20	(Ca^{19+})	.0154	(54.5)	.0129	(45.5)	.0283
22	(Ti^{21+})	.0133	(55.0)	.0109	(45.0)	.0242
24	(Cr^{23+})	.0116	(55.5)	.00931	(44.5)	.0209
26	(Fe^{25+})	.0102	(55.9)	.00807	(44.1)	.0183
28	(Ni^{27+})	.00908	(56.3)	.00706	(43.7)	.0161
30	(Zn^{29+})	.00813	(56.6)	.00623	(43.4)	.0144

Table V-A-3/2. Contributions of Excitation and Ionization to Sum Rule Cross Sections for One-Electron Ions Incident on Atomic Nitrogen.

$Z_N^{(1)}$	(Ion)	Excitation $I_{ex,el}+I_{ex,in}$	(%)	Ionization $I_{ion,el}+I_{ion,in}$	(%)	Total $I_{in,el}+I_{in,in}$
2	(He^{+})	.946	(20.3)	3.71	(79.7)	4.66
4	(Be^{3+})	.740	(31.3)	1.62	(68.7)	2.36
6	(C^{5+})	.539	(37.0)	.917	(63.0)	1.46
8	(O^{7+})	.405	(40.5)	.597	(59.5)	1.00
10	(Ne^{9+})	.316	(48.9)	.423	(51.1)	.828
12	(Mg^{11+})	.255	(44.5)	.317	(55.5)	.572
14	(Si^{13+})	.210	(45.8)	.248	(54.2)	.458
16	(S^{15+})	.177	(47.0)	.199	(53.0)	.376
18	(Ar^{17+})	.151	(47.9)	.164	(52.1)	.315
20	(Ca^{19+})	.131	(48.7)	.138	(51.3)	.269
22	(Ti^{21+})	.115	(49.4)	.117	(50.6)	.232
24	(Cr^{23+})	.102	(51.0)	.0980	(49.0)	.200
26	(Fe^{25+})	.0908	(50.6)	.0885	(49.4)	.179
28	(Ni^{27+})	.0816	(50.5)	.0799	(49.5)	.162
30	(Zn^{29+})	.0738	(51.6)	.0692	(48.4)	.143

by Eq. (1), where the appropriate collision strength is $I_{in,el} + I_{in,in}$. As expected, this cross section decreases as one goes to higher charge states, but the change is modest. A reduction of about 30% is found in going from Hg^{2+} to Hg^{10+}; 61% in going to Hg^{20+}.

Table V-A-3/3 also gives results for the total elastic collision strength ($I_{el,el}$) as well as for the parameter $\mathcal{J}_1-\mathcal{J}_2$ which appears in the cross section for the inelastic scattering of the target atom. [$\frac{1}{2}(\mathcal{J}_1 - \mathcal{J}_2)$ is essentially the effective collision strength $I_{el,in}$.] These parameters increase with increasing net charge of the ion, as expected, but again the change is modest for the lower charge states.

Table V-A-3/3. Results for Selected Hg Ions Incident on N.

Incident Ion	$I_{el,el}$	$I_{in,el}$	$I_{in,in}$	$\mathcal{J}_1-\mathcal{J}_2$
Hg^{2+}	4.74×10^{3}	9.98×10^{1}	2.95×10^{1}	2.03×10^{3}
Hg^{10+}	5.06×10^{3}	6.95×10^{1}	1.83×10^{1}	2.11×10^{3}
Hg^{20+}	6.25×10^{3}	3.98×10^{1}	9.29	2.31×10^{3}
Hg^{34+}	1.06×10^{4}	2.44×10^{1}	5.50	3.47×10^{3}
Hg^{52+}	1.94×10^{4}	6.71	1.36	5.81×10^{3}

SUMMARY

All of the theoretical work carried out to date suggests strongly that the sum rule method, for calculating upper bound cross sections, will not grossly overestimate the electron stripping cross sections (i.e., is within a factor of 2) provided that the charge state of the ion is not too high. The theory is, of course, only valid at high velocities, and only the leading order cross sections have been considered here. The next order terms can be evaluated, and have been in selected cases.[2] Again, if the charge state is not too high, it appears that the leading order is sufficient for velocities greater than that corresponding to a few MeV/nucleon. This leads to the conclusion that for the purpose of establishing vacuum requirements of most ions currently under consideration for accelerators, storage rings or transport systems (with the possible exception of the low-β region), this method provides rigorous upper bound cross sections which are not gross overestimates of the actual electron stripping cross sections.[5]

For problems such as neutralized beam transport, and propagation of the beam in the high density gas or plasma present in a reaction chamber, the high-velocity atomic data required is more detailed than that necessary for establishing vacuum transport requirements. While the theoretical approaches used in the latter can provide some information for these types of problems, in most cases, some alternative approaches will probably be necessary.

ACKNOWLEDGEMENTS

Many of the ideas considered here are the outgrowth of discussions with a large number of people. The collaboration with Y.-K. Kim and K. T. Cheng has clearly been fruitful. In addition, conversations with S. Yu, of Lawrence Livermore Laboratory, on reaction chamber problems have been very useful. The support of the Physical Dynamics' Independent Research and Development Fund is, again, greatly appreciated.

References

1. R. O. Bangerter, W. B. Herrmannsfeldt, D. L. Judd and L. Smith, editors, ERDA Summer Study of Heavy Ions for Inertial Fusion, Final Report, LBL-5543 (1976).

2. G. H. Gillespie, Y.-K. Kim and K. T. Cheng, "Born Cross Sections for Ion-Atom Collisions", submitted for publication.

3. The calculated data in Fig. V-A-3/1 for He^+ are from Tables V-A-3/1 and V-A-3/2; that for Li^+, Cs^+ and Au^+ are from Ref. 2. The data for Na^+ utilizes the incoherent scattering function as calculated by K. Tanaka and F. Sasaki [Int. J. Quantum Chem. 5, 157 (1971)]. The results for U^+ were calculated by Y.-K. Kim and K. T. Cheng during this workshop, and represent about 30% reduction from the estimates of last year's summer study [Ref. 1].

4. The values for the total (sum rule) and ionization collision strengths were calculated directly using the known hydrogenic-like incoherent scattering function and generalized oscillator strength for continuum final states. The excitation collision strengths given were obtained by subtracting the values of these two. However, the excitation strengths were checked by calculating directly the excitations up to the n = 8 level for the one-electron ions again using the known hydrogenic-like inelastic form factors. In each case, the discrete excitations up to and including the n = 8 level, reproduced the total excitation collision strengths given in Tables V-A-3/1 and V-A-3/2 to within 97%.

5. While the confidence in the theory at this level of accuracy is good, a direct experimental verification for a heavy ion, with many electrons, in this velocity regime, would clearly be very desirable. There are experimental verifications for light ions over a significant velocity range, but not for the low charge state heavy ions of interest here.

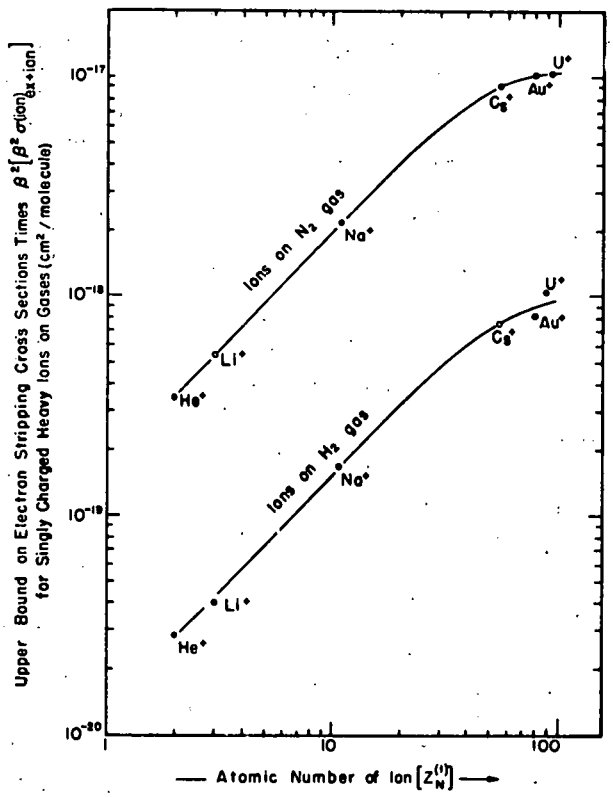

Fig. V-D-3/1. Sum rule cross sections times β^2, which provide upper bounds to the electron stripping cross sections, for singly charged ions as a function of the ion atomic number. The open circles are the results of calculations for the specific ions indicated (see Note 3), the solid lines are simply smooth curves drawn through these points.

4. ATOMIC DATA NEEDS FOR BEAM TRANSPORT IN GAS

Simon S. Yu

INTRODUCTION

Determination of the parameters Z_{eff}, electrical conductivity, plasma density, and the plasma temperature is essential in the study of heavy ion beam transport in gas. The calculation of these parameters require input from atomic physics. This note is an attempt to make these needs known to atomic physicists.

DISCUSSION

The following list summarizes some of the data needs for the study of heavy ion beam transport in a gas-filled reactor:

1. Secondary electron energy spectra from the ionization of background gas by fast heavy ions.
2. Secondary electron energy spectra from the ionization of background gas by slow electrons ($\lesssim$ 50 eV).
3. Excitation cross sections for background gas by slow electrons.
4. Multiple ionization cross sections of heavy ions by background gas.

One of the critical issues of the heavy ion fusion program is the feasibility of transporting an ion beam through a gaseous medium without severe disruptions. The motion of the beam, (and therefore, its stability) is determined by the interplay between the beam current and the plasma response. In the determination of both the beam current and the plasma response, certain parameters directly related to atomic collisions play a major role. The purpose of this note is to draw attention to these parameters.

To determine the beam current, the effective charge of the ion Z_{eff} is needed. The plasma response is characterized by three related quantities: the electrical conductivity σ, the plasma density n_e, and the plasma temperature T_e. If the energy spectra of low energy electrons in the medium, $f(\epsilon)$ are known, the latter three parameters are determined.

As the heavy ion beam traverses the gas medium, it goes through a continuous process of stripping, which results in an increase in the beam current. The total beam current is

$$I_b = Z_{eff}\, I_o$$

where I_o is the incoming beam current (of charge state +1) and Z_{eff} is a function of the ion position in the gas medium, given by

$$Z_{eff} = \sum Z N_z \Big/ \sum N_z \ .$$

N_z is the number density of ions with charge Z, and the sum is performed over all charge states. Since the current represents the primary driving force in the beam transport problem, the determination of Z_{eff} as a function of the beam position in the reactor is crucial.

It is clear that in order to determine the relative population of various charge states at a given point in time (or space), it is necessary to know its collisional history. This requires not only the knowledge of the total stripping cross sections, but also the individual cross sections for multiple ionization. A direct computation of the evolution of charge states would involve a transport equation with the individual ionization cross sections as input.

The present calculation (1) of Z_{eff} is based upon a classical binary encounter model with binding energies obtained from relativisitic Hartree-Fock-Slater type calculations. The assumption of independent particle model permits us to bypass the problem of calculating multiple ionization cross sections. In Table V-A-4/1, the total ionization cross sections computed from the binary encounter model are compared with the total inelastic Born cross sections computed by Gillespie and Kim[2]. A conclusion regarding the validity of the classical binary encounter calculations at this point may be premature. In any case, it would be desirable to have results from several different calculational schemes.

The question of the needed accuracy for Z_{eff} is somewhat difficult to answer, since it depends strongly on the specific effect under consideration. In the example of the self-pinch effect, the magnetic force which is responsible for pinching the ion beam is proportional roughly to Z_{eff}^2. Thus an error of 2 in Z_{eff} will result in an error of 4 in the determination of the self-pinch force.

The major parameter of interest in determining the plasma response is the conductivity σ. In the simplest approximation, the conductivity is given in terms of the density of low energy electrons in the medium n_e, and their average energy, or, the plasma temperature T_e. The relation is

$$\sigma = \frac{e^2}{m} \frac{n_e}{\nu_m(T_e)}$$

where ν_m is the frequency of momentum transfer collisions, and can be obtained from direct measurements.

As the heavy ion beam passes through the medium, plasma electrons are created through ionization processes. When a few percent of the gas is ionized, (which occurs not far from the head of the pulse in the case of a pencil-shaped beam) ν_m is determined by electron-ion collisions and is

proportional to $n_e T_e^{-3/2}$. The conductivity then becomes independent of the plasma density, and depends only on the plasma temperature. Thus, a correct determination of the plasma temperature is an essential part of the conductivity calculation. The plasma density is relevant for the conductivity calculation before the gas medium becomes highly ionized. It is also of interest independently for other instability questions.

To calculate the temperature of the plasma, one would need to know $f(\epsilon)$, the energy spectrum of slow electrons in the medium. The plasma density is just the integral of $f(\epsilon)$ over all energies. Furthermore, in more sophisticated calculations, the relation of the conductivity to n_e and T_e is bypassed, and the conductivity is related directly to $f(\epsilon)$. For example, the conductivity in a predominantly neutral medium is given by

$$\sigma = -\frac{2}{3}\frac{e^2}{m}\int_0^\infty d\epsilon \, \frac{\epsilon^{3/2}}{\nu_m(\epsilon)} \frac{d}{d\epsilon}\left(\frac{f(\epsilon)}{\epsilon^{1/2}}\right)$$

Thus, the determination of $f(\epsilon)$ is essential for studying the plasma response.

The production of these low energy electrons, as well as their evolution with time, are consequences of the interplay between the electric field due to the beam and the atomic processes which take place in the medium.

Direct ionization of the background gas by stripped heavy ions is an important source of the low energy electrons. The quantities of interest are the secondary electron spectra from direct ionization by various charge states of the heavy ion. During the passage of the beam, the background medium can become highly ionized. Thus, we are interested not only in the ionization of neutral background gas, but also of the gas in various ionized and excited states. If the detailed calculation of all possible configuration is too cumbersome, it would be useful at least to know the relative importance of the various processes.

Another important source of electrons is the "avalanche" effect. An intense ion beam passing through the medium creates an electric field which could accelerate slow electrons to energies above the ionization threshold. These electrons then undergo ionizing collisions to create more electrons. The quantities of interest are the secondary electron spectra from the ionization of background gas by electrons in the threshold region ($\lesssim$50 ev). At gas pressures of around 1 torr, the "avalanche" effect is comparable to direct ionization. Thus, it is important to account for this effect properly. If the secondary electron spectra at these low energies are hard to obtain, the total ionization cross sections above threshold can be quite useful for making estimates.

The electrons produced by the above effects go through a continuous process of evolution due to all other atomic processes which take place in the medium. In a monatomic gas like Li, one expects electronic excitation to be the only additional process of importance. However, in a molecular gas, like N_2, or air, there are many more possible processes, e.g. vibrations, dissociative recombination, etc. The history of evolution can be traced by a Boltzman Equation with the atomic and molecular cross sections as input.

While the total number of possible atomic and molecular processes in the gas medium may be large, one may not necessarily have to consider all of them for the heavy ion beam problem. The reason is that we are interested primarily in the plasma response <u>during</u> the passage of the beam. The pulse time of interest is quite short. Any process with a collision time long compared to the pulse length may be neglected. At pressure of $\sim$1 torr, the fast atomic processes have collision times which are comparable to the pulse time. Thus, we do not expect drastic modifications of the secondary energy spectrum from direct ionization and avalanche by other atomic processes to take place during the pulse-on time.

The author wishes to thank Ed Lee for some very helpful comments on the writing of this manuscript.

Table V-A-4/1. Cross Sections for the Stripping of Heavy Ions: A comparison of the Born inelastic cross sections and binary encounter model calculations of the ionization cross section.

Ion	Target	$A^{(Born)} \approx \sigma_{in}\beta^2(A^2)$	$A^{(BE)} \approx \sigma_{ion}\beta^2(A^2)$
Hg^{52+}	N_2	6.04×10^{-3}	1.87×10^{-3}
Hg^{34+}	N_2	2.24×10^{-2}	1.18×10^{-2}
Hg^{20+}	N_2	3.68×10^{-2}	2.18×10^{-2}
Hg^{2+}	N_2	9.71×10^{-2}	2.16×10^{-1}

References

1. "Propagation of a Heavy Ion Beam in a Gas-Filled Reactor", S. S. Yu, H. L. Buchanan, F. W. Chambers, E. P. Lee. The Present Proceedings.
2. See "Atomic Cross Sections for Heavy-Ion Fusion", K. T. Cheng, G. Das, Y. K. Kim, and R. C. Raffenetti. Presented at the Brookhaven Heavy Ion Fusion Workshop.

B. PLASMA AND NEUTRALIZATION EFFECTS

1. SUMMARY

D. A. Tidman

The plasma working group considered the question of whether an intense heavy ion beam could be transported and accurately focussed across a target chamber radius of $\sim$ 10 m on to a pellet of radius $\sim$ 0.1 cm at the center of the chamber (a typical beam was taken as 3 kA, 40 GeV uranium injected into the reactor vessel with initial beam radius $\sim$ 10 cm). Here we give a brief summary of our considerations, the details of which are included in papers 2-6 of this section of this report. The conclusions were that focussing through relatively dense reactor chamber gases appears to be possible. Instabilities, if they arise, are expected only within the last few 10's of cm from the pellet, by which time they are unlikely to significantly degrade the beam focussing.

The beam interaction processes that occur depend on the environment (gas and possible fields) in the chamber. The gas pressure range taken to be of most interest was approximately 10^{-2} torr $< p <$ 10 torr, i.e., assuming cool gas to be present just before a pellet ignition event. This corresponds roughly to a number density range $3\cdot10^{14} < n_o < 3\cdot10^{17}$ cm^{-3}. This range of relatively high densities (for which beam stripping occurs) was viewed as desirable in that it is consistent with use of a liquid Li waterfall reactor chamber (the vapor pressure of liquid Li at 500°C is $\sim 5\cdot10^{-3}$ torr), and such a modest vacuum is easy to maintain. The higher vacuum range that avoids stripping (emphasized more in the summer study report LBL-5543) remains an option if this higher density liquid Li reactor environment gives difficulties not perceived by our group. The upper limit in density is set by noting that above about 10 torr multiple scattering spreads a typical beam beyond 0.1 cm in 10 m. We also note that the chemical composition of gas actually present in the chamber, apart from Li, can to some extent be chosen by other considerations, such as its ability to produce high conductivity when traversed by the beam pulse.

In addition to the gas environment, there may also be stray magnetic fields (1 - 10 G) present in the target chamber that were generated by the previous pellet explosion. These are discussed in paper 5 of this section and may have to be swept out of the chamber (this may occur automatically in the Li waterfall case).

As the ion pulse propagates it undergoes stripping (e.g. a 100 GeV U ion strips to $Z_b \approx 70$ in traversing 10 m of N_2 at 1 torr). This process, together with focussing, can elevate the beam current density by several orders of magnitude as it approaches the pellet. At the head of the pulse, gas ionization is produced both by beam-gas collisions and by electron avalanching in the strong electric fields in this region (Fig. V-B-1/1) These processes continue through the pulse until some limiting process such as recombination or finite pulse length limits the electron density and its attendant conductivity to a maximum value. This conductivity allows a return current density j_e to flow in the plasma in response to the induced field, which in turn reduces the net current j_n in the pulse below that of the bare beam j_b. Charge neutralization occurs within a few cm of the pulse head.

The strength of the pinch magnetic field associated with the net current $j_n = j_b + j_e$ determines the growth rate of instabilities such as the resistive firehose, or filamentation, etc. Micro-instabilities may also derive from interaction between the beam ions and background electrons (e - b mode) and background electrons with background ions due to j_e (e - i) mode.

In papers 2 and 3 of this section, and also in the appendix to this summary, some results for propagation models are given. The important feature on which they agree is that for pressures in the 1 torr range current neutralization is better than 98% even though stripping occurs. This is because as the beam ions strip they become more effective at producing background plasma, both via collisional ionization ($\sim Z_b^2$) and via gas breakdown. This results in a more rapid rise in conductivity at the head of the pulse where the induced E field drives the return current.

For this high degree of current neutralization resistive firehose instability does not grow significantly during a beam transit time across the chamber radius (for the case of an injected beam radius of 10 cm as in Fig. V-B-1/1). The possibility of resistive filamentation of the beam close to the pellet is still an open question. However, in paper 2 of this section it is pointed out that finite emittance may stabilize this instability.

Investigation of micro-instabilities (papers 2, 4 and 5 of this section) found that they would grow, if at all, only when the beam is within a few 10's of cm from the pellet. These modes tend to be pushed towards stability by the effects of collisions (for pressures of $\sim$ 1 torr) and by phase mixing due to the finite beam velocity spread. Although micro-instabilities may well occur close to the pellet, it was thought that this would be too late to significantly degrade the beam focussing.

The Livermore group (paper 2 of this section) has suggested a more ambitious beam propagation mode, namely that it might be possible to transport the ion beam across the entire chamber radius in a pinched state, i.e., inject it at the edge with a radius of $\sim$ 0.5 cm. Micro-instability could be potentially more damaging in this case in that it gives rise to decreased conductivity which in turn influences the return current decay and the attendant resistive firehose growth rate. This interplay between micro and MHD instabilities is not described in any of the existing computer models. However, experimental evidence with electron beams ($\sim$ 10 kA, γ = 3) indicates stable pinched propagation for a pressure range window of 1 - 5 torr, although the beams in these experiments were propagated down the axis of a cylinder (typically of radius $\sim$ 10 cm) which may play a stabilizing role.

Our group also noted that the high degree of current neutralization predicted by the propagation models may have other desirable consequences. For example one expects the interaction between several beams (Fig. V-B-1/2) to be reduced in comparison to the corresponding vacuum case. The field of a single beam near the pellet is approximately $B = f\, I_{bo}\, Z_b/5r\, Z_o$, so that for an injected current and charge $I_{bo} = 3\cdot10^3$A, $Z_o = 3$, which strips to a charge state $Z_b = 70$ near the pellet where r = 0.1, and assuming the fractional current neutralization is $f = 10^{-2}$, we find $B \approx 4$ kG. The field of a given beam has insufficient time in the pulse duration time ($\sim$ 5 nsec) to diffuse into the plasma channel of a neighboring pulse. The attractive body forces between neighboring pulses thus act on the combined mass density, ρ, of beam plus plasma which would produce lateral beam motions characterized by the Alfven velocity $B/\sqrt{4\pi\rho}$. This velocity is typically $\leq 10^{-3}c$ near the pellet and would produce negligible deflections. Similarly the electron deficit created at the outer edge of a pulse by charge neutralization near the pulse head would be slightly redistributed by the E field of a neighbor. The result is equivalent to an electric force that acts on the combined beam plus plasma mass density as in the magnetic case.

APPENDIX

The general pulse propagation problem involves solving a set of equations in axi-symmetry, i.e., for independent variables r, z, ξ, where r is the radial position, ξ is measured from the pulse tail, and z is the displacement of the pulse from the accelerator injection point. The equations have been simplified by integrating over beam radius assuming Bennet distributions for both the beam and plasma currents. The result is a coupled system of equations consisting of an equation for the electron density containing avalanching, direct production by beam-gas collisions, and dissociative recombination, together with an equation for the net pulse current derived from a transmission line model.

The variables are,

N_e = plasma electron density/cm
E = z-field in V/cm
a = radius of pulse, cm.
I_n = net current, amps.
I_b = beams current, amps, = $\pi a^2 j_b$
z = displacement of pulse from the injection point.
ξ = position along pulse measured from tail, cm., i.e., $\xi = L_p$ = nose position, $\xi = 0$ is tail.
σ = radial average conductivity
ξ_c = charge neutralization distance measured back from nose
p = air pressure in torr corresponding to air density, i.e., p = 760/D
D = n_o/n = air density at 1 Atm/air density (note, D > 1 for low densities)
L = radiation length (= $3\cdot10^4$ cm for air)
R_c = estimate of displaced charge radius used in ℓn factor of transmission line model
T_e = electron temperature in eV (typically fairly constant).

A system of equations describing pulse propagation for the case of an air atmosphere are the electron density equation,

$$-\frac{\partial N_e}{\partial \xi} = 2\cdot10^{10}\,\frac{I_b}{D}\left(\frac{Z_b}{\beta_b^3}\right) - \frac{6\cdot10^{-20}N_e^2}{a^2}$$

(ionizing collisions) (dissociative recombination of O_2^+)

$$+ 6.3\cdot10^{-6}\, EN_e e^{-222p/E}\left\{\frac{(E/p)^{\frac{1}{2}}}{1 + 4\cdot10^{-4}E/p}\right\},$$

(avalanching)

and net current equation

$$\frac{2\pi a^2 \sigma}{c}\frac{\partial}{\partial \xi}\left\{\left(\ell n\,\frac{R_c}{a} + \frac{1}{4}\right) I_n\right\} + I_n = -I_b\ ,$$

with the conductivity σ given by

$$\frac{1}{\sigma} = \frac{a^2 T_e^{\frac{1}{2}}}{5.7\cdot10^{-5} N_e D} + \frac{\ell n \Lambda}{1.7\cdot10^{14} T_e^{3/2}}\ ,$$

and T_e is in eV. The beam current I_b is

$$I_b = I_{bo}\left(\frac{Z_b}{Z_o}\right)$$

where Z_o, I_{bo}, are the injected beam charge state and current. The charge state Z_b was modeled by an exponential ramp

$$Z_b = Z_o + (Z_{b\infty} - Z_o)\ (1 - e^{-z/\ell}) \quad ,$$

where the final stripped state $Z_{b\infty}$ for an ion of given energy was approached in a characteristic stripping length ℓ.

The pinch magnetic field, and axial electric field used in the N_e equation, were given by

$$B(a) = \frac{2I_n}{ac}$$

$$E = 60\ \frac{\partial}{\partial \xi}\left\{\left(\ell n\ \frac{R_c}{a} + \frac{1}{4}\right) I_n\right\}\ S \text{ volts/cm}$$

$$S = 1 - \exp\ -\frac{(L_p - \xi)^2}{\xi_c^2}$$

and the spatial dependence of the beam envelope radius $a(\xi,z)$ was determined from the injection radius and focussing requirement as in Fig. V-B-1/1.

The above system of equations can be solved for various assumed beam current profiles. An example is shown in Fig. V-B-1/3 that illustrates the 98% current neutralization referred to in the text, in approximate agreement with Papers 2 and 3. I am grateful to Dr. D. Spicer who wrote the code that gave these results.

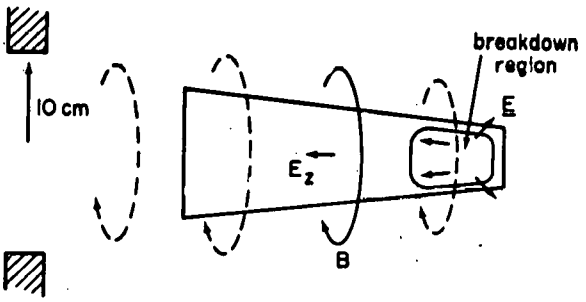

Fig. V-B-1/1. Focussed ion beam pulse and its self fields.

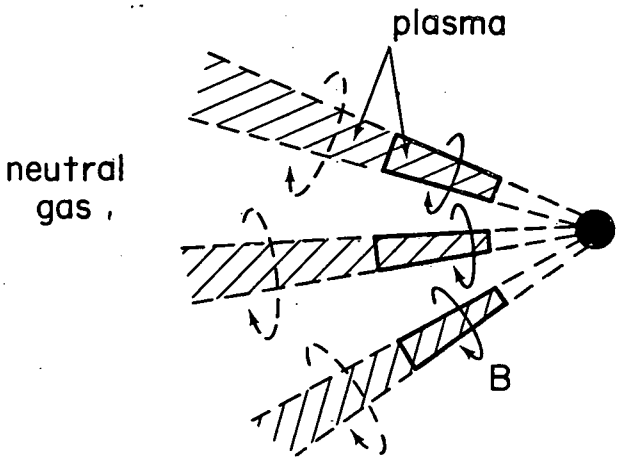

Fig. V-B-1/2. Convergence of several beams on a target.

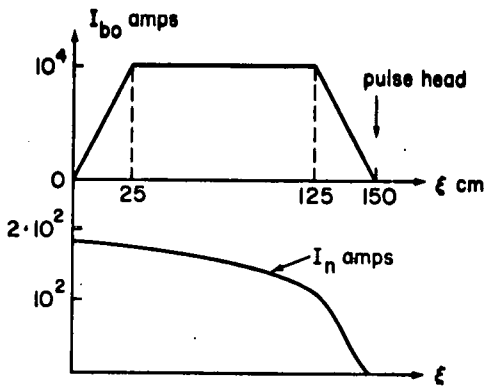

Fig. V-B1/3. Net current and injected beam current along a 10 nsec pulse of U ions traveling with velocity c/2 (energy 34.5 GeV) through air at 7.6 torr. Pulse rise time is 1.66 nsec, injected charge state 3, injected beam radius 10 cm, and the ions have stripped to a charge state $Z_b = 50$. This particular plot of $I_n(\xi)$ is taken when the head of the pluse has just reached the pellet of radius 0.1 cm.

2. PROPAGATION OF A HEAVY ION BEAM IN A GAS-FILLED REACTOR

S. S. Yu, H. L. Buchanan,
F. W. Chambers and E. P. Lee

INTRODUCTION

A gas-filled reactor vessel (P ≈ 1 Torr) has several advantages compared with a highly evacuated vessel. The pumping requirements are not as stringent, and the gas provides some shielding for the reactor wall from ablative x-rays and energetic charged particles. A liquid Li "waterfall" layer, which has finite vapor pressure, is consistent with such an environment. In addition, gas propagation may allow a greater range of beam parameters.

The subject of our investigation is to determine whether a heavy ion beam can be transported in gas, without severe disruption, to hit a mm-sized target at ranges ~ 10 m. We are interested primarily in the propagation of a pencil-shaped self-pinched ion beam which enters the chamber through a small aperture, although our transport code also treats other cylindrically symmetric configurations. It has been demonstrated both theoretically and experimentally that an intense electron beam can be stably transported over large distances in the 1 torr pressure range (1). The critical question is whether these results can be extended to high energy heavy ion beams. We discuss first the propagation characteristics of ion beams and then the instabilities which may disrupt beam propagation.

PROPAGATION

An important feature of the transport problem is that the heavy ions go through a continuous process of stripping as they traverse the target chamber. Our calculations indicate that, in the example of a 100 GeV U^{+}_{238} beam traversing 10 meters of N_2 at 1 torr, the effective charge state of the ions can be as high as 70 when they reach the target. The effective charge as a function of the distance travelled for these parameters is plotted in Figure V-B-2/1.

The effect of this stripping process on the self-fields of the beam is quite interesting. On the one hand, stripping causes the beam current to increase rapidly as a function of distance travelled. This strong current could in principle lead to large self-fields and disruption of propagation. On the other hand, the stripped beam ions are very effective in ionizing the background gas, thus generating a highly conductive medium in a very short time. This leads in turn to a high degree of charge and current neutralization, cancelling the potential disruptive effects of a strong beam current. Our calculations indicate that, for typical parameters, we have more than 99% current neutralization and complete charge neutralization over most of the pulse length.

The effect of this small net current on the motion of the beam is not obvious. The self-pinch force acting on the beam is proportional to the product $Z_{eff}\ I_{net}$. While I_{net} is small as a result of the high degree of current neutralization, Z_{eff} is large because of stripping. Quantitative predictions for the beam radius can be made only from a detailed analysis of a beam envelope equation. To do this, we have developed a beam propagation code. The technical details of this code are given in the Appendix. In addition to the magnetic self-pinch, the code also includes the effects of the initial beam emittance, small angle multiple scattering, and phase-mix damping of oscillations

We do not anticipate drastic developments in the motion of the beam envelope basically because of the very high mass of the ions; i.e., the beam is stiff. Nevertheless, the code does reveal many interesting features in the interplay of the various factors which affect the envelope.

Figure V-B-2/2 summarizes the results of one calculation. In this run, one kA of 100 GeV U^{+}_{238} is injected into a reactor with 1 torr of N_2. The initial radius of the beam is 0.5 cm, and the initial emittance is .3 mrad-cm. The pulse length is 10 nsec, and the rise time is 1 ns. The plot gives the rms radius of the beam R as a function of z, the distance into the chamber and x = vt - z, which is the position of a beam segment measured from the head of the pulse. At the head of the pulse, (x = 0), the net current always vanishes. Thus, the head experiences free expansion as a result of the finite emittance. As x increases (moving towards the back of the pulse), the net current builds up and the pinching effect of the self-field becomes evident. The body of the pulse is thus compressed and reaches the target with small radius. This plot gives a typical example of a pencil beam propagating in a self-pinch mode.

INSTABILITIES

Experiments (1) with a 15kA, 1.5 MeV electron beam have shown that stable propagation is possible in gas for a narrow window of pressure (1-5 torr N_2 and similarly for other gases.). For P < 1 torr, there is strong evidence for disruption by microinstability of the two-stream type. Above 5 torr gross sideways deflection occurs and is interpreted as the resistive hose instability. The window of good propagation is believed to result from the simultaneous suppression of both instabilities (2).

TWO-STREAM MODE

The two-stream interaction, a high frequency mode in which the beam drives a plasma wave, is suppressed by increasing gas pressure as follows. The instability occurs in the collisional plasma regime with electron-neutral collisions dominant, leading to decreasing growthrate with increasing pressures. The mode is stabilized by spread beam velocity ($\Delta V_{\parallel}$); for a fully pinched, monoenergetic, relativistic beam the perpendicular velocity

spread arises from the particle betatron motions, the parallel velocity spread follows since $V_{\parallel}^2 + V_{\perp}^2 = V^2 = \text{constant}$. Including the spread beam velocity in the collisional two-stream dispersion relation a stability boundary in n_e and P is determined. As gas pressure is increased, the plasma density required to suppress the two-stream mode decreases. However, plasma production by the beam increases with pressure such that above $\cong 1$ torr, the density very rapidly exceeds that necessary to suppress the mode.

In extending these ideas from electrons to heavy ions, we note that the anticipated current, pressure, beam velocity, beam radius and propagation distance are similar. Two principal differences are (a) the much greater rigidity of the ion beam due to the large mass (although this is mitigated somewhat by the high charge state) and (b) the large plasma density and high conductivity produced by the ions due to their large charge.

Considering the two-stream interaction for a heavy ion beam, we again find that for sufficiently high plasma density the mode is stabilized. Differences from the electron case are that electron-ion collisions are dominant in the plasma and we allow a spread in beam energy to produce $\Delta V_{\parallel}$. Proceeding as before, we consider a Uranium beam with particle current $I_{BO} = 1000$ A, effective charge state $Z_{eff} = 70$, radius R = .5 cm, with 100 GeV and a 1% parallel velocity spread. The minimum stabilizing plasma density is found to be $3 \times 10^{15}/cm^3$. For background gas pressures ≥ 1 torr, this plasma density will be achieved very early in the beam pulse so the two-stream instability will not present a serious obstacle to ion beam propagation.

We also note that when instability does occur, it provides a mechanism for transferring beam momentum to the plasma electrons. For a relativistic electron beam this leads to increased net current by a factor of 1-3; this effect has been observed (1) and simulated (3). For an ion beam momentum transfer by instability leads to current cancellation or reversal (4) which can result in beam defocusing. Hence, it is important to operate in the stable regime.

RESISTIVE MODES

Considering first the hose instability of a relativistic electron beam, this mode is suppressed by sufficiently rapid generation of electrical conductivity. As a rule of thumb, the beam will be hose stable if the magnetic decay time is comparable to or greater than the pulse length (5). This condition fails in the diode experiments as pressure increases above $\cong 10$ torr primarily because electric field breakdown of the gas shuts off-thus less conductivity is generated by the pulse hose. For the ion beam, very high conductivity is generated directly by the beam; this, coupled with the rigidity of the beam, will completely suppress hose growth.

A second possible source of instability is the resistive filamentation modes. These are not important for the electron beam because the net current is comparable to the beam current, resulting in large transverse velocity spread. However, in the ion beam case, where there is a high degree of current neutralization, this mode may be important. If the beam does break into filaments, it is possible that propagation will not be severely degraded since there is no net deflection. The question of filamentation is not settled and is now being investigated for ion beams. Preliminary results indicate that finite emittance will stabilize filamentation even in the presence of current neutralization.

Finally we mention the resistive sausage mode which involves a cylindrically symmetric "breathing" or radial expansion and contraction of the beam. The growth rate for this mode scales inversely with the magnetic neutralization time (6) and hence is unimportant in the high conductivity regime as encountered with the ion beam. However, even in the lower conductivity experienced by the electron beam this instability is suppressed by spread betatron frequency.

APPENDIX

In this appendix, the essential elements of the heavy ion beam transport code are described.

The stripping process is calculated in a classical binary encounter model, with binding energies for the heavy ion obtained from relativistic Hartree-Fock-Slater type calculations (7). In this model, a bound electron in the heavy ion acquires energy by Coulomb interaction with the gas nucleus of atomic number Z_g. In the rest frame of the heavy ion, gas nuclei are moving with the speed v, which is equal to the ion velocity in the lab frame. The energy ΔE acquired by the bound electron in the ion rest frame is given by

$$\Delta E = \frac{2 Z_g^2 e^4}{m_e v^2 b^2},$$

where b is the classical impact parameter. Ionization of a bound electron is assumed to occur if and only if $\Delta E = E_i$ where E_i is the binding energy. Thus, we obtain the cross section for ionization as

$$\sigma_i = \pi b_o^2 = \frac{2\pi Z_g^2 e^4}{m_e v^2 E_i}$$

The characteristic length for the ionization of this particular electron is

$$\lambda_i = \frac{1}{\sigma_i n_g}$$

where n_g is the gas atomic density.

An effective charge of the heavy ions at a

position z in the chamber is given by

$$Z_{eff}(z) = Z_I - \sum_i n_i e^{-z/\lambda_i}$$

where Z_I is the atomic number of the heavy ion. The sum is performed over all orbitals, n_i being the occupation number of a particular shell. The binding energies are obtained from Scofield's tabulation (7).

The stripped heavy ions are very effective in ionizing the background gas. Except at the head of the pulse (where a short period of time is required to build up the plasma density) the conductivity is predominantly that of a highly ionized gas, and is adequately approximated by Spitzer's formula (8). In this regime, the conductivity is very sensitive to the electron temperature but not to the plasma density.

To determine the electron temperature, we first note that the pulse length is exceedingly short compared to the time required for the plasma electrons to thermalize. During this short period, the plasma electron energy distribution looks more like the secondary distribution from direct ionization than a thermal Maxwellian. The secondary electrons produced from direct ionization are mostly slow ($E \leq E_I$, the ionization energy). We therefore approximate the average electron energy by $E_I/2$.

Our model of conductivity is basically that of Spitzer (8). However, to include the effects of electron-neutral collisions during the plasma buildup phase at the head of the pulse, we write

$$\sigma = \frac{e^2}{m} \frac{n_e}{\nu_m}$$

where

$$\nu_m = \left[2.0 \times 10^{-5} \left(\frac{E_I}{2}\right)^{-3/2} n_e + 2.0 \times 10^{-7} \left(n_g - n_e\right) \right] \text{ sec}^{-1}$$

E_I is the ionization energy (in ev). The plasma density n_e is generated from direct ionization and is given by

$$\left(\frac{\partial n_e}{\partial t}\right)_z = \frac{I_o/e}{\pi R^2} \frac{S}{W}$$

where I_o/e is the beam particle current, S the Bethe stopping power, and W the energy expended per ion pair.

$$W = 34.8 \text{ for } N_2 \quad (10)$$

As the beam traverses the medium, the conductivity rises rather quickly to an equilibrium value, and beyond that point, additional ionization will produce a higher plasma density, but does not change the effective electron temperature; hence, conductivity remains constant.

Once the effective beam current $Z_{eff}\ I_o$ and conductivity are known, the net current I is determined from the circuit equation (11)

$$I + \frac{\pi\sigma\nu R^2}{c^2} \left(\frac{\partial(LI)}{\partial x}\right)_z = Z_{eff}\ I_o .$$

The quantity $\pi\sigma\nu R^2/c^2$ is the "resistive decay time" for plasma currents, with inductance L a slowly varying function of R, given by

$$L = \log\left(\frac{b^2}{R^2} + e\right) .$$

b is the large radius at which the charge imbalance appears ($\sigma \to 0$), and is set at 10 cm throughout our calculations, e = 2.71828.

Finally, the ion radius R is controlled by the net current and emittance E via an evelope equation (12)

$$\frac{\partial^2 R}{\partial z^2} + \frac{e}{Mc^2} \frac{Z_{eff}}{\nu\gamma} \frac{I}{R} - \frac{E^2}{R^3} = 0$$

M is the mass of the heavy ion and γ its relativistic factor. The envelope radius is therefore determined by two competing effects, the self-magnetic field which causes the beam to pinch, and the emittance which causes the beam to expand.

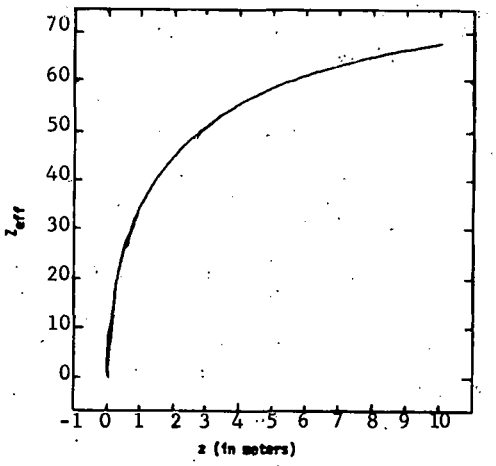

Fig. V-B-2/1. Effective charge of 100 GeV Uranium at various points (z) in a reactor with 1 Torr of N_2.

The initial emittance E_o of the beam is modified by multiple scattering as well as the phase mixing effects due to anharmonic pinch field (11). These processes are described by the equation

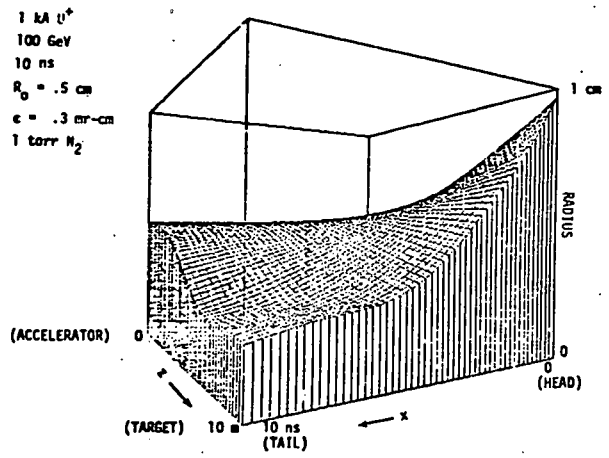

Fig. V-B-2/2. Radius of ion beam over the length of the beam (x = vt - z) at various points in the chamber (z).

$$\frac{\partial(E^2)}{\partial v} = \frac{8\pi Z_g (Z_g + 1) e^4 n_g Z_{eff}^2 \log\left(\frac{a}{b}\right)}{M^2 v^4 \gamma^2} R^2$$

$$- \alpha \frac{e Z_{eff} I}{Mc^2 \gamma v E} R^3 \frac{\partial^2 R}{\partial z^2} .$$

The parameters a and b in the multiple scattering term correspond to the atomic and nuclear radii respectively. The constant α is a phenomenological parameter of the order 0.5 selected to reproduce the damping effect observed in a particle simulation.

The above equations form a closed system of coupled equations which are solved numerically.

References

1. R. J. Briggs, J. C. Clark, T. J. Fessenden, R. E. Hester, E. J. Lauer, Livermore preprint UCRL-79958.
2. E. P. Lee, F. W. Chambers, L. L. Lodestro, S. S. Yu, Livermore preprint UCRL-79886.
3. F. W. Chambers, Bull. Am. Phys. Soc. 22 1097 (1977).
4. R. N. Sudan, Phys. Rev Lett 37, 1613 (1976).
5. E. P. Lee, Bull. Am. Phys. Soc. 22 1097 (1977).
6. E. P. Lee, Livermore internal report UCID-16268.
7. J. Scofield, (1972) unpublished. See e.g. Livermore UCRL-75542.
8. L. Spitzer, Physics of Fully Ionized Gases, J. Wiley & Sons (1967) p. 138.
9. V. Fano, Ann Rev. Nucl Sci. 13, 1 (1963).
10. H. Bichsel, private communication (1977).
11. E. P. Lee, Livermore preprint UCRL-79913.
12. E. P. Lee and R. K. Cooper, Particle Accelerators 7, 83 (1976).

3. CURRENT NEUTRALIZATION OF CONVERGING ION BEAMS

D. Mosher

It is desired to consider the problem of current neutralization of heavy ion beams traversing gas backgrounds in which the conductivity changes due to beam heating and beam convergence. The procedure is to determine Green's-function solutions to the magnetic-diffusion equation derived from Maxwell's equations and an assumed scaler-plasma conductivity σ for the background-electron current density j_e. The present calculation is more general than some previously carried out (see the ERDA Berkeley Summer Study Proceedings) in that arbitrary time variations for the beam current j_b and conductivity are allowed and the calculation is valid for both weak and strong neutralization. Results presented here must be combined with an appropriate energy-balance equation for the heated background in order to obtain the neutralization self-consistently.

A diffusion equation for j_e is determined by simultaneous solution of the Maxwell's equations

$$\nabla \times \underset{\sim}{E} = -\frac{1}{c}\frac{\partial \underset{\sim}{B}}{\partial t} \; ; \quad \nabla \times \underset{\sim}{B} = \frac{4\pi}{c}\left(\underset{\sim}{j}_b + \underset{\sim}{j}_e\right) \qquad (1)$$

and Ohm's law,

$$\underset{\sim}{j}_e = \sigma \underset{\sim}{E} , \qquad (2)$$

where the time and length scales for the problem at hand allow neglect of displacement currents.

The axial component of the diffusion-like equation for $\underset{\sim}{j}_e$ is

$$\frac{\partial}{\partial t} j_{ez} = -\frac{c^2}{4\pi}\frac{1}{r}\frac{\partial}{\partial r}\left\{r\left[\frac{\partial}{\partial z}(j_{er}/\sigma) - \frac{\partial}{\partial r}(j_{ez}/\sigma)\right]\right\} - \frac{1}{4\pi}\frac{\partial^2}{\partial t^2}(j_{ez}/\sigma) - \frac{\partial}{\partial t} j_{bz} \qquad (3)$$

If R_o is the beam radius at injection and L is the distance to the pellet, then both j_r/j_z and $\frac{\partial}{\partial z}/\frac{\partial}{\partial r}$ are expected to scale like R_o/L. The

$$\frac{\partial}{\partial z}(j_{er}/\sigma)$$

term is then down by R_o^2/L^2 and can be neglected in Eq. (3). Similarly,

$$\frac{\partial^2}{\partial t^2}(j_{ez}/\sigma) \cong \beta^2(R_o^2/L^2)\frac{\partial^2}{\partial r^2}(j_{ez}/\sigma)$$

can be neglected. Additionally, it is assumed that thermal conductivity smoothes the radial background-temperature profile to the extent that

$$\frac{\partial}{\partial r}\ell n\sigma \ll \frac{\partial}{\partial r}\ell n j_{ez} ,$$

so that σ can be treated as a function of z and t only. With these approximations, Eq. (3) reduces to

$$\frac{4\pi\sigma}{c^2}\frac{\partial j}{\partial t} = \frac{\partial j}{\partial \tau} = \frac{1}{r}\frac{\partial}{\partial r}\left(r\frac{\partial j}{\partial r}\right) - \frac{\partial j_b}{\partial \tau} \qquad (4)$$

where subscripts have been dropped ($j \equiv j_{ez}$, $j_b = j_{bz}$) and the time variable has been transformed according to

$$\tau = \frac{c^2}{4\pi}\int_o^t \frac{dt'}{\sigma(z,t')} \qquad (5)$$

The solution to Eq. (4) follows from the infinite-domain Green's function for the transverse plane

$$j(r,t) = -\int_o^\tau d\tau_o \int_o^\infty r_o dr_o d\theta \; g(r,\theta,\tau|r_o,\theta_o,\tau_o) \times \frac{\partial j_b(r_o,\tau_o)}{\partial \tau_o} \qquad (6)$$

where

$$g(r,\theta,\tau|r_o,\theta_o\tau_o) = \frac{1}{4\pi(\tau-\tau_o)}\exp\left[-\rho^2/4(\tau-\tau_o)\right]$$

and

$$\rho^2 = r^2 + r_o^2 - 2rr_o\cos(\theta-\theta_o). \qquad (7)$$

Integrating over θ_o results in

$$j(r,t) = -\int_o^\tau d\tau_o \int_o^\infty r_o dr_o G(r,\tau|r_o,\tau_o)\frac{\partial j_b}{\partial \tau} \qquad (8)$$

with

$$G(r,\tau|r_o,\tau_o) = \frac{1}{2(\tau-\tau_o)} I_o\left[\frac{rr_o}{2(\tau-\tau_o)}\right]\exp\left[\frac{(r^2+r_o^2)}{-4(\tau-\tau_o)}\right]. \qquad (9)$$

The integration over r_o can be carried out when j_b is chosen to have a Gaussian profile

$$j_b(r,t) = \frac{I_b(z,t)}{\pi R^2} e^{-r^2/R^2} \qquad (10)$$

where convergence onto the pellet requires $R = R_o z/L$ and the transit-time z-dependence of I_b is given by

$$I_b(z,t) = I_b\left(L, t - \frac{L-z}{V}\right)$$

for monoenergetic ions of axial velocity V. Performing the integration over r_o

$$j(r,t) =$$

$$-\frac{1}{\pi}\int_o^\tau d\tau_o \frac{\partial I_b}{\partial \tau_o}\frac{1}{R^2+4(\tau-\tau_o)}\exp\left[-\frac{r^2}{R^2+4(\tau-\tau_o)}\right] \tag{11}$$

Noting that in the limit of negligible diffusion ($\tau-\tau_o\to 0$), Eq. (11) demonstrates that $j+j_b=0$, and that most cases of interest correspond to small fractional non-neutralization, the net current can be approximated by expanding the integrand for small values of $4(\tau-\tau_o)/R^2$. To lowest significant order

$$j_n = j+j_b = \frac{4}{\pi R^4}\left(1-\frac{r^2}{R^2}\right)e^{-r^2/R^2}\int_o^\tau I_B(\tau_o)d\tau_o \tag{12}$$

where integration by parts has been employed. This expression is useful everywhere except close to the pellet where the magnetic-diffusion length may be comparable to the beam radius. The net current contained within radius r is given by

$$I_n(,t) =$$

$$2\pi\int_o^r r'dr' j_n(r',t) =$$

$$\frac{c^2}{\pi R^2}\cdot\frac{r^2}{R^2}e^{-r^2/R^2}\int_o^t \frac{dt' I_b(z,t')}{\sigma(z,t')} \tag{13}$$

from Eq. (12), and

$$I_n r,t) = \tag{14}$$

$$\int_o^\tau d\tau_o\left\{\frac{\partial I_b}{\partial\tau_o}\exp\left[-\frac{r^2}{R^2+4(\tau-\tau_o)}\right]\right\} - I_b(z,t)e^{-r^2/R^2}$$

for the more general case of arbitrary neutralization given by Eq. (11). From Eq. (13), maximum net current occurs at r=R while maximum self field occurs at $r = R/\sqrt{2}$.

If I_b is uniform in time, Eq. (13) reduces to

$$\frac{I_n(max)}{I_b} = e^{-1}\int_o^t \frac{dt'}{\tau_D(t')} \tag{15}$$

for r = R with

$$\tau_D = \frac{\pi\sigma R^2}{c^2}$$

The ratio I_n/I_b calculated here is down by a factor e over that estimated in the ERDA-Berkeley Summer Study proceedings partially because of the Gaussian profile for j_b.

For I_b constant in τ, the ratio $I_n(r)/I_b$ is from Eq. (14)

$$I_n(r)/I_b = \exp\left(-\frac{r^2}{R^2+4\tau}\right)-\exp\left(-\frac{r^2}{R^2}\right) \tag{16}$$

Maximum net current occurs at

$$\frac{r^2}{R^2} = \frac{1+\nu}{\nu}\ell n(1+\nu)\ ;\ \nu = \frac{4\tau}{R^2} = \frac{t}{\tau_D} \tag{17}$$

where t = 0 corresponds to the time the front of the beam crosses the axial position observed.

Although the simple relations Eqs. (15) - (17) are useful, required shaping of the beam-current pulse due to pellet requirements, and the variations with time of the plasma conductivity due to return-current heating make Eq. (13) the most useful for a comprehensive study.

4. LINEAR MICROSTABILITY ANALYSIS OF A HEAVY ION BEAM - PLASMA SYSTEM

P. F. Ottinger and D. Mosher

In order to investigate the propagation and focussing of a beam of heavy ions, it is necessary to consider the effects of a background plasma in the reactor chamber. Although this background provides charge and current neutralization of the beam, it may also cause excitation of certain microinstabilities. Here, interactions involving the background electrons with the beam ions (e-b mode), and the background electrons with the background ions (e-i mode) are investigated to determine if these modes are unstable in the parameter regimes appropriate for a fusion device.

The conditions for a good charge and current neutralization are

$$n_e \simeq Z_i n_i, \tag{1}$$

and

$$V_e \simeq Z_b n_b V_b / n_e, \tag{2}$$

which requires

$$n_b \ll Z_i n_i / Z_b, \tag{3}$$

and

$$R \gg c/\omega_{pe}. \tag{4}$$

Here Z_α, m_α, n_α and V_α are respectively the charge, mass, density, and mean-streaming velocity of species α (=i,e,b), R is the beam radius (variable as the beam is focussed), and $\omega_{p\alpha}^2 \equiv 4\pi n_\alpha Z_\alpha^2 e^2/m_\alpha$. Typically, a 3 kA 40 GeV uranium beam is injected into the reactor vessel with radius $R_o \simeq 10$ cm, and converges onto a spot 10 meters downstream. Such a beam provides the 100 TW power expected to be necessary for a reactor system. It is assumed here that $Z_b = Z_i = 1$ and that the background density is sufficiently low to insure that the beam ions are not stripped further. Under these conditions, the distribution of particles in velocity space exhibits relative drifts among the three species which may lead to growth of the e-i mode and/or the e-b mode.

Because a 40 GeV beam of uranium ions is only mildly relativistic ($\gamma \simeq 1.25$), a nonrelativistic, electrostatic, linear-stability analysis will be employed. Relativistic corrections should only effect the results presented for the e-b mode where it is expected that the growth rates will be decreased slightly. Assuming that the distribution function, f_α, for all species can be written as a drifting Maxwellian (with the thermal energy of species α given by T_α), the dispersion relation for perturbations of the form $e^{i(kz-\omega t)}$ becomes

$$D = 0 = 1 + \sum_\alpha \frac{\omega_{p\alpha}^2}{k^2} \frac{m_\alpha}{T_\alpha} \left[1 + \eta_\alpha Z(\eta_\alpha)\right]. \tag{5}$$

Here, $\eta_\alpha \equiv (\omega/k - V_\alpha)/u_\alpha$, $u_\alpha \equiv (2T_\alpha/m_\alpha)^{\frac{1}{2}}$ is the thermal velocity of species α, and $Z(\eta_\alpha)$ is the usual plasma dispersion function. When considering the e-i mode, the beam contribution to D is negligible, so that for $|\omega_r/k| > u_i$ and $|\omega_r/k - V_e| < u_e$ (where $\omega = \omega_r + i\omega_i$), the usual result for the ion-acoustic instability is obtained.

$$\omega_r = kc_s/(1 + k^2\lambda_D^2)^{\frac{1}{2}}, \tag{6}$$

$$\omega_i = \frac{-\sqrt{\pi/8}\,|\omega_r|}{(1 + k^2\lambda_D^2)^{3/2}} \left\{\left(\frac{T_e}{T_i}\right)^{3/2} \exp\left[-\frac{T_e}{2T_i(1+k^2\lambda_D^2}\right]\right.$$

$$\left. + \left(\frac{m_e}{m_i}\right)^{\frac{1}{2}} \left[1 - \frac{V_e}{c_s}(1 + k^2\lambda_D^2)^{\frac{1}{2}}\right]\right\}. \tag{7}$$

Here, $c_s^2 \equiv T_e/m_i$ and $\lambda_D^2 \equiv T_e/(4\pi n_e e^2)$. Thus, when $T_e \gg T_i$, e-i mode is unstable if

$$V_e > \omega_r/k = c_s/(1 + k^2\lambda_D^2)^{\frac{1}{2}}. \tag{8}$$

When $T_e \simeq T_i$, the e-i mode is stablized by ion Landau damping unless $V_e \gtrsim u_e$.

For $T_i \simeq T_e \simeq 1$ eV at injection, the e-i mode is stable ($u_e \simeq 6 \times 10^7$ cm/sec $> V_e$) when $n_{bo}/n_e < 3.3 \times 10^{-3}$. Here, n_{bo} is the beam density at injection. However, as the beam is focused, there is still the possibility of unstable growth. During focussing, if V_e (R) increases in order to maintain local current neutrality and T_e(R) increases due to return-current heating, the local instability criterion may be satisfied for some $R < R_o$. An upper limit on the local growth rate is given by ($k \lesssim 1/\sqrt{2}\,\lambda_D$)

$$\omega_i \lesssim 7.7 \times 10^9 \left(\frac{n_{bo}}{n_e} \frac{T_e(R)_o}{T_e(R)}\right)^{\frac{1}{2}} \frac{R_o}{R^2} \text{ rad/sec} \tag{9}$$

as long as $u_e(R) \gtrsim |\omega_r/k - V_e(R)| \simeq V_e(R) \gg c_s$ and $T_e(R) \gg T_i$, and by

$$\omega_i \lesssim 1.7 \times 10^8 (n_e/n_{bo})^{\frac{1}{2}} \text{ rad/sec} \tag{10}$$

for cold electrons where $u_e(R) \ll |\omega_r/k - V_e(R)| \simeq V_e(R)$. The relation $n_b(R) = n_{bo}R_o^2/R^2$ has been employed. If electron heating is insignificant so that $T_e(R) \simeq T_e(R_o) \simeq T_i$ holds, then growth first occurs when $V_e(R)$ becomes larger than u_e or when

$$R/R_o \lesssim 17.4\,(n_{bo}/n_e)^{\frac{1}{2}}. \tag{11}$$

When studying the stability of the e-b mode, the background-ion contribution to D is negligible and V_e can be ignored compared with $|\omega_r/k| \simeq V_b$. Furthermore, because of the smallness of $m_e n_b/m_b n_e$, u_b/V_b does not have to be very large in order to consider the beam warm in this analysis. Thus, for $|\omega_r/k| > u_e$ and $u_b > \sqrt{3}/2(\omega_{pb}^2/2\omega_{pe}^2)^{1/3} V_b$, the maximum growth of the e-b mode occurs for

$$\omega_r \simeq \omega_{pe}\left(1 - \frac{\omega_{pb}^2}{k^2 u_b^2}\right) \qquad (12)$$

and

$$k^{MAX} \simeq \frac{\omega_{pe}}{V_b}\left(1 + \frac{u_b}{\sqrt{2}\, V_b}\right) \qquad (13)$$

with

$$\omega_i^{MAX} \simeq -\frac{\nu_e}{2} + \sqrt{\frac{\pi}{2}}\, e^{-\frac{1}{2}} \frac{\omega_{pb}^2}{\omega_{pe}} \frac{V_b^2}{u_b^2} \qquad (14)$$

Here, $\nu_e = 2.9 \times 10^{-6}\, n_e \lambda_{ei}/T_e^{3/2}$ is the electron collision frequency and λ_{ei} is the Coulomb logarithm for electron-ion collisions. The quantity ν_e was introduced in the dispersion relation though the electron contribution which was written in the standard form as $-\omega_{pe}^2/\omega(\omega + i\nu_e)$. From (4), it is clear that growth of the e-b mode occurs if

$$\frac{n_e}{n_b} < 0.032\, R_o^{\frac{2}{3}} \left(\frac{V_b}{u_b}\frac{R}{R}\right)^{4/3} \frac{T_e(R)}{T_e(R_o)}, \qquad (15)$$

where $\lambda_{ei} \simeq 7.0$ was used. Again, if $T_e(R) \simeq T_e(R_o)$, then the e-b mode is unstable for

$$R/R_o < 0.076\, (n_{bo}/n_e)^{3/4}\, V_b/u_b\, R_o^{\frac{1}{2}} \qquad (16)$$

with the growth rate given in (14). Note that for both the e-i mode and the e-b mode, the wavelengths of the most unstable perturbations are much shorter than the radial and axial scale lengths of the beam. Thus, if these modes do grow to significant levels, they will only produce microscopic effects such as anomolous resistivity, rather than directly producing any macroscopic disruption of the beam.

Figure V-B-4/1 shows typical marginal stability curves as functions of n_e/n_{bo}, R/R_o and T_b/E_b for a 40 GeV beam of U^{+1} ions with $R_o = 10$ cm. Curves for both the e-i mode and the e-b mode are shown. An arrow on the R/R_o axis indicates the radius of a 1 cm pellet. Regions to the right of any given curve are stable and regions to the left are unstable. Thus for a target 1 cm in radius, it is required that $n_e/n_{bo} \geq 10^4$ in order for the e-i mode and the e-b mode ($T_b/E_b > 10^{-4}$) to be stable for the entire time of transport. This requirement is consistent with (3) which is one of the conditions for good charge and current neutrality. Figure V-B-4/2 shows the marginal stability curves for a 7 GeV beam of Xe_{136}^{+1} ions with I = 14 kA and R_o = 10 cm.

Although primary-current heating will be negligible, return-current heating may increase T_e of order 10 eV in the case of U^{+1} and higher for Xe^{+1} as the beam approaches the pellet. Marginal-stability curves for T_e = 10 eV are also shown. It should also be pointed out that although instability may set in for $R < R_o$, the growth only occurs during the last segment of the transport process. Thus, even when linearly unstable because of smaller pellet dimensions or lower background density, the growth may not reach a sufficient level to affect the propagation or focussing of the beam.

In summary, the linear growth rates of two microinstabilities, the e-i mode and e-b mode, have been investigated under conditions of good charge and current neutralization in a heavy ion beam-plasma system. It was found that both modes can be stabilized in parameter regimes which are consistent with these conditions for charge and current neutrality and which are appropriate for a fusion reactor. If occurring at all, these instabilities can grow only when the beam is quite close to the pellet. Thus, it is unlikely that either of the electrostatic modes will significantly

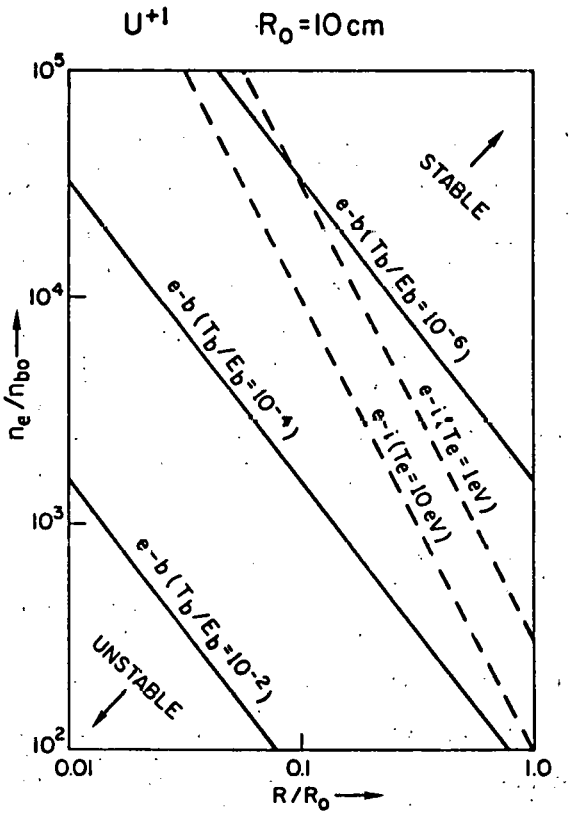

Fig. V-B-4/1. Typical marginal stability curves as functions of n_e/n_{bo}, R/R_o and T_b/E_b for a 40 GeV beam of U^{+1} ions with R_o = 10cm.

degrade beam transport or focussing. The stability of electromagnetic modes is currently under investigation.

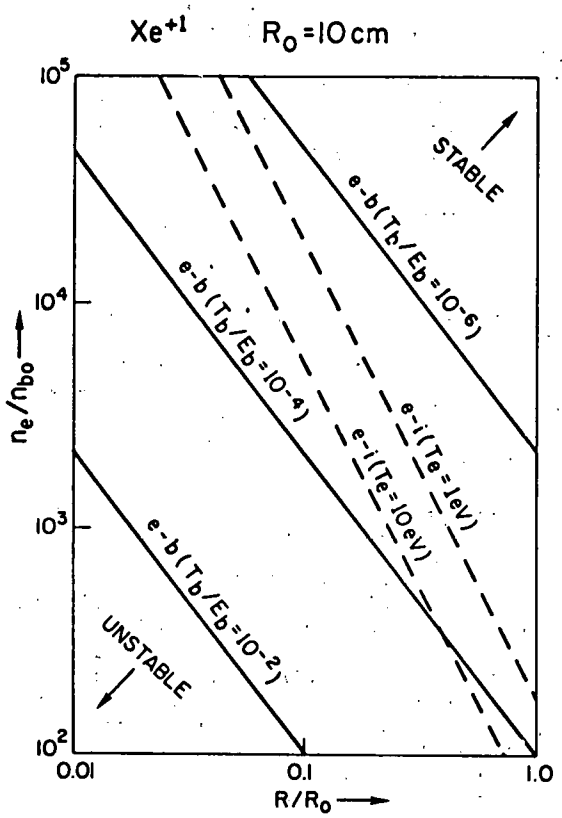

Fig. V-B-4/2. Marginal stability curves for a 7 GeV beam of Xe^{+1}_{136} ions with I = 14 kA and R_o = 10cm.

5. TARGET CHAMBER MAGNETIC FIELDS IN PELLET FUSION REACTORS

D. A. Tidman

ABSTRACT

Stray magnetic fields are expected to be generated by various mechanisms following a fusion pellet explosion in a reactor target chamber. These fields, which would be partially trapped in the chamber between explosions, may present a complication for the accurate aiming of focussed ion beams on to a target pellet. Various schemes could be used to remove these fields.

INTRODUCTION

In this note we discuss the expected generation of stray magnetic fields in a target chamber containing a fusion micro-explosion. Such fields can be generated by a variety of mechanisms[1-7] and may become embedded and trapped in the Li blanket surrounding the chamber. The sources discussed in Sec. 3 include debris ion currents, wall photoelectron currents, residual fields in the pellet plasma generated during the pellet burn, and possible turbulent dynamo effects. It appears that fields of a few Gauss are likely, and transient fields of > 10 G immediately following an explosion would not be surprising. The question therefore arises as to whether the existence of such fields would make it difficult to repeatedly aim focussed particle beams accurately at a series of target pellets.

The actual fields present at the time of an ignition event depends on how quickly they decay between explosions, the degree to which field may become embedded and persist in the wall and surrounding conducting structures, and design-dependent features such as whether the fireball could be swept out of the chamber before much field diffused into the wall. In this regard we note that an azimuthal flux loop takes a time

$$\tau \approx 4\pi\sigma(\Delta R)^2/c^2 \approx 10^{-3}(\Delta R)^2 \text{ sec} \qquad (1)$$

to diffuse through a spherical shell of Li ΔR cm thick, i.e., $\sim$ 10 sec for a blanket 1 meter thick. If the target chamber wall was a static structure, we note that plasma and field could be either quenched or swept out of the chamber in a few sound transit times ($\sim 10^{-2}$ sec). However, field would have time to diffuse a distance $\sim$ 3 cm into the wall in this case and might still accumulate in the blanket structures after a series of shots. On the other hand in a liquid lithium waterfall target chamber, field may be automatically swept out between explosions.

ION BEAM DEFLECTION

Magnetic fields in the target chamber can be expected to have a spectrum of wavelengths. Provided long wavelength components exist ($\lambda \sim R$), significant beam deflection effects can occur. Spectral components with $\lambda \ll R$ however would have less effect.

As a simple measure of the importance of the long wavelength B field components for beam aiming, consider an ion injected along a radial direction at the wall, with a uniform field component B perpendicular to its motion. It would then miss the chamber center by a distance $\Delta r \approx R^2/2r_c$ where $r_c = 3.16.10^6$ $(\gamma A\beta/ZB)$ is the ion cyclotron radius in cm and we assume $R \ll r_c$. This displacement can be written

$$\frac{\Delta r}{B} = \frac{0.16\ Z}{\gamma A\beta}\left(\frac{R}{10^3}\right)^2 \approx \frac{3.5\ Z}{(A\epsilon_{MeV})^{\frac{1}{2}}}\left(\frac{R}{10^3}\right)^2, \qquad (2)$$

where the second expression is for a non-relativistic ion of energy ϵ MeV, atomic weight A, and charge state Z. At high ambient gas densities the plasma electrons may partially shield out the B field from the inner part of the ion pulse. However, this more complex beam plasma deflection problem is not considered here, although it may significantly reduce the deflection.

In Fig. V-B-5/1 we have plotted $\Delta r/B$ as a function of A for several ion beam charge states. The ion energy $\epsilon(A)$ used in Eq. (2) for this figure was taken to be the energy for which an ion of atomic weight A has a range of 250μ in Au which is a possible target material and stopping distance. We see for example that if an accuracy of Δr = 0.1 cm is required, then fields of 10 Gauss would cause difficulties for all except high A ions in low charge states. Stray fields of 1 G however becombe a problem only for light to moderate atomic weight ions, or high A ions that are nearly fully stipped.

MAGNETIC FIELD ESTIMATES FOR SOME SOURCES

Field sources divide into those in the background gas and wall environment, and sources generated in the pellet plasma debris in the course of the fusion burn and its subsequent expansion. In the following sections we derive some simple parametrized estimates for several of the mechanisms involved. Detailed modeling would require development of a computer code for anisotropic pellet explosions and the chamber environment.

DEBRIS ION CURRENTS

After the pellet debris has expanded a relatively short distance radially, its density will fall below that of the ambient photo-ionized gas in the chamber (for chamber pressures above about 10^{-4} torr and mm size pellets). At this point a pellet ion with energy ϵ_d (keV) and charge Z_d has a mean-free-path in the background plasma,

$$\lambda \approx \frac{7.7\ 10^{18}\epsilon_d^2}{Z_d^2\ N_e\ \ell n\Lambda}\ \text{cm}, \qquad (3)$$

where N_e cm^{-3} is the background electron density after photo-ionization by the explosion.

For example $Z_d = 5$, $\ell n\Lambda \approx 5$, $\epsilon_d = 3$ keV, $N_e = 5.10^{13}$ cm^{-3}, gives $\lambda \approx 10^2$ meters, so that debris ions will strike the wall for low background pressures.

Now in streaming radially through the background plasma the pellet ions provide a current $\underline{j}_d$ which is initially neutralized by the plasma electron current. However, as the electrons respond to their friction with background gas ions, a magnetic field grows according to

$$\frac{\partial \underline{B}}{\partial t} \approx \frac{c^2}{4\pi\sigma} \nabla^2 \underline{B} + \frac{c}{\sigma} \underline{\nabla} \times \underline{j}_d \qquad (4)$$

where

$$\sigma = \frac{1.7\ 10^{14}\ T_o^{3/2}}{Z_o\ \ell n\Lambda_o} \qquad (5)$$

is the background plasma conductivity[1] (assumed homogeneous), T_o its temperature in eV and Z_o the background ion charge. Since the magnetic diffusion term is relatively small for the gradient scales involved in $\underline{j}_d$,

$$\underline{B}(\underline{r},t) \approx \frac{c}{\sigma} \int_o^t dt' \ \underline{\nabla} \times \underline{j}_d \qquad (6)$$

To evaluate this field we require a model for the pulse of debris ions, $j_d(\underline{r},t)$, emitted by the pellet explosion. If we assume this pulse has a velocity dispersion $\nabla v_d \sim v_d$ where $m_d v_d^2/2 = \epsilon_d$ is the average ion kinetic energy, then the pulse broadens out as it advances radially. A simple model giving rise to an azimuthal field B (Fig. 2) is to assume

$$\underline{j}_d = \hat{r}\ j(\theta) \left(\frac{R}{r}\right)^3 \frac{3}{4}\ I\ , \qquad (7)$$

where $\underline{j}_d$ is radial but has dependence on polar angle θ represented by $j(\theta)$ which is the ion current pulse arriving at the wall r = R, and I is a square pulse function with I = 1 for $2r/3v_d \le t \le 2r/v_d$ and I = 0 otherwise. The factor $(R/r)^3$ conserves the total number of debris ions in the pulse and applies for r sufficiently large for the debris ions to become dilute enough to stream freely through the background plasma.

The maximum value of B is reached at the end of the pulse (for $t \ge 2r/v_d$) and follows from Eqs. (6) and (7) as

$$B_m = -\frac{c}{\sigma v_d} \left(\frac{R}{r}\right)^3 \frac{\partial j}{\partial \theta}\ . \qquad (8)$$

Noting that the total debris ion energy arriving at the chamber wall is

$$w_d = 2\pi R^2 \int_o^\infty dt' \int_o^\pi \sin\theta\ d\theta \left(\frac{j_d}{eZ_d}\right) \epsilon_d\ , \qquad (9)$$

and using Eq. (5), B_m can be expressed as

$$B_m = B_R \left(\frac{R}{r}\right)^3 \qquad (10)$$

where $B_R(\theta)$ is the field at the wall (r = R),

$$B_R = -\ 8.4\ 10^{-2}\ \frac{Z_o\ Z_d\ \ell n\Lambda_o}{\epsilon_d\ T_o^{3/2}} \left(\frac{10^3}{R}\right)^3 W\left(\frac{W_d}{W}\right) \phi, \qquad (11)$$

and the asymmetry factor ϕ is

$$\phi = \frac{\partial j}{\partial \theta} \Big/ \int_o^\pi d\theta\ j\ (\theta) \sin\theta\ , \qquad (12)$$

with the total explosion energy W in MJ, ϵ_d the average debris ion energy in keV, T_o in eV, and R in cm. If we also assume a model for $j(\theta)$, namely

$$j = j_o + \delta j \cos n\theta \qquad (13)$$

with $\delta j < j_o$, the asymmetry factor ϕ becomes

$$\phi \approx -\ n \left(\frac{\delta j}{2 j_o}\right) \sin n\theta \qquad (14)$$

large values for n would then correspond to a fine-structure jetting of debris material, and the case n = 1 to a simple pole-to-pole variation δj in the ion current. The symmetric case n = 0 gives $B_m = 0$.

Now $B_m(r,\theta)$ is the azimuthal magnetic field (Fig. V-B-5/2) left at r,θ immediately after traversal by the debris ion pulse. Considering some plausible numerical values, $W_d/W = 0.1$, W = 500 MJ, R = 10^3 cm, ϵ_d = 3 keV, T_o = 20 eV, $\ell n\Lambda \sim 5$, $Z_o = 3$, $Z_d = 6$ gives

$$B_m \approx 0.7\ n \sin n\theta \left(\frac{\delta j}{j_o}\right) \left(\frac{R}{r}\right)^3\ . \qquad (15)$$

If the ion current asymmetry between two hemispheres is substantial, say $\delta j/j_o \sim 0.5$ and n = 1, we find in the equatorial plane a field $B_m \approx 0.35\ (R/r)^3$, i.e., about 0.35 Gauss at the chamber wall, but several 100 Gauss towards the center ($R/r \sim 10$).

It should be noted that these approximate formulas apply for $r_{crit} < r <$ (smaller of R or a debris ion range), where r_{crit} is the radius at which debris ions first stream freely through the background plasma instead of sweeping it up. After the impulsive generation of these fields the $(R/r)^3$ dependence would be rapidly smeared out by diffusion and convection so that the stronger fields at small r would tend to approach the chamber wall.

In concluding this section we also note that the factor ϕ in Eq. (14) can become large for large values of n, corresponding to small scale jetting effects in the debris. This would create larger fields, but their subsequent diffusive mixing would also proceed more quickly.

WALL PHOTO-ELECTRON CURRENTS

Photo-emission from various regions of the chamber wall would be non-uniform if the pellet radiation flash was asymmetric. Under these circumstances photo-electrons emitted from the wall produce currents that can generate magnetic fields. A simple model for this is similar to that in the previous Section, but where instead of debris ions we consider photo-electrons with energies $\hbar\nu > T_o$ flowing radially inward from the wall. A rough upper limit to the field produced is then given by using Eq. (11) but with the replacements $Z_d \rightarrow -1$, W_d = total energy emitted as wall photo-electrons with $\hbar\nu > T_o$, and $\epsilon_d \rightarrow \hbar\nu$ is the mean photo-electron energy in this range. We then see that this source of B field is relatively small compared to the debris ion source, due to the small photo-efficiency of light elements such as liquid Li which would probably be used as a thin ablative layer on the inner wall.

RESIDUAL PELLET FIELDS

In the compressed burning fuel several mechanisms exist that generate very strong magnetic fields. They arise when the pellet departs from spherical symmetry and examples are: thermo-electric sources at fuel-pusher boundaries[4], anisotropic α-particle fluxes generated by the burn[6], or small scale composition fluctuations arising because of Rayleigh- Taylor mixing of pieces of the pusher into the fuel, etc.

Defining the plasma beta during burn, $\beta = 2NT/(B^2/8\pi)$, we have a maximum field (corresponding to $\beta = 1$) $B_{max} = (16\pi NT)^{\frac{1}{2}} = 6.10^7 (NT_{keV}/N_s)^{\frac{1}{2}}$, where $N_s = 4.5\ 10^{22}$ cm^{-3} is a characteristic solid state density for DT. For example for a fuel compression of $N/N_s = 10^4$, and T = 100 keV during burn, $B_{max} = 6.10^{10}$ Gauss.

Regardless of detailed mechanisms we note that fields generated in the compressed fuel sphere and its surroundings are embedded in the plasma and thus decrease as r^{-2} as the pellet fireball expands. The field strength at a radius R equal to the chamber radius is thus

$$B \approx 6.10^7 \left(\frac{N\ T_{keV}}{N_s}\right)^{\frac{1}{2}} \left(\frac{r_o}{R}\right)^2 \frac{1}{\sqrt{\beta}}\ , \qquad (16)$$

where N cm^{-3}, T_{keV}, β, and radius r_o, refer to the compressed pellet plasma. For example taking $r_o \approx 10^{-2}$, R = 10^3 cm, $B \approx 1$, $N/N_s = 10^4$, T = 100 keV gives $B \approx 6$ Gauss as an upper limit for the residual field.

TURBULENT DYNAMO EFFECTS

If the magnetic Reynolds number, R_M, of a turbulent plasma is large, the fluid kinetic energy tends to do work on the field by line stretching faster than the field can diffuse through the fluid eddies in which it is embedded. An adequate theory or computer simulation for the complex 3D motion that is involved in this process is not available. However, some 2D MHD computer models by Fyfe, Montgomery, and Joyce[7], show that provided both the magnetic and mechanical Reynolds numbers are large, the magnetic energy tends to increase with an e-folding time $\sim \lambda/\delta V$ and approaches the fluid kinetic energy density.

The magnetic Reynolds number for a plasma is $R_M = \lambda\ \delta V/\eta$ where $\eta = c^2/4\pi\sigma$ is the magnetic viscosity, λ the fluid motion scale, and δV the turbulent velocity amplitude. Using the plasma conductivity for σ this becomes

$$R_M = \frac{7.5\ 10^{-2}\ \lambda\ \delta V\ T_{keV}^{3/2}}{Z\ \ell n\Lambda}\ . \qquad (17)$$

The maximum value for δV is of order the sound speed, c_s, so that at early times in the expanding fireball a situation $R_M >> 1$ can in principle exist. However, as the expansion proceeds and T decreases to say 1 - 10 eV, the final chamber filled state (even if turbulent with $\delta V \sim c_s$) would have a small R_M. Thus, only if turbulence occurs in the early-time expanding fireball would this large fluid kinetic energy source become available for magnetic field generation.

The question as to whether turbulence actually occurs however is difficult to answer. At first sight one would expect the fluid expansion of the pellet plasma to be principally a laminar radial motion, in which case dynamo action would not occur. However, suppose the pellet retains its layered structure (consisting of a high atomic weight shell containing a low atomic weight pusher and fuel plasma inside) well into its radial expansion. We then note that the sound speed in the interior can be larger than the radial expansion velocity of the tamping shell, in which case fluid turbulence of the interior fireball plasma may be superposed on the radial expansion.

References

1. S. I. Braginskii, in Reviews of Plasma Physics, edited by M. A. Leontovich (Consultants Bureau, New York, 1965), p. 205.
2. J. A. Stamper and B. H. Ripin, Phys. Rev. Lett. 34, 138 (1975).
3. D. G. Colombant, K. G. Whitney, D. A. Tidman, N. K. Winsor, and J. Davis, Phys. Fluids 18, 1687 (1975).
4. D. A. Tidman, Phys. Fluids 18, 1454 (1975); Phys. Rev. Lett. 37, 1397 (1976).
5. J. B. Chase, J. M. Leblanc, and J. R. Wilson, Phys. Fluids 16, 1142 (1973).
6. D. A. Tidman, Phys. Rev. Lett. 35, 1228 (1975).
7. D. Fyfe, D. Montgomery, and G. Joyce, Dissipative Forced Turbulence in Two-Dimensional Magnetohydrodynamics, submitted to J. of Plasma Physics, 1976.

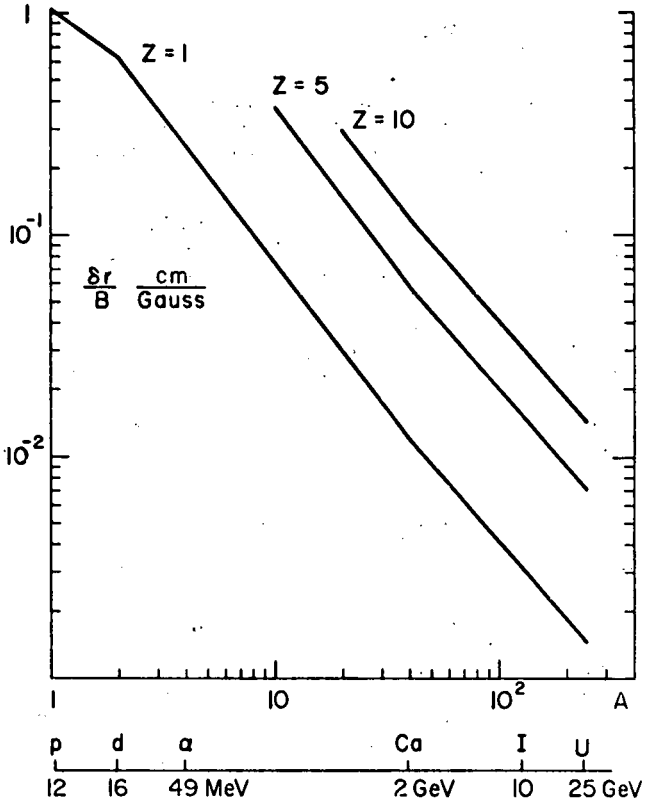

Fig. V-B-5/1. Displacement of an ion trajectory, δr, in traversing a distance of 10^3cm across a uniform field, B Gauss, for ions of various atomic weights and charge states. Ion energies are taken as those corresponding to a range of 250 μ in Au.

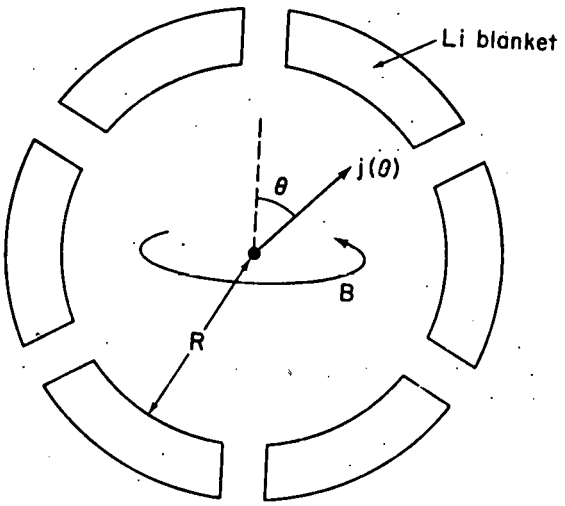

Fig. V-B-5/2. Azimuthal magnetic field produced by the pellet debris ion current flowing with axisymmetry through background plasma in a target chamber. Radiation from the pellet micro-explosion preionizes the background. A typical chamber radius would be R = 10^3cm, and Li blanket thickness of 150cm.

6. BEAM STABILITY IN THE TARGET CHAMBER

W. B. Thompson, S. Jorna

In these notes we consider the stability of a heavy ion beam propagating through the target chamber. In most schemes the beam has energies of several tens of GeV, carries currents of ~1,000 amps (equivalent); and is focused geometrically from an aperture of radius $r_i \sim 10$ cm to a target spot of $r_f \sim 1$ mm over a distance of $L \sim 10$ m. The propagation mode must thus be highly stable.

If the target chamber were empty, the beam properties could easily be calculated and the stability investigated. In that case the only serious instability is the wriggle or fire hose mode which has a growth rate

$$\Gamma^2 = \pi \frac{nZ^2e^2}{M} (k^2 r_0^2) \log \left(\frac{1}{kr_0} \right)$$

or $\Gamma \leq 0.21\ \omega_B$ where $\omega_B^2 = 4\pi n(Z^2e^2/M)$ is the square of the beam plasma frequency. For our beam $N = \pi n r^2 = 2.1 \times 10^8\ I_{eq}/\beta \simeq 4 \times 10^{11}$ cm^{-1}, and with $(L - x)$ the distance from the head of the beam,

$$n \simeq \frac{4 \times 10^{11}}{\pi r^2} = \frac{4 \times 10^{11}\ I(kA)}{\pi[r_0 + (r_f - r_0)(x/L)]^2} =$$

$$\frac{1.3 \times 10^9}{[1 - 0.99x/L]^2}\ I\ (kA)$$

or for a limiting current of 1 KA the density is in the range

$$1.3 \times 10^9 \leq n \leq 1.3 \times 10^{13}\ \text{cm}^{-3}$$

$$\omega_B = \left(4\pi n \frac{Z^2e^2}{M}\right)^{1/2} = 1.3 \times 10^3\ Z(n/A)^{1/2}\ \text{sec}^{-1}.$$

Ions suggested vary from singly charged U, A = 238, to 5 times charged I, A = 126. In the first case

$$3 \times 10^6 < \omega_B < 3 \times 10^8\ \text{sec}^{-1},$$

while in the second

$$2 \times 10^7 < \omega_B < 2 \times 10^9\ \text{sec}^{-1}.$$

The total growth equals ($\omega_B^0 \equiv \omega_B(x = 0)$)

$$\frac{1}{5} \int \omega_B\ dt \simeq \frac{1}{5} \int \omega_B \frac{dx}{v} = \frac{1}{5} \omega_B^0 \frac{L}{v} \int_0^1 \frac{dy}{[1.01 - y]}$$

$$\simeq \frac{1}{5} \omega_B^0 \frac{L}{v} \ln 100 \simeq 6 \times 10^{-8}\ \omega_B^0 \simeq 0.2 \text{ for } U^+$$

$$\simeq 1 \text{ for } I^{5+}$$

and is not important.

There is no intention, of course, of propagating beams through a vacuum, but as we shall show, beam effects are still characterized by ω_B, even in the presence of a background.

The environment through which the beam travels depends strongly on the pressure in the target chamber. Pressures considered have ranged from 10^{-2} torr, about the lowest that could be reached with a repetition rate of 1 Hz for the reactor vessel dimensions contemplated, to ~ 1 torr, which is close to the limit set by multiple scattering of the beam particles (for the self-constricted beam it may be possible to exceed this).

In the former case, the chamber might be filled initially with an at least partially ionized gas at a temperature of ~ 1 eV. In the second case, the first few centimeters of the beam produce enough ionization, both directly and by avalanching to ionize the plasma fully and to establish a temperature of between 1 and 5 eV, yielding a channel substantially wider than the beam, but surrounding it. In both cases, the plasma rapidly neutralizes both the beam charge and (almost completely) the beam current, so that the net current might be reduced to $I_{net} < 0.01\ I_B$. An immediate consequence is that the growth rate of the wriggle or fire hose mode is reduced by a factor of 100 (assuming that the entire current channel shares the gross motion; since the plasma current and the beam current almost coincide in space, this seems a reasonable assumption; but we shall examine it further).

The background plasma is characterized by its plasma frequency $\omega_p = 5.6 \times 10^4 \sqrt{n}\ \text{sec}^{-1}$ and its electron collision frequency $\nu \simeq 3 \times 10^{-6}\ n \log \Lambda / T^{3/2}\ \text{sec}^{-1}$. Here $\log \Lambda \simeq 22.3 - 1.15 \log_{10} n + 3.5 \log_{10} T$, T being the temperature in electron volts.

For 0.01 torr ($n \simeq 10^{14}$ cm^{-3}) and T = 1 eV

$$\omega_p \simeq 5.6 \times 10^{11}\ \text{sec}^{-1},$$

$$\nu \simeq 1.9 \times 10^9\ \text{sec}^{-1},$$

for 1 torr ($n \simeq 10^{16}$ cm^{-3})

$$\omega_p = 5.6 \times 10^{12}\ \text{sec}^{-1},$$

$$\nu = 1.2 \times 10^{11}\ \text{sec}^{-1} \text{ at } T = 1 \text{ eV}$$

$$\nu = 1.7 \times 10^{10}\ \text{sec}^{-1} \text{ at } T = 5 \text{ eV}.$$

In our analysis we propose to describe the background plasma by its dielectric coefficient

$$\epsilon_p = 1 - \frac{\omega_p^2}{\omega(\omega - i\nu)} .$$

Stripping of the beam particles must also be taken into account. Since the relevant cross-sections are $\sim 10^{-17}$ cm^2, this is important at densities of order 10^{16} cm^{-3} with stripping to $Z_f \sim 40$,, while at $n_p = 10^{14}$ cm^{-3} $Z_f \sim 2$. In the following we let $Z = Z_0(Z_f/Z_0)^{x/L}$ represent the change of charge state with distance along the pulse.

The easiest way to describe the wriggle mode is to compute the effective electric charge line density in the rest frame of the beam, then to calculate the unbalanced force acting on a curved part of the beam. The effect of a plasma environment is then to reduce the electric field by a factor $1/\epsilon_p$: hence to reduce the growth rate Γ_0 by $\epsilon_p^{-1/2}$. The mode grows for $kr_0 < 1$ with maximum growth for $kr_0 \sim 0.6$ or $\vec{k}\cdot\vec{v} \simeq 9.2 \times 10^9$ sec$^{-1} \ll \omega_p$. Thus

$$\Gamma \sim \Gamma_0 \frac{\vec{k}\cdot\vec{v}}{\omega_p\sqrt{2}} \left[1 + \left(1 + \left(\frac{\nu}{\vec{k}\cdot\vec{v}} \right)^2 \right)^{1/2} \right]^{1/2}$$

which for $\nu \gg \vec{k}\cdot\vec{v}$ reduces to $\Gamma \sim \Gamma_0 (\nu\vec{k}\cdot\vec{v}/2\omega_p)^{1/2}$ The total gain involves ($\omega_B^0 \equiv \omega_B(x = 0)$, $\alpha L = \ln Z_f/Z_0$)

$$\int_0^t \omega_B \, dt = \omega_B^0 \frac{1}{v} \int_0^L e^{\alpha x} \, dx/(1-0.99\, x/L) \simeq$$

$$-\omega_B^0 (L/v)\, e^{\alpha L} \, [\ln (0.01\, \alpha L + 0.5772]$$

and

$$\int_0^t \Gamma \, dt \simeq \left[\int_0^t \Gamma_0 \, dt \right] \frac{Z_f}{Z_0} \frac{I_{net}}{I_0} \frac{\vec{k}\cdot\vec{v}}{\omega_p} \, 2^{-1/2} \cdot$$

$$\times \left[1 + \left(1 + \left(\frac{\nu}{\vec{k}\cdot\vec{v}} \right)^2 \right)^{1/2} \right]^{1/2}$$

$$\simeq 7 \times 10^{-4} \int_0^t \Gamma_0 \, dt, \text{ for } n = 10^{14} \text{cm}^{-3}$$

$$\simeq 3 \times 10^{-3} \int_0^t \Gamma_0 \, dt, \text{ for } n = 10^{16} \text{cm}^{-3}.$$

In the latter case one scheme requires propagating the beam constricted by the residual current to its final radius. The gain then increases by a factor of about 37 to $0.1 \int \Gamma_0 \, dt$ which is still small.

A second mode that may deform the beam is a ripple mode. To understand this, let us first forget about beam geometry and consider a plane sheet of charge (again in vacuum) whose surface is distorted sinusoidally by a displacement $\xi = \xi_0 \cos kz$. The effective surface charge density produced by this is $\Sigma = -n_0 Ze\zeta_n \cos kz$, where ζ_n is the normal displacement drawn out of the surface. This produces an electric field

$$E = 2\pi\Sigma = - n_0 2\pi Ze\zeta_n \cos kz$$

and a local acceleration

$$\zeta = \frac{Ze}{M} E = -2\pi n_0 \frac{Z^2 e^2}{M} \zeta$$

and ζ oscillates with the frequency $\omega_B/\sqrt{2}$. In the presence of a plasma this result must be modified by the dielectric coefficient, and the dispersion relation becomes the cold two-stream dispersion relation with $\omega_B \to \omega_B/\sqrt{2}$. The resonant modes ($\vec{k}\cdot\vec{v} \simeq \omega_p$) grow at the rate $\sim \omega_p(\omega_B/\omega_p)^{2/3}$ (for small ν) and easily saturate. The associated wavelengths are now ~ 0.2 cm at $n = 10^{14}$ cm^{-3} and 0.02 cm at $n = 10^{16}$ cm^{-3} and it seems unlikely that these are dangerous, although targeting at 0.1 cm may be impaired. Non-resonant modes grow as ω_B and are not neutralized by the return current, and hence grow fifty times faster than the wriggle mode, still not fast enough to have much effect. The constricted case is an exception, for here the gain is about 11.5 e-foldings saturating at rather long wavelengths. Hence, surface ripples which significantly expand the beam could limit the use of self-pinched beams.

MICRO-INSTABILITIES

In addition to the modes which disrupt the spatial distribution of the beam, there are velocity-space modes which do not appear to have much direct effect on the beam, but may affect the degree of beam current neutralization by the induced plasma current. The beam driven two-stream mode is the best studied of these.

TWO-STREAM MODES

We consider these first in the hydrodynamic approximation and include both the velocity spread of the beam and plasma electron collisions. For the beam

$$\frac{\partial \vec{v}_+}{\partial t} + \vec{v}\cdot\nabla\vec{v}_+ = - \frac{1}{nM} \nabla p + \frac{Ze}{M} \vec{E} ,$$

$$\frac{\partial n_+}{\partial t} + \vec{v}\cdot\nabla n_+ = -n_0(\nabla\cdot\vec{v}_+) .$$

While for the plasma electrons

$$\frac{\partial \vec{v}_-}{\partial t} + \nu\vec{v}_- = -\frac{e\vec{E}}{m} ,$$

$$\frac{\partial n_-}{\partial t} = -n_0(\nabla\cdot\vec{v}_-) ,$$

and on combining these equations with Poisson's equation we obtain the dispersion relation

$$1 - \frac{\omega_B^2}{(\omega - \vec{k}\cdot\vec{v})^2 - (\vec{k}\cdot\vec{\Delta v})^2} - \frac{\omega_p^2}{\omega(\omega - i\nu)} = 0$$

or, with $x = \omega/\omega_p$, $y = \vec{k}\cdot\vec{v}/\omega_p$, $\mu = \nu/\omega_p$, $\epsilon = \omega_B^2/\omega_p^2$, and $\theta = \vec{k}\cdot\vec{\Delta v}/\omega_p = y(\Delta v/v)$:

$$[(x(x - i\mu)) - 1][(2 - y)^2 - \theta^2] - \epsilon x(x - i\mu) = 0.$$

We note that for θ, $\mu = 0$, $y = 1$, and $x = 1 + u$ that $u \simeq (\epsilon/2)1/3$ for $u^2 \ll 1$. Near the resonant point $y \simeq 1$ with $x = 1 + u$ this expression reduces to (if we neglect ν)

$$u(u^2 - \theta^2) = \frac{1}{2}\epsilon$$

which has real roots provided $\epsilon \leq (4/3\sqrt{3})\theta^3$. For the unstripped beam $\epsilon/\theta^3 \simeq 0.14$ for $\theta = 0.01$ and this mode is suppressed by the velocity spread in the beam. For the stripped beam the ratio increases by a factor $Z^2/100$ and the instability is excited for $Z > 16$. The self-pinched beam is then unstable by this criterion for much of its path. For the converging beam, however, the stability condition is not violated except very close to the target leaving only little time for gain. One might object that the hydrodynamic model is inadequate here, and that the beam dynamics should include Landau damping, or growth. The approximate effect is easily obtained by modeling the beam as a flat-topped distribution of width Δv, going linearly to zero at $v \pm (\Delta v + \delta v)$. The charge induced on the beam (in the beam frame) is then

$$4\pi\delta_q = 4\pi\frac{Z^2e^2}{M}\int \frac{k(\partial f/\partial v)}{(\omega - k\cdot v)}\phi \simeq$$

$$\frac{\omega_B^2 k^2}{2\Delta v n}\int_{v-\Delta v}^{v+\Delta v} f(v)(\omega - k\cdot v)^{-2}\,dv\,\phi$$

$$\simeq \left[\omega_B^2 k^2 \frac{1}{(\omega - k\cdot v)^2 - k^2\Delta v^2} \pm \frac{i\omega_B^2\pi}{2\delta v\Delta v}\right]\phi$$

$$= \omega_B^2 k^2\left[\frac{1}{(\omega - k\cdot v)^2 - k^2\Delta v^2} \pm \frac{i\pi}{2(k\delta v)(k\Delta v)}\right]\phi$$

where the last term is present only if ω/k lies between $v \pm \Delta v$ and $v \pm (\Delta v + \delta v)$. The effect on the dispersion relation is to add a term

$$\epsilon(x\cdot x - i\nu - 1)[(x - y)^2 - \theta^2]\left[\frac{i\pi}{\theta^2}\frac{\Delta v}{\delta v}\right]$$

and to alter the coefficient of $(u^2 - \theta^2)$ from 1 to $1 \pm i\pi\epsilon\Delta v/\theta^2\delta v$ and the growth rate, already small, is altered by a complex factor less than 1. Henc kinetic effects do not seem important.

TRANSVERSE MODES

There is a non-convective electromagnetic mode that will grow for wavelength small compared to the beam radius with a growth rate of $\sim \beta\omega_B$. This grows only for the beam duration $\sim 10^{-8}$ sec and in the worst case, the highly ionized iodine beam, grows by a factor exp 20, or for highly ionized uranium by a factor $\sim$ exp 6. Its effects are not clear; any beam shredding occurs right at the end of the beam, and it may produce significant magnetic fields near the target. On the other hand, it does not appear to be disruptive.

PLASMA MODES

Near the end of its path, the current density in the beam reaches values of $I \sim 2 \times 10^5$ amp/cm^2 for the low pressure case and because of enhanced ionization $\sim 8 \times 10^6$ amp/cm^2 in the high pressure case. The electron velocity need to neutralize these currents is of the order

$$v_s \approx 6 \times 10^{18}\frac{j}{n} \approx c \text{ for } n = 10^{14}\ \text{cm}^{-3}$$

$$\simeq 0.4c \text{ for } n = 10^{16}\ \text{cm}^{-3}.$$

Hence in both cases the electron velocity exceeds the electron thermal speeds and in the absence of collisions one would expect ion-acoustic instabilities to induce an anomalous resistance. The associated frequencies $\omega < \omega_f \simeq 10^8 \sim 10^9$ are much less than the collision frequencies, hence one could scarcely expect the usual collisionless theory to hold. On the other hand the collisions themselves appear to drive a similar mode unstable. To analyze this roughly, note first that the electron-electron collision frequency is great enough to keep the electrons close to Boltzmann equilibrium. On the other hand, the ratio between the momentum transfer frequency between electrons and ions is about a factor of 100 below the ion plasma frequency. We can then write the ion momentum balance equation in the form (neglecting the pressure):

$$\dot{v} + \nu_{+-}v - \delta\nu_{+-}v_D = eE/M$$

where

$$\delta\nu = \nu\frac{\delta n_-}{n_-} = \nu\frac{k_D^2}{en_0}\phi$$

hence

$$v_+ = \frac{-(e/M)ik\phi + v\nu(k_D^2/en_0)\phi}{[i(\omega - kv) + \nu]}$$

and

$$4\pi\delta q_+ = \frac{\omega_{p_+}^2 k^2}{(\omega - k\cdot v)(\omega - k\cdot v - i\nu)}\left[1 + i\frac{k\cdot v\nu}{k^2 v_-^2}\frac{M}{m}\right]\phi,$$

where v_- is the electron thermal speed, and the dispersion relation becomes

$$(\omega - k\cdot v)(\omega - k\cdot v - i\nu) = \omega_{p_+}^2 \frac{k^2}{k^2 + k_D^2}\left[1 + i\frac{k\cdot v_D}{k^2 v_-^2}\nu\frac{M}{m}\right]$$

where $\nu = (m/M)\nu_-$. From this

$$(\omega - k\cdot v) = \frac{1}{2} i\nu \pm \sqrt{\omega_{p_+}^2 \frac{k^2}{k^2 + k_D^2}\left[1 + i\frac{v_D}{v_-}\frac{\nu_-}{\omega_{p_-}}\frac{k_D}{k}\right] - \frac{1}{4}\nu^2}.$$

Now if $k^2/(k^2 + k_p^2) \gg (\nu/2\omega_p)^2$, we can neglect ν^2 and

$$\omega - k\cdot v \simeq \frac{1}{2} i\nu \pm \omega_p \frac{k}{\sqrt{k^2 + k_p^2}}\left[1 + i\frac{v}{v_-}\frac{\nu_-}{\omega_{p_-}}\frac{k_D}{k}\right]^{1/2}$$

and a growing mode is possible, with a growth

$$\frac{1}{2}\nu \pm \frac{\omega_p}{\sqrt{2}}\frac{k}{\sqrt{k^2 + k_D^2}}\left[\sqrt{1 + \left(\frac{v}{v_-}\frac{\nu_-}{\omega_{p_-}}\frac{k_D}{k}\right)^2} - 1\right]^{1/2}.$$

This is unstable if

$$\sqrt{2}\frac{\nu_+}{\omega_{p_+}} < \frac{k_D}{\sqrt{k^2 + k_D^2}}(v/v_-)(\nu_-/\omega_{p_-}).$$

$$v/v_- \simeq 3 \times 10^{10}\, IZ/n\Gamma^2\sqrt{T}$$

and the stability criterion is satisfied for 1000 ampere beams, for $R > 1$ cm at $n = 10^{14}$ cm^{-3}, $Z = 1$: $R > 0.3$ cm for $n = 10^{16}$ cm^{-3}. The remaining flight path is $x \simeq 1$ m, or 6 nsec. In the low density case $\omega_B < 6 \times 10^7$ and the growth of the wriggle mode would still be less than exp (0.6) even if the currents were completely destroyed. For the high density case where $Z = 40$, the growth $\sim$ exp $(40 \times 10^7 \times 6.10^{-9}) \approx 11$ and even if the current were completely neutralized by anamoulous effects, there would be no great effect on the U beam. For the I case a more careful calculation is required.

Note that the arguments presented here are quite crude. Beam geometry has been handled in a very primitive fashion, the plasma has been treated as if uniform and all relativistic effects have been omitted. A completely convincing version will correct these deficiencies and treat the nonlinear consequences of the instabilities.

7. ARGONNE NEUTRALIZATION EXPERIMENT

S. Fenster

Argonne is setting up an experiment on the charge neutralization of beams of heavy ions using a 3 mA dc source of Xe^{+1} at 100 keV. This beam will pass through a 3-inch bore triplet with gradient variable up to 15 Tesla/m. The ion beam will tend to trap electrons with an inward radial electrical field.

$$E_r = -60.\pi \frac{J}{\beta_i} r \text{ volts/m} .$$

Where J is the ion current density ($amps/m^2$), $\beta_i = \frac{v_i}{c}$ and r is the distance to the axis. Electrons will revolve around the magnetic field lines at gradients of 15 Tesla/m. The experiment will determine whether enough lower energy electrons are present to achieve neutralization.

The potential at the edge of such a beam is +90 volts with respect to its center. If a 200 V. electrode ring surrounds the beam, the neutralizing electrons may be removed. By pulsing the electrode on with a rise time $\tau_r < .1$ μsec and observing electronically the increase in beam spot size as a function of time, one can determine the time constant for removal of neutralizing electrons. Pulsing in the opposite direction gives the reverse time constant for producing neutralization. With this setup, electrons inside a quadrupole may get trapped around magnetic field lines, so it may be necessary to place clearing electrodes inside the magnets. A 10 MHz. A. C. clearing field may also be tried.

We expect to vary the vacuum from the usual 10^{-5} Torr down to 10^{-8} Torr to check the effect of residual gas on neutralization.

A listing of beam sizes against the phase advance per period and the parameter P in a FODO Lattice has been set up, neglecting space charge.

C. REACTORS

1. SUMMARY

J. A. Maniscalco

INTRODUCTION

The Laser Fusion Program System Studies Group at Lawrence Livermore Laboratory has been engaged in scoping studies to identify attractive reactor concepts for producing power with inertial confinement fusion. The scoping studies were carried out by developing several reactor concepts and then comparing them on the basis of their ability to cope with the major problems affecting the technical feasibility of an inertial confinement fusion power plant. These include:

1) The effects of the fusion microexplosion on the first wall.
2) The effects of high energy neutrons and cyclical stresses on the blanket structure.
3) The effects of the fusion microexplosion on the final focussing elements.

During these comparative studies a fluid wall reactor design called the liquid lithium waterfall emerged as a most promising reactor concept for generating electricity with laser fusion. In this section we will briefly describe the reactor concept and analyze it with regard to the technical problems listed above.

High energy yield per shot can be used to minimize the effects of both driver and target fabrication costs on the cost of electricity. Conversely, high energy yield per pulse characteristics increase the damaging effects of the radiation from the microexplosion on the first wall and blanket structure. This is one of the reasons that led us to select a fluid wall concept for our reactor. More importantly, in this approach, the first wall and blanket structure are shielded from x-rays, target debris, and neutrons by a thick falling region of liquid lithium. We consider target irradiation from a few sides with long focal length ion beams. At focal lengths on the order of 10 m, it appears possible to design a final focussing magnet that could survive the damaging effects of the thermonuclear microexplosion for a year or longer, sufficiently long to avoid an excessive effect on the plant capacity factor.

REACTOR DESIGN

The lithium waterfall reactor design was strongly influenced by our desire to develop a simple concept that could be constructed with existing materials using current state-of-the-art technology so that the decade or so required for advanced material development and testing could be circumvented.

The reactor concept (Fig. V-C-1/1) features a thick continuously recyclable first wall of liquid lithium that protects the first structural wall from direct exposure to the microexplosion. The waterfall is disassembled by each shot, and it is reestablished between each shot. The lithium is continually pumped to the top of the vacuum chamber through a reservoir region which separates the first structural wall from the pressure vessel. A small fraction of the lithium flow circulates as the primary coolant to the heat exchanger. The return flow from the heat exchangers is injected through a vortex generator to provide protection to the top of the chamber.

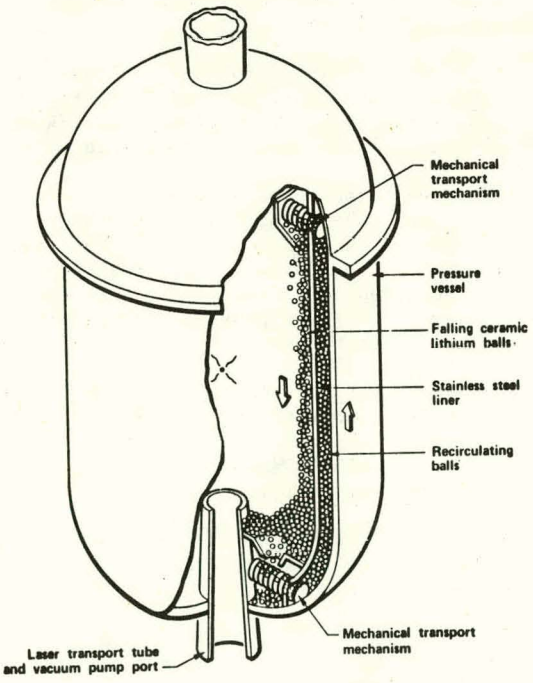

Fig. V-C-1/1. Falling balls concept.

The principal purpose of the fall is to reduce the neutron radiation damage in blanket structural materials, allowing them to survive for the useful life of the plant. Besides moderating neutrons, the fall also absorbs the x-ray output and pellet debris. By keeping the fall separated from the chamber wall, any shock wave produced in the fall will not be directly transmitted to the structural wall.

The primary neutron damage mechanisms to reactor structural materials are atomic displacements and gas production. For an unprotected steel wall operating at a neutronic wall loading of 1 MW/m^2, the damage limits would be reached in only a few full-power-years. This would present a severe maintenance problem and result in the generation of large amounts of radioactive waste. One MW/m^2, is generally considered to be the lower flux limit for an economically attractive fusion reactor. At this wall loading, a fusion reactor would operate with power densities that are an order of magnitude lower than a light water reactor.

The product of neutron wall loading, in MW/m^2, and the wall lifetime, in years, is a figure of merit for any fusion reactor design. This product, the allowable first-wall fluence, increases exponentially with the protective thickness of the lithium fall. We have evaluated the requirements of a system that maintains a minimum protective lithium thickness of 60 cm, and found it provides an allowable fluence of $\sim$ 90 $MW\text{-}Yr/m^2$. In other words, the system could be operated at $\sim$ 4 MW/m^2 for the 30-year plant life at a 75% capacity factor. Thus, for a given power, the reactor can be made smaller with structures that never require replacement.

It should be pointed out that fluids other than liquid lithium could be used to perform the functions of the fall. The primary constraints on the fall material are that the substance must:

1) Have a reasonably low melting point (less than about 300° C) so the fluid state can be effectively maintained.
2) Have a low enough vapor pressure at the selected operating temperature (>400° C but as high as possible) to permit an adequate vacuum condition to be maintained.
3) Have neutronic characteristics that permit an adequate tritium breeding ratio to be achieved.
4) Be compatible with the selected structural materials.

Tritium breeding considerations preclude the use of a neutron absorber and require that lithium be incorporated in the reactor system in a suitable manner.

Other possibilities for the fall are lead and lead-lithium alloys such as Pb_4Li. Lead, as the primary constituent of the fall, degrades the neutron energy through (n, 2n) and inelastic scatterings. Our neutronic calculations indicate that a few volume percent of ^6Li in the lead would be enough to maintain a tritium breeding ratio greater than one. The use of Pb or Pb_4Li would allow a lower system tritium inventory to be maintained. On the negative side, recirculation pumping power would significantly increase and grain boundary corrosion of steels may present compatibility problems. The various aspects of these systems are being investigated.

The pumping power required to recirculate the lithium fall has been estimated on the basis of the kinetic and static head requirements with the fall inlet conditions determined by two constraints:

- The fall must have sufficient velocity to reestablish itself between microexplosions.
- A minimum attenuating thickness of 60 cm must be maintained.

The required pumping power increases with chamber size and with pulse repetition rate. For 1-2 Hz, the power required is less than 5% of the gross electric power production of the reactor. Since the ion beam system operates more economically at higher repetition rates, multiple reactor chambers may be coupled with a single driver.

The beam propagation group at the workshop generally felt that it would be possible to focus the heavy ion beam in a chamber with a background pressure in the neighborhood of 1 Torr. This relatively high allowable pressure makes it possible to use liquid lithium in the vacuum chamber. Corrosion considerations require that, for use with stainless steel, lithium temperatures must be less than 500° C. As shown in Fig. V-C-1/2, the vapor pressure of lithium at this temperature is less than 5×10^{-3} Torr.

If fusion chamber pressures less than 10^{-3} Torr are needed to focus the ion beam, the attractive features of the lithium waterfall reactor concept can be retained by replacing the liquid fall with a falling region of solid ceramic-lithium pellets. In this concept (Fig. V-C-1/3) ceramic pellets are continuously recirculated to the top of the fusion through a resevoir region between the first wall and the pressure vessel. The ceramic pellets can be either transported through heat exchangers or cooled by the flow of high pressure helium gas in the resevoir region. Tritium is bred in the ceramic compounds and recovered as it diffuses out into the helium. The use of lithium in ceramic form eliminates both the corrosive problems and chemical hazards associated with lithium metal. On the negative side major uncertainties need to be addressed such as the structural integrity of the ceramic pellets and finding a means of efficiently transporting the pellets into and out of the vacuum chamber. We intend to address these questions this year.

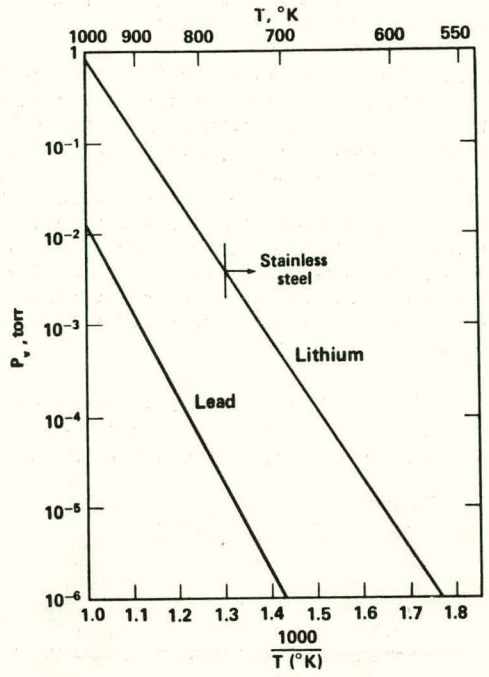

Fig. V-C-1/2. Vapor pressure vs temperature for lithium and lead.

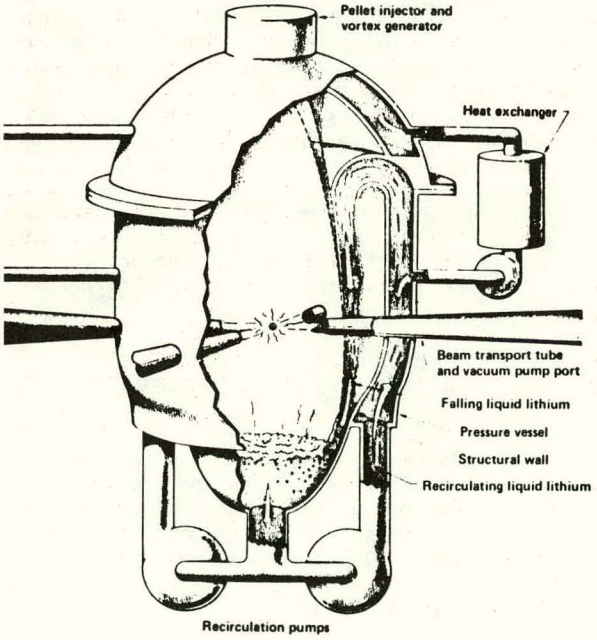

Fig. V-C-1/3. Ceramic pellet concept.

CONCLUSIONS

The lithium waterfall reactor has emerged as a promising concept which alleviates the major problems associated with inertial confinement fusion systems. It eliminates the first wall problems resulting from x-rays and pellet debris, and minimizes cyclical thermal stresses. Also, the thick falling region of lithium attenuates neutrons to the point where the blanket structure could survive for the lifetime of the power plant at high power densities. The concept appears to be adaptable to any inertial confinement fusion system which can operate with fusion chamber pressures greater than 10^{-2} Torr.

2. CONSTRAINTS DUE TO NUCLEAR INTERACTIONS IN HEAVY-ION INDUCED FUSION, AND SHIELDING REQUIREMENTS

R. Silberberg and C. H. Tsao

INTRODUCTION

There are several aspects of the heavy-ion induced fusion process for which a detailed knowledge of nucleus-nucleus interactions is essential: (1) The modification of the distribution of energy deposition in the fusion pellet due to nuclear fragmentation and constraints on the composition of the pellet, (2) the background radiation of protons and neutrons at energies of ~ 200 MeV due to interactions of heavy ions near the reactor chamber and the accumulator ring while the reactor is in operation, and (3) the background radioactivity at the reactor and accumulator ring while the reactor is shut down. We shall present here some preliminary results obtained in two weeks work in this field, and point out areas in which further work is required.

CONSTRAINTS ON THE COMPOSITION OF THE PELLET

In the present sample calculation we shall adopt an energy of 300 MeV/nucleon (henceforth abbreviated as MeV/u) for the beam particles at the target. For ^{209}Bi, the corresponding energy is 63 GeV, and a few per cent less for other prospective beam particles like Hg or Au.

Above 100 MeV/u, the total inelastic cross section per proton-nucleus collision can be approximated by the empirical equation (formulated by us):

$$\sigma\ (p + A) = 1.31^2\ .10\ \pi\ A^{2/3}\ (1 - 0.47/A^{0.4})$$

and for nucleus with mass number A_1 colliding with one having mass number A_2 by

$$\sigma\ (A_1 + A_2) = 1.26^2.\ 10\ \pi \left[A_1^{1/3} + A_2^{1/3} - 0.4\right]^2 ;$$

both cross sections are given in units of mb. A more rigorous expression for the latter (including energy dependence) is given by Karol (1975).[1]

The fraction of nuclei that come to rest without undergoing a nuclear collision is given approximately by

$$F = \exp\left[\frac{-R\ (g/cm^2)\ \sigma(mb)}{1673\ A_2}\right].$$

Here R is the residual range (in g/cm^2) of the beam particle in the medium of mass number A_2. It is assumed that the residual range of the particle is negligible when its energy has been reduced to a value such that the above cross section equations are no longer applicable.

We shall now determine the initial "surviving fraction" F, i.e., prior to the turning of the target into plasma. The actual value of F will be larger due to reduction of the residual range R in the plasma (Nardi et al 1977).[2]

The beam particles (^{209}Bi) become nearly fully stripped; the electrons retained are evaluated by the procedure outlined by Barkas (1963).[3] The residual range R and fraction F of ^{209}Bi nuclei at 300 MeV/u that have not collided is given in Table V-C-2/1, for target media of hydrogen, carbon; copper and lead, respectively. Since the calculation is an extrapolation to heavier nuclei, the uncertainty in the estimate of R is ~ 2%. A more detailed computer calculation, based on the number of electrons retained as a function of energy, is desirable.

Table V-C-2/1. Residual range and fraction of non-colliding Bi nuclei.

Target	R(g/cm^2)	F
H	0.80	0.42
C	1.86	0.75
Cu	2.48	0.90
Pb	3.36	0.98

One can see from Table V-C-2/1 that if the medium in which the Bi (or Au or Pb) nuclei lose most of their energy is light, e.g., consisting of hydrocarbon, about half of the beam particles will undergo nuclear collisions, and the forward "tail" (or snout) of the Bragg peak can be appreciable in regions of the target where it is undesirable. This could especially be the case with a uranium beam--since most of the nuclear interactions result in fission, the residual range of the fission fragment is nearly double that of the parent uranium nuclide.

If the target medium, on the other hand, consists of heavy nuclei like Pb, the interacting fraction 1-F is ~ 2%, and the distortion of the Bragg peak due to nuclear interactions is negligible.

THE BACKGROUND RADIATION IN REACTOR CHAMBER AND THE ACCUMULATOR RING WHILE THE REACTOR IS IN OPERATION.

For this sample calculation, we assume an energy release of 4×10^9 joules per pellet, a ratio of energy output to energy input of 100, and 10 pulses per second. This corresponds to an energy input of 2.5×10^{20} MeV per pulse, or 4×10^{15} Bi nuclei (or Au or Pb) per pulse, i.e., 4×10^{16} Bi nuclei per sec.

The richest source of neutrons in the fusion reactor is the deuterium-tritium fusion, yielding (for the above parameters) ~ 10^{22} neutrons/sec. But the energy of these neutrons, and of their progeny is about 14 MeV. On the other hand, the neutrons from the fragmentation of the beam particles (e.g., Bi) are dominant in the outer portion of the shield as shown in the next three paragraphs below.

In p-Bi collisions at 300 MeV, the atomic number Z of Bi changes on the average by $\Delta Z \leq 10$, and the number of neutrons emitted is ~ 1.5 larger. In heavy nucleus-nucleus collisions, however, the degree of breakup is much greater (Schroeder, 1977).[4] Probably ~ 25 protons and ~ 35 neutrons are emitted per collision of bismuth nucleus. Assuming 2% Bi nuclei collide in the target, $\sim 3 \times 10^{16}$ neutrons with an average energy $E \approx 200$ MeV are generated per second.

Assuming a permissible radiation dose of 0.1 rem/week corresponds to 1.3×10^6 neutrons/cm^2 per week at 10 MeV (Goussev, 1968).[5]

We shall now explore the shielding necessary to reduce the neutron flux to these limits. The half-value thickness (in which the neutron flux is reduced 50%) for the fragmentation neutrons from Bi, (i.e. at 200 MeV) is 42 cm of concrete, and only 9 cm for the 14 MeV fusion neutrons (Wallace, 1970).[6] Table
that the nuetrons from Bi, though fewer in number, require more shielding.

Table V-C-2/2. Shielding required to reduce the neutron dose to 0.1 rem/week, at distance r from reactor.

r(m)	Shielding (m of concrete)	
	fusion neutrons	Bi fragmentation neutrons
30	4	14
1000	3	11

Appreciable shielding is also required at the accumulator ring. Assume 1% of Bi nuclei are lost from the beam and enter a medium of iron or steel. Assume again a beam of Bi nuclei of 4×10^{16}/sec; and an energy of 300 MeV/u. About 90% of the Bi nuclei come to rest, while 10% undergo nuclear reactions. The number of neutrons per interaction is again assumed to be 35. Then $\sim 1.4 \times 10^{15}$ neutrons are generated per second, i.e. $\sim 5\%$ of that from interactions of Bi in the reactor area. The required shielding is 12 m of concrete if the working areas are 30 m from the accumulator ring, and 9 m if the working areas are 1 km away.

The required shielding for the linac can be a little less than 10 m of concrete—the exact value depends on the fraction of Bi nuclei lost per unit path length in the linac.

The accelerator and reactor can be underground, at depths approximately comparable to the shielding discussed above.

BACKGROUND RADIOACTIVITY WHEN THE ACCELERATOR (i.e. REACTOR) IS SHUT DOWN.

The background radioactivity in the reactor is derived from (a) interactions of neutrons produced in the $^2H + {}^3H$ fusion process, (b) fragments of the Bi nucleus and its collision partner in the fusion pellet, as the latter evaporates, and (c) fast protons and neutrons from the fragmenting Bi nucleus that interact in the reactor walls. Since $\sim 10^{22}$ neutrons per second are generated in process (a) compared to $\sim 10^{15}$ in process (b) and 10^{16} in process (c), the radioactivity generated by the first process should be dominant. Probably $\geq 1\%$ of the fusion neutrons ($\sim 10^{20}$/sec) will interact in the pellet ablator layer, generating radioactive nuclei that will splash on the reactor wall.

Also in the accumulator ring, the radioactivity after shut-down will be high. About 4×10^{13} Bi nuclei/sec will interact yielding a variety of radioactive products, and nuclides that go on and collide at the rate of $\sim 10^{15}$/sec. Thus, the γ-ray production rate in the accumulator and the surrounding shielding can build up to 10^{15}/sec.

A detailed calculation of the background radioactivity is warranted, but requires detailed information on the configuration and composition of the accumulator, the surrounding walls and also of the reactor chamber walls. Since the 14 MeV fusion neutrons can induce only a limited number of nuclear reactions, e.g. (n,p), (n,α), a choice of shielding material is possible that minimizes the number of radioactive nuclei formed, or restricts them to a very short-lived species. Yet, the radiation level may be so high, that procedures may have to be designed for remote control of required repairs or replacement of parts.

References

1. P. J. Karol, Phys. Rev. C 11, 1203 (1975).
2. E. Nardi, E. Peleg, and Z. Zinamon, Weizmann Institute of Science, 1977, WIS-77/28-PH.
3. W. H. Barkas, Nuclear Research Emulsions, 1 (1963), Academic Press.
4. L. S. Schroeder, Research/Accelerators, LBL, 2, No. 2, p. 44 (1977).
5. N. G. Goussev, Engineering Compendium on Radiation Shielding, I, p. 12 (1968), Springer Verlag.
6. R. Wallace, Engineering Compendium on Radiation Shielding, III, p. 157 (1970), Springer Verlag.

3. TARGET INPUT REQUIREMENTS FOR HEAVY ION FUSION

R. O. Bangerter

INTRODUCTION

This paper summarizes the requirements a heavy ion accelerator must meet in order to initiate practical thermonuclear microexplosions. Particular emphasis is given to the question of maximum allowable ion energy.

ACCELERATOR REQUIREMENTS

Although fusion target design was not an official part of the workshop, there were a sufficient number of questions on the topic to justify writing a brief note for the Workshop Proceedings.

Just as there are many possible accelerator designs, there are also many possible fusion target designs. Some of these target designs have not fully been evaluated. Furthermore we expect that improved targets will continue to be developed. Consequently a number of iterations involving close communication between target designers, accelerator designers and reator designers will be required to arrive at an optimized target - accelerator-reactor system.

The target requirements which we have provided are based on our best designs so far, on rather universal target design considerations, and on our projections of future improvements in target performance.

At the beginning of this workshop we decided to focus our efforts on two sets of target requirements. These are given in Table V-C-3/1. The reactor corresponds to the moderate confidence level target described in Table 1-I of the 1976 Summer Study Report.[1] Progress during the last year has increased our confidence in this case. We are reasonably confident that the heavy ion demonstration experiment (HIDE) target parameters can produce scientific breakeven.

The specific energy column has been a source of some confusion and since it sets an upper limit on the range (particle energy) of the incident ions it has a large impact on accelerator design. Consequently, I have written a small program to calculate the range-energy curves shown in Fig. V-C-3/1. The curves are for various ions incident on lead at a density of 2 g/cm^3 and a temperature of 200 eV. These conditions are typical of densities and temperatures in the beam deposition region of a fusion target. In any case the curves are only weakly dependent on density and temperature. For example, the calculated range of a 30 GeV uranium ion is 1.12 g/cm^2 in lead at a density of 11.3 g/cm^3 and room temperature and 0.95 g/cm^2 at a density of 2.0 g/cm^3 and a temperature of 200 eV. The calculations include the effects of both bound and free electrons and are similar to the calculations presented by Mosher in Appendix A1-2 of Reference 1.

The new curves differ somewhat from those given in F. 1-1 of Reference 1. Using again 30 GeV uranium as an example, the new curves give a range that is about 1.5 times as large as the old curves. I consider the new curves more reliable; however, to my knowledge ranges of intense, energetic ion beams in hot, dense material have never been measured. It does not seem most unlikely that the calculated ranges are in error by more than a factor of two, but additional theoretical work is underway to improve the accuracy of the calculations. It is also possible that some relevant experiments can be performed at existing heavy ion accelerators.

With the above qualifications in mind, I have used the curves of Fig. V-C-3/1 to produce curves of upper limits on ion energy as a function of atomic weight. The specific energy is given by $\varepsilon = E/m = E/2\ \pi r^2 R$ where r is the focal spot radius and R is the range in g/cm^2 (or other units of area density). The factor of 2 in the denominator results from the fact that at least 2 beams are required for adequate implosion symmetry. For targets having an input energy $\sim$ 1 MJ the minimum reasonable focal spot radius is $\sim$ 1 mm although for smaller 100 kJ targets 0.5 mm may be allowable. Using these facts and assuming a minimum specific energy of 20 MJ/g we obtain the curves shown in Fig. V-C-3/2.

It should be emphasized that these curves do not represent a sharp upper limit in the sense that any ion energy above the curve will not work at all and all ion energies below the curve are equally effective. In terms of specific energy we expect target gain to increase rapidly as the specific energy is increased from $\sim$ 10 MJ/g to $\sim$ 30 MJ/g. It is probably also true that for a given specific energy there is some advantage in going to a larger focal spot size and shorter range; or, in terms of accelerator parameters, there is some advantage in low ion-energy, high emittance beams. However, it seems likely that ranges less than $\sim$ 0.03 g/cm^2 or focal spot sizes larger than $\sim$ 1 cm are useful for targets in the 1 to 10 MJ input range.

We also note that ions have shorter ranges by nearly a factor or 2 (in g/cm^2) in low Z materials than in high Z materials. It may be possible to take advantage of this fact to increase the upper limits on ion energy, but in so doing we decrease the flexibility in target design. For this reason I have excluded upper limits based on low Z range-energy relations from Fig. V-C-3/2. In so doing, I am placing the 35 GeV synchrotron case studied at the Workshop about the upper limit. However, an increase in total energy from 1 to 1.3 MJ (for a uranium beam) would bring 35 GeV back within limits.

There have also been some questions about pulse shape. Different target designs require different pulse shapes. The typical pulse shape taken from Reference 1 is reproduced in Fig. V-C-3/3. A research accelerator should have the capability of producing variations of this pulse

shape and also simpler shapes such as a relatively square pulse. Sufficient flexibility in pulse shaping would be provided by a capability of approximating this shape via a series of ≥ 5 shorter pulses.

Finally it should be noted that the fall time or shape of the pulse after the power has reached its peak value for a time Δt is not important. Energy arriving after this time is simply wasted. Our design efforts are currently oriented toward taking advantage of energy that is delivered over a time greater than the Δt shown in Table V-C-3/1.

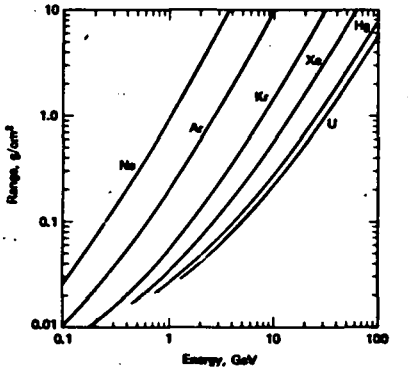

Fig. V-C-3/1. Range as a function of energy for various particles incident on lead at a density of 2 g/cm^3 and a temperature of 200 eV.

Reference

1. ERDA Summery Study of Heavy Ions for Inertial Fusion, LBL-5543, December 1976.

Table V-C-3/1. Summary of Accelerator Requirements.

TARGET	E (MJ)	Δt (ns)	P (TW)	ϵ (MJ/g)
Moderate Confidence Reactor Target	1.	6	100	≥20
HIDE Target	0.1	1.2	50	≥20

E is the total beam energy, Δt is the pulse length at peak power, P is peak power, ϵ is specific energy (energy/mass) deposited in the target.

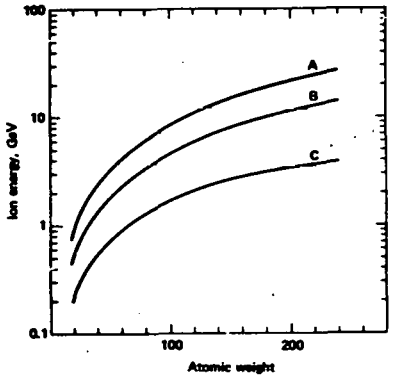

Fig. V-C-3/2. Upper limit on beam energy as a function of atomic weight assuming a specific energy of 1 MJ and a beam radius of 1 mm. Curve B is for 100 kJ and 0.55 mm and curve C is for 100 kJ and 1 mm.

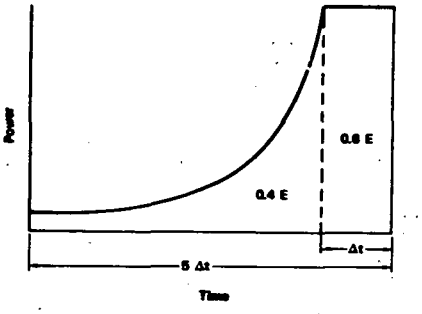

Fig. V-C-3/3. Typical pulse shape for an ion beam fusion target.

4. FINAL FOCUSING OF 35 GeV BISMUTH IONS

Eugene Colton

In this note we investigate the parameters of a final focusing system for Bismuth ions of kinetic energy 35 GeV in charge states +4 and +1. These options were discussed at the recent IBF Workshop convened at Brookhaven in October, 1977.

For simplicity, we just utilize a symmetric quadrupole triplet to fulfill a point to parallel condition in both transverse planes. Space-charge effects are not included. The outer quadrupoles are horizontal focusing, and of effective length L_o. The inside quadrupole has an effective length L_i, and is vertically focusing. The quadrupoles are separated by 0.5 m drift lengths and are placed as shown in Fig. V-C-4/1.

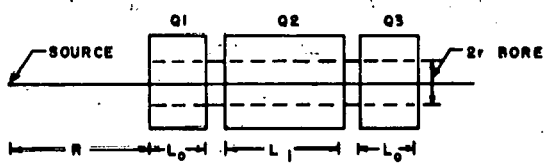

Fig. V-C-4/1. Schematic quadrupole arrangement.

R is the first drift length (e.g., radius of the reaction chamber). For this exercise we utilized T = 35 GeV Bismuth ions (P = 121.9 GeV/c), and a fixed pole tip field of 50 kG (superconducting quadrupole).

The optical constraints were satisfied by varying the quadrupole lengths; the program TRANSPORT was utilized in the studies. Results were obtained assuming bore radii of both 30 cm and 50 cm, each for two R values (5 m and 10 m). In Table V-C-4/1, we list the quadrupole lengths for the four cases mentioned, for an ion charge of +4 ($H\rho$ = 101.6 x 10^6 gauss-cm). We also list the normalized transverse emittance/π passed by the system $\epsilon_x = X_o\, X_o'\, \beta\gamma$, and $\epsilon_y = Y_o\, Y_o'\, \beta\gamma$, where X_o (Y_o) is the half-source width in the horizontal (vertical) plane. X_o' and Y_o' represent the largest initial divergences which can be transmitted through the system. For this case, we assumed a spherical source (pellet) with $X_o = Y_o = 0.1$ cm. We show in Table V-C-4/2 similar cases assuming a ion charge of +1 ($H\rho$ = 406.2 x 10^6 gauss-cm). It should be noted that the allowed emittance increases with increasing ion charge under identical conditions (because of the shorter quadrupole lengths required).

Finally, and for illustration we display in Fig. V-C-4/2 the transverse plane beam envelopes for normalized emittance of 1.0 cm-mr (solid curve), and 2.0 cm-mr (dashed curve). The conditions are for the third row down in Table V-C-4/2, namely, ion charge +1, R = 10 m, and r_{bore} = 30 cm. It appears that beam envelopes must enter the quadrupole system (from the left) with a size of about half the aperture in order to be successfully transported. These conditions can be altered somewhat by making the triplet asymmetric, but no big gains are to be expected.

Table V-C-4/1. Results for Ion Charge of +4.

R (m)	Bore Radius (cm)	L_o (m)	L_i (m)	ϵ_x (cm-mr)	ϵ_y (cm-mr)
5.0	30	1.40	2.57	1.75	2.01
5.0	50	1.96	3.58	2.36	3.02
10.0	30	1.16	2.18	1.34	1.28
10.0	50	1.67	3.12	2.00	2.00

TABLE V-C-4/2. Results for Ion Charge of +1.

R (m)	Bore Radius (cm)	L_o (m)	L_i (m)	ϵ_x (cm-mr)	ϵ_y (cm-mr)
5.0	30	3.39	6.14	0.93	1.48
5.0	50	4.48	8.28	1.19	2.14
10.0	30	3.00	5.54	0.88	1.03
10.0	50	4.13	7.59	1.19	1.54

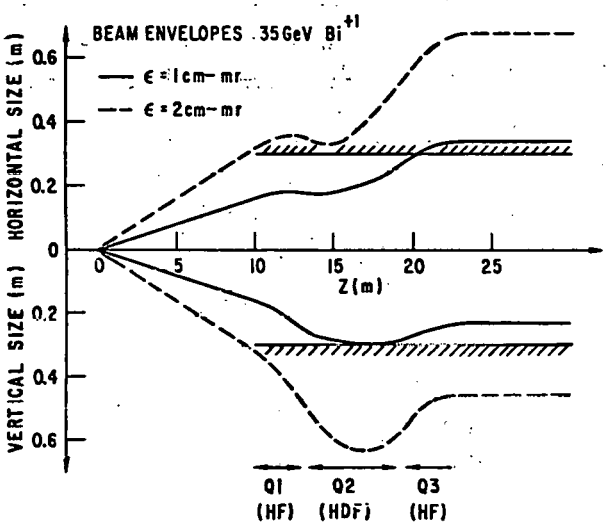

Fig. V-C-4/2. Monoenergetic beam envelopes expected with use of a symmetric quadrupole triplet which satisfies a focus to parallel condition. We assume T = 35 GeV Bi^{+1} ions, a reaction chamber radius of 10 m, and bore radius of 30 cm (shown cross-hatched). See text for other details.

D. ION SOURCES AND PREACCELERATORS

1. SUMMARY

Everette F. Parker

Since this workshop has the HIDE development as its main function, participation in the ion source/preaccelerator (S/P) working group was rather limited.

Most of the time was spent reviewing the S/P programs at the various laboratories. These programs were described briefly in the three (ANL, BNL, LBL) program summary talks given at the beginning of the workshop. More detailed descriptions of these S/P programs are given in following papers in this section of the proceedings.

The S/P working group also received very interesting presentations on the space charge neutralization studies being carried out at BNL; the collective acceleration work at the University of Maryland; and the heavy ion source work going on in the Chemistry Department at BNL.

The key R&D issues in the S/P areas are the development of high intensity, high brightness heavy ion sources, the development of high voltage (1-3 MV) accelerating columns and associated high voltage power supplies and the development of an understanding of space charge neutralization, and charge changing interactions at low energies. Each of these issues is being studied at one or more of the involved laboratories, and within the next 1 - 2 years we should have a firm understanding of the mass, charge state, brightness, current and energy practically available for HIF.

While firm specifications must await the results of the presently planned R&D program, the S/P working group is highly confident that an S/P system producing 100 mA of Xe^{+1} at 1 MeV with a normalized emittance of 0.02 π cm mrad can be built. It should also be possible to produce higher charged states but at much lower currents. For Xe^{+2}, one might expect 5 particle mA at 2 MeV; or for Xe^{+3}, 1 - 2 particle mA at 3 MeV.

The production of higher charge states is better accomplished by stripping a Xe^{+1} beam at several mega electron volts. It appears that a Xe^{+1} beam can be converted to a Xe^{+3} beam by gas stripping with He. At 1 MeV, the conversion efficiency should be about 33%, and the emittance growth due to scattering noticeable, but acceptable (rms scattering angle of 2 -3 mrad). A peak conversion efficiency of 36% occurs at about 3 MeV where the gas scattering is less than 1 mrad.

Although with considerably less confidence, the S/P working group feels a factor of 1.5 to 2 increase in the preaccelerator voltage and ion source current may be possible.

2. ANL IBF ION SOURCE/PREACCELERATOR PROGRAM

Everette F. Parker

The IBF system inputs to the source/preaccelerator (S/P) area are the specification of the ion mass and charge state, the minimum acceptable beam brightness and current, and the minimum acceptable injection velocity for the second stage accelerator. The S/P area program then becomes the development of an adequate ion source, accelerating column, and a high voltage power supply.

The S/P input to the system studies required to arrive at the ion mass and charge state specification will be a push for charge state +1 and for a mass which exists naturally in a gaseous, monatomic, pure isotopic state. All of these requirements stem from the desire to avoid the equipment complexities, brightness dilution, space charge effects, and power loss associated with mass and charge state mixtures. The noble gases represent convenient candidates for masses up to $\sim$ 130 except for the isotopic distribution of Kr (57% at Kr^{84}) and Xe (27% at Xo^{132}). At higher masses, Hg is available but it, too, suffers from a poor isotopic distribution (30% at Hg^{202}). Natural isotopic and chemical purity is limited to Bi, I, and Cs in the mid and heavy mass range. These elements are, unfortunately, not very convenient to deal with.

In the first phase of the ANL S/P program, we will develop a noble gas source. The low β linac stages under development at ANL will be able to use an unseparated beam for some time. This source will also have a Hg capability if a higher mass is required. Before isotopic purity becomes a practical problem we will, of course, have to develop a separation technique or a source using a naturally pure isotopic element.

Like all of the other IBF system parameters, the preinjector beam current and brightness requirements have not been accurately specified. Some very preliminary considerations indicate, however, that for one IBF approach, 50 mA in a normalized area of 0.1 cm mrad is required for injection into a collector ring. Assuming an overall transmission efficiency of 50% and that the source emittance will be diluted by a factor of 4 or 5 by the time the beam reaches the collector ring, we have set as an initial source design goal, 100 mA in 2×10^{-2} cm mrad. The ANL source program is discussed in Ref. 1.

The optimum preaccelerator voltage must be determined by a cost (difficulty and dollars) trade-off study between the preaccelerator and low β linac. The costs to the S/P people scales as some large positive power of the voltage; whereas, the cost to the low β linac people scales as some large negative power of the voltage. We have not yet carried out such a trade-off study in any detail, but a cursory review indicates that the optimum voltage may be between 1.0 and 3 MV. Design studies of a low β structure operating at 12.5 MHz indicates that $\sim$ 25 mA will be the current limit for Xe^{+1} at 750 KeV. This limit should scale as $\beta_{2/3}$, so a 50 mA linac would require an injection energy of 2 MeV if this analysis is correct.

The development of a 3 MeV, 100 mA Xe^{+1} beam with a reasonable emittance represents a significant advancement beyond presently available heavy ion accelerators, so we have set our sights somewhat lower than this for our initial effort. Our initial design goal is 1.5 MeV. The accelerating column, while being designed for 15 mA/cm^2 of Xe^{+1} and 1.5 MeV, will be built in such a way as to allow lower current densities and energies to be used. The details of the column design are given in Ref. 2.

The power supply is a modified Radiation Dynamics, Inc. 4 MV dynamitron. This machine was selected originally because it was available as excess NASA equipment. We now feel that it, or something similar, is more appropriate than the Cockcroft-Walton we have more experience with. The major reason for this belief is its compactness at these high voltages and its small stored energy relative to a "bounced" C-W. This latter characteristic should help keep arc-down damage to a minimum. The ANL development plans for this machine are discussed in Ref. 3.

References

1. R. L. Seliger, R. P. Vahrenkamp, Ion Source for Ion Beam Fusion, this workshop.
2. E. P. Parker, ANL IBF Column Development, this workshop.
3. J. M. Watson, ANL Heavy Ion Preaccelerator Development, this workshop.

3. ION SOURCE FOR ION BEAM FUSION

R. L. Seliger and R. P. Vahrenkamp

The selection of the best ion source for ion beam fusion must be based on the ability of the source to provide the desired beam current, emittance, and long-life operation on heavy ions. The performance of an ion source is basically determined by its ionization mechanism and the configuration of the extraction electrode.

The ion source we are currently investigating for ion beam fusion uses a low-voltage Penning ion discharge and has a single-aperture Pierce extraction electrode configuration. This choice was based on our experience with it, which includes demonstration of many of the desired performance features. Figure V-D-3/1 contains a schematic of an early (1973) version of such a source and a Table of performance that was obtained for three different Pierce electrode configurations. This material comes from an earlier study[1] in which aperture diameters of 1 mm and 4 mm were considered for current densities ranging between 9 and 37 mA/cm^2 of argon. The beams produced in all cases were far superior to the beams in our existing ion implantation systems, which were produced by low-voltage extraction (~3 kV) and low-gradient (4 kV/cm) linear acceleration. We now know that the improved beam quality was caused by the low emittance of the Penning-discharge Pierce-extraction (PDPE) source.

In 1974, we further refined our PDPE source to improve its utility. An intermediate electrode, in the shape of an equipotential surface, was inserted between the focus and the extraction electrodes to provide a simple means of controlling the focus of the emerging beam. Figure V-D-3/2 is a diagram of the beam envelope obtained for the three-electrode PDPE source; the beam current was 4 mA of argon at a final energy of 90 keV. The narrow beam angle (α= 15 mrad) was obtained by adjusting the intermediate electrode voltage to make the beam waist coincide with the plane of neutralization. Expansion of the neutralized beam was then linear with z, which made it straightforward to determine the beam angle. With a waist diameter of 2 mm, the source emittance was 1.5 mrad-cm. Comparing this measured emittance with the minimum theoretical emittance

$$E_{th} = \frac{D_A}{2} \quad \frac{V_t}{V_z}$$

obtainable from a source of emitting radius $D_A/2$ (which produces ions with transverse ion energy eV_t and accelerates the ions to axial energy eV_z without aberrations) shows the transverse ion energy to be ~2.3 eV. Thus, the PDPE source has low emittance because it can produce a high-energy (90 keV) beam with only 2.3 eV of transverse energy. The Penning-type discharge is essential to achieving this because of its inherently low energy spread; the Pierce-type electrode configuration is essential because of its low aberration.

Other desirable features of the PDPE source are that it can generate heavy ions and can be scaled to higher currents. On 30 September 1977 Hughes delivered a three-electrode PDPE source to Argonne National Laboratory (ANL) that had been modified to operate on the heavy ions Xe, Bi, and Hg. Figure V-D-3/3 shows some operating points taken at Hughes before delivery.

The complete source was not tested on Hg because we felt certain of successful performance, and we wanted to delay Hg contamination until absolutely necessary. Source operation on Xe was very stable and reproducible. Xe appears to be an excellent candidate for initial demonstration of the high-voltage dc accelerator. A Bi beam was also demonstrated in the PDPE source, but the electrode surfaces became coated rapidly (in a few hours) and arcing began to occur. When the high-voltage insulator also became coated, we stopped experimenting with Bi. We conclude that if long-life operation of a PDPE source on Bi is possible at all, it will only be achieved by a large engineering effort to provide strategically heated surfaces (e.g., electrodes at ~800°C), cool surfaces to intentionally collect the Bi and baffles to shield the insulators. A similar strategy is needed for Hg, but surfaces will remain uncoated at a much lower temperature (e.g., 100°C). The 2-mA Xe PDPE source will be evaluated in a test stand at ANL beginning next month. This will generate much important data on source emittance, beam neutralization, and heavy ion scattering, which will help develop the beam dynamics of ion beam fusion.

Work has also begun on a PDPE ion source scaled up to 100 mA for ion beam fusion. A critical parameter in the scaling is the diameter of the extraction aperture D_A. The choice of D_A governs the required plasma density in the source and the current density of the beam in the subsequent stages of acceleration. The primary wearout mechanism in the discharge chamber is ion sputtering erosion; the erosion rate is directly proportional to the plasma density. Although source lifetime is not an immediate concern, high plasma densities should be avoided. The ion source current density dramatically affects the design of the dc accelerator. Figure V-D-3/4 shows the electric field necessary to balance the divergent space-charge forces in a collimated beam with current density J and atomic mass M as the beam accelerates in a dc accelerator at a constant radius. As shown, the electric field is a weak function of the mass; $M^{\frac{1}{2}}$ only varies from 2.51 for Ar (M = 40) to 3.76 for Hg (M = 200). The electric field is a stronger function of the current density ($J^{\frac{1}{2}}$); depending on the value of J chosen, the electric field could be changed by up to a factor of three. We have tentatively chosen J = 15 mA/cm^2 for Xe, which corresponds to a reasonable electric field of 60 kV/cm at 0.4MV. In this region of acceleration, the Pierce accelerator electrode design that will be used will couple perfectly with the Pierce extraction system and provide a high-energy, parallel, low-emittance beam. Geometric scaling of the 2mA Xe

PDPE source by a factor of five is required to obtain 100 mA of Xe at J = 15 mA/cm^2. The extraction aperture diameter D_A would then be 3cm. Two significant goals of the ion source development program are to demonstrate that a stable plasma sheath can be formed with this size extraction aperture and that a low-emittance beam can be extracted. Work toward these goals is about to begin on an ANL/Hughes program.

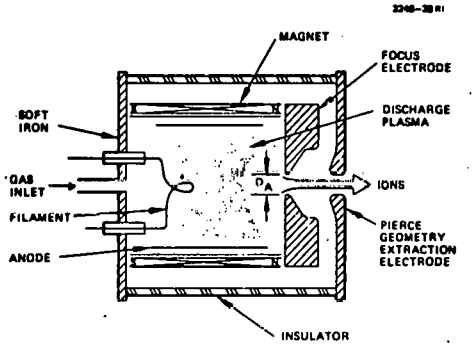

CONFIGURATION	D_A (mm)	V (kV)	I (mA) ARGON	J (mA/cm^2) ARGON
A	1.0	20	0.1	12.3
B	4.0	100	1.2	9.2
C	4.0	100	4.5	37.0

Fig. V-D-3/1. Ion source configuration.

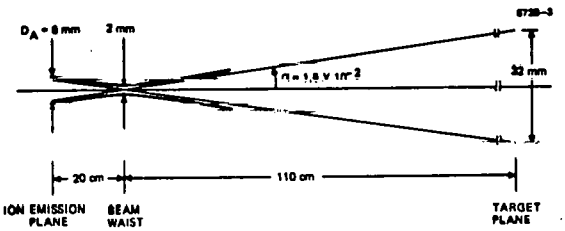

Fig. V-D-3/2. Beam envelope for three-electrode PDPE ion source.

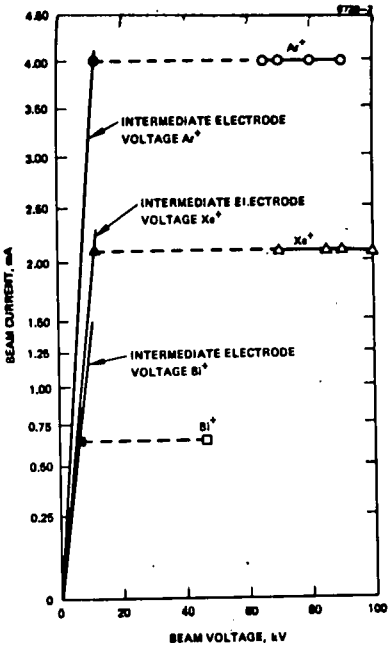

Fig. V-D-3/3. Three-electrode PDPE source: operating points on Ar, Xe, and Bi.

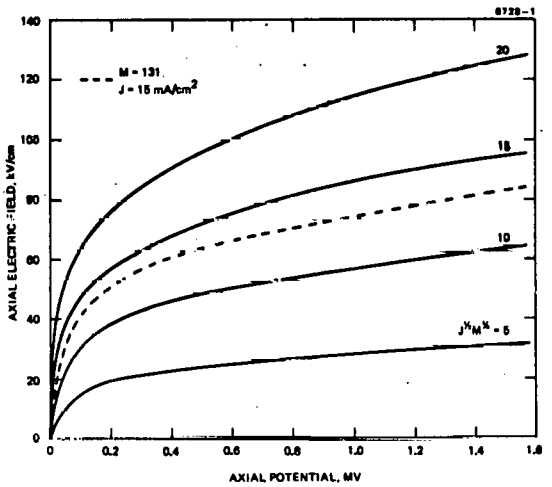

Fig. V-D-3/4. Effect of beam current density and ion mass on the accelerator gradient required for parallel ion flow.

Reference

1. R. L. Seliger and J. W. Ward. "Low Perveance Ion Beam Extraction from an Electron Bombardment Discharge," Electron and Ion Beam Science and Technology, Sixth International Conference.

4. ANL HEAVY ION PREACCELERATOR DEVELOPMENT

J. M. Watson

A substantial part of the IBF program at Argonne National Laboratory is the development of a high-current high-voltage preaccelerator for heavy ions. There are several advantages in making the preaccelerator voltage as high as possible. The large space-charge force of 100 mA heavy-ion beams makes their transport difficult at low energies through reasonable apertures with desirable current densities. A higher preaccelerator energy would also alleviate some of the expense and complexity of low-beta linac cells. Although most of us are acquainted with high-power 750 k V dc supplies used as injectors at high energy accelerators, reliable high-current accelerators capable of several MV have been developed and marketed since 1960.[1] Above 1 M V these newer power supplies appear superior to the Cockcroft-Walton preaccelerators. They have very little stored energy, so spark damage is minimal, and they are much more compact through the use of an insulating gas. The pressurized gas vessel is only a minor inconvenience if adequate pumping and gas storage are provided and the vessel is equipped with quick-opening flanges.

In July of this year we obtained a 4 MV Dynamitron from Goddard Space Flight Center for our preaccelerator development program. Our initial objective is to generate pulsed 100 mA beams of 1.5 MeV Xe^{+1} ions. This is twice the voltage at which most of us have experience, so the accelerating column for this energy and current density will be a challenge, but hopefully the extrapolation of our present techniques will be successful. The designs of the source and accelerating column are also described in this workshop.[2]

The Radiation Dynamics, Inc. (RDI) Dynamitron[3] is a parallel-input, series-output voltage multiplier which converts high-frequency ac power into high-voltage dc power with good efficiency (60%). The radio-frequency (125 kHz) power is capacitively coupled to the rectifier stages via a pair of semi-cylindrical electrodes (dees) which surround the rectifier column. The rectifiers are connected to a series of semi-circular corona shields which together form an inner, cylindrical envelope around the column. The corona shields perform the combined functions of receiving rf power from the driving electrodes, filtering the dc potentials and preventing corona discharges from the rectifier terminals and other high-voltage components. Since no capacitors or transformers are used in the rectifier column, the stored energy is very low and the risk of component damage due to spark breakdown is minimal.

We have reassembled the Dynamitron minus source and accelerating column and are presently carrying out high voltage tests. The rf oscillator is shown in Figs. V-D-4/1 and V-D-4/2 and the rectifier column and rf electrodes in Fig. V-D-4/3. The experimental hall (Fig. V-D-4/4) where it is located will house both the preaccelerator and the beginning cells of the low-beta linac. This will transport the beam into an adjacent hall where the higher energy systems will be developed.

At the conclusion of the high voltage tests in November, the Dynamitron will be disassembled for the modifications needed to accept the new column and source and to achieve intense pulsed currents. The pressure vessel will be lengthened three feet, have a new flange added for mounting the column downstream of the rectifier stack, and have a quick-opening flange inserted at the terminal end. The present stack has 94 high-vacuum rectifier tubes which have a maximum dc current rating of 25 mA and output voltage of 50 k V dc per stage. These will be replaced by 82 solid-state rectifier modules (Fig. V-D-4/5) rated at 50 mA and 50 kV dc per stage. The new stack will also be reconfigured to a full-wave circuit which will allow twice as much current at a maximum voltage of 2 MV. The dees will also be reshaped and moved closer to the stack to increase the capacitive coupling since the voltage holdoff spacing can be reduced.

In January, the preaccelerator will be reassembled and pulsed high voltage tests will be conducted. In preparation for 500 μ sec pulsed beams at a repetition rate of 1/sec, we expect the accelerator will have to operate at the desired voltage for approximately 10 msec per pulse to achieve good regulation. The voltage between pulses will depend on what leads to the most reliable operation of the column. The source will also have its gas and extractor voltage pulsed, so it is not obvious whether the column will operate better by lowering the voltage between pulses or by going to a higher voltage to condition it for the next beam pulse.[4] The pulsed power capability will be measured during these tests by using a variable-resistance water load. It is expected to be at least 50 mA with the present oscillator. An attempt will be made to boost this to pulsed currents of 100 mA by adding energy storage to the oscillator high-voltage supply and new or additional pass tubes if necessary. If this should prove too extensive, a RDI oscillator capable of this power is already commercially available.

The 100 mA Xe^{+1} source and column should be installed by June 1978. The conditioning and reliability tests will then begin in an effort to provide an intense low-emittance beam suitable for injection into the first cells of the low-beta linac.

If the 1.5 MV, 100 mA goals are successful, we intend to pursue the development of higher voltage machines in collaboration with RDI. The accelerators would probably have the accelerating column within the rectifier stack as in the original design. This simplifies and stabilizes the voltage division down the column, but it would require a short, large-diameter stack to match

the columns needed for intense heavy-ion beams. Of course, several-MV accelerators such as this would be very useful as injectors for high energy accelerators as well as having many practical applications.

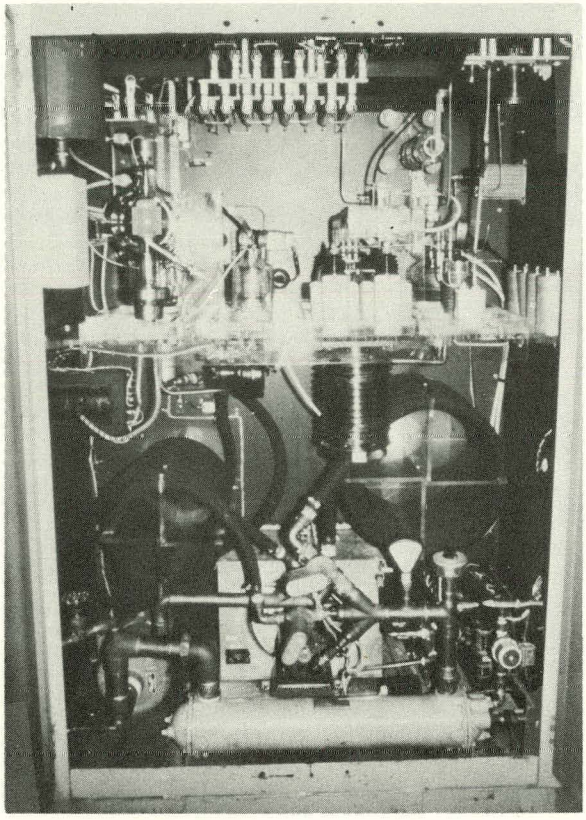

Fig. V-D-4/1. Dynamitron rf oscillator: Series pass tube compartment.

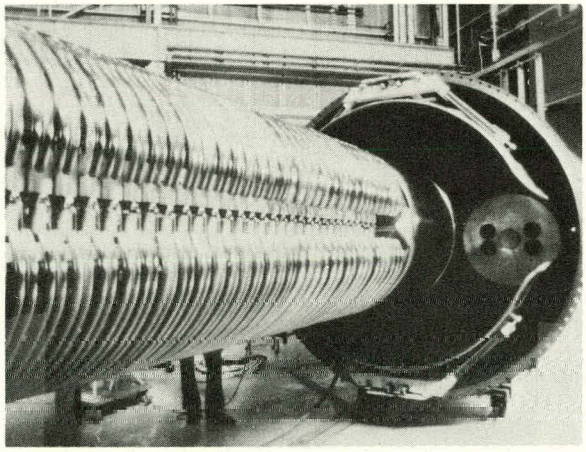

Fig. V-D-4/3. Dynamitron cascaded rectifier system with vacuum tubes.

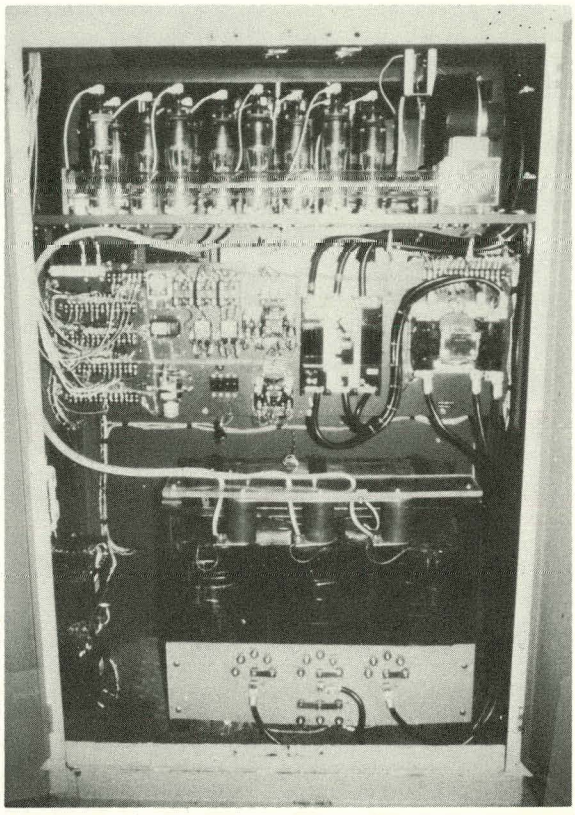

Fig. V-D-4/2. Dynamitron rf oscillator: High voltage power supply compartment.

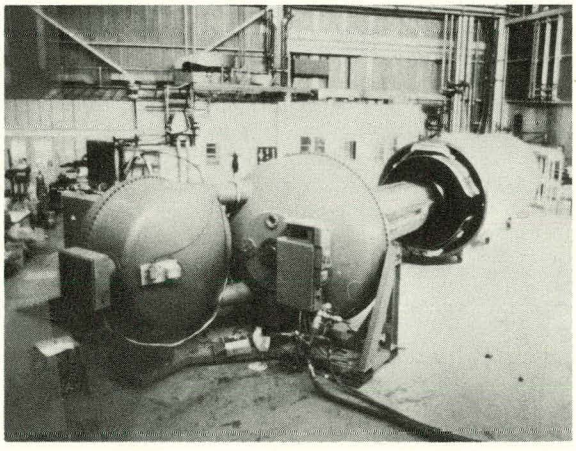

Fig. V-D-4/4. IBF Preaccelerator hall. Low beta linac will penetrate wall in far corner into adjacent hall.

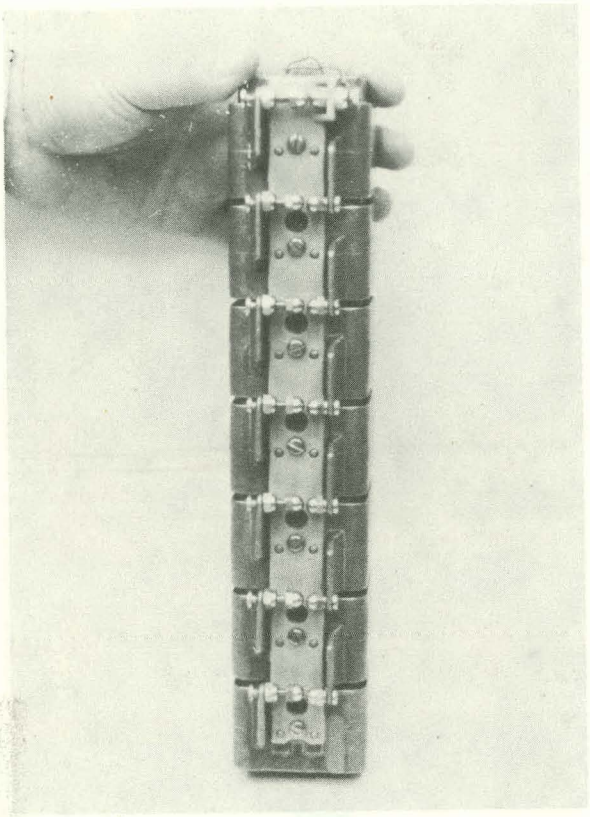

References

1. These are available from four firms: Radiation Dynamics, Inc., High Voltage Engineering Corp. Nishin HV and Mitsubishi.
2. R. L. Seliger and R. P. Vahrenkamp, "Ion Source For Ion Beam Fusion", this workshop. E. F. Parker, "ANL High Voltage Column Development", this workshop.
3. M. R. Cleland and K. H. Morganstern, "A New High-Power Electron Accelerator", Nucleonics, August 1960.
   M. R. Cleland and K. H. Morganstern, "A New High Power Electron Accelerator", IRE Transactions on Industrial Electronic, Vol. 1E-7, No. 2, July 1960.
   M. R. Cleland and P. Farrell, "Dynamitrons of the Future", IEEE Transactions on Nuclear Science, Vol. NS-12, No. 3, June 1965, p. 227.
   C. C. Thompson and M. R. Cleland, "Design Equations for Dynamitron Type Power Supplies in the Megavolt Range", IEEE Transactions on Nuclear Science, Vol. NS-16, No. 3, June 1969, p. 124.
4. Alexander Langsdorf, Jr. Private communication.

5. LARGE-APERTURE PULSED 1-AMPERE CESIUM SOURCE

W. W. Chupp, A. Faltens, W. B. Herrmannsfeldt,
D. Keefe, S. Abbott, and E. Hoyer

We have begun the development and construction of a large aperture (10 inches diamter) pulsed heavy-ion source. This source is designed to produce 2 microsecond bursts of 500 keV Cs^{+1} ions with a current in the one-ampere range. Cs^{+1} are produced by directing bursts of neutral Cs atoms onto an iridium hot plate. This development is well underway.

In addition to this we have set up a smaller test system to test components which may influence the design of the large ion source and also to obtain early information about unusual difficulties that might not have been anticipated for the big source. In this test we have installed and tested a puff valve using Xe gas and nude ionization gauge detectors. Hot tungsten wire detectors have now been installed in the system and tests with cesium vapor are underway. Cs^{+1} ions have been observed with these detectors from the hot surface in about the approporiate quantity expected for the test conditions.

Concurrently, a heated iridium plate has been installed in the test tank and an existing submicrosecond Marx generator has been modified to generate pulses a few microseconds long over a voltage range variable from 100 kV to 200 kV. This will permit application of voltages and fields in the presence of Cs ions and vapor comparable with those expected in the large aperture source. Because cesium contamination can enhance electron emission we feel it necessary to check tolerable voltage gradient levels in this test set-up before proceeding to the final "one-ampere" source.

6. ANL IBF COLUMN DEVELOPMENT

Everette F. Parker

At this early stage in the IBF program there are no firm specifications on the preaccelerator, so the selection of initial design goals in this area is somewhat arbitrary. From the studies completed to date, it appears reasonable to conclude that an ion mass of 150 ± 50 will be required at a current of some tens of milliamperes at the highest practical energy. We have therefore chosen 100 mA (~15 mA/cm^2) of Xe^{+1} at 1.5 MeV as our initial preaccelerator design goals.

There are a number of problems associated with the design of an accelerating column capable of meeting these goals and, unfortunately, many of them do not lend themselves to any kind of optimization analysis. Instead, one is forced to use "educated guesses," "gut feelings," and "rules-of-thumb." The design we have arrived at is shown in Fig. V-D-6/1. Its key parameters are listed in Table V-D-6/1.

The problems we are most concerned about are: protecting the insulators from ions and sputtered metal, minimizing the electric field gradients at the metal-insulator joints, and producing an adequately high field gradient to keep the space-charge-induced beam size growth to an acceptable level.

The insulator protection is provided by the double "T" arrangement shown in Fig. V-D-6/1. Any ion or metal reaching the ceramic surface is the result of at least a two-step cascade, unless it is produced locally as a result of X-rays,or field emission. The thick shields, while incorporated to minimize fabrication costs, will provide some protection from X-rays. The lower "T's" concentrate the field at the center of the ceramic-washer gap, thereby reducing the field gradient at the metal-ceramic joint to a minimum.

The diameter of the column was kept as small as possible, and a large number (30) of gaps were used to minimize the stored energy per gap.

The ceramic-metal joint is shown in Fig. V-D-6/2. It consists of the epoxy-indium ring joint used on the AGS column, but also incorporates the step in the ceramic used on the FNAL columns. A high gradient column using this joint has given trouble-free service on the ZGS for the past three years.

In order to carry a Xe^{+1} current density of 15mA/cm^2 to 1.5 MeV in a Pierce geometry, a peak field of 83 kV/cm is required. While this might be obtainable, we will not count on it. We will use a Pierce geometry to as high an energy as practical, then use a constant gradient the rest of the way. This means that the beam will exit the column with a divergence, the magnitude of which depends upon the current density and the amount of constant gradient acceleration. Fig. V-D-6/3 shows the approximate divergence vs current density for two values of peak gradient. Practical considerations of quadrupole construction indicate that divergences up to about 15-20 mrad can be handled by a focussing triplet mounted in the ground end of the column. From Fig. IV-D-6/3, we see that this implies a peak field gradient of almost 60 kV/cm for the desired 15 mA/cm^2 current density. Sixty kV/cm is higher than any gradient in service that we are aware of and may be difficult or impossible to realize. Should this be the case, we will have to use stronger quadrupoles and/or lower current densities.

The column will be designed in a manner which will allow both the peak and average field gradients to be adjusted moderately easily.

The ground end quadrupole triplet is about one meter long and has a bore diameter of 8 cm and a gradient of 25 T/m.

The detail design of this column will be completed by early November and part procurement is underway. Assuming no delivery problems, we expect to complete this column and be ready for initial testing by the spring of 1978.

Table V-D-6/1. 1.5 MV, Xe^{+1} High Gradient Column Parameters.

Voltage	≤1.5 MV
Current density	≤15 mA/cm^2
Current	≤100 mA
Total length	117.3 cm
Accelerating gap length	34 ± 10 cm
Wall field gradient	15 kV/cm
Number of sections	30
Insulators	Coors AD 90 ceramic (90% Al_2O_3)
Lens and shields	Titanium
Metal-ceramic bond	Epoxy with indium vacuum seal
Accelerating field geometry	"Pierce" up to 400 kV, then constant gradient to 1.5 MV

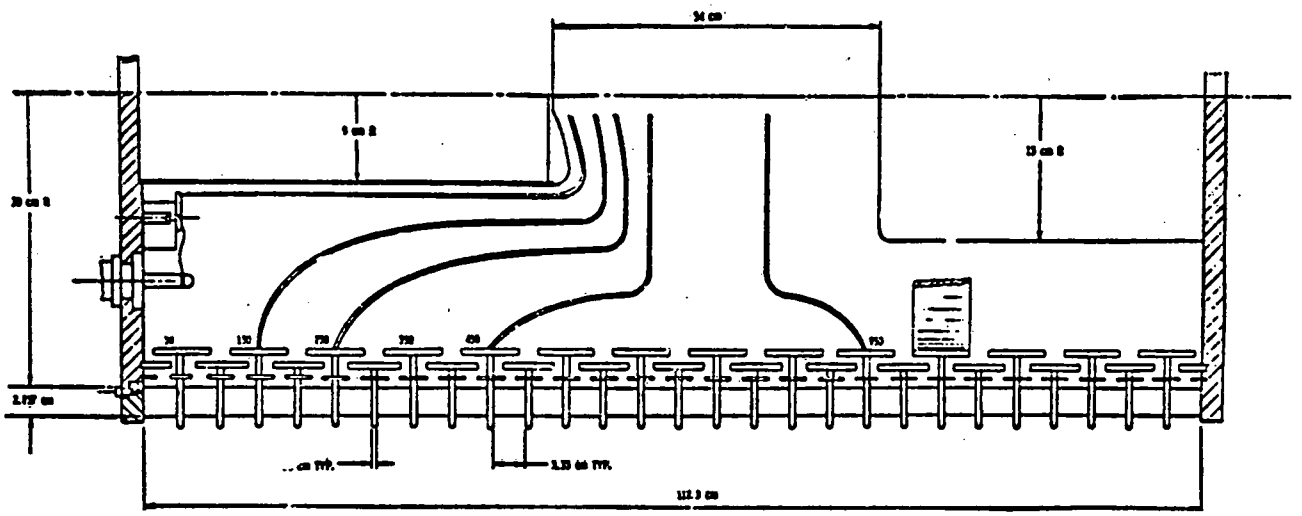

Fig. V-D-6/1. 1.5 MeV Column.

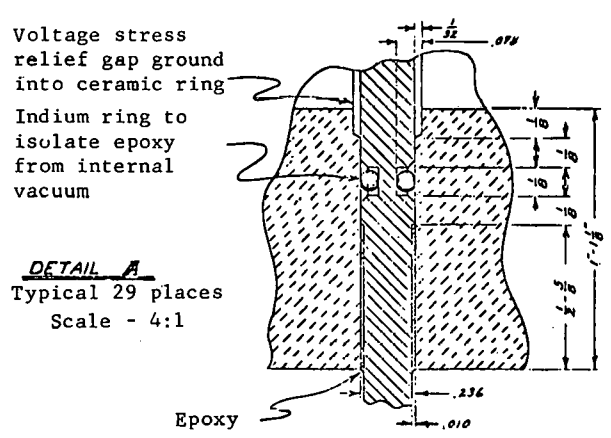

Fig. V-D-6/2. Ceramic Metal Joint.

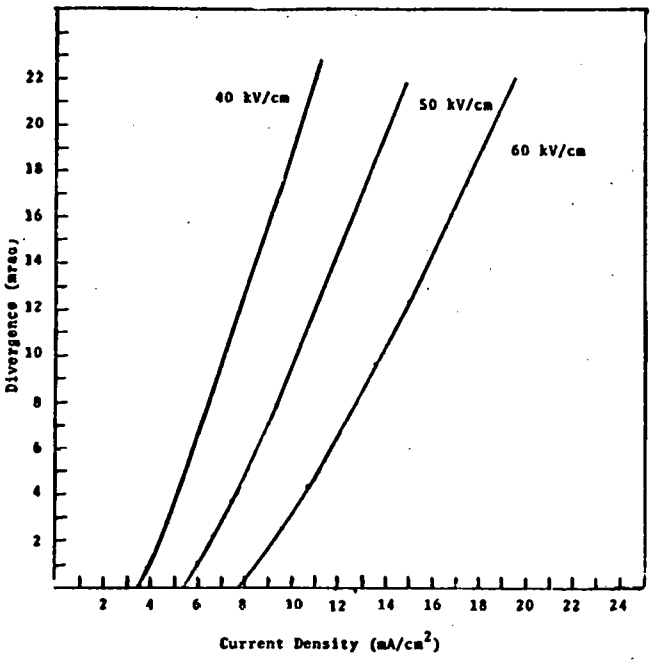

Fig. V-D-6/3. Exit divergence as a function of current density.

7. TESTS AND DEVELOPMENT OF DUOPLASMATRON AND MULTIAPERTURE HEAVY ION SOURCES FOR AN RF LINAC

D. J. Clark, R. M. Richter, E. Zajec,
R. Brokloff and J. E. Osher

The goal of the program of ion source development for an rf linac has been to produce currents of up to 100 mA of the heavier gaseous ions such as argon and xenon, of good emittance (.02 π cm mr, normalized) and charge state 1^+ following the recommendation of the 1976 Summer Study.[1] Existing facilities and hardware utilized included the 470 kV Bevatron injector, the 750 kV injector for the 50 MeV ESCAR linac, the 80 kV Bevatron test stand, a 20 kV LLL test stand and existing duoplasmatron and CTR sources. A summary of test results is shown in Table V-D-7/1. We have also befited from the experience of the CTR source groups at LBL and LLL, and discussions with K. Ehlers.

At the Bevatron injector beams of 30 mA of neon and 25 mA of xenon were accelerated through the low gradient column to 470 kV, using the Bevatron duoplasmatron source. The beams were pulsed with 0.5 ms duration at 2/sec. No beam emittance or charge state measurements were made in this set-up.

The 750 kV injector with its high gradient column was used to accelerate neon to 500 kV, using the standard duoplasmatron. Fifteen mA was measured, with an emittance of .02 - .05 π cm mr., normalized, with mainly 1^+ charge state. The transmission was not optimum for Ne^{1+}, but only

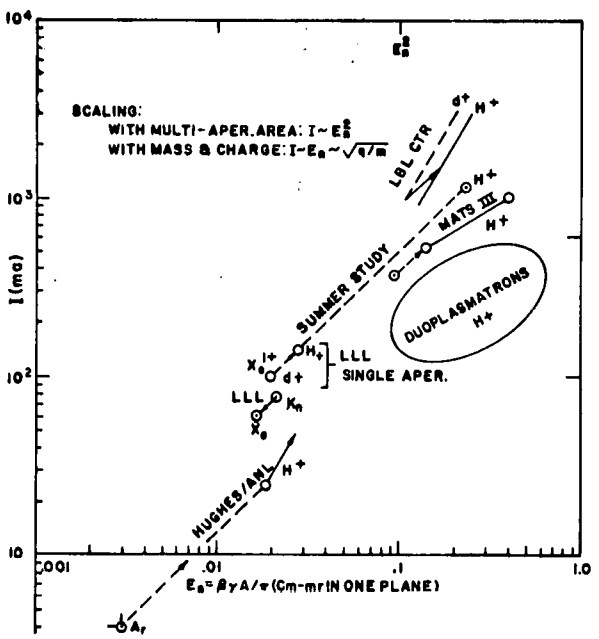

Fig. V-D-7/1. Survey of ion source current vs. emittance, before accelerating column. Emittance is divided by 2 before plotting for those duoplasmatron measurements made after a column, to allow for column blow-up.

for Ne^{3+} and above, because of the column quadrupole strength limitation. Ne^{3+} was about 1% of the total beam.

The requirement of 100 mA of Xe^{1+} corresponds to an equivalent (scaled) proton current of 1.1 amps from the same source at the same extraction voltage, so the high output current capability of the multi-aperture source (tens of amperes of protons) matches the requirement better than a single-aperture duoplasmatron or PIG source. Figure V-D-7/1 shows a survey of source current and emittance. The CTR sources of LBL and LLL appear brighter than duoplasmatrons, so one of these was selected for development on the 80 kV Bevatron test stand. A source previously used by the LBL CTR group[2] was kindly loaned to us and was modified by adding an accel.-decel. extraction system similar to that used in J. E. Osher's MATS III source.[3] The LBL source is shown in Figs. V-D-7/2 and V-D-7/3. Thirteen circular holes of 2 mm dia. within a 1.5 cm diameter are used in the extraction aperture plates. The predicted current is 10 mA Xe^{1+}. Development has been aimed at transporting the beam 1.3 meters to a Faraday cup using a magnetic quadrupole triplet, and understanding the effect of various source parameters upon beam intensity, divergence and transport. Typical source operating parameters for good transmission are: +20 kV on source, +10 kV on extractor (accel.-accel.), arc pulse 1 ms wide, 2/sec. Langmuir probe measurements show the plasma to be uniform to 5% across the apertures. Beam current is 5 mA at the source and 1.2 mA focused into a 4 cm dia. cup 1.3 m downstream, expected to be mostly Xe^{1+}. Tests with a biased mesh in the beam gave no improvement in transmission, indicating space charge neutralization is probably adequate. Gas pressure measurements along the beam line show pressures of $1\text{-}5\times10^{-5}$ Torr, giving a calculated 10% loss due to charge exchange to Xe^{o}. A larger aperture single extraction hole (4mm instead of 2mm dia.) has been recently tested and gives a factor of 3 increase in brightness compared to the 2 mm hole case. The extraction mode in this case was 18 kV accel. and 1 kV decel. Future measurements are planned on beam divergence, emittance, and charge state distribution. A beam profile monitor and more pumping will be added.

A test on krypton using a MATS III source[3] was done by J. Osher at Livermore. A 25 aperture accel.-decel. extraction system was used. A dc current of 75 mA at 20 kV was measured calorimetrically at 1.1 meters from the source. The emittance appeared to be comparable to the .02π cm mr required. The beam current scaled approximately as $V^{3/2}$ over the range 10-20 kV. This excellent space-charge neutralized transport comes close to meeting the Summer Study goal.

Also under study is the design of a new type of structure for a high gradient column. In seeking a simple, low-cost design the insulators will be made of two flat plates rather than a series of circular rings. A preliminary model is planned using lucite instead of ceramic; later a

Table V-D-7/1. Heavy Ion Beam Summary.

Source Type	Ion Type	Source Voltage (kV)	Source I (mA)	Source ϵ_n (π cm mr)	Column (kV)	Column Gradient	After Column I (mA)	After Column ϵ_n (π cm mr)
Duoplasmatron	Ne				470	Low	30	
	Xe				470	Low	25	
	Ne				500	High	15	.03-.05
LBL-CTR								
13-2mm aper.	Xe	20	11→1.2					
1-4mm aper.	Xe	18	6→1.2					
LLL MATS III	Kr	20	75	~.02				

Note: Charge state of ions is believed to be mostly +1.

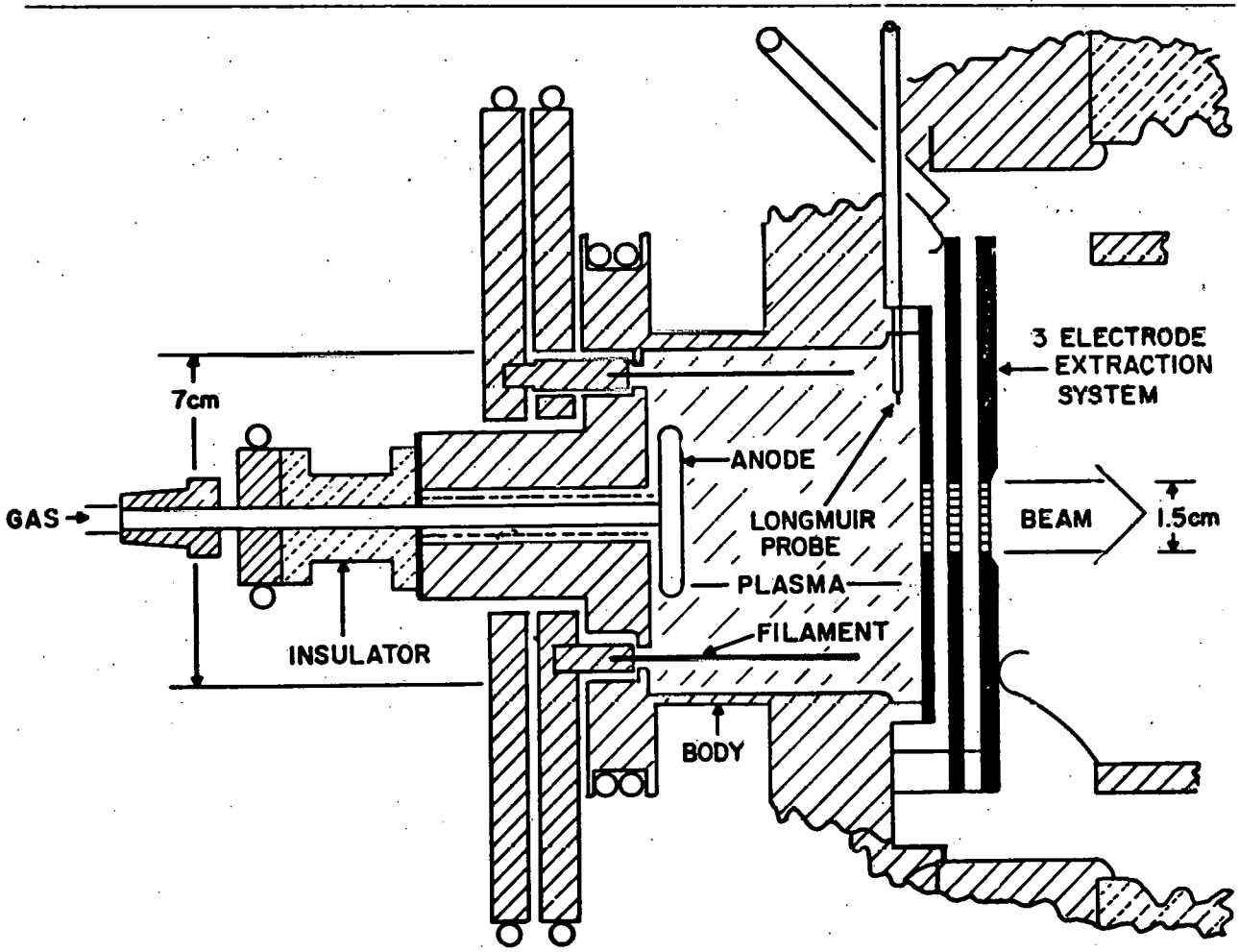

Fig. V-D-7/2. LBL CTR multi-aperture source, adapted from early model.

ceramic version will be designed if first tests are promising.

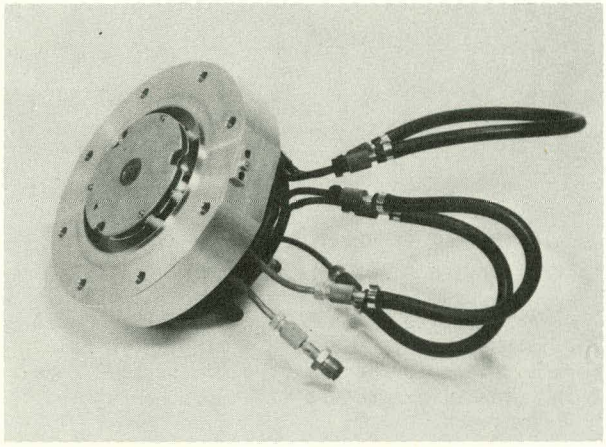

Fig. V-D-7/3. LBL CTR multi-aperture source.

References

1. ERDA Summer Study of Heavy Ions for Inertial Fusion, LBL-5543, p. 4 (1976).
2. W. R. Baker, et al., BNL 50310, p. 145 (1971).
3. J. E. Osher and G. W. Hamilton, LBL-3399 p. VI - 7-1, (1974).

E. LOW BETA LINACS

1. SUMMARY

R. Kustom, A. Moretti, J. Staples,
T. K. Khoe, J. Keane

INTRODUCTION

The Low Beta Linac group interacted mainly with the Preinjector Source group and the HIDE Linac group. It became apparent earlier on that the main problems faced by the group were: 1. the transport of high intensity beam through the low-β linac and therefore, the determination of the space charge limit of beam transport and 2. the structure or structures to accelerate the beam up to the first Alvarez structure in an optimum economical manner. The most severe design problem for the low-β linac is the first accelerating linac tank after the pre-accelerator where, of course, β is the lowest. It was the consensus of the group that every effort be expended to increase the terminal voltage of the ion source to at least 1 MV with 2 MV being most desirable. Since the first stage is both source and transport limited; it was decided to cascade the first linac tank and its source in a tree fashion with frequency jumps of two at the branch point to reach final required beam current. Scenarios which take Xe^{+3} to 240 emA, $200A^{1+}$ to 400 emA and $200A^{1+}$ with stripping to A^{3+} to 400 emA were developed.

In the event that it was not possible within the time frame for HIDE to develop the 1 MV to 2 MV source terminal, other linac structures were examined which could transport intense ion beam currents at very low β. It was determined that the most beam current that could reasonably be expected from future multiple charged ion sources was about 60 emA. With 50% capture efficiency, the first linac tank would have to accelerate 30 emA. Linac structures deemed possible to transport 30 emA at a low β of 0.004 were a long set of independently phased cavities with single drift tube and strong quadrupole focusing operating at 12.5 MHz (1) and a 5 MHz, π-3π Wideröe structure similar to the GSI and LBL designs (2,3), however, scaled to a lower frequency.

SPACE CHARGE LIMIT IN THE LOW BETA LINAC

The method used to determine the transverse and longitudinal space charge limit on beam transport is described below. In all cases the transverse space charge forces dominated and they primarily determine the transport limit.

ESTIMATING THE SPACE CHARGE LIMIT FOR A LINAC

A linearized method is derived which predicts the transverse space charge limit in the adiabatic approximation. Numerical results of the procedure agree within reason with macro-particle procedures.

The beam envelope equation

$$\frac{d^2r}{dz^2} = k_Q r - k_\Delta r - k_s r + \frac{\varepsilon^2}{r^3}$$

is linearized by setting the l.h.s. to zero and replacing the beam radius by an averaged envelope radius $\bar{a}$. In a periodic focussing channel of cell (not period) length L, the focussing term is

$$k_Q = \left(\frac{\Delta\mu}{L}\right)^2$$

where $\Delta\mu$ is the phase advance per cell. For a packing factor $\Lambda = \frac{1}{2}$ the required gradient is

$$B' = \frac{\theta_o^2 R}{L^2}$$

where R is the beam rigidity and $\theta_o^2 = 3.5$ for a FD sequence, 1.12 for a FFDD sequence, or .52 for a FFFDDD sequence. A constraint that must be imposed on the overall problem is that the quadrupoles be physically realizable with sufficient aperture to result in the required acceptance of the linac.

The electrostatic gap defocussing term per gap is $k_\Delta = \frac{\delta}{L}$ where

$$\delta = \frac{\Delta\theta}{r} = -\pi\left(\frac{q}{A}\right)\left(\frac{eV_{gap}}{m_p c^2}\right)\frac{1}{\beta^2}\frac{1}{\beta\lambda} T \sin\phi_s$$

is the deflection parameter for an off-axis particle.

The space charge force is considered to be a linear defocussing force.

$$F = \frac{qe}{4\pi\epsilon_o c}\,\frac{6I}{\beta b}\,(1-f)\,\frac{1}{2\bar{a}}$$

operating over the cell L which gives

$$k_s = 90\Omega\,\frac{q}{A}\,\frac{e}{m_p c^2}\,\frac{I}{B}\,\frac{(1-f)}{\beta^3 a^{-2}}$$

where $B \le 1$ is the bunching factor, I the average electrical current in the macropulse and f is a form factor related to the beam shape, approximated by

$$f = \frac{\bar{a}}{2r_z + \bar{a}}$$

where r_z is the bunch half-length.

The three focussing terms can be combined to give the saturation current as a function of averaged beam radius $\bar{a}$:

$$I = \frac{B}{90\Omega}\left(\frac{A}{q}\right)\left(\frac{m_p c^2}{e}\right)\frac{\beta^3}{1-f}\left\{\left[\left(\frac{\Delta\mu}{L}\right)^2 - \sum_{gaps}\frac{\delta}{L}\right]a^{-2} - \frac{\epsilon^2}{a^{-2}}\right\}$$

where ϵ is the unnormalized emittance area/π of the beam.

If the expression within [ ] is negative, the focussing is outside the classical stability limit. The emittance term serves notice that some additional beam aperture is needed for finite emittance beams. The minimum beam size required for zero current is

$$\bar{a} = \left[\frac{\epsilon^2}{\left(\frac{\Delta\mu}{L}\right)^2 - \sum_{gaps}\frac{\delta}{L}}\right]^{1/4}$$

indicating that $\bar{a} \propto L^{\frac{1}{2}}$, approximately, But for large transported current,

$$\bar{a} = \frac{L}{\Delta\mu}\left[90\Omega\,\frac{I}{B}\left(\frac{q}{A}\right)\left(\frac{e}{m_p c^2}\right)\frac{1-f}{\beta^3}\right]^{1/2}$$

indicating that in the presence of space charge, $\bar{a} \propto L$.

As far as longitudinal motion is concerned, for the linacs considered here, the longitudinal space charge force is smaller than the longitudinal restoring force. A minimum gap voltage can be established as

$$V_{min} = \frac{90\Omega}{\pi}\,\frac{I}{B}\,\frac{L_c\lambda}{a^{-2}}\,\frac{f}{T\sin\phi_s}$$

where L_c is the length of the accelerating cell, and f is defined above. This V_{min} is usually far below the gap voltage given in the linac study.

An upper limit to the gap voltage exists also, related to electrostatic gap defocussing force derived above for the requirements for transverse stability. This upper limit has been frequently imposed in the numerical examples given for the low-β sections.

An additional constraint that limits the harmonic number for a structure is given by the bucket depth and phase acceptance of the linac. The formalism is not reproduced here, but its practical consequences limit one to $n \le 5$ in low-β π-nπ Widerŏe type structures before the phase acceptance suffers.

LONGITUDINAL SPACE CHARGE LIMIT IN LOW β LINAC

In the presence of space charge the bunch width is given by (see ARF report ACC-1: Hearthfire, 5/31/77), where,

$$\Delta\phi = 3\,(1-k)\phi_o \qquad (1)$$

$$k = \frac{3\,I\,Z_o\,\beta\,\lambda^2}{2\pi^2\,L^3\,E\sin\phi_o}\,(0.8\,\frac{L}{d} - 0.134)$$

I = average beam current (electric)

$Z_o = 120\pi$ ohm

d = beam diameter

L = bunch length

E = average axial field

ϕ_o = synchronous phase angle from rf peak

$\lambda = c/f$ = free space wave length.

Substitution of

$$L = \frac{\Delta\phi}{2\pi}\beta\lambda = \frac{3\,(1-k)\,\phi_0\,\beta\lambda}{2\pi}$$

in Equation (1) and solving for I gives

$$I = \frac{3\,\phi_o^2\,\beta\,d\,E\sin\phi_o}{1.6\,Z_o}\,\frac{k\,(1-k)^3}{1-k-a} \qquad (2)$$

where $a = \dfrac{0.134\,\pi\,d}{1.2\,\phi_o\,\beta\lambda}$. (3)

The right hand side of Equation (2) has it maximum value for .

$$k = 1/3\,[1 + 0.5\,a + 1.125\,a^2]\,.$$

Substituting this into Equation (2) one obtains

$$I_{max} = \frac{\phi_o^2 \beta d E \sin\phi_o}{3.6 Z_o} [1 + 1.5a + 2.5A^2]$$

Example

$d = 0.04$ cm,

$E = 1.5$ MV/m,

$\lambda = 24$ m ($f = 12.5$ MHz)

$\phi_o = 30^o$,

$\beta = 0.004$

Equations (2) and (4) given

$a = 0.2792$

$I_{max} = 40$ mA

LOW BETA LINAC STRUCTURES

ANL, BNL and LBL are currently designing low-β linacs to accelerate intense heavy ion beams. The work at ANL centers on independently-phased cavities using Xe^{1+} from a dynamitron source. The dynamitron source is being developed to produce 100 mA of Xe^{1+} at a final energy of 1.5 MV. It is expected to be operational by June 1978. The BNL work centers around a coaxial quarter wave folded line resonator with 12 drift tubes. The drift tubes can be easily changed in this design to study beam blow-up and rf sparking. They expect to accelerate 5 to 10 mA of Xe^{1+} from a 750 kV Cockcroft-Walton by December 1977. The work at LBL centers around a 23.4 MHz Wideröe accelerator for SuperHilac (3). They expect to accelerate 8 to 10 ema of Xe^{3+} from a 750 kV Cockcroft-Walton terminal by late 1980.

INDEPENDENTLY PHASED CAVITIES (ANL)

The low β linac concept under development at Argonne to accelerate and transport high intensity heavy ion beams is the use of independently phased cavities with single drift tubes and strong quadrupole magnetic focusing in between the cavity drift tubes (1). Models for the independent linac cavity are shown in (Fig. V-E-1/1, 2, 3). They are the ½-wavelength folded line resonator (Fig. V-E-1/1), the capacity-loaded coaxial line resonator (Fig. V-E-1/2) and lumped-inductor resonator (Fig. V-E-1/3). The cavities have been designed to resonate at 12.5 MHz with an aperture of 4 cm. The beam transport limit has been calculated to be 30 mA Xe^{1+}. The shunt impedance of the resonators is high enough so that only 12 kW is required for the rf copper wall losses.

The current plans are to build high power test models of the capacity loaded coaxial resonator and the lumped inductor resonator. The ½-wavelength coaxial resonator is thought to be too expensive to construct at this time so the decision to build a high power test model of it has been delayed. Construction of the other models is scheduled to begin in December 1977. High- wer testing is sceduled to begin in February 1978. It is planned to have five resonators with their rf power amplifiers installed by October 1978 when testing with the 100 mA Xe^{1+} 1.5 MV dynamitron will commence.

BROOKHAVEN LOW BETA PROGRAM

In order to conduct experiments on emittance blow-up, longitudinal acceptance as well as experiments in rf sparking phenomena, three steps have been taken:

1. Completion of a 750 keV Cockcroft-Walton preaccelerator with a Xe source that is expected to deliver 5.0 to 10 mA. It has been run at over 1 mA Xe^{+1}.

2. Construction of a 12 cell heavy ion $\beta\lambda/2$ accelerator structure.

3. Recommissioning of a 20 kW-50 MHz rf transmitter.

The rf transmitter on loan from LBL was modified to deliver 20 kW rf power at a frequency of 16.6 MHz. It can run pulsed or C-W. Center frequencies up to 60 MHz can be set-up in less than 8 hours. This unit has supplied 20 kW at 16 and 50 MHz into a resistive load.

The low-beta accelerator section has been constructed. The resonator is a folded $\lambda/4$ resonator with a variable short to tune to 16 MHz. The accelerating section has been built so that acceleration gaps can be easily changed, so that various types or number of drift tubes can be inserted. Presently the drift tubes contain no quadrupole focusing but π-3π or 3π-3π cells could easily be installed in the future. In the present configuration kinetic energies of 1.1 MeV are expected to be reached. It should be noted that this type resonator could have a window back in the coaxial section where the gradient is down by a factor of 10-20. Since the resonating structure is not in vacuum, machine costs are reduced.

Presently, all units have been run with the exception of the accelerating structure which was just assembled in our lab. It is expected that Xe ions will be accelerated in December.

RF DEFLECTORS FOR COMBINING TWO LINAC BEAMS

The output of two linacs operating at frequency f_o, 180° apart, which are combined and further accelerated by a following linac at frequency $2f_o$ can be accomplished with minimal transverse emittance dilution with an rf sweeper. However, with beams of finite transverse emittance and high rigidity, a single rf electrostatic or magnetic sweeper is hopelessly inadequate in strength. A method is described here which would allow, in principle, this obstacle to be overcome. This combiner is analyzed here as a sweeper turned end-for-end.

Consider a FODO magnetic focussing structure of the same period as the following linac, which

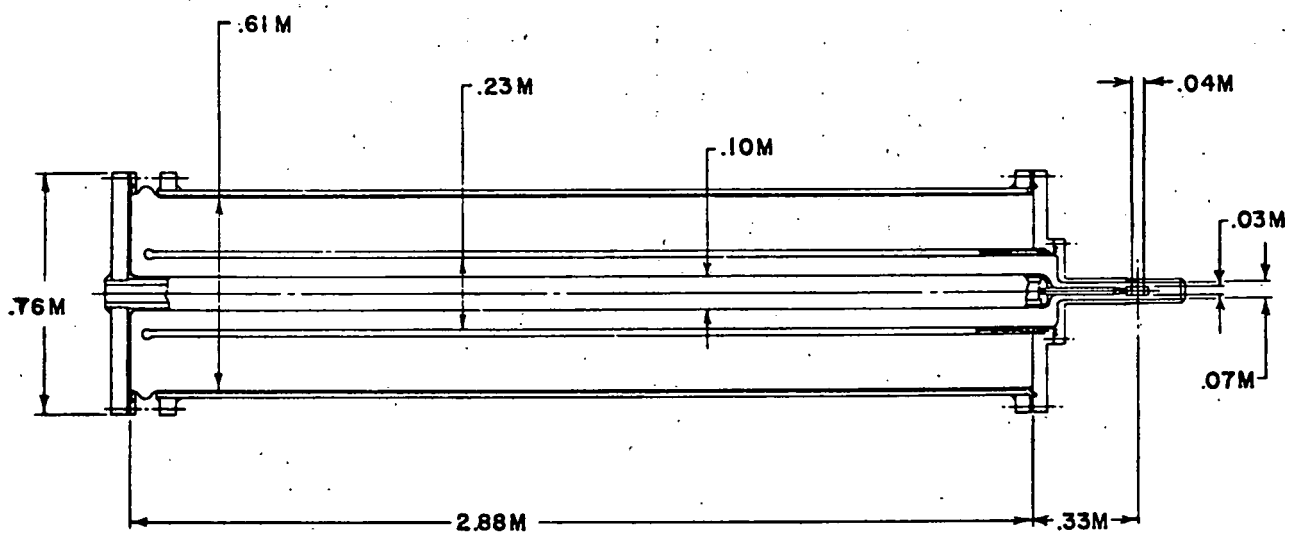

Fig. V-E-1/1. 12.5 MHz 1/4 Wavelength Folded Line Resonator.

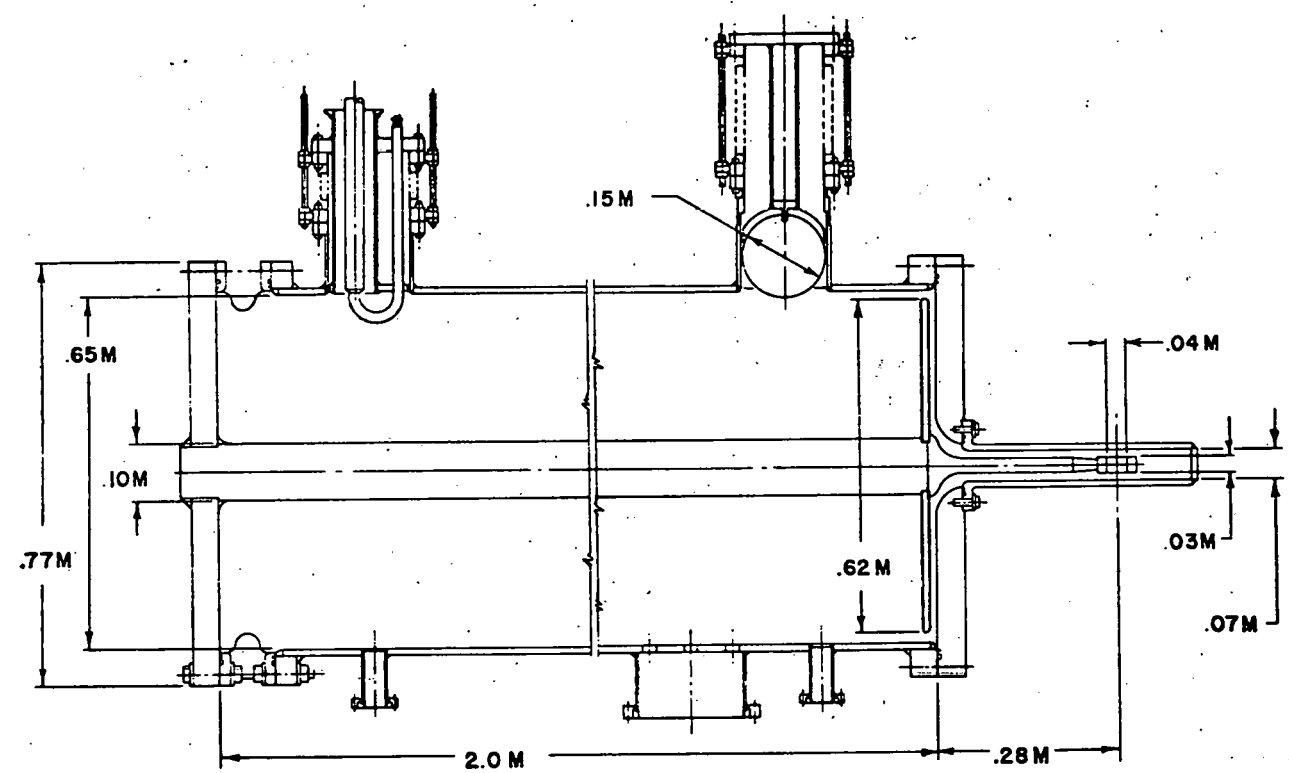

Fig. V-E-1/2. 12.5 MHz Capacity Loaded Coaxial Resonator.

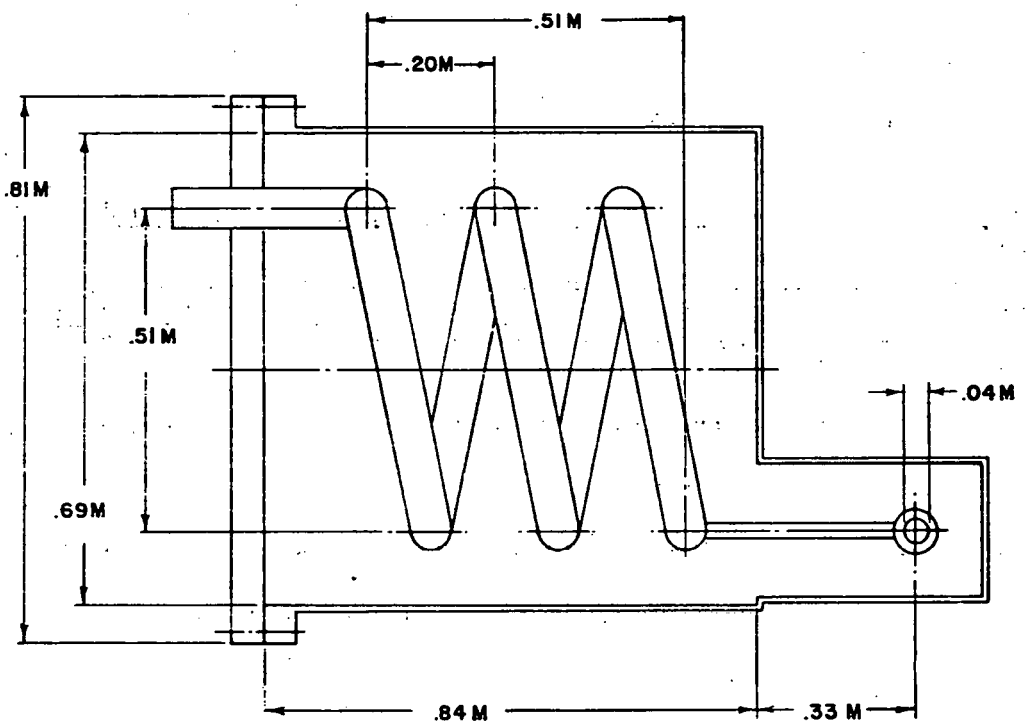

Fig. V-E-1/3. MHz Lumped Inductor Resonator.

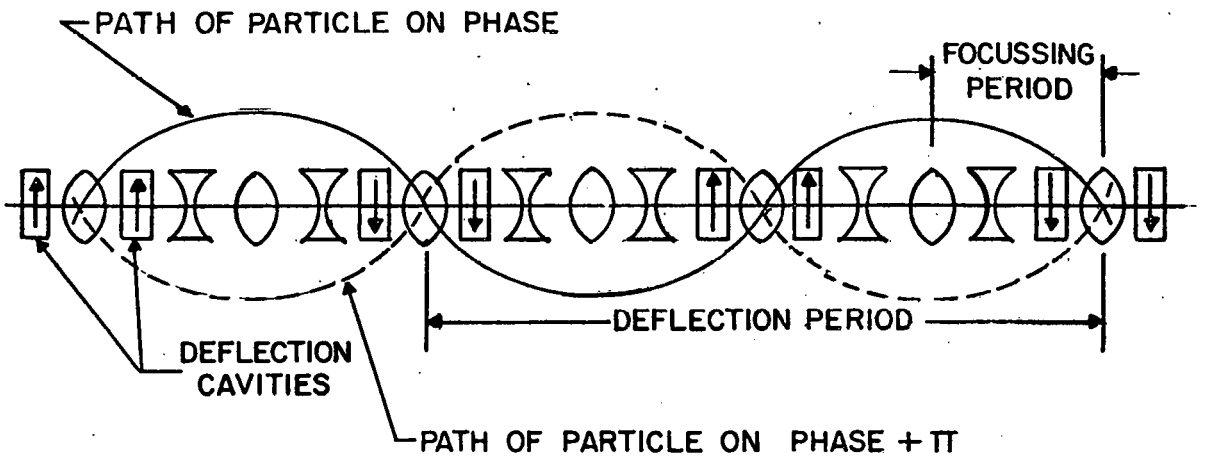

Fig. V-E-1/4. Periodic Deflector.

in a typical case, would be a π-3π Wideröe structure operating at $\lambda = c/f_o$. The magnet period is $4\beta\lambda$ with a filling factor $\Lambda = .5$, each magnet and drift section having a length of $\beta\lambda$. If the quadruple gradient $B' = 3.47R/(2\beta\lambda)^2$, the phase advance per period is $\pi/2$, where R is the beam rigidity. If a small angular deflection $\Delta\theta$ is introduced every 2 periods, with appropriate sign, then the total net deflection θ for N deflectors is $N\,\Delta\theta$, as shown in Fig. 1. The averaged beam size will remain constant through the length of the FODO channel.

If the beam is allowed to exit the channel at a waist with size parameter β_o, then the size function will grow as $\beta = \frac{1}{\beta_o}(\beta_o^2 + L^2)$ in a drift length of length L. The net deflection θ L must be greater than the beam size $y = \sqrt{\beta\,\epsilon}$ at the end of L for the beams to be effectively separated by a septum magnet, as in Fig. 2. This effectively fixes the parameter N.

If

$$R = \left[\frac{\beta\gamma}{c}\right]\left[\frac{m_p c^2}{e}\right]\left[\frac{A}{q}\right]$$

is the particle rigidity, then the angle $\Delta\theta$ from an electrostatic (magnetic) deflector of length ℓ

of field strength E (B) is

$$\Delta\theta = \frac{E}{c}\frac{\ell}{R} \cdot T = \frac{B\ell}{R} \cdot T$$

where T is a transit time factor approximated by

$$T = \frac{\sin \frac{\pi\ell}{\beta\lambda}}{\frac{\pi\ell}{\beta\lambda}}$$

for a uniform field cavity and by 1 for a slow wave structure matched to the velocity of the beam, such as a helically wound deflection plate. Uniform field structures that are an appreciable fraction of $\beta\lambda$ would be avoided for beams with all but the shortest bunch length to avoid deflecting different sections of the bunch different amounts.

As a numerical example, consider the difficult case of combining two $_{200}A^{1+}$ beams of β = .2771 with a maximum allowable beam radius of .01m and an unnormalized emittance $E/\pi = 2.10^{-5}$ m-rad. Each cavity, one per 4 $\beta\lambda$ period, is assumed to be $\beta\lambda/4$ long, λ = 7.5m, (T = .90). With a transverse E - field of 5 MV/m, each cavity deflects the beam of an angle $\Delta\theta = 4.32 \cdot 10^{-5}$ radian.

Table V-E-1/1 lists the beam β function, radius a, required total deflection angle θ and N, the number of cavities required. To limit the transverse beam growth in the drift space to a reasonable value, L should be kept below 5 meters, requiring at least 65 cavities. A lower limit of L is set by a practical upper limit to the number of deflection cavities needed. A few longitudinal cavities would also be located at points where the deflected beam crosses the axis, every π phase advance, Fig. V-E-1/6.

Table V-E-1/1. Number of Deflections vs Drift Length.

L(m)	β(m)	a(m)	θ(rad)	N
0	5.0	.0100		
1	5.2	.0102	.0102	236
2	5.8	.0108	.0054	125
3	6.8	.0117	.0039	90
5	10.0	.0141	.0028	65
10	25.0	.0224	.0022	51

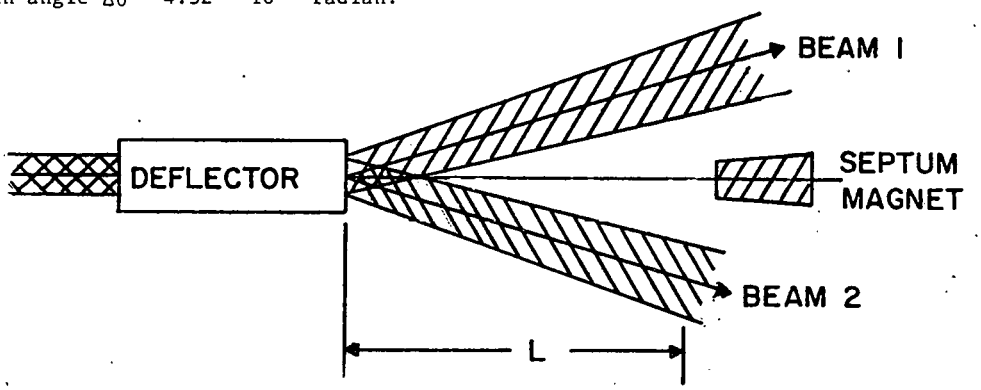

Fig. V-E-1/5. Deflector Followed by a Drift Space L and Septum.

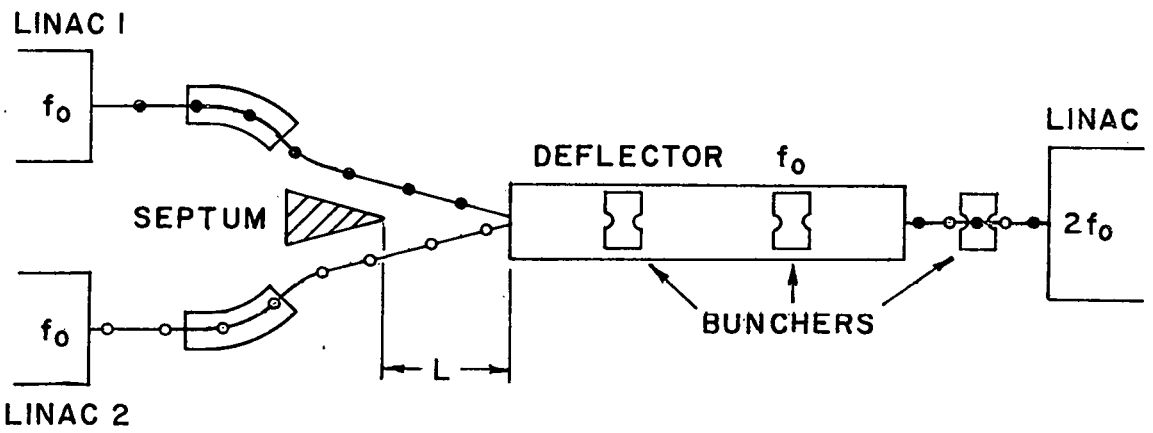

Fig. V-E-1/6. Inflector Combining Two Linacs. Focussing not Shown in Beam Lines.

References

1. R. J. Burke, et al., "Hearthfire Design Base for the High Current Low Velocity RF Linac," ANL, ARF report ACC-1, May 31, 1977.
2. K. Kasper, "The Prestripper Accelerator of the Unilac, "Proc. of the 1976 Proton Linear Accelerator Conference, Chalk River, Sept. 1976.
3. J. Staples, et al., "A Wideröe Pre-accelerator for the SuperHilac," Proc. of the 1976 Proton Linear Accelerator Conference, Chalk River, Sept. 1976.

EQUILIBRIUM PHASE-SPACE DISTRIBUTIONS

W. P. Lysenko

This will summarize some work done at the Los Alamos Scientific Laboratory[1] which may be relevant to the heavy-ion fusion program. Limits on beam current and emittance in proton or heavy ion linear accelerators may be calculated by determining equilibrium phase space distributions. This is a matching procedure which takes into account space charge forces. We make use of the following result: If the distribution function is a function of the conserved single-particle Hamiltonian

$$f(\vec{x},\vec{p}) = F(H) \qquad (1)$$

then the distribution is time independent. We use the following model

$$H = \frac{p^2}{2m} + \frac{kr^2}{2} + \frac{k_z z^2}{2} + e\phi(r,z) \qquad (2)$$

in which ϕ is the unknown space charge potential. Thus we assume linear restoring forces which are constant in time. Azimuthal symmetry is assumed so that there are only two degrees of freedom. For the function F we use one of the following

$$F(H) = \begin{cases} nB(H_0 - H)^{n-1}, & H < H_0 \\ 0, & H \geq H_0 \end{cases} \qquad (3)$$

in which B and H_0 are constants and n is a non-negative integer. These are the same functions considered in the original work of Gluckstern, Chasman, and Crandall[2] which treated the corresponding one-degree-of-freedom problem in the coordinate r.

To solve for the space charge potential we integrate the distribution function over momentum and use the Poisson equation. After normalizing the variables in a certain way the following nonlinear Poisson equation is obtained

$$\nabla^2\Phi = \begin{cases} -\mu u^{n+1/2}, & u > 0 \\ 0, & u \leq 0 \end{cases} \qquad (4)$$

where $u(r,z) = 1 + \Phi(0,0) - \Phi(r,z) - \frac{r^2 + \alpha z^2}{2 + \alpha}$.

The space charge parameter μ is defined by

$$\mu = \frac{2\mu_r + \alpha\mu_z}{2 + \alpha} \qquad (5)$$

in which μ_r and μ_z are the ratios of the space charge forces to the external restoring forces at the bunch center in the radial and axial directions, respectively. The constant α is the ratio of the two force constants

$$\alpha = k_z/k. \qquad (6)$$

Equation (4) may be solved numerically for the space charge potential which consequently specifies completely the distribution in phase space.

We may now write results in terms of physical parameters to give some scaling laws. The current and beam radius may be written

$$I = G_1(\mu,\alpha,n)\ (\eta f)^{3/2} \left(\mu^0_{shr}\right)^{1/2} \left(\frac{A}{q}\right), \qquad (7)$$

$$\frac{r}{\beta\lambda} = G_2(\mu,\alpha,n) \left(\frac{\eta f}{\mu^0_{shr}}\right)^{1/2} \beta, \qquad (8)$$

where G_1 and G_2 describe the space charge physics of the problem. In these formulas, η is the normalized emittance, f is the accelerator frequency, A is the atomic mass, and q is the charge state of the ion. Instead of the force constant k we have written the results in terms of μ^0_{shr}, the transverse phase shift per length $2\beta\lambda$, in order to relate these results to an alternating gradient focussing system. As an aid to understanding these scaling laws let us note that for a fixed pole-tip field, the phase shift varies as

$$\mu^0_{shr} \sim \left(\frac{q}{A}\right)^{1/2} f^{-1}. \qquad (9)$$

A general conclusion that we may draw is that for a fixed emittance, higher currents may be obtained with higher frequency accelerators although there is an upper limit because the beam radius measured in terms of the cell length (which scales with the bore radius) also increases with frequency. If we disregard emittance and just fix the quantity $r/\beta\lambda$ so that the beam occupies a certain fraction of the bore, then we see that low frequency accelerators are favored for high currents when beam quality is of no concern. The space charge physics effects contained in G_1 may be summarized simply by noting that, for a given accelerator and a given current, the emittance decreases with the space charge parameter μ.

References

1. W. P. Lysenko, "Equilibrium Phase-Space Distributions and Space Charge Limits in Linacs," Los Alamos Scientific Laboratory report LA-7010-MS (October 1977).

2. R. L. Gluckstern, R. Chasman, and K. Crandall, "Stability of Phase Space Distributions in Two Dimensional Beams," Proc. 1970 Proton Linear Accelerator Conf., National Accelerator Laboratory, 1970, p. 823.

F. HIGH CURRENT BEAM TRANSPORT

1. SUMMARY

Ingo Hofmann

INTRODUCTION

A goal of this workshop has been to understand the actual physical processes that lead to limitations in the power transmittable through a long periodic transport system in a regime where space charge defocusing is no longer small compared with the externally applied focusing. A strongly justified formula describing the actual current limit in a given structure as imposed by transverse space charge effects is crucial in the design of accelerator systems for heavy ion fusion. In an rf linac this limiting current is impoortant at the low energy front end, while the induction linac technique with pulse shortening during acceleration makes operation at the space charge limit desirable throughout acceleration.

Other major topics of the workshop has been addressed to the possibilities of correcting for aberrations in the final focusing system and to the question of space charge neutralization within the beam. Additional work presented in the workshop will be found in other sections of these proceedings.

CALCULATIONS LEADING TO CONSTRAINTS IN BEAM TRANSPORT

The use of scaled equations for studying beam transport in a FODO system and subsequent descaling have suggested a "figure of merit" $\frac{Q}{u_{max}^{2/3}}$, such that the constant C employed in the formula for power transport (originally suggested by Maschke, Ref. 1)

$$P = C \left(\frac{A}{q}\right)^{4/3} B_Q^{2/3} (\beta\gamma)^{5/3} \varepsilon_N^{2/3} (\gamma-1)$$

is found as $C=3.43\cdot10^{15} \frac{Q}{u_{max}^{2/3}}$ (ref. 2). Actual values of this "figure of merit" derived on the basis of a stability analysis (Ref. 3, 4, 5) presented in the workshop are given by Laslett in this section. The analytic work has considered perturbations of a matched K-V beam within the framework of the Vlasov equation. It reveals a series of unstable modes of oscillation for arbitrary values of phase advance σ_o leading to inhomogeneous density across the beam with thresholds in terms of tune depression $\frac{\sigma}{\sigma_o}$ ($\leq.4$) that are quite independent of whether a continuous solenoid or a periodic focusing structure is considered. These unstable modes are not fluid-like and require consideration of evolution in the velocity space. In addition to these unstable eigenmodes of the K-V beam, resonances of eigenmodes with the period of the structure have been discovered to further reduce the range of stable values of intensity in an interrupted solenoid and even more in a FODO lattice. The unstable envelope mode occuring for $\sigma_o > 90^o$ falls in this class of resonances, while higher order resonant modes have been found dangerous also for $\sigma_o < 90^o$. For $\sigma_o < 90^o$ a tune depression of $\frac{\sigma}{\sigma_o} > .5$ was suggested as safe (Ref. 5).

The complete absence of Landau damping makes the K-V beam appear as a very singular model. In addition, the linearized Vlasov theory becomes invalid after very modest growth of the unstable modes due to the evolution of a highly non-linear space charge force (except for the envelope modes). This necessitated consideration of other than K-V models and study of non-linear saturation of instabilities, possibly through computer simulation where analytic methods fail.

A study of the scaling laws for power transportation applying to different situations with varying constraints on some of the parameters appearing in the general formula has provided very useful formula for designers of beam lines and reconciled different standpoints. This study is also (see Reiser in this section of these Proceedings) useful in that it compares the different notations being used by various authors. It presents an approximate analytic expression for the matched envelope solution, which is fairly accurate for small σ.

Lawson and Reiser, in the next paper of these Proceedings, summarize a discussion of the physical nature of some parameters of interest in a continuous solenoid. It compares the theoretical predictions with existing experimental work done in the past in connection with electron guns. While the effect of mismatch in the experiment requires additional consideration, the comparison does not show any incompatibility.

COMPUTER SIMULATION

Results of computer simulation of a large number of particles ($\geq 10^4$) distributed on a four-dimensional hyper-ellipsoid in transverse space as initial condition and propagated along a quadrupole system with thin lenses have been presented (Ref. 6). The simulations follow orbits in the self-consistent electric field. They give evidence of unstable growth even at $\sigma_o = 90^o$ (where envelope modes are stable) and support in this respect the analytic results. Non-linear saturation and growth in phase space more than in real space were observed. A detailed comparison with the theoretical predictions was not possible during the Workshop, but it was felt that systematic computer studies are essential for a better understanding of the stability of realistic beams. Analytic predictions should serve as guide line for such studies.

Another type of orbit tracing code was based on summing up Coulomb interactions between a moderately large number of infinitely long rods (Ref. 7). Applications of the code and an increase of its speed by possibly applying a poisson solver are in progress.

CORRECTION OF CHROMATIC AND GEOMETRIC ABERRATIONS IN THE FINAL FOCUSING SYSTEM

Target requirements necessitate the production of achromatic spots and corrections for geometric aberrations. Three contributions have opened possibilities for corrections through the use of a series of quadrupole and sextupole components. Space charge effects have been neglected in these approaches, though they are likely to be important for the dispersive properties of the lenses and also at waists that might be produced at different positions along the channel. Hence, consideration of space charge appeared to be highly justified for future work (see Brown, Bruck, and Halbach in this section of these Proceedings).

SPACE CHARGE NEUTRALIZATION

The participants were aware that limitations imposed by some of the phenomena mentioned in this summary might be substantially relaxed by the introduction of space-charge neutralization within the beam. The lack of a theoretical model describing the process of electron accumulation in the bunch was strongly felt. Experimental work on this topic is in progress at Brookhaven National Laboratory and planned at Argonne National Laboratory (see Fenster, in section V-B of these Proceedings).

References

1. A. W. Maschke, ERDA Summer Study of Heavy Ions for Inertial Fusion, July, 1976, unpublished.
2. G. Lambertson, L. J. Laslett, L. Smith, IEEE Trans. NS-24, p. 993 (1977).
3. L. Smith, HIFAN-13, LDL-6771, Lawrence-Berkeley Laboratory (1977).
4. S. Chattophadhyay, HIFAN-14, Lawrence-Berkeley Laboratory (1977).
5. I. Hofman and L. J. Laslett, HIFAN-15, Lawrence-Berkeley Laboratory (1977).
6. I. Haber, Naval Research Laboratory, unpublished (work in progress).
7. S. Penner, National Bureau of Standards, unpublished (work in progress).

2. TRANSVERSE SPACE CHARGE LIMITS - SOME NOTES AND SOME QUESTIONS

J. D. Lawson and M. Reiser

INTRODUCTION

Recent work by the Berkeley group[1] on the transport of focused K-V distributions suggest that under some conditions the distribution is unstable. This is found also in numerical simulations by Haber in matched periodic systems though a clear correspondence between simulations and theory has not yet been achieved. Based on the theoretical studies, the Berkeley group recommends (a) that the phase shift per period in a periodic lattice should not exceed $\pi/2$ and (b) that the relative betatron phase shift with and without space-charge, (μ/μ_o), should not fall below 0.4-0.5. It is interesting to note that the second rule applies also to continuous solenoids.

Since perfect "Brillouin flow" corresponds to $\mu/\mu_o = 0$, well below the stability criterion suggested above, and further, many experiments have been made on beams which do not appear to depart greatly from Brillouin flow, it seems relevant to investigate the experimental evidence.

In order to see more clearly how these effects might relate to other known and understood phenomena, it is also interesting to look at the physical nature of some of the parameters involved. In this discussion, we confine attention to the continuous solenoid.

PARAMETERS FOR A UNIFORM SOLENOID

The simplest form for the envelope equation of the beam in the solenoid is

$$a'' + \frac{a}{\lambda_o^2} - \frac{K}{a} - \frac{\epsilon^2}{a^3} = 0 \qquad (1)$$

where λ_o is the orbit wavelength in the absence of space-charge, K the "generalized perveance,"[2] and $\pi\epsilon$ the (un-normalized) emittance. For a matched beam a" = 0, and from equation (1),

$$\epsilon^2 + Ka^2 = \frac{a^4}{\lambda_o^2} = \alpha^2 , \qquad (2)$$

where $\pi\alpha$ is the acceptance of the channel of radius a when K = 0. The condition $\epsilon = 0$ represents "Brillouin flow" so that from equation (2)

$$\frac{K\lambda_o^2}{a^2} = 1 . \qquad (3)$$

We note that this is equivalent to the commonly quoted result

$$\omega_p^2 = 2\omega_L^2 , \qquad (4)$$

where $\omega_L = eB/2\gamma m_o$ and $\omega_p = \sqrt{K}\,\beta c/a$ is the plasma frequency.

In this Brillouin case, the flow is laminar, i.e., all particles move on concentric helical orbits in the laboratory frame and on straight lines in the rotating Larmor frame. When the beam has a finite emittance and, hence, condition (4) is not satisfied, the individual particles oscillate in the Larmor frame with a frequency ω given by

$$\omega = \sqrt{\omega_L^2 - \frac{1}{2}\omega_p^2} = \omega_L\sqrt{1 - \frac{1}{2}\left(\frac{\omega_p}{\omega_L}\right)^2} . \qquad (5)$$

In terms of the frequencies ω_L and ω_p, equation (2) may be written as

$$\omega_L^2 = \frac{1}{2}\omega_p^2 + \frac{\epsilon^2}{a^4}\beta^2c^2 , \qquad (6)$$

so that if we know ω_L, ω_p, a, and β, the emittance ϵ can be determined. Dividing through by ω_L^2, and noting that $\alpha = a^2\omega_L/\beta c$, one can put equation (6) into the form

$$\frac{\epsilon^2}{\alpha^2} = 1 - \frac{1}{2}\frac{\omega_p^2}{\omega_L^2} . \qquad (7)$$

By comparing (5) and (6), we obtain the relation

$$\frac{\omega^2}{\omega_L^2} = \frac{\epsilon^2}{\alpha^2} = 1 - \frac{1}{2}\frac{\omega_p^2}{\omega_L^2} . \qquad (8)$$

This is equivalent to

$$\frac{\omega^2}{\omega_L^2} = \left(\frac{\mu}{\mu_o}\right)^2 = \frac{\epsilon^2}{\alpha^2} = 1 - \frac{Q}{2u^2} , \qquad (9)$$

where $Q/2u^2$ represents the Berkeley notation.[1]

According to the Berkeley studies,[1] the beam is unstable when $\omega/\omega_L \leq 0.4$, and hence

$$\frac{\omega_L}{\omega_p} \leq 0.77 . \qquad (10)$$

Note that the Brillouin-flow condition, where $\epsilon = 0$, $\omega/\omega_L = 0$, corresponds to $\omega_L/\omega_p = 0.707$.

SIGNIFICANCE OF $K\lambda_o^2/a^2$

The parameter $K\lambda_o^2/a^2$, $\omega_p^2/2\omega_L^2$, or $Q/2u^2$ varies from zero for a matched beam in the absence of space charge to unity for Billouin flow in which $\epsilon = 0$. It expresses the extent to which the space charge force or external force dominates the beam behavior. It is interesting to note in this connection that it can be written in yet another form:

$$\frac{K\lambda_o^2}{a^2} = \left(\frac{a}{2\lambda_D}\right)^2 \qquad (11)$$

where λ_D is a length corresponding to the Debye

length in a Maxwellian plasma. For a K-V distribution, we define λ_D as

$$\lambda_D^2 = \epsilon_o \langle kT \rangle / nq^2 \qquad (12)$$

where

$$\langle kT \rangle = \frac{1}{2} m \left(\frac{a^2}{\lambda^2} \right) \beta^2 c^2 . \qquad (13)$$

Thus, if $\lambda_D \ll a$, $\mu/\mu_o \sim 0$, but if $\lambda_D \gg a$, $\mu/\mu_o \sim 1$.

From our understanding of plasma equilibrium and stability, can we draw any concluions from this result?

BEAM RIPPLE

Before we compare theory with experiment, it is important to understand the nature of the "beam ripple" observed on imperfectly matched beams.

The envelope equation of small perturbations, $a \to a + \rho$, may be found by linearizing equation (1) about the matched solution. This yields

$$\rho'' + \left(\frac{1}{\lambda_o^2} + \frac{K}{a^2} + \frac{3\epsilon^2}{a^4} \right) \rho = 0 . \qquad (14)$$

If λ_r is the ripple wavelength, then

$$\frac{1}{\lambda_r^2} = \frac{1}{\lambda_o^2} + \frac{K}{a^2} + \frac{3\epsilon^2}{a^4} = 2 \left(\frac{\epsilon^2}{a^4} + \frac{1}{\lambda_o^2} \right) , \qquad (15)$$

where use has been made of equation (2). When the oscillation amplitude is large, non-linearities will be introduced, and there may perhaps exist resonances between harmonics of the wavelengths λ_r and λ, where λ is the orbit wavelength. Writing $\epsilon = a^2/\lambda$, equation (15) can be written

$$\frac{1}{\lambda_r^2} = 2 \left(\frac{1}{\lambda_o^2} + \frac{1}{\lambda^2} \right) . \qquad (16)$$

Further parametric effects may occur if the focusing structure is periodic rather than uniform.

COMPARISON WITH EXPERIMENT

One problem in the comparison of the theory with the experiment is that actual distributions are not K-V. A good gun or source will have a uniform distribution in real space at the exit, but the velocity space distribution arises from thermal emission velocities, aberrations, and (if applicable) grid structure effects. Even in the absence of space-charge, the transverse density a distance $\lambda_o/4$ beyond the gun is nonuniform because of the rotation through $\pi/2$ of the "phase space diagram." After an additional distance $\lambda_o/4$, a futher rotation produces an image of the cathode. For a gaussian velocity distribution, the intensity distribution across the beam can be determined once the focusing properties of the channel (which can vary with z) are known.[3]

In the presence of space-charge, of course, the problem becomes quite intractable analytically because of the aberrations associated with the nonuniformity of the distribution.

Despite these difficulties, it is worthwhile making a comparison with experiment; to do this, we return to equation (8). We have not yet had time to discuss this with tube experts, but, as a start, a comparison can be made with experiments published by Brewer[4] in 1959.

Brewer injected an electron beam from a magnetically shielded gun into a long solenoid. The aperture radius a at the entrance into the solenoidal region was fixed, and from the electron current and kinetic energy, he calculated the electron plasma frequency ω_p at this point. The magnetic field, and thus the Larmor frequency ω_L, was then changed in a systematic way to determine under what conditions a smooth, matched (or unrippled) beam in the solenoid could be achieved. Brewer used an apertured plate with a 0.002-in.-diam. hole which was passed across the beam to obtain a plot of current density versus radius at many axial positions along the beam. The best beam with practically no variation of the density profile along the entire distance within the solenoid was achieved for

$$\frac{\omega_L}{\omega_p} = 0.9, \text{ which implies } \frac{\omega}{\omega_L} = 0.62. \qquad (17)$$

This value is higher than the ideal Brillouin flow case, i.e., the beam had a finite emittance which could be calculated from equation (6), and thus a higher magnetic field was required to achieve a matched beam. We note that the corresponding frequency ratio ω/ω_L is safely above the instability limit predicted by the Berkeley group. On the other hand, Brewer also obtained a reasonably good beam closer to the Brillouin value. For

$$\frac{\omega_L}{\omega_p} = 0.75 \text{ and thus } \frac{\omega}{\omega_L} = 0.333 , \qquad (18)$$

the beam had only a small ripple in the variation of the cross section with axial distance. This ripple could be explained by the fact that the beam was not perfectly matched. At any rate, there was no clear indication of a destructive instability even though the frequency was somewhat below the theoretical threshold found by the Berkeley group. We do not feel, however, that this data is conclusive, and the matter needs further study.

CONCLUDING REMARKS

A vigorous ongoing program on these questions can be foreseen, perhaps more computational than analytical. It is worth checking whether something can be learned from existing tube experience

and from new experiments with electron beams.

References

1. See papers by Smith, Chattopadhyay, Hofman, and Laslett entitled, "Stability of the K-V Distribution in Long Periodic Transport Systems." referred to in the summary.
2. J. D. Lawson, "The Physics of Charged Particle Beams," Clarendon Press, Oxford, 1977.
3. Kirstein, Kino, Waters, "Space Charge Flow," McGraw Hill, 1967.
4. G. R. Brewer, J. Appl. Phys. 30, 1022 (1959).

3. A DESIGN PROCEDURE FOR CORRECTING SECOND-ORDER GEOMETRIC AND CHROMATIC ABERRATIONS IN A BEAM TRANSPORT SYSTEM

Karl L. Brown

DISCUSSION

Consider a beam transport system consisting of a periodic array of static-magnetic-optical elements as a function of distance s, along the optic-axis. At any position s, the first order optical properties may be described by a matrix R and the initial conditions of an arbitrary ray represented by the vector $\vec{\chi}$, such that $\vec{\chi}(s) = R(s)\vec{\chi}(0)$. The components of the vector χ are the transverse position and angle coordinates of the ray x, x', y, y' and the deviation in momentum $\frac{\Delta p}{p} = \delta$ of the arbitrary ray from the central trajectory.

Now assume that the periodic array of magnetic elements is composed of a series of magnetic multipole components $M_n(s)$, such that the subscript n = o refers to the dipole components, n = 1 to the quadrupole component, and n = 2 to the sextupole components. The following five conditions are imposed upon the design of the system:

(1) $R_{11}(s + \ell) = - R_{11}(s)$ — x plane

(2) $R_{12}(s + \ell) = - R_{12}(s)$ — x plane

(3) $R_{33}(s + \ell) = - R_{33}(s)$ — y plane

(4) $R_{34}(s + \ell) = - R_{34}(s)$ — y plane

and the multipole components are distributed according to the rule

(5) $M_n(s + \ell) = M_n(s)$ — physical layout of the system.

CONCLUSIONS

i) The optic axis of the system is determined by the distribution of the dipole components via equation (5); i.e., by $Mo(s + \ell) = Mo(s)$.

ii) Equations (1) through (4) may be satisfied by choosing a periodic array that has equal focusing power in both the x and y planes, such as a FODO array of quadrupole components well known to AGS machine designers.

iii) If conditions (1) through (4) are satisfied, then it follows that $R(\ell) = - I$ (minus the unity matrix) for the monoenergetic trajectories and $R(2\ell) = + I$ to first order for all trajectories independent of their momentum. In other words, at position $s = 2\ell$ the system is achromatic to first-order in the components of the vector $\vec{\chi}(s)$.

iv) Because of the symmetries imposed by Equations (1) through (5), it follows from the driving terms of the differential equation[I] that <u>all</u> of the second-order geometric matrix elements (aberations) are zero at position $s = 2\ell$ where $R(s) = + I$.

v) We are now left (to second order) with only the chromatic aberrations of the system. <u>All</u> of these may be eliminated by the appropriate distribution and strengths of the sextupole components $M_2(s + \ell) = M_2(s)$ without disrupting the monoenergetic trajectories.

To understand how this is possible, note that the monoenergetic matrix transformation between any two positions a distance ℓ apart is $R(s + \ell, s) = - I_{x,y}$ in both the x and y planes. Therefore two identical sextupole components located a distance ℓ apart exactly cancel each other far as monoenergetic trajectories are concerned <u>if</u> the intervening system is linear. However, this conjugate pair of se tupoles <u>may</u> couple to the chromatic aberrations if there are dipoles present in the system to create a dispersive trajectory. In order to couple to all possible trajectories, a minimum of two such conjugate pairs is necessary in each transverse plane (x and y) separated by a sufficient distance to couple to both normal-modes of the harmonic-oscillator, i.e., to the trajectories represented by $R_{11}(s)$ and $R_{12}(s)$ in the x plane and $R_{33}(s)$ and $R_{34}(s)$ in the y plane. Thus a total of at least 4 sextupoles (2 conjugate pairs) is needed in each transverse plane to correct for all possible chromatic aberations within a + I transport section. If these two conjugate pairs in each plane are positioned 90° phase shift apart then the system is degenerate and all four sextupoles in each plane will have the same strength. In this case only two variables are needed (4 sextupoles tied together in the x plane and 4 tied together for the y plane). Thus the transformation matrix is equal to + I at position $S = 2\ell$ to both first- and second-order in the geometric and chromatic terms.

The best location for the sextupoles for each plane is where the beam envelope "Beta" function is a maximum for that plane (i.e., within or close to the focusing quadrupole - components for that plane). Thus there is a "natural" location for the x plane sextupoles components and also for the y sextupole components in a typical periodic array such as a FODO array of quadrupoles.

Chromatic aberrations for systems external to the + I section may in principle be corrected by the sextupole pairs within the + I section if enough free sextupole variables (conjugate pairs) are available in each plane. How successful this will be depends upon the magnitude of the corrections required and the resulting sextupole strengths needed for the correction. If the sextupole strengths required are too high then the

interlacing of sextupole pairs will ultimately disrupt the "assumed linearity" between conjugate pairs and the correction scheme will run into difficulties from higher-order trajectory distortions.

It has been subsequently shown that the above results may be extended to a more general result as follows:

Assume that a periodic array of N identical unit cells, each composed of dipole, quadrupole, and sextupole components, is adjusted to have a phase shift of $(2\pi/N)$ per cell. Then if the phase shift per cell is equal to or less than 90°, the total system of N cells will have a phase shift of 2π and the system may be adjusted such that all second-order geometric and chromatic aberrations are essentially zero. The geometric aberrations are zero by virtue of the 2π phase shift and symmetry of the system. The chromatic aberrations may be adjusted to be essentially zero by two families of sextupoles (one for the x plane and one for the y plane) and again because of the total system symmetry.

References

1. See, e.g., K. L. Brown, SLAC-75.

4. OUTLINE OF AN ABERRATION CORRECTED OPTICAL CHANNEL WITHOUT SPACE CHARGE

H. Bruck

INTRODUCTION

This beam transport line guides a particle bunch from a storage ring to the target, located at the center of the ring.

The present device has been conceived to prevent spectral analysis and coma aberration, owing to the deflecting sector, and also chromatic and spherical aberrations. Space charge is not considered here.

The device includes the following elements: (1) extraction from the storage ring, (2) adaptation to (3) the deflecting magnet sector, (4) collimator lens, and (5) 10m drift space to the target plane.

The full circle of a storage ring offers room for about 15 exit channels of this type. Nevertheless, if these channels are each slightly inclined with respect to the storage ring plane, there may be enough room for $\sim$ 50 channels, half of them accepting beam bunches from above, and half of them from beneath the storage ring.

SPECTRAL ANALYSIS AND COMA ABERRATION

No noticeable aberrations are caused prior to the deflecting sector. But the latter, beside chromatic and third order aberrations, causes momentum analysis and coma, decreasing thus the brilliance and the homogeneity of the beam.

The sector has a periodic AG structure and some further symmetry properties:

(a) Let the total number of trajectory oscillations per sector be an integer of the same value in x and in z.

(b) Let the sector field structure be a sequence of symmetrical periods, each period having the length of half a trajectory oscillation. Such a period is formed for instance by the lattice ½F M D M ½F or by this lattice, several times repeated.

Furthermore one supposes that the chromatic aberration (of type $\zeta_1 = C\ (\Delta p/p)\alpha$) and the third order aberration (essentially spherical of type $\zeta_3 = C_3\ \alpha^3$) of the sector are corrected in the usual way by conveniently located hexa- and octopoles, preserving the symmetry condition (b).

Under these conditions, not only spectral analysis, chromatic, coma and spherical aberrations are corrected, but furthermore the sector exit plane forms an afocal image of the entry plane. (See more in appendix.)

COLLIMATOR LENS

Leaving the deflector, the beam enters the collimator. The collimator system first enlarges the beam section, and then projects a very small image of it onto the target plane, 10m away. The collimator behaves like a low-β insertion in a storage ring, except that it acts not only in the x-, but also in the z-plane. The collimator comprises two focalizing multiplets with optical properties similar in x and z.

Unfortunately, the small first order image in the target plane is prohibitively enlarged by the collimator's chromatic and spherical aberrations, which can each be estimated at about ± 10mm under current conditions (incident beam angle at the target $\alpha \sim 5.10^{-2}$, momentum spread $\Delta p/p \sim 5.10^{-3}$).

The spherical aberration can be corrected by octopole lenses, located in the vicinity of the collimator. The chromatic aberration cannot be corrected by hexapole lenses in the same location, because all particle momenta are superimposed.

Nevertheless, this latter aberration can be corrected within the magnet sector, by the condition that the beam there is <u>not</u> adapted to the sector:

If the beam is adapted, its section forms a circle in phase space representation. Chromatic aberration rotates the phase space. But a rotated circle remains a circle.

On the contrary, an unadapted beam, if it is monochromatic, resembles in phase-space a diameter of a circle. If there is momentum dispersion and chromatic aberration, the corresponding diameters are dispersed and rotated. This dispersion and rotation can be compensated by hexapoles, located in the sector in places where the momenta are separated. It can be overcompensated, correcting simultaneously the chromatic aberration of the subsequent collimator.

APPENDIX

ACHROMATIC AND AFOCAL DEFLECTING SECTOR

The present theory applies to periodic transport channels of various shapes and arbitrary lengths. For simplicity of language we suppose the sector to be an arc of angular extent

$$-\frac{\pi}{2} \leqslant \theta \leqslant +\frac{\pi}{2}$$

The equations of the trajectory in the deflexting sector are

$$\left.\begin{aligned} \frac{d^2x}{d\theta^2} + K_x\, x &= f \\ \frac{d^2z}{d\theta^2} + K_z^z &= \sigma \end{aligned}\right\} \qquad (1)$$

The function f contains zero order and second order terms in x and z:

$$f = a_o + a_2 x^2 + a_2' x'^2 + b_2 z^2 + b_2' z'^2 \qquad (2)$$

The term $a_o = (R^2/\zeta)\,\Delta p/p$ is responsible for spectral analysis of the beam, and the four following terms for coma aberration.

The dependence of focalisation on momentum and on the third order terms do not appear in these equations. They are supposed to be corrected by hexa- and octo-pole fields. Orders higher than three are not considered.

Solutions of the homogeneous equation (1) (with $f \equiv 0$) is

$$\left.\begin{aligned} x_H &= A\,c_x + B\,s_x \\ z_H &= C\,c_z + D\,s_z \end{aligned}\right\} \qquad (3)$$

$c_{x,z}$ and $s_{x,z}$ being the pseudo-cosine and sine functions. Given the previously defined symmetry properties of the sector fields and the connection between the periodicities of field and of trajectory oscillations, the functions $c_{x,z}$ and $s_{x,z}$ have also strong symmetry properties, so that the trajectories, equations (3) form in the sector exit plane $\theta = +\frac{\pi}{2}$ an afocal image of the entry plane $\theta = -\frac{\pi}{2}$.

It has to be shown that this is still true for the trajectories, satisfying the full equations (1) with $f \neq 0$:

Solution of this full system (1) is

$$\left.\begin{aligned} x &= x_H + P \\ z &= z_H \,, \end{aligned}\right\} \qquad (4)$$

where

$$P(\theta) = -c_x \int_{-\frac{\pi}{2}}^{\theta} s_x\, f\,d\theta + s_x \int_{-\frac{\pi}{2}}^{\theta} c_x f\,d\theta \,. \qquad (5)$$

The function $P(\theta)$ expresses a deflection. In the entry plane $\theta = -\frac{\pi}{2}$, we have according to (5):

$$P(-\tfrac{\pi}{2}) = P'(-\tfrac{\pi}{2}) = 0. \qquad (6a)$$

By virtue of (2) and (3) and the symmetry properties of $c_{x,z}$ and $s_{x,z}$ one easily realizes, that $p(\theta)$ is an even function with the same periodicity as $c_{x,z}$ and $s_{x,z}$. Consequently also

$$P(+\tfrac{\pi}{2}) = P'(+\tfrac{\pi}{2}) = 0. \qquad (6b)$$

Therefore the image formed by trajectories, satisfying equations (4), solution of the full perturbed equations (1), is still afocal, independent of trajectory amplitude or particle momentum.

The influence of parametric resonance and coupling have not been considered, given the small number ($\lesssim 5$) of trajectory oscillations in the sector. Furthermore it is also possible to spoil slightly the symmetry conditions, allowing for a small, but nevertheless notably reduced amount of spectral analysis and coma.

This report, in its conclusions, is in accordance with a paper presented by K. L. Brown.

5. PRODUCTION OF ACHROMATIC SPOTS WITH A BEAM TRANSPORT SYSTEM CONSISTING ONLY OF QUADRUPOLES AND/OR SOLENOIDS

Klaus Halbach

INTRODUCTION

It is the purpose of this note to describe some unfinished work that may have a bearing on the problem of producing a small beam spot on a target for HIF. One of the important results obtained so far is an existence proof that shows that it is possible, at least in principle, to design systems, containing only quadrupoles and/or solenoids, with vanishing first and second derivatives of the spotsize with respect to momentum both at the target and at the exit of the last lens.

FORMULATION OF THE PROBLEM

If we assume that an accelerator produces a populated region of transverse phase space that can be represented by an ellipse of area $\pi\epsilon$ in each transverse dimension, and if we describe the spotsize in the customary manner by defining (spotradius in a transverse dimension)^2 = $\beta\epsilon$, then the minimum β_T obtainable at the target, for a given β_L at the exit of the last lens, is given by

$$\beta_T = L^2/\beta_L, \qquad (1)$$

where L is the distance from the last lens to the target. The design objective is to obtain that spotsize over a range of momentum without significant increase of β_L.

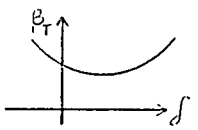

Fig. V-F-5/1

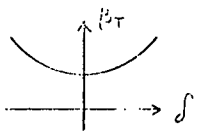

Fig. V-F-5/2

Fig. V-F-5/1. β_T vs $\delta(=\frac{\delta p}{p})$ for a poorly designed system.

Fig. V-F-5/2. β_T vs $\delta(=\frac{\delta p}{p})$ for a system in which $\left.\frac{d\beta_T}{d\delta}\right|_{\delta = o} = 0$.

Figure V-F-5/1 represents β_T vs $\delta(= \Delta p/p)$ for a poorly designed system. Clearly, it is advantageous to scale all magnetic fields such that $d\beta_T/d\delta = \beta_T' = 0$ for $\delta = 0$ as shown in Fig. V-F-5/2. In general, even for this system the increase of β_T over the desired momentum range may be much too large. We therefore require, possibly as a starting point for further optimization, that $\beta_T'' = 0$ also. Since a blow up of the beam is undesirable at the last lens, we also require that $\beta_L' = 0$, and $\beta_L'' = 0$. Transforming all of the above mentioned conditions to the end of the last lens, it follows that one has to satisfy the following conditions at the reference momentum:

$$\beta_L' = 0;\ \beta_L'' = 0;\ \alpha_L' = 0;\ \alpha_L = \beta_L/L, \qquad (2)$$

where α_L is the off-diagonal element of the phase space matrix at the end of the last lens. Its value, expressed by the last of Eq. (2), is required in order to satisfy Eq. (1). In addition to satisfying Eq. (2), the beam also has to fill the given aperture of the last lens.

RESULTS

The existence of systems satisfying Eq. (2) has been proved by designing a system, consisting of three thin dispersive lenses, that satisfies Eq. (2). That particular system is not reproduced here because it was designed only to demonstrate that there are no basic prohibitions against satisfying Eq. (2) by a linear system, and because its characteristics (lens strengths, distance between last lens and target, etc.) are such that it is useless for practical purposes.

Work on the design of a usable system has progressed far enough that one can state that:

a) It is very likely that such systems can be built with realistic elements for realistic phase spaces and target requirements, satisfying Eq. (2) for both transverse dimensions.

b) It is unlikely that one can design these systems for beams with large Bρ without producing several small waists. Even though these waists do not occur simultaneously in both transverse dimensions, they are likely to produce space charge problems when very large beam currents are used.

6. THE "FIGURE OF MERIT", $Q/u_{max}^{2/3}$, FOR BEAM TRANSPORT THROUGH PERIODIC FOCUSSING SYSTEMS

L. Jackson Laslett

LIMITS FOR FODO FOCUSSING SYSTEMS

Recent investigations[1] of the stability of high intensity beams (Kapchinskij-Vladimirskij distribution) have indicated that it may be prudent to design and operate transport systems in such a manner that

(i) the zero-intensity phase advance of individual particle betatron oscillations per period of the structure (σ_o) not exceed 90 degrees.

and

(ii) the intensity be limited to values such that σ not be depressed below 40% or 50% of σ_o.

These two conditions may impose substantial restrictions on the beam current that one can plant to transport. The implications of these conditions can first be examined by reference to the scaled envelope equations[2] and then by de-scaling in accordance with additional restrictions (e.g., maximum pole-tip field for a quadrupole transport system). In this case the de-scaling procedure indicated the significance of the "figure of merit", defined as $Qu/_{max}^{2/3}$ in terms of the scaled variables. [Thus

$$I = C_2 \left(\frac{A}{q}\right)^{1/3} B_Q^{2/3} (\beta\gamma)^{5/3} \epsilon_N^{2/3} \frac{Q}{u_{max}^{2/3}}$$

where

$$C_2 = \frac{1}{4}\left(\frac{4\pi}{\mu_o}\right)^{5/6}\left(\frac{m_p c^2}{r_p}\right)^{1/6}$$

$$= 3.66 \times 10^6 \text{ MKS·A units}$$

-- as given by the second of Eqns. (3) of Ref. 2]

We accordingly present below a table of this quantity $Q/u_{max}^{2/3}$ for $\sigma_o = 90$ deg. and for the slightly less marginal $\sigma_o = 80$ deg., and for the tune depressions $\sigma/\sigma_o = 0.50$ and $\sigma/\sigma_o = 0.40$ (the latter value σ/σ_o perhaps being close to marginal). The lattice designated by p = 0 is a symmetrical FODO structure with no gaps between the individual quadrupole elements, while that designated by p = 2 employs inter-quadrupole gaps of length equal to the length of the individual quadrupole elements themselves. These data thus serve to supplement results recorded earlier in Ref. 3. [The quantity θ ($= \sqrt{K}\,L$) is the half-period of the focussing structure, expressed in scaled units.]

Table V-F-6/1. Figures of Merit for FODO Systems.

For $\sigma/\sigma_o = 0.50$					For $\sigma/\sigma_o = 0.40$				
p = 0,					$\theta = 1.570796326795$				
				$\sigma_o = 90^\circ$					
σ	Q	u_o	v_o	$Q/u_o^{2/3}$	σ	Q	u_o	v_o	$Q/u_o^{2/3}$
45°	1.457	2.902_5	1.490	0.716	36°	2.035_5	3.223	1.674	0.933
p = 0,					$\theta = 1.49668994341$				
				$\sigma_o = 80^\circ$					
40°	1.375	2.879	1.586	0.679	32°	1.922	3.204	1.780	0.884
p = 2,					$\theta = 1.86361748098$				
				$\sigma_o = 90^\circ$					
45°	1.228	3.234_6	1.599	0.562	36°	1.716	3.592	1.797	0.731
p = 2,					$\theta = 1.77643752505$				
				$\sigma_o = 80^\circ$					
40°	1.158	3.201	1.705	0.533	32°	1.619	3.562	1.913	0.694

Somewhat more detailed data are recorded as an Addendum.

LIMITS FOR SOLENOIDAL FOCUSSING SYSTEMS

The quantity $(u^2 - \frac{1}{u^2})$ can play the role of a figure of merit for a focussing system formed by a continuous solenoid -- thus, from the second of Eqns. (4) in Ref. 2,

$$I = C_4 B_s (\beta\gamma) \epsilon_N (u^2 - \frac{1}{u^2}),$$

where

$$C_4 = \frac{1}{4}\left(\frac{4\pi}{\mu_o}\right) = 2.5 \times 10^6 \text{ MKS-A units},$$

or more simply [e.g., from the definition of Q]:

$$I = \frac{1}{8}\left(\frac{4\pi}{\mu_o}\right) B_s (\beta\gamma) \epsilon_N Q$$

$$= 1.25 \times 10^6 B_s (\beta\gamma) \epsilon_N Q.$$

A limit to transportable intensity in such a system (and probably also for an interrupted-solenoid transport system) again must lie close to a value such that $\sigma/\sigma_o \cong 0.4$.

For the continuous solenoid, one obtains (from the envelope equation in scaled variables)

$$u^2 = \sqrt{1 + \left(\frac{Q}{4}\right)^2} + \frac{Q}{4}$$

$$\frac{1}{u^2} = \sqrt{1 + \left(\frac{Q}{4}\right)^2} - \frac{Q}{4}$$

$$u^2 - \frac{1}{u^2} = \frac{Q}{2}$$

and from the single-particle equation

$$\omega/\omega_o = \sqrt{1 - \frac{Q}{2u^2}}.$$

For $\omega/\omega = 0.50$, one obtains $Q = 3.0$ and

$$u^2 - \frac{1}{u^2} = 1.5 \quad (u^2 = 2.0)$$

For $\omega/\omega_o = 0.40$, one obtains $Q = 4.2$ and

$$u^2 - \frac{1}{u^2} = 2.1 \quad (u^2 = 2.5).$$

IMPLICATION CONCERNING THE MASCHKE-COURANT FORMULA

For quadrupole focussing in a FODO lattice, descaling of the results obtained from study of the scaled equations leads to a transportable beam current given by[2]

$$I = 3.66 \times 10^6 \left(\frac{A}{q}\right)^{1/3} B_Q^{2/3} (\beta\gamma)^{5/3} \epsilon_N^{2/3} \times$$

$$\times \frac{Q}{u_{max}^{2/3}} \text{ [MKS-A units]}^*$$

if the "pole-tip field" limitation $B'(a_x)_m = K[B\rho](a_x)_m \leq B_Q$ is imposed. Expressed as beam power, through introduction of the factors $(\gamma-1)\frac{A}{q}\frac{M_p c^2}{e}$,

$$P = 3.43 \times 10^{15} \frac{Q}{u_{max}^{2/3}} \times$$

$$\times \left(\frac{A}{q}\right)^{4/3} B_Q^{2/3} (\beta\gamma)^{5/3} \epsilon_N^{2/3} (\gamma-1).$$

The factor $\frac{Q}{u_{max}^{2/3}}$ has been seen to assume values in the range 0.53 - 0.93 if the limitations suggested earlier are adopted. One thus obtains

$$P = C \left(\frac{A}{q}\right)^{4/3} B_Q^{2/3} (\beta\gamma)^{5/3} \epsilon_N^{2/3} (\gamma-1),$$

where the coefficient C falls in the range (2 to 3) $\times 10^{15}$. For $Q/u_{max.}^{2/3} = 0.7$, $C = 2.4 \times 10^{15}$ and thus is 1.5 times the value (1.67×10^{15}) suggested by Maschke.

It is gratifying that the result obtained here indicates a coefficient quite close to that proposed by Maschke in 1976. It will be recalled that Courant indicated at that time that Maschke's formula appeared to be conservative.

*$\pi\epsilon_N$ is the normalized emittance, so that the actual emittance is $\pi\epsilon_N/(\beta\gamma)$.

References

1. Lloyd Smith, HI-FAN-13; Ingo Hofmann and L. Jackson Laslett, HI-FAN-15 (Lawrence Berkeley Laboratory; October 1977).

2. G. R. Lambertson, L. J. Laslett, and L. Smith, IEEE Trans. Nucl. Sci., p. 993 (June 1977) -- LBL-5552.

3. Victor O. Brady and L. Jackson Laslett, "Figure of Merit", $Q'/u_m^{2/3}$, for Beam Transport Through a Periodic Quadrupole Lens System" (LBL Internal Notes, Hi-Fan-11, 1977).

ADDENDUM

Background Data

σ_o (deg.)	p = 0	p = 2
90.	1.570796326795	1.86361748098
80.	1.49668994341	1.77643752505
60.	1.31844943075	1.56609291708
30.	0.94733104711	1.12622633002

COMPUTATIONAL RESULTS

p = 0, θ = 1.570796326795

Q'	u_o	v_o	σ, deg.	$Q/u_o^{2/3}$
0.	2.1932800_5	1.	90.000000	(0.)
1.45742	2.9025023	1.4898640	45.000057	0.7162583
2.03553	3.22339166	1.67445715	36.000003	0.9328292

p = 2 θ = 1.86361748098

Q'	u_o	v_o	σ, deg.	$Q/u_o^{2/3}$
0.	2.4447567	1.0729641	90.000000	(0.)
1.2284	3.2345569	1.5991859	45.000056	0.5616468
1.7157	3.5920809	1.7974079	35.999510	0.7314937

p = 0 θ = 1.49668994341

Q'	u_o	v_o	σ, deg.	$Q/u_o^{2/3}$
0.	2.1282038	1.0826523	80.000000	(0.)
1.37491	2.8790852	1.5864476	40.000082	0.6793679
1.9218	3.2039376	1.7803018	32.000141	0.8842712

p = 2 θ = 1.77643752505

Q'	u_o	v_o	σ, deg.	$Q/u_o^{2/3}$
0.	2.3667256	1.1631666	80.000000	(0.)
1.158387	3.2012124	1.7049021	40.000000	0.5333071
1.619155	3.5623385	1.9132891	32.000027	0.6941686

7. HIGH-CURRENT BEAM TRANSPORT CALCULATIONS: SCALED VARIABLES, CONSTRAINTS, AND SCALING LAWS

M. Reiser

INTRODUCTION

The limitation of the beam current due to space charge effects is one of the most crucial problems in the design of accelerator systems for heavy ion fusion. What is the maximum current that can be transported in a given periodic focusing channel? How does it vary with the experimental parameters, i.e., what are the "scaling laws"? What are the consequences of constraints on the pole-tip field, the ratio of the aperture to the length of the magnets, the choice of the zero-intensity phase shift, and the lower limit for the phase shift with space charge? These are some of the major questions that are being asked by the designer and that were discussed by members of the beam transport group at this workshop. The following is a brief description and comparison of the numerical and analytical methods of solving these beam transport problems. Various useful analytical formulae for FODO and solenoid channels are presented, and the underlying constraints and limits of validity will be discussed.

THE K-V ENVELOPE EQUATIONS, COMPARISON OF NOTATIONS

All of the theoretical work on beam transport done so far involves the solution of the Kapchinskij-Vladimirskij (K-V) equations, either by numerical or by analytical methods. One of the difficulties in the comparison of results is the fact that there is no general consensus on notation. Different workers and groups use different symbols, and sometimes the same authors change the notation from one report to the next. It would be confusion to survey and compare all relevant papers with regard to notation, computational approach, etc. Most of the numerical work so far was done by the Berkeley group. The most accurate analytic approach, on the other hand, is the smooth approximation method presented in reference 2. We will therefore restrict ourselves to a comparison of these two techniques. In the table below, we compare the Berkeley notation, particularly that adopted in reference 1, with our notation used in reference 2. (MKS-A units are used unless noted otherwise.)

For easy reference and comparison, we present first the K-V envelope equations in the Berkeley[1] form [Eq. (1)] as well as in our notation[2] [Eq. (2)]. The independent variable in both cases is the path length $s = vt = \beta ct$ along the focusing channel.

$$\frac{d^2a_x}{ds^2} + K_x a_x - \frac{4q^2}{A}\frac{NR_p}{\beta^2\gamma^3}\frac{1}{a_x+a_y} - \frac{\epsilon^2}{\beta^2\gamma^2}\frac{1}{a_x^3} = 0$$

$$\frac{d^2a_y}{ds^2} + K_y a_y - \frac{4q^2}{A}\frac{Nr_p}{\beta^2\gamma^3}\frac{1}{a_x+a_y} - \frac{\epsilon^2}{\beta^2\gamma^2}\frac{1}{a_y^3} = 0 \,, \qquad (1)$$

$$\frac{d^2X}{ds^2} + \kappa_x X - \frac{2K}{X+Y} - \frac{\epsilon^2}{X^3} = 0$$

$$\frac{d^2Y}{ds^2} + \kappa_y Y - \frac{2K}{X+Y} - \frac{\epsilon^2}{Y^3} = 0 \,, \qquad (2)$$

where

$$\kappa_{x,y} = \frac{ZeB_o c^2}{AM_o c^2 a} \quad \text{for quadrupoles} \qquad (3)$$

and

$$\kappa_{x,y} = \left(\frac{ZeB_s c^2}{2AM_o c^2}\right)^2 \quad \text{for solenoids} \qquad (4)$$

$M_o c^2$ is the mass unit. The Berkeley group chooses it to be the proton mass, i.e., $m_p c^2 = 9.3826 \times 10^8$ eV; we use the atomic mass unit based on ^{12}C, i.e., $M_o c^2 = 9.3148 \times 10^8$ eV. The difference is obviously negligible in beam transport calculations.

Table V-F-7/1. Comparison of Symbols.

Berkeley Group (Ref. 1)	Description	Ref. 2
A,q	Atomic mass number and charge state of ion	A,Z
β,γ	Relativistic velocity and energy factors $\gamma=(1-\beta^2)^{-\frac{1}{2}}$	β,γ
$\pi\epsilon$ (also $\pi\epsilon_N$)	Normalized emittance Un-normalized emittance	$\pi\epsilon_N = \pi\beta\gamma\epsilon$ $\pi\epsilon$
a	Semi-aperture of magnets* Length of magnets Length of space between magnets	a ℓ L
2L	Length of one channel Period	S
$\frac{2}{p+2}$	Fraction of lattice occupied by magnets	$\ell/(L+\ell)$
a_x, a_y	Beam envelope in x and y direction	X,Y
a	Maximum envelope radius for matched beam with same emittance $\pi\epsilon$ in x and y (i.e., $\epsilon_x=\epsilon_y=\epsilon$) and with space charge*	$X_{max} = a$
	Maximum envelope radius for matched beam without space charge	$X_{o,max}$
K_x, K_y	Focusing function in K-V envelope equations	κ_x, κ_y

$\frac{4q^2}{A}\frac{Nr_p}{\beta^2\gamma^3}$	Space-charge factor in K-V envelope equations (N= number of particles per unit lenth, r_p=classical proton radius; K="generalized perveance")	2K
B_Q	Pole-tip field in quadrupoles*	B_o
B_s	Axial field in solenoids	B_s
I	Electrical beam current	I
I/q	Particle current	I/Z
P	Beam power	P
μ_o or σ_o	Phase shift (or "advance") per channel period ("cell") with no space charge	μ_o
μ or σ	Phase shift with space charge	μ
	Maximum of amplitude (or Courant-Snyder) function with no space charge	$\beta_{o,max} = w^2_{o,max}$
	Maximum of amplitude function with space charge	$\beta_{max} = w^2_{max}$
	Acceptance	$\pi\alpha$
$\textcircled{\sim} = \sqrt{K}\,L$	Focusing parameter	$\theta = \sqrt{\kappa}\,\ell$
$\textcircled{\sim} = 2\theta$		

*Comment: In the formulae for a matched beam, "a" is always understood to be the maximum beam radius and B_Q or B_o as the magnetic field at r=a although we often refer to them as the magnet semi-aperture and pole-tip field.

NUMERICAL SOLUTION OF THE K-V ENVELOPE EQUATIONS

For numerical integration of the K-V equations, it is useful to introduce dimensionless, "scaled variables" as was done by the Berkeley group. They define a scaled envelope function

$$u_{x(y)} = (\beta\gamma)^{1/2} K_{x(y)}^{1/4} \epsilon^{-1/2} a_{x(y)} \qquad (5)$$

and a space charge parameter

$$Q = \frac{4q^2}{A}\frac{Nr_p}{\beta\gamma^2 \epsilon K^{1/2}} \qquad (6)$$

which measures the ratio of the space charge force to the amplitude of the applied focusing force and the emittance ϵ. The advantage of this method is that one has only one parameter, Q, rather than three, and one only needs to calculate the scaled envelope $u_{x(y)}$ and the phase shift $\mu_{x(y)}$ as a function of Q. For a matched beam in a FODO channel, the transportable current is determined by the maximum of the scaled envelope function, u_m, and Q according to the relation[1]

$$I = C_2\left(\frac{A}{q}\right)^{1/3} B_o^{2/3}(\beta\gamma)^{5/3}\epsilon_N^{2/3}\frac{Q}{u_m^{2/3}} \qquad (7)$$

where $C_2 = 3.66 \times 10^6$ (MKS-A units). Laslett calls the ratio $Q/u_m^{2/3}$ the "figure of merit" (F.M.) It can be calculated from plots of u_m and μ versus Q by specifying the zero-intensity phase shift μ_o and the lower limit of μ/μ_o due to instabilities.[3] The recommended numbers are $\mu_o = 80^\circ$ and $\mu = 30^\circ$ which yields the result F.M. = 0.7 and for the beam power[3]

$$P_{[W]} = 2.4\times10^{15}\left(\frac{A}{q}\right)^{4/3}(\beta\gamma)^{5/3}(\gamma-1)B_o^{2/3}\epsilon_N^{2/3} \qquad (8)$$

ANALYTICAL SOLUTION OF THE K-V ENVELOPE EQUATIONS

The K-V equations can be solved analytically by the smooth approximation method.[2] In the parameter regime of interest to heavy ion fusion, i.e., $\mu_o \leq 90^\circ$ and high currents, this method is quite accurate (the maximum error is in the range of a few percent compared with the exact numerical results). For a periodic focusing channel, the following general results are obtained (in the notation of reference 2) for a matched beam:

$$K = \frac{\mu_o}{S}\alpha[1 - (\epsilon/\alpha)^2] \qquad (9)$$

where

$$\alpha = \frac{a^2}{w^2_{o,max}}, \quad \epsilon = \frac{X^2_{o,max}}{w^2_{o,max}} \qquad (10)$$

and hence

$$\left(\frac{\epsilon}{\alpha}\right)^2 = \frac{X^4_{o,max}}{a^4} \qquad (11)$$

The generalized perveance K is related to the beam current I by

$$K = \frac{I}{I_o}\frac{2}{\beta^3\gamma^3} \qquad (12)$$

where

$$I_o = I_1\frac{A}{Z} = 3.1 \times 10^7\frac{A}{Z} \quad [\text{amperes}] \qquad (13)$$

is the limiting current. Thus, one gets from (9) for the electric beam current that can be transported through a periodic channel the relation

$$I = 0.5\, I_1\frac{A}{Z}\beta^3\gamma^3\frac{\mu_o}{S}\alpha[1 - (\epsilon/\alpha)^2]. \qquad (14)$$

The interpretation of these results is straightforward: The transportable beam current I is proportional to the average force per channel period (represented by μ_o/S) and increases with the channel acceptance $\pi\alpha$. High current transport requires that the emittance $\pi\epsilon$ is significantly less than the acceptance. A matched beam with given emittance $\pi\epsilon$ would in the absence of the space charge force have a maximum radius of $X_{o,max}$. Due to the space charge, it acquires a larger cross section with maximum radius $X_{max} = a$. The "acceptance" $\pi\alpha$ may be understood in two ways, namely, as the available transverse phase space area that the matched beam can occupy in a channel with given semi-aperture a, or, alternately, we can say that the beam with emittance $\pi\epsilon$ and with space charge looks like a beam with effective emittance $\epsilon_{eff} = \alpha$ and no space charge.

We now define a space charge parameter u (analogous to Q of the Berkeley group) by

$$u = \frac{KS}{2\mu_o\epsilon} = \frac{I}{I_o}\frac{S}{\mu_o}\frac{1}{\beta^3\gamma^3\epsilon} \tag{15}$$

The phase shift μ with space charge and the maximum value of the amplitude function w_{max} with space charge are then found to be simple functions of u and given by the expressions

$$\mu = \mu_o\left[\sqrt{1+u^2} - u\right], \tag{16}$$

$$w_{max} = w_{o,max}\left[\sqrt{1+u^2} + u\right]^{1/2}. \tag{17}$$

Furthermore, Eq. (9) may be written in the form

$$u = \frac{1}{2}\frac{\alpha}{\epsilon}\left[1 - \left(\frac{\epsilon}{\alpha}\right)^2\right] \tag{18}$$

Solving (18) for ϵ/α yields

$$\frac{\epsilon}{\alpha} = \sqrt{1+u^2} - u \tag{19}$$

and hence, in view of (16),

$$\frac{\epsilon}{\alpha} = \frac{\mu}{\mu_o}. \tag{20}$$

Our theory thus yields the surprisingly simple result that the ratio of the emittance ϵ to the acceptance α (or effective emittance, ϵ_{eff}) is equal to the ratio of the phase shift with and without space charge, μ/μ_o.

The relationship between the parameters Q, u_m of the Berkeley group and our parameters is as follows:

$$Q = \frac{2K}{\kappa^{1/2}\epsilon} = \frac{2K\ell}{\theta\epsilon}, \tag{21}$$

or

$$Q = \frac{2\mu_o}{(1 + L/\ell)\theta}\,u \quad \text{for FODO channels,} \tag{22}$$

and

$$Q = \frac{4\mu_o}{(1 + L/\ell)\theta}\,u \quad \text{for solenoid channels.} \tag{23}$$

$$u_m = \kappa^{1/4}\frac{w_{max}}{\sqrt{\ell}} = \frac{\sqrt{\theta}}{(\epsilon/\alpha)^{1/2}}\frac{w_{o,max}}{\sqrt{\ell}}, \tag{24}$$

or

$$u_m = \sqrt{\theta}\,\frac{w_{o,max}}{\sqrt{\ell}}\left[\sqrt{1+u^2} + u\right]^{1/2}. \tag{25}$$

QUADRUPOLE CHANNELS OF THE FODO TYPE

It is convenient to express the factor $\mu_o\alpha/S$ as well as $w_{o,max}$ in terms of the focusing parameter $\theta = \sqrt{\kappa}\,\ell$, and the ratio a/ℓ. For FODO channels, one finds

$$\frac{\mu_o}{S}\alpha = \left(\frac{a}{\ell}\right)^2 H(\theta, L/\ell), \tag{26}$$

where

$$\theta = 0.5675\left(\frac{Z}{A}\frac{B_o}{\beta\gamma a}\right)^{1/2}\ell, \tag{27}$$

and L/ℓ is the ratio of free-space distance L between magnets to the length of the quadrupoles. Analytical expressions for the functions $H(\theta,L/\ell)$ and $w^2_{o,max}/\ell$ and a plot of $H(\theta,L/\ell)$ versus θ for different values of L/ℓ may be found in reference 2. Table V-F-7/2 lists some values for μ_o, θ, $H(\theta,L/\ell)$, and $w_{o,max}/\sqrt{\ell}$ for a FODO channel with $L/\ell = 1$.

SOLENOID CHANNELS

For a periodic channel with solenoids, one finds the equivalent expressions

$$\frac{\mu_o}{S}\alpha = \left(\frac{a}{\ell}\right)^2 F(\theta, L/\ell), \tag{28}$$

where

$$\theta = 0.16\,\frac{Z}{A}\frac{B_s\ell}{\beta\gamma}. \tag{29}$$

The functions $F(\theta,L/\ell)$ and $w^2_{o,max}/\ell$ for the solenoid channel are given in reference 2, and Table V-F-7/3 shows a few values for $L/\ell = 1$.

CONSTRAINTS AND SCALING LAWS

The analytical theory is particularly useful in elucidating the parametric dependence of the beam current and the effects of various constraints on the scaling laws. For design studies, it is very important to know the scaling laws which show how the beam current or power varies with the experimental parameters (A,Z,β,γ,ϵ,B_o,a,

ℓ,L). This was recognized very early by A. Maschke, who first derived a power law of the form (8) for a quadrupole channel, except that his coefficient was slightly different (1.67 versus 2.4).

We shall see below that this scaling law can be obtained from our general formula (14) under the condition that μ_o and μ/μ_o are fixed. The consequences of these as well as other constraints and the validity of relation (8) and other scaling laws that can be derived from Eq. (14) will be discussed.

FODO CHANNELS

The expression (14) for the beam current in a periodic channel is a general analytic solution of the K-V envelope equations (for a matched beam). Note that it is not an explicit function of all experimental parameters, and that different scaling laws can be derived from it depending on the constraints that are imposed. In the following we list the most important formulae beginning with the general expression for a FODO channel.

(a) Beam current in FODO channel with no constraints: By substituting (26) into (14), one obtains

$$I_{[A]}=1.55\times10^{7}\,\frac{A}{Z}\,\beta^{3}\gamma^{3}\left(\frac{a}{\ell}\right)^{2}H(\theta,L/\ell)[1-(\epsilon/\alpha)^{2}]\,, \tag{30}$$

Where θ is given by (27), ϵ/α by (10), (11), and $H(\theta,L/\ell)$ is defined in reference 2. To determine how the beam current varies with a given parameter, say, B_o, one first calculates the value of θ, the $H(\theta,L/\ell)$ and $w_{o,max}$ using the formulae in reference 2 (or interpolating from the values given in Table V-F-7/2 if $L/\ell = 1$).

(b) $\theta \ll 1$, $\mu_o \ll \pi$: In this case, $H(\theta,L/\ell) \approx \theta^4 g(L/\ell)$, and one gets

$$I_{[A]} = 1.61\times10^{6}\,\frac{Z}{A}\,\beta\gamma(B_o\ell)^{2}g(L/\ell)[1-(\epsilon/\alpha)^{2}] \tag{31}$$

where $g(L/\ell)$ is defined in reference 2; for $L/\ell = 1$, $g(1) = 0.167$. Note that in this limit, the particle current, I/Z, is independent of the charge state Z. For high-current beam transport, one tries to operate at a phase shift μ_o close to 90°, and thus formula (31) is not very useful.

(c) μ_o and L/ℓ fixed: This condition implies that the focusing strength θ of the quadrupoles, the function $H(\theta,L/\ell)$, and $w_{o,max}^2/\ell$ is fixed. Hence, from (27)

$$\frac{Z}{A}\,\frac{B_o}{\beta\gamma}\,\frac{\ell^{2}}{a} = C_1\,, \tag{32}$$

and from (10)

$$a^{2} = \frac{w_{o,max}^{2}}{\ell}\,\alpha\ell = C_3\alpha\ell \tag{33}$$

Therefore,

$$\left(\frac{a}{\ell}\right)^{2} = \left(\frac{ZB_o}{A\beta\gamma}\right)^{2/3}\left(\frac{C_3}{C_1}\right)^{2/3}\alpha^{2/3}. \tag{34}$$

Eq. (30) then becomes

$$I = C_2\left(\frac{A}{Z}\right)^{1/3}(\beta\gamma)^{7/3}\,B_o^{2/3}\,\alpha^{2/3}[1-(\epsilon/\alpha)^{2}] \tag{35}$$

The constant C_2 depends on the value of θ. For $\mu_o = 80°$, $L/\ell = 1$, one finds (from Table V-F-7/2) $\theta = 0.888$, $H(\theta,L/\ell) = 0.553$, $w_{o,max}/\sqrt{\ell} = 2.5113$ which yields $C_1 = 2.45$, $C_3 = 6.307$, $C_2 = 1.6 \times 10^{6}$, and thus

$$I_{[A]}=1.6\times10^{6}\left(\frac{A}{Z}\right)^{1/3}(\beta\gamma)^{7/3}B_o^{2/3}\alpha^{2/3}[1-(\epsilon/\alpha)^{2}]. \tag{36}$$

The corresponding beam power (for $\mu_o = 80°$, $L/\ell = 1$) is

$$P_{[W]} = 1.5\times10^{15}\left(\frac{A}{Z}\right)^{4/3}(\beta\gamma)^{7/3}B_o^{2/3}\alpha^{2/3}(\gamma-1)\,[1-(\epsilon/\alpha)^{2}] \tag{37}$$

(d) μ_o, L/ℓ, and μ/μ_o fixed: If instabilities impose a lower limit to the phase shift with space charge, $(\mu/\mu_o)_{min}$, as inferred from the studies of the Berkeley group, the acceptance α cannot exceed the value

$$\alpha_{max} = \frac{\epsilon}{(\mu/\mu_o)_{min}} = f_1\epsilon \tag{38}$$

in accordance with relation (20). In this case, we have

$$\alpha^{2/3}[1-(\epsilon/\alpha)^{2}] = f_1^{2/3}\,\epsilon[1-1/f_1^{2}] = f_2\epsilon\,, \tag{39}$$

and the maximum beam current is given by

$$I = C_2 f_2\left(\frac{A}{Z}\right)^{1/3}(\beta\gamma)^{7/3}B_o^{2/3}\,\epsilon^{2/3}. \tag{40}$$

This has the form of Maschke's scaling law. For $\mu_o = 80°$, $L/\ell = 1$, and $\mu = 30°$, we find $f_2 = 1.65$, and hence

$$I_{[A]}=2.64\times10^{6}\left(\frac{A}{Z}\right)^{1/3}(\beta\gamma)^{5/3}B_o^{2/3}\epsilon_N^{2/3}\,, \tag{41}$$

$$P_{[W]}=2.48\times10^{15}\left(\frac{A}{Z}\right)^{4/3}(\beta\gamma)^{5/3}\,B_o^{2/3}\,\epsilon_N^{2/3}(\gamma-1) \tag{42}$$

Note that the numerical factor in (42) differs by only 3% from the result (8) obtained by exact numerical integration. This demonstrates that the smooth approximation method is indeed remarkably accurate in the parameter regime that is of interest to heavy-ion fusion. From the derivation, it is obvious that one must be cautious in the interpretation and application of the scaling laws (41) and (42). These formulae are useful for design purposes, i.e., as long as one can assume that with increasing emittance of the beam, the acceptance of the channel can be increased proportionally. However, once a focusing channel is built and actual parameters differ from the design values, one must use the more general relations (35) or (30) (depending on whether the phase shift μ_o remains fixed or not when parameters are varied). Specifically, in a channel with fixed acceptance α, the beam current can be increased only by reducing the emittance ϵ. The seeming contradiction between the scaling laws (35) and (40) is thus explained by the fact that the latter implies that α increases proportionally to ϵ while in (35) α is an independent parameter.

(e) μ_o, L/ℓ, μ/μ_o, and B_o fixed: The additional constraint that the magnetic field B_o has a given value, uniquely determines the two geometry parameters a, ℓ (i.e., the magnet size) when particle mass, charge state, and energy are given. The values of a and ℓ follow from Eqs. (32) and (33). Since the ratio a/ℓ cannot become too large[1] ($a = \ell/2$ would appear to be a reasonable limit), quadrupole channels are not useful below a kinetic energy that can be calculated from Eq. (34). With $a/\ell = 0.5$, $\alpha = f_1\epsilon$, one gets from (34) the relation

$$\frac{A\beta^2\gamma^2}{ZB_o\epsilon_N} \geq 8 f_1 \frac{C_3}{C_1} . \qquad (43)$$

For our example of $\mu_o = 80^o$, $\mu = 30^o$, $L/\ell = 1$, we get

$$8f_1 \frac{C_3}{C_1} = 54.9 . \qquad (44)$$

Using (44) and the nonrelativistic relation for the voltage,

$$V = \frac{1}{2}\frac{A}{Z}\frac{M_o c^2}{e}\beta^2 ,$$

one can express the relation (43) in the form

$$V_{[MV]} \geq 2.56\times10^4 B_{o[T]}\epsilon_{N[m\text{-}rad]} . \qquad (45)$$

Thus, when $B_o = 5$ T, $\epsilon_N = 2\times10^{-5}$ m-rad, one finds that the use of FODO magnets in low-energy beam transport is no longer practical at voltages below 2.56 MV. Note that this lower limit for V is independent of the mass and charge state of the particles.

SOLENOID CHANNELS

Similar scaling laws may be derived from Eq. (14) for periodic solenoid channels. The results are summarized in the same order as in the FODO case.

(a) Beam current in solenoid channel with no constraints [from (14) and (28)]:

$$I_{[A]} = 1.55\times10^7 \frac{A}{Z}\beta^3\gamma^3\left(\frac{a}{\ell}\right)^2 F(\theta, L/\ell)[1-\epsilon/\alpha)^2] , \qquad (46)$$

where θ is given by (29) and $F(\theta, L/\ell)$ is defined in reference 2.

(b) $\theta \ll 1$, $\mu_o \ll \pi$: In this approximation, $F(\theta, L/\ell) \approx \theta^2/(1+L/\ell)$; hence, with (29),

$$I_{[A]} = 4.0\times10^5 \frac{Z}{A}\beta\gamma(B_s a)^2 \frac{\ell}{\ell+L}[1-(\epsilon/\alpha)^2] . \qquad (47)$$

(c) μ_o and L/ℓ fixed:

$$\frac{Z}{A}\frac{B_s \ell}{\beta\gamma} = c_1 \qquad (48)$$

$$a^2 = \frac{w_{o,max}^2}{\ell}\alpha\ell = c_3\alpha\ell \qquad (49)$$

$$\left(\frac{a}{\ell}\right)^2 = \frac{c_3}{c_1}\frac{ZB_s}{A\beta\gamma}\alpha , \qquad (50)$$

$$I = c_2\beta^2\gamma^2 B_s\alpha[1-(\epsilon/\alpha)^2] . \qquad (51)$$

For $\mu_o = 80^o$, $L/\ell = 1$, one finds (using Table V-F-7/3 $\theta = 0.9644$, $F(\theta, L/\ell) = 0.42$, $w_{o,max}/\sqrt{\ell} = 1.2893$ which yields $c_1 = 6.03$, $c_3 = 1.66$, $c_2 = 3.0\times10^5$, i.e.,

$$I_{[A]} = 1.79\times10^6\beta^2\gamma^2 B_s\alpha[1-(\epsilon/\alpha)^2] . \qquad (52)$$

(d) $\mu_o, L/\ell, \mu/\mu_o$ fixed: In this case we get with $\alpha = f_1\epsilon$ and

$$\alpha[1-\epsilon/\alpha)^2] = f_1\epsilon[1-1/f_1^2] = f_3\epsilon \qquad (53)$$

the scaling law

$$I = c_2 f_3\beta^2\gamma^2 B_s\epsilon , \qquad (54)$$

which has the same form as Courant's Eq. (17) in reference 4. For $\mu_o = 80^o$, $L/\ell = 1$, and $\mu = 30^o$, one obtains $f_1 = 2.667$, $f_3 = 2.29$,

$$I_{[A]} = 4.1\times10^{6}\beta\gamma B_s \epsilon_N \ , \qquad (55)$$

$$P_{[W]} = 3.73\times10^{15}\,\frac{A}{Z}\,\beta\gamma(\gamma-1)B_s\epsilon_N \ . \qquad (56)$$

Note that, in contrast to the FODO case, the beam power varies only linearly with the parameters (A/Z), $\beta\gamma$, B_s, and ϵ_N. For the ratio of the beam current in a FODO channel to that in a solenoid channel (with the same constraints) one obtains from (41) and (55)

$$\frac{I_{FODO}}{I_{SOL}} = 0.64\left(\frac{A}{Z}\right)^{1/3}(\beta\gamma)^{2/3}\,\frac{B_o^{2/3}}{B_s}\,\epsilon_N^{-1/3} \ . \qquad (57)$$

(e) μ_o, L/ℓ, μ/μ_o, and B_s fixed: As in the FODO case, the parameters a, ℓ are fixed by these constraints when A, Z, and $\beta\gamma$ are given. Their values can be calculated from (48) and (49). For $\mu_o = 80^o$, $L/\ell = 1$, $\mu = 30^o$, one finds

$$\frac{a}{\ell} = \frac{0.857}{\beta\gamma}\left(\frac{ZB_s\epsilon_N}{A}\right)^{1/2} \ . \qquad (58)$$

The voltage where $\ell = 2a$ is given by

$$V_{[MV]} = 1.37\times10^{3}B_{s[T]}\epsilon_{N[m\text{-}rad]} \ , \qquad (59)$$

which, for the same magnetic field and emittance, is seen to be more than an order of magnitude lower than in the FODO case. It is interesting to compare the current-carrying capability of solenoid and FODO systems at the low-energy point where quadrupoles become impractical since $\ell = 2a$. By substituting $\beta\gamma$ from (43), using (44) for the constants, into (57), one finds for this limit

$$\frac{I_{FODO}}{I_{SOL}} = 2.4\,\frac{B_o}{B_s} \ . \qquad (60)$$

This relation depends only on the ratio of the quadrupole field B_o to the solenoidal field B_s. For $B_o = B_s$, we see that, at the low-energy quadrupole limit $\ell = 2a$, the FODO channel can transport 2.4 times more current than the solenoid channel. (The ratio ℓ/a for the solenoid magnets would of course be greater than 2 in this case.)

QUESTIONS AND COMMENTS

The preceding analysis, like most beam transport studies done so far, is based entirely on the K-V equations and matched-beam conditions. In a critique of this approach, the Berkeley group[1] discussed a number of questions that can be raised, such as the effects of image fields, more realistic phase-space distribution functions, etc.

Table V-F-7/2. Parameter data for a FODO channel with $L/\ell = 1$.

μ_o	θ	$w_{o,max}/\ell$	$H(\theta,L/\ell)$
90°	.9318	2.5328	.0612
85°	.9107	2.5178	.0585
80°	.8882	2.5113	.0553
75°	.8643	2.5134	.0518
70°	.8388	2.5243	.0479

Table V F 7/3. Parameter data for a solenoid channel with L/ℓ - 1.

μ_o	θ	$w_{o,max}/\ell$	$F(\theta,L/\ell)$
90°	1.0769	1.2469	.5052
85°	1.0211	1.2659	.4629
80°	.9644	1.2893	.4200
75°	.9071	1.3175	.3771
70°	.8491	1.3507	.3348

We want to briefly comment on two of these questions, namely, (a) the current limit at low energy where the potential well due to the space charge becomes comparable to the kinetic energy of the particles, and (b) the effects of mismatch between beam emittance and channel acceptance.

With respect to the first question, the potential V_o on the axis of an axially summetric beam is given in terms of the beam current I, and mean axial velocity, βc, by

$$V_o = \frac{I}{4\pi\epsilon_o\beta c} \ . \qquad (61)$$

A particle is stopped when all its kinetic energy is converted into potential energy, i.e., when (nonrelativistically)

$$(\gamma-1)AM_oc^2 \approx \frac{1}{2}\,AM_oc^2\beta^2 = ZeV. \qquad (62)$$

By substituting (61) into (62), one finds for the limiting current $I = I_L$:

$$I_L = 3.1\times10^{7}\,\frac{A}{Z}\,\beta(\gamma-1) \approx 1.55\times10^{7}\,\frac{A}{Z}\,\beta^3 \qquad (63)$$

le compare this with the focusing limit (55) of a solenoid channel and find the energy where this current is equal to I_L. From (55) and (63), we find for the ratio I/I_L the expression

$$\frac{I}{I_L} = 0.264 \frac{B_s \epsilon_N}{\beta^2} \frac{Z}{A}, \qquad (64)$$

and, hence, for β^2 when $I = I_L$:

$$\beta^2 = 0.264 \frac{Z}{A} B_s \epsilon_N \qquad (65)$$

The equivalent voltage is

$$V_{[MV]} = 123\, B_{s[T]} \epsilon_{N[M\text{-rad}]}. \qquad (66)$$

For $B_s = 5$ T, $\epsilon_N = 2 \times 10^{-5}$ m-rad, one gets

$$V = 0.0123 \text{ MV} = 12.3 \text{ kV}.$$

The initial accelerating voltages at the ion source are in the range of 100 kV to 1 MV and thus safely above this limit. We conclude therefore that this effect should not pose a limit to the transportable beam current.

Concerning the second question on beam mismatch, a definitive answer is not yet available at this point. The beam current propagates in the form of pulses which experience various processes (acceleration, transverse stacking, longitudinal bunching, etc.). Under ideal conditions, one can match only a slice of the pulse along which the current and emittance are the same. The rest of the beam (particularly in the leading and trailing edge of the pulse) could presumably be mismatched. The Berkeley group argued in reference 1 that the rate of increase of current with time (or distance) is sufficiently slow that the transverse motion will adjust itself adiabatically to the matched conditions if it is matched at the entrance to the channel where the current is low. However, Lemaire showed results from numerical integration of the K-V envelope equations which appear to indicate that small changes in beam current may lead to mismatch and relatively large oscillations of the transverse beam cross section.[5] This question was only briefly discussed by the beam transport group at the end of the workshop. Clearly, further studies are necessary to determine whether mismatch is an important effect, and, if so, what provisions must be made in the design of the focusing systems (larger apertures, etc.) to avoid unnecessary particle losses.

References

1. G. Lambertson, L. J. Laslett, L. Smith, "Transport of Intense Beams", IEEE Trans. NS-24, 993 (1977).
2. M. Reiser, "Periodic Focusing of Intense Beams", Physics Publication No. 77-261 (Oct. 1977), Univ. of Maryland; to be published in Particle Accelerators.
3. See papers by Laslett in these workshop proceedings.
4. ERDA Summer Study of Heavy Ions for Inertial Fusion, LBL-5543, Dec. 1976, p. 73.
5. J. L. Lemaire, private communication.

8. SATURATION OF SPACE CHARGE DRIVEN INSTABILITIES IN BEAM TRANSPORT SYSTEMS

I. Haber and A. W. Maschke

Instabilities in the presence of space charge can limit the power which may be transported in a focused channel. Several classes of perturbations to a matched Kapchinskij-Vladimirskij[1] system have in fact been found to be unstable[2,3]. Numerical simulations have been performed[4] which indicate that a parameter range exists where these instabilities saturate without major growth in the beam emittance.

Figure V-F-8/1a is a plot of four views of the initial four-dimensional $x\text{-}p_x\text{-}y\text{-}p_y$ phase space of the numerical system. Two thousand of the approximately 16 thousand simulation particles in the system are plotted. The thin lens quadrupole focusing system has a tune of 90° per lens system, which is detuned by space charge to 30°. This system goes unstable and evolves in a complicated fashion until a steady state is reached after about forty magnet pairs and little subsequent evolution occurs. Fig. V-F-8/1b shows the phase space after 100 magnet pairs. Numerical tests have shown that these results are essentially independent of

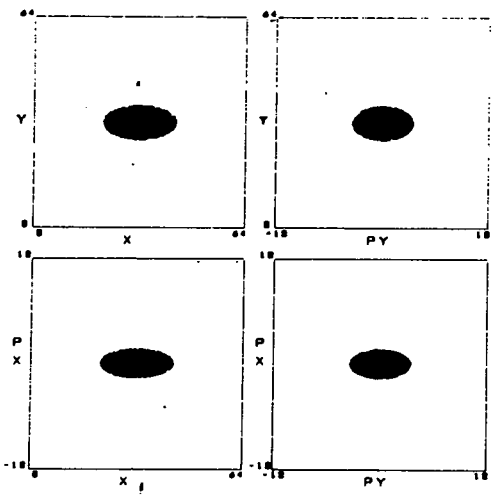

1a

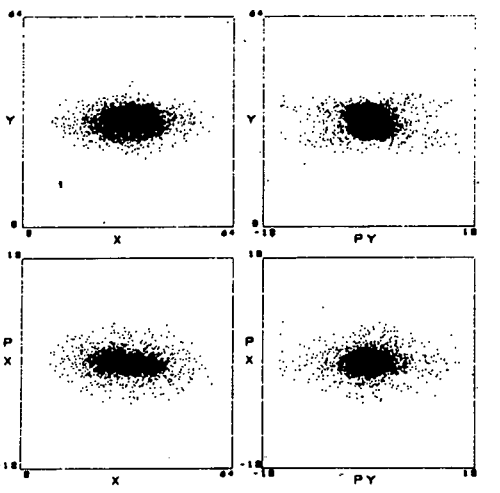

1b

Fig. V-F-8/1. Phase space of 90° focused system in the presence of space charge. At t = 0 (a), and after 100 magnet pairs (b).

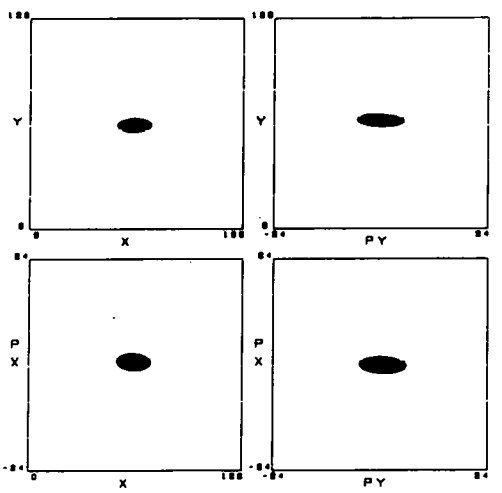

2a

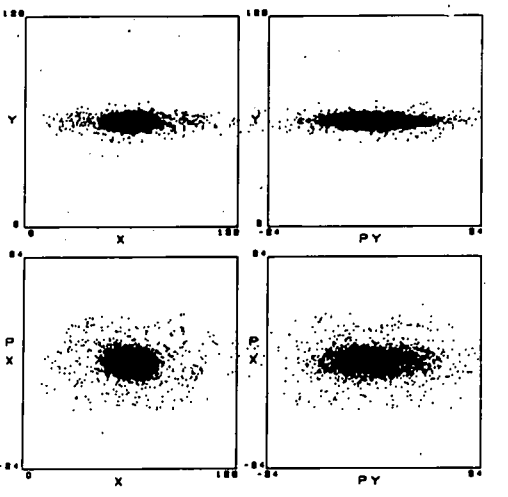

2b

Fig. V-F-8/2. Phase space of 130° focused system in the presence of space charge. At t = 0 (a), and after 100 magnet pairs (b).

variations of numerical parameters such as time step, system resolution, and number of particles when they are varied by factors of two from the conditions used.

Even a system subject to instabilities of the K-V envelope equations is found to saturate, although the emittance growth in reaching steady state is much greater. Fig. V-F-8/2a shows the initial phase space of a 130° per magnet system detuned by sapce charge to 70°. Fig. V-F-8/2b shows the steady state this system has reached after 100 magnet pairs.

Though the detailed parametric behavior of these steady distributions has not yet been examined, the results here appear to be typical of those obtained in several runs. The optimistic conclusion appears to be that these instabilities present no barrier to transporting beam powers in the vicinity of the Maschke current limit.

References

1. I. M. Kapchinskij and V. V. Vladimirskij, Proc. Internat. Conf. on High Energy Accelerators, CERN 1959, p. 274.
2. Discussion with the High Current Beam Transport Group.
3. S. Chattopadhyay, I. Hofmann, L. J. Laslett, and L. Smith, Paper WB15, Topical Meeting on Inertial Confinement Fusion, San Diego, California, February, 1978. Proceedings to be published.
4. I. Haber, T. F. Godlove and A. W. Maschke, Bull. Am. Phys. Soc., 22, p. 1198 (Oct. 1977).

9. ESTIMATE OF THE LONGITUDINAL SELF ELECTRIC FIELD OF AN ION BEAM

A. A. Irani

INTRODUCTION

The self electric field on the axis of an ion beam of radius a in a conducting cylinder of radius b is given by

$$E_z = -\frac{g}{\gamma^2}\frac{d\lambda}{dz} \tag{1}$$

where λ is the charge per unit length and g, the geometrical factor, is a function of the radii a and b. The above formula assumes that the radius of the conducting cylinder is much smaller than the length of the ion beam ($b \ll L$) and that E_z is calculated away from the edge of the beam ($|z|<|\frac{L}{2}|$). For the HIDE parameters[1], i.e., loosely speaking a 50 TW, 100 JK, multi-GeV heavy ion beam, the assumption $b \ll L$ is no longer valid and hence Eq. (1) cannot be used. Since for an unneutralized heavy ion beam it is necessary to apply ramp voltages to compensate for the longitudinal self fields it is desirable to know exactly what these fields are. Here, exact expressions for E_z on the axis of the ion beam are obtained and are compared under different circumstances with the approximate results given by Eq. (1).

THEORETICAL CALCULATIONS

We consider the Green's Function approach; i.e., we calculate the fields due to a point charge moving inside a cylinder of radius b. The calculations are carried out in the frame of reference of the moving particle and the fields are later transformed back to the laboratory frame. Then according to Poisson's Equation

$$\nabla^2\delta\phi = -4\pi q\,\delta(\underset{\sim}{x} - \underset{\sim}{x}'). \tag{2}$$

Now, as is usually done for simplicity, we pick our origin of coordinates to be at the point $\underset{\sim}{x}'$ and after obtaining the final result generalize our solution. Then, in cylindrical coordinates

$$\nabla^2\delta\phi = -4\pi q\cdot\frac{\delta(r)}{2\pi r}\cdot\delta(z) \tag{3}$$

and we obtain

$$\frac{1}{r}\frac{\partial}{\partial r}\,r\,\frac{\partial}{\partial r}\,\delta\bar{\phi} - k_z^2\delta\bar{\phi} = -2q\frac{\delta(r)}{r} \tag{4}$$

where $\delta\bar{\phi} = \int_{-\infty}^{\infty} dz\, e^{-ik_z z}\,\delta\phi$ is the Fourier Transform of $\delta\phi$.

The solution to the differential equation given by (4) using the boundary condition $\delta\bar{\phi} = 0$ at $r = b$ is

$$\delta\bar{\phi} = -2q\,\frac{K_o(k_z b)\,I_o(k_z r)}{I_o(k_z b)} + 2q\,K_o(k_z r) \tag{5}$$

where the standard notation has been used for the Bessel functions.

Then using $\delta\phi = \int_{-\infty}^{\infty}\frac{dk_z}{2\pi}\,e^{ik_z z}\,\delta\bar{\phi}$, solving the integrals by contour integration and generalizing the result we obtain

$$\delta\phi = \frac{\pi q}{b}\sum_{n=1}^{\infty}\frac{J_o[k_n(r-r')]\,Y_o(k_n b)}{J_1(k_n b)}\,e^{-k_n(z-z')} \tag{6}$$

where the k_n are given by $J_o(k_n b) = 0$ and

$$\delta E_z = -\frac{\partial}{\partial z}\,\delta\phi = \left\{\frac{z-z'}{|z-z'|}\right\}\frac{\pi q}{b} \times \sum_{n=1}^{\infty}\frac{k_n\,J_o[k_n(r-r')]\,Y_o(k_n b)}{J_1(k_n b)}\,e^{-k_n|z-z'|} \tag{7}$$

Now, for the charge distribution

$$\rho_1 = \frac{6Q}{\pi a^2 L^3}\left[\frac{L^2}{4} - z^2\right]$$

which is constant in the r direction but parabolic in the z direction and where Q is the total charge in the bunch we get on axis (i.e. at $\underset{\sim}{x}_\perp = 0$)

$$E_z = -\frac{\pi}{b}\cdot\frac{6Q}{\pi a^2 L^3}\cdot 2\pi\int_o^a r'\,dr'\sum_n\frac{k_n Y_o(k_n b)\,J_o(k_n r')}{J_1(k_n b)} \times \begin{cases} \displaystyle\int_{-L/2}^{L/2} dz'\left[\frac{L^2}{4} - z'^2\right]e^{-k_n(z-z')} & \text{for } z \geq L/2 \\ \displaystyle\left[\int_{-L/2}^{z} dz'\left[\frac{L^2}{4} - z'^2\right]e^{-k_n(z-z')} - \int_{z}^{L/2} dz'\left[\frac{L^2}{4} - z'^2\right]e^{k_n(z-z')}\right] & \text{for } -L/2 \leq z \leq L/2 \\ \displaystyle -\int_{-L/2}^{L/2} dz'\left[\frac{L^2}{4} - z'^2\right]e^{k_n(z-z')} & \text{for } z \leq -L/2. \end{cases} \tag{8}$$

Solving the integrations and transforming back to the laboratory frame coordinates we obtain

$$E_z = \frac{12\pi Q}{ab\gamma^2 L^2} \sum_n \frac{Y_o(k_n b)\, J_1(k_n a)}{k_n^2\, J_1(k_n b)} \cdot f(z) \qquad (9)$$

where

$$f(z) = \begin{cases} \left(1-\frac{2}{k_n\gamma L}\right)e^{-k_n\gamma(z-L/2)} + \left(1+\frac{2}{k_n\gamma L}\right)e^{-k_n\gamma(z+L/2)} & \text{for } z \geq L/2 \\ \frac{4z}{L} - \left(1+\frac{2}{k_n\gamma L}\right)\left(e^{k_n\gamma(z-L/2)} - e^{-k_n\gamma(z+L/2)}\right) & \text{for } -L/2 \leq z \leq L/2 \\ -\left(1+\frac{2}{k_n\gamma L}\right)e^{k_n\gamma(z-L/2)} - \left(1-\frac{2}{k_n\gamma L}\right)e^{k_n\gamma(z+L/2)} & \text{for } z \leq -L/2 \end{cases}$$

and with the k_n given by $J_o(k_n b) = 0$.

Picking another charge distribution

$$\rho_2 = \frac{12Q}{\pi a^4 L^3}(a^2-r^2)\left(\frac{L^2}{4} - z^2\right)$$

which is parabolic in both the r and z directions and carrying out the calculations as before we obtain that on axis:

$$E_z = \frac{48\pi Q}{a^3 b\gamma^2 L^2} \sum_n \left[\frac{2J_1(k_n a) - k_n a J_o(k_n a)}{k_n^4}\right] X$$

$$X \quad \frac{Y_o(k_n b)}{J_1(k_n b)} \cdot f(z) \qquad (10)$$

RESULTS

From Eq. (1) for $\lambda = \frac{6Q}{L^3}\left[\frac{L^2}{4} - z^2\right]$

$$E_z = \frac{120g}{\gamma^2 L^3} z \qquad (11)$$

with $g = 1+2\ \mathrm{Ln}.\left(\frac{b}{a}\right)$ for $\rho_1 = \frac{\lambda}{\pi a^2}$

and $g = \frac{3}{2} + 2\ \mathrm{Ln}.\left(\frac{b}{a}\right)$ for $\rho_2 = \frac{2\lambda}{\pi a^4}(a^2-r^2)$.

As an example consider a 50 TW, 100 KJ, 25 GeV Uranium beam. The length of the ion beam is L = 26 cms. Then taking a = 10 cms. and a charge state Z =5 for the Uranium beam, we plot E_z obtained from Eqs. (9) - (11) for b = 20 cms. in Figure V-F-9/1 and for b = 13 cms. in Figure V-F-9/2 and conclude that since the assumption $b \ll L$ is not satisfied the results obtained from Eq. (11) for E_z in the region away from the center are higher by a factor of 2-3. Figure V-F-9/3 is a plot for b = 20 cms. and L = 260 cms. Here the linear esults of Eq. (11) are pretty accurate except near the edge of the ion beam. Note also that because of the charge distribution of the beam the maximum value of E_z is not at the edge of the beam. A simpler example illustrates the point. For example--for a sphere of constant density $E_r = \frac{Qr}{R^3}$ for r ≤ R with E_r max. at r = R and of density $\rho = \frac{15Q}{8\pi R^5}(R^2-r^2)$, $E_r = \frac{5Qr}{2R^5}\left[R^2 - \frac{3}{5}r^2\right]$ for r ≤ R with E_r max. at $r = \frac{\sqrt{5}}{3}R$.

Finally, since analytical expressions for E_z are possible only for certain charge distributions of the beam and only on the axis of the beam numerical computation seems necessary. An interesting charge distribution under consideration is

$$\rho = \frac{8Q}{\pi^2 a^4 L^2}(a^2-r^2)\sqrt{\frac{L^2}{4} - z^2}$$

which corresponds to a uniformly populated ellipse in phase space[2] and for which Eq. (1) breaks down at the edges giving an infinite value for E_z there. Also using Eq. (6) we can make numerical estimates of $E_r(r,z)$ and compare it with the results obtained from the axially infinite beam case.

References

1. HIF Workshop--Brookhaven National Laboratory October 17-21, 1977
2. R. Chasman, Proceedings of 1968 Linear Accelerator Conference, May 20-24, 1968, Brookhaven National Laboratory, BNL 50120 (C-54)

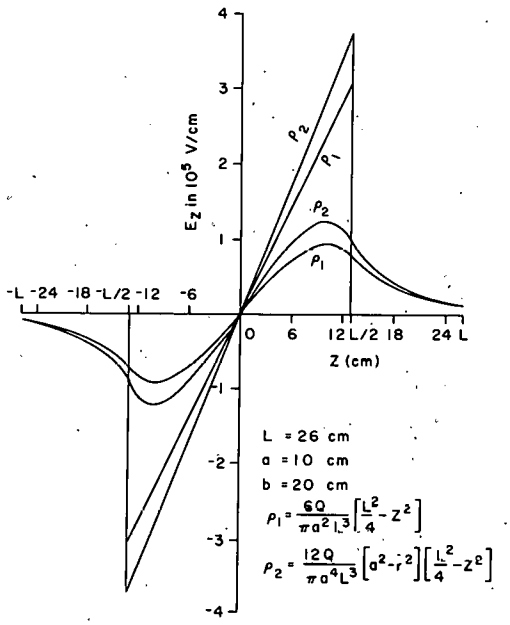

Fig. V-F-9/1. Plot of E_z vs Z for b/L = 10/13.

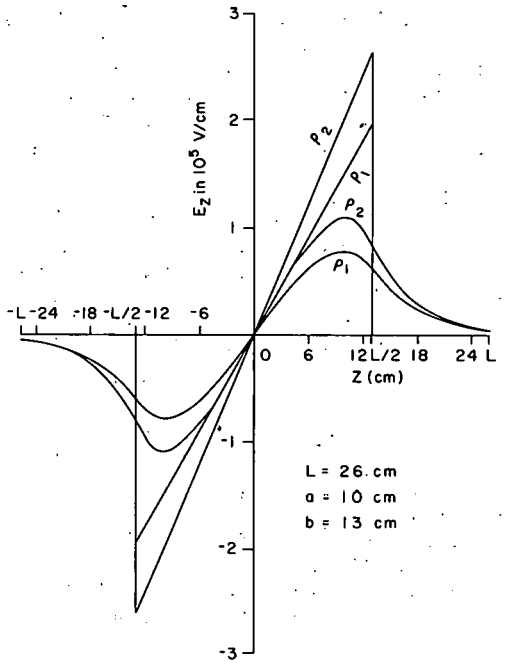

Fig. V-F-9/2. Plot of E_z vs Z for b/L = 1/2.

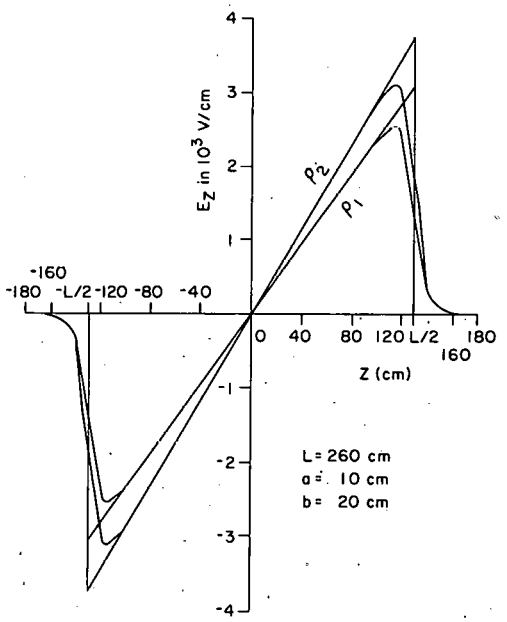

Fig. V-F-9/3. Plot of E_z vs Z for b/L = 1/13.

10. EMITTANCE GROWTH IN HIGH CURRENT BEAM TRANSPORT

Samuel Penner

INTRODUCTION

The possibility of using high-current beams of heavy ions to initiate an inertially-confined fusion reaction has stimulated interest in the acceleration and transport of very intense beams. The Kapchinsky-Vladimirsky (KV) envelope equations[1] provide a first guide to the current-carrying capability of a transport channel for the particular case of a beam whose charge distribution in the four-dimensional transverse phase space is such that all of its two-dimensional projections are uniform charge distributions within a boundary ellipse. The Berkeley group has studied the stability of the solutions to the KV envelope equations analytically by the method of linearization of the Vlasov equation about the KV solution coupled with appropriate perturbations.[2,3,4] The unrealistic beam distribution contained in the KV equations, the inability of the analytic approach to predict further beam development beyond the initial perturbation, and the need for a mechanism for studying a more general and realistic problem (including, for example, beam image forces, non-linearities in the focusing fields, energy spread in the beam, etc.), led us to the development of a numerical simulation approach to the high-current beam transport problem.

In our approach, we solve numerically the coupled equations for individual particle orbits within the beam, subject to external (focusing, accelerating, etc.) forces as well as the space charge forces generated by the beam itself. We report here our initial results for the transport of a high-current beam through a symmetric FODO quadrupole channel. We find (for sufficiently high currents) rapid initial growth of the emittance of the beam during which the beam transforms to a non-KV space charge density, followed by a much more gradual increase in emittance as the beam continues to propagate along the channel.

CALCULATIONAL METHOD

The equations of motion for individual particle orbits in the paraxial ray approximation can be written:

$$\frac{d^2x}{ds^2} = -K_x(s)\,x + \frac{Q}{2N}\int_{x'}\int_{y'} \frac{(x-x')n(x',y')dx'dy'}{(x-x')^2+(y-y')^2},$$

$$\frac{d^2y}{ds^2} = -K_y(s)\,y + \frac{Q}{2N}\int_{x'}\int_{y'} \frac{(y-y')n(x',y')dx'dy'}{(x-x')^2+(y-y')^2}. \qquad (1)$$

Our notation is the same as that of Lambertson, Laslett and Smith[5] (LLS), except that here

$$Q = \frac{4q^2Nr_p}{A\beta^2\gamma^3} \qquad (2)$$

is an (unnormalized) measure of the beam current. The charge density in the beam, n(x,y) is normalized such that

$$\int_x\int_y n(x,y)\,dx\,dy = N, \qquad (3)$$

where, as in LLS, N is the number of particles per unit length of the beam.

If the charge density n is chosen to be constant within a boundary ellipse with semi-axes a_x and a_y, and zero outside the ellipse, our Eq. (1) reduces to the KV individual particle equations of motion given by Eqs. (39) and (40) of Ref. 1.

We approximate Eqs. (1) with a finite set of equations:

$$\frac{d^2x_i}{ds^2} = -K_x(s)\,x_i + \frac{Q}{2M}\sum_{\substack{j=1\\ j\neq i}}^{M} \frac{x_i - x_j}{(x_i-x_j)^2+(y_i-y_j)^2} \qquad (4)$$

and similarly for y_i. We solve this set of equations numerically to obtain $x_i(s)$ and $y_i(s)$ for all particles i as a function of s, using a fast Adams method differential equation solver.[6] Two aspects of the numerical method require particular attention: The choice of initial conditions $x_i(o)$, $\frac{dx_i}{ds}(o)$, $y_i(o)$, $\frac{dy_i}{ds}(o)$, and the handling of the singularity in the space charge term of Eq. (4). A detailed discussion of these problems is beyond the scope of the present paper, but we briefly sketch our approach in the following paragraphs.

An initial set of orbits can be chosen from any desired distribution function by random sampling techniques. To date we have used the KV distribution as the sample function. All possible one and two dimensional projections of the sample set are compared with the corresponding projections of the KV distribution and are found to differ from it in a way which is completely consistent with the statistics of the sample size. This test and others convince us that the initial orbit distributions chosen represent the KV distribution with random noise superimposed. We do not impose any particular perturbation, as is done in the analytic work, but the randomness assures that our distributions contain components corresponding to all the perturbations examined.[2,3] By examining the beam behavior for several different randomly chosen initial orbit sets, we test the sensitivity of the results to the magnitude and character of the perturbations. Our small-sample results (M = 249) indicate considerable sensitivity to the

details of the perturbation.

The singularity of the space charge force is a well-known problem inherent in the simulation of a real particle beam by a relatively small number of representative orbits. We avoid the singularity by making the replacement

$$(x_i - x_j)^2 + (y_i - y_j)^2 \rightarrow r^2$$

in the denominator of Eq. (4) if $(x_i - x_j)^2 + (y_i - y_j)^2 < r^2$. The cutoff radius $r(s)$ is chosen to be

$$r^2 = a_x(s) \cdot a_y(s) \cdot C/M \ , \qquad (5)$$

where C is an adjustable cutoff parameter. We find experimentally that the transport calculation results are quite insensitive to the value of C (in the range $.1 \leq C < 10$ at least). The dependence on sample size M will be discussed later.

CHARACTERIZATION OF RESULTS

There is a problem of how to present the results of a transport calculation in a compact but meaningful way. Phase space plots of the individual orbits of the type presented to the workshop by I. Haber[7] are very informative but not immediately quantitative. A useful concept is the RMS emittance [8]

$$\bar{\epsilon}_x = 4(\langle x_i^2 \rangle \langle (\frac{dx_i}{ds})^2 \rangle - \langle x_i \frac{dx_i}{ds} \rangle^2)^{1/2} \ , \qquad (6)$$

and similarly for the y plane. Here the symbol $\langle\rangle$ indicates averaging over the values of the enclosed variable. For present purposes, we average the RMS emittance over the two transverse planes.

$$\bar{\epsilon} = (\bar{\epsilon}_x \, \bar{\epsilon}_y)^{1/2} . \qquad (7)$$

This measure of emittance is easily calculated numerically, and for a KV distribution is identical to the emittance defined by the beam envelope in phase space. For our randomly-generated initial orbit sets chosen from the KV distribution, the mean deviation of the sample $\bar{\epsilon}$ from the KV distribution was 0.3% for a group of samples each consisting of M = 249 orbits.

In our calculations of high-current transport through a symmetric FODO channel, we observe growth in all quantities which are obviously related to the beam quality, e.g., the envelope size $a_x(s)$, the emittance defined by the envelope of the beam in phase space (ϵ), and the RMS emittance $\bar{\epsilon}$, as defined above. The "noise" relative to the average growth of $a_x(s)$ is quite large, presumably because of our small sample sizes. The envelope emittance, ϵ, is also quite noisy in its growth, but defining this measure of emittance is ambiguous and awkward, even for large samples.

On the other hand, the RMS emittance growth shows much less noise than a_x or ϵ, even for quite small samples. In the limited number of cases we have examined, the fractional growth of $\bar{\epsilon}$ is larger than that of a_x and smaller than that of ϵ. This observation implies that the space charge distribution changes from a KV distribution ($\epsilon = \bar{\epsilon}$) to one with a more diffuse density in its exterior regions than at its center, and that most of the growth is in the momentum variable (i.e. $\frac{dx}{ds}$) rather than in the coordinate variable (x). These trends are illustrated in Figs. V-F-10/1a,b.

NUMERICAL EXAMPLES

Our program uses dimensioned variables. The examples we give here correspond to the transport of 100 GeV singly charged ^{238}U ions in a channel in which each quadrupole magnet and each intervening drift space is 5.076 meters long (p = 2 in the notation of Ref. 3). The magnetic field gradient in the quadrupoles is 2.381 kG/cm, and the initial (unnormalized) beam emittance is 0.95 cm mr. The phase shift per period of the structure is μ_o = 80.0 degrees (when Q = 0). These results can be scaled for other energies, ion types, charge states, etc., as shown in Ref. 5. The only free variable, once μ_o and p are specified is the parameter $Q' = Q/\epsilon K^{\frac{1}{2}}$, which measures the beam current. We report our results solely in terms of Q'. For each value of Q', the initial orbits are chosen corresponding to a matched input beam, as determined numerically with the KV envelope equations. We have made a number of approximations to speed up the calculation. These include

a. Forces due to image currents in the beam pipe are ignored.

b. The quadrupoles are idealized - they have no higher multipole components and their magnetic fields start and end abruptly.

c. The beam can be represented by a small number of orbits (usually 249), and a cutoff on the interparticle force can be used as discussed above.

Approximations a and b are not essential, and we can easily investigate their effects in future work. Computer time limitations do not permit a major increase in the number of orbits carried since computing time is very nearly proportional to M^2. This limitation can be circumvented by changing the method of calculating the space charge force, and will also be examined in future work.

As mentioned above, each random sample of the initial orbits represents a different perturbation about the KV distribution. In order to allow for different perturbations, we repeat the calculation for each value of Q' with several statistically independent samples. In Table V-F-10/1 we summarize our results for the percentage growth in $\bar{\epsilon}$ in the first period of the FODO structure. For comparison, we give numerical values for the beam envelope growth rate calculated by Laslett and Brady[4] from the theory of Refs. 2 and 3.

Table V-F-10/1. Emittance Growth in One Period[a]

	Percentage emittance growth[b]					
Q^1	1	2	3	4	5	Ref. 4 Results[c]
.31	0.0	0.2	-0.3	0.0	0.0	0.0
1.00	1.3	1.8	0.1	0.6	1.0	2.8
1.35	1.9	3.5	0.4	1.7	4.4	26.9
2.20	4.7	9.3	0.1	5.3	4.8	22.2 28.3
4.00	16.9	27.3	6.6	16.2	17.0	32.2 23.0
5.00	32.4	38.4	12.4	25.3	25.8	28.9 17.3 23.7

(a) Samples of 249 orbits.

(b) The various columns represent different samples. The initial orbits are basically the same in each column, but scaled to the proper matching conditions for each Q^1.

(c) Multiple entries for one Q^1 value represent growth rates for different initial perturbations.

CONCLUSIONS

Our calculations indicate beam emittance growth at high currents for space charge densities similar to the KV distribution, in qualitative agreement with the Berkeley work. (2,3,4) From Table V-F-10/1, it appears that growth rates of the instabilities may be significantly smaller than the Berkeley results, except perhaps at the highest current (Q^1 = 5.0) studied.

The initial rapid growth in emittance appears to damp out rapidly in the few examples studied, as illustrated by Fig. V-F-10/2 which also indicates that our qualitative conclusions are not strongly sensitive to the small size of the samples studied.

The need for further more detailed studies is clearly indicated. In particular, we plan to study the propagation of beams whose initial phase space density is more characteristic of physical particle beams than the KV distribution.

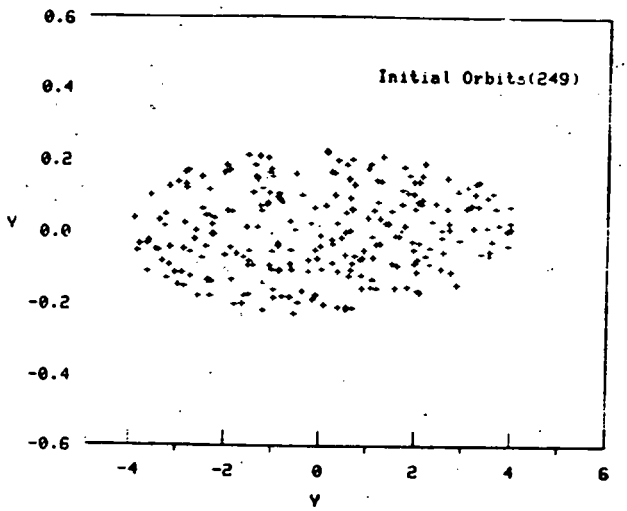

Fig. V-F-10/1a. Phase space distribution of initial orbits in y, y' phase space ($y' = \frac{dy}{ds}$ in the test).

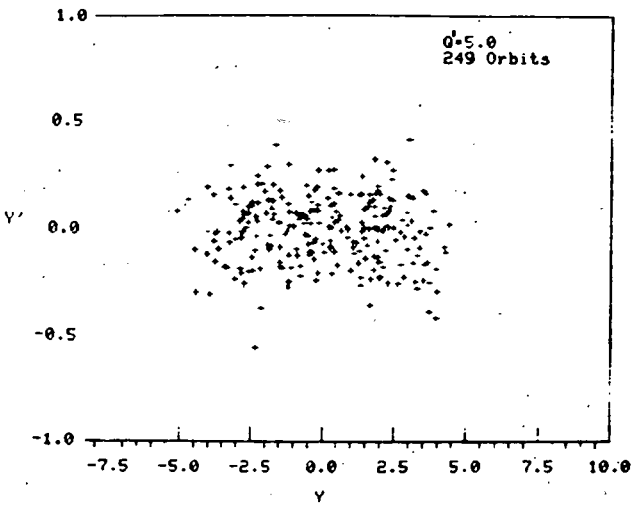

Fig. V-F-10/1b. Same orbits after propagation through 10 periods of the FODO structure, with Q^1 = 5.0. The beam size has increased by more than a factor of two. The RMS emittance in the y, y' plane has increased by 52%.

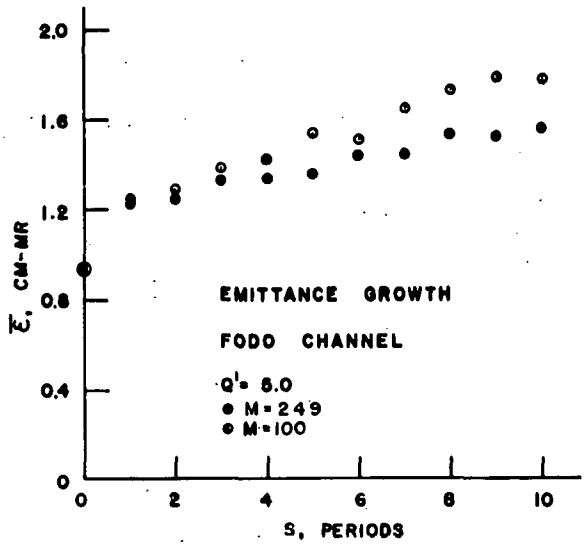

Fig. V-F-10/2. RMS emittance growth in a FODO channel with $Q^1 = 5.0$, comparing calculations with M = 100 orbits and M = 249 orbits.

References

1. I. M. Kapchinsky and V. V. Vladimirsky, Proc. Int. Conf. on High Energy Accelerators, CERN, p. 274 (1959).
2. "Stability of the K-V Distribution in Long Periodic Transport Systems - Part I: General Formulation," Lloyd Smith, HIFAN-13, Lawrence Berkeley Laboratory (Rough Draft 10/4/77).
3. "Stability of the K-V Distribution in Long Periodic Transport Systems, Part III--Computational Results," Inge Hofman and L. Jackson Laslett, HIFAN-15, Lawrence Berkeley Laboratory, October 12, 1977 (unpublished).
4. L. Jackson Laslett and V. O. Brady, private communication from L. J. Laslett (letter November 7, 1977).
5. G. R. Lambertson, L. J. Laslett, and L. Smith, IEEE Trans. on Nucl. Sci. NS-24, 993 (1977).
6. "Computer Solution of Ordinary Differential Equations: The Initial Value Problem," L. F. Shampine and M. K. Gordon, W. H. Freeman and Company, San Francisco, California (1975).
7. I. Haber, presentation to this workshop.
8. P. M. Lapostolle, IEEE Trans. Nucl. Sci. NS-18, No. 3, 1101 (1971) F. J. Sacherer, loc. cit. p. 1105. We wish to thank J. D. Lawson for pointing out these papers to us.

G. LONGITUDINAL BUNCHING

1. THE EFFECTS OF THE LONGITUDINAL SPACE CHARGE ON BUNCH COMPRESSION

T. K. Khoe

INTRODUCTION

Expressions are derived in this note for the voltages, times, and drift distances required for longitudinal bunch compression either in a single pass device followed by a drift space or in a ring.

Assuming a parabolic linear density distribution, the longitudinal space charge force on a particle at the end of a bunch is (S. I. units)

$$F_\ell = \frac{3\,N\,(q\,e)^2\,g}{8\pi\,\epsilon_o\,\gamma^2\,L^2} \qquad (1)$$

where N is the number of particles in the bunch, q is the charge state of the particle, 2L is the bunch length = $\beta\,c\,\Delta\,t$, and g is a geometrical factor. For a cylindrical bunch of radius a and length 2L ($L \gg a$), we find

$g = \ln \frac{4\,\gamma\,L}{a}$ with no vacuum chamber (free space)

$g = 1 + 2\,\ln \frac{b}{a}$ in a cylindrical vacuum chamber of radius $b << L$

$g = 1 + 2\,\ln \frac{2h}{\pi a}$ halfway between two parallel plates; distance between the plates $h << L$.

BUNCHING IN A STRAIGHT LINE

Defining a longitudinal beam emittance by the relation

$$\epsilon = L\,\frac{dL}{ds} = \frac{\beta\,c}{2\gamma^2}\,\Delta t_o \left(\frac{\Delta p}{p}\right)_o \qquad (2)$$

one can write the differential equation for the longitudinal beam envelope variation in the form

$$\frac{d^2 L}{ds^2} = \frac{\epsilon^2}{L^3} + \frac{3\,N\,q^2\,r_o\,g}{2\,A\,\gamma^5\,\beta^2\,L^2}\,, \qquad (3)$$

where

A is the atomic weight of the particle,

$r_o = \frac{e^2}{4\pi\,\epsilon_o\,m\,c^2} = 1.547 \times 10^{-18}$ m, and

mc^2 is the rest energy of a nucleon (931.5 MeV).

Multiplication of Eq. (3) by $\frac{dL}{ds}$ and integration gives

$$\left(\frac{dL}{ds}\right) - \left(\frac{dL}{ds}\right)_o^2 = \epsilon^2 \left(\frac{1}{L_o^2} - \frac{1}{L^2}\right) + 2\,Q^2\left(\frac{1}{L_o} - \frac{1}{L}\right) \qquad (4)$$

where

$$Q^2 = \frac{3\,N\,q^2\,r_o\,g}{2\,A\,\gamma^5\,\beta^2}\,. \qquad (5)$$

The bunch length has a minimum value when $\frac{dL}{ds} = 0$. Using the relation $L = \frac{1}{2}\beta\,c\,\Delta\,t$, this gives

$$\left(\frac{dL}{ds}\right)_o^2 + \left(\frac{2\,\epsilon}{\beta\,c\,\Delta\,t_o}\right)^2 \left\{1 - \left(\frac{\Delta t_o}{\Delta t_{min}}\right)^2\right\} + \frac{4Q^2}{\beta\,c\,\Delta t_o}\left(1 - \frac{\Delta t_o}{\Delta t_{min}}\right) = 0. \qquad (6)$$

Now

$$\left(\frac{dL}{ds}\right)_o = \left(\frac{\Delta\,\beta}{\beta}\right)_o \approx \frac{q\,e\,U}{\gamma\,(\gamma+1)\,T}\,, \qquad (7)$$

where U is the buncher voltage and T is the kinetic energy of the particle in the center of the bunch. Substituting Eq. (7) in Eq. (6) gives

$$\left(\frac{1}{\gamma(\gamma+1)}\,\frac{q\,e\,U}{T}\right)^2 = \left(\frac{2\,\epsilon}{\beta\,c\,\Delta t_{min}}\right)^2 \left[1 - \left(\frac{\Delta t_{min}}{\Delta t_o}\right)^2\right] + \frac{(2\,Q)^2}{\beta\,c\,\Delta t_{min}}\left(1 - \frac{\Delta t_{min}}{\Delta t_o}\right). \qquad (8)$$

Substituting equations (2) and (5) in equation (8) and solving for $\frac{eU}{T}$, we obtain the expression for the buncher voltage,

$$U = \left\{ \left[\frac{(\gamma+1)}{\gamma q} \left(\frac{\Delta p}{p}\right)_o \frac{\Delta t_o}{\Delta t_{min}} \right]^2 \left[1 - \left(\frac{\Delta t_{min}}{\Delta t_o}\right)^2 \right] \right.$$

$$\left. + \frac{6\, N\, r_o\, (\gamma+1)^2\, g}{A\, \gamma^3\, \beta^3\, c\, \Delta t_{min}} \left(1 - \frac{\Delta t_{min}}{\Delta t_o}\right) \right\}^{1/2} . \quad (9)$$

To find the drift distance one has to integrate Eq. (4). First this is written in the form

$$\frac{dL}{ds} = \frac{1}{L} \left[C\, L^2 - 2\, Q^2 - \epsilon^2 \right]^{1/2} ,$$

where

$$C \doteq \left(\frac{dL}{ds}\right)_o^2 + \frac{2\, Q^2}{L_o} + \left(\frac{\epsilon}{L_o}\right)^2 .$$

Performing the integration, we find

$$S = \frac{1}{C} \left\{ \left(\frac{dL}{ds}\right)_o L_o - \left[C\, L_{min}^2 - 2\, Q^2\, L_{min} - \epsilon^2 \right]^{1/2} \right. \quad (10)$$

$$\left. + \frac{Q^2}{\sqrt{C}}\, \ell n \frac{\sqrt{C} \left(\frac{dL}{ds}\right)_o L_o + C\, L_o - Q^2}{\sqrt{C} \left[C\, L_{min}^2 - 2\, Q^2 L_{min} - \epsilon^2 \right]^{1/2} + C\, L_{min} - Q^2} \right\} .$$

where $L_o = \frac{1}{2} \beta\, c\, \Delta t_o$ and $L_{min} = \frac{1}{2} \beta\, c\, \Delta t_{min}$. In the case that $L_o >> L_{min}$ we find, using equations (2), (5) and (8), that

$$S = \frac{\gamma\, (\gamma+1)\, T}{q\, eU} L_o . \quad (11)$$

The requirements are illustrated by the following example. Taking A = 238, q = 1, T = 150 GeV, γ = 1.6766, $\gamma\, \beta$ = 1.346, $\Delta t_{min} = 10^{-8}$ sec, $\Delta t_o = 2.9 \times 10^{-8}$ sec, $\left(\frac{\Delta p}{p}\right)_o = \frac{1}{\gamma\, \beta} \left(\frac{\Delta p}{mc}\right)_o = 1.56 \times 10^{-4}$, $N = 2 \times 10^{13}$ and g = 2, we find $\frac{eU}{T} = 1.2 \times 10^{-3}$, or U = 180 MV and S = 11,262 m.

BUNCHING IN A CIRCULAR COMPRESSOR

For bunching in a ring, the longitudianl emittance can be written in the form

$$\epsilon = \Delta\phi\, \frac{d\Delta\phi}{dt} = h\, \eta\, \omega\, \Delta\phi\, \frac{\Delta p}{p} , \quad (12)$$

where h is the harmonic number = number of bunches in the ring,

$$\eta \doteq \frac{1}{\gamma_t^2} - \frac{1}{\gamma^2} \approx \frac{1}{\nu_x^2} - \frac{1}{\gamma^2} \approx -\frac{1}{\gamma^2}$$

γ_t = transition energy

ν_x is the number of radial betatron oscillations per turn,

ω is the rotation frequency $\frac{\beta c}{R}$,

R is the mean radius of the compressor, and

$$\Delta\phi = \frac{h\, \beta\, c}{2\, R}\, \Delta t .$$

The differential equation for the longitudinal beam envelope becomes

$$\frac{d^2 \Delta\phi}{dt^2} + \Omega^2\, \Delta\phi - \frac{Q^2}{\Delta\phi^2} - \frac{\epsilon^2}{\Delta\phi^3} = 0 \quad (13)$$

where

$$\Omega^2 = \left(\frac{c}{R}\right)^2 \frac{h\, |\eta|\, q\, e\, U}{2\, \pi\, \gamma\, A\, m\, c^2} \quad (14)$$

$$Q^2 = \frac{3\, N\, q^2\, h^3\, |\eta|\, r_o\, c^2\, g}{2\, A\, \gamma^3\, R^3} \quad (15)$$

U = bunching voltage per turn

The definitions of the other quantities are the same as the preceding sections.

Initially $\Omega^2\, \Delta\phi - \frac{Q^2}{\Delta\phi^2} - \frac{\epsilon^2}{\Delta\phi^3} > 0$, and $\frac{d\Delta\phi}{dt}$ decreases. If $\left(\frac{d\Delta\phi}{dt}\right)_o \leq 0$, $\frac{d\Delta\phi}{dt}$ reaches its minimum value when $\Omega^2\, \Delta\phi - \frac{Q^2}{\Delta\phi^2} - \frac{\epsilon^2}{\Delta\phi^3} = 0$ and starts increasing since $\Delta\phi$ continues to decrease. One has $\Delta\phi = \Delta\phi_{min}$ when $\frac{d\Delta\phi}{dt} = 0$. On the other hand if $\left(\frac{d\Delta\phi}{dt}\right)_o > 0$, one has $\Delta\phi = \Delta\phi_{max}$ when $\frac{d\Delta\phi}{dt} = 0$ for the first time. From this point on, the bunch behaves as in the case of $\left(\frac{d\Delta\phi}{dt}\right)_o \leq 0$; and $\Delta\phi = \Delta\phi_{min}$ when $\frac{d\Delta\phi}{dt}$ is equal to zero again.

Multiplication of equation (13) by $\frac{d\Delta\phi}{dt}$ and integration give

$$\left(\frac{d\Delta\phi}{dt}\right)^2 - \left(\frac{d\Delta\phi}{dt}\right)_o^2 = \Omega^2 \left(\Delta\phi_o^2 - \Delta\phi^2\right) +$$

$$2\, Q^2 \left(\frac{1}{\Delta\phi_o} - \frac{1}{\Delta\phi}\right) + \epsilon^2 \left(\frac{1}{\Delta\phi_o^2} - \frac{1}{\Delta\phi^2}\right) . \quad (16)$$

To simplify the discussion, we assume that $\left(\frac{d\Delta\phi}{dt}\right)_o = 0$. In this case, we have

$$\Omega^2 \left(\Delta\phi_o^2 - \Delta\phi_{min}^2\right) = \frac{2\, Q^2}{\Delta\phi_o\, \Delta\phi_{min}} \left(\Delta\phi_o - \Delta\phi_{min}\right)$$

$$+ \left(\frac{\epsilon}{\Delta\phi_o\, \Delta\phi_{min}}\right)^2 \left(\Delta\phi_o^2 - \Delta\phi_{min}^2\right) .$$

ince $\Delta\phi_o - \Delta\phi_{min} \neq 0$, this equation can be reduced to

$$\Omega^2 \left(\Delta\phi_o + \Delta\phi_{min} \right) = \frac{2Q^2}{\Delta\phi_o \Delta\phi_{min}} + \left(\frac{\epsilon}{\Delta\phi_o \Delta\phi_{min}} \right)^2 \left(\Delta\phi_o + \Delta\phi_{min} \right) .$$

From Eqs. (11), (13) and (14), we derive

$$\frac{\epsilon U}{2\pi\gamma A m c^2} = \frac{3 N q h^2 r_o g}{A\gamma^3 R \Delta\phi_o \Delta\phi_{min}\left(\Delta\phi_o + \Delta\phi_{min}\right)} + \frac{h |\eta| \beta^2}{q \Delta\phi_{min}^2} \left(\frac{\Delta p}{p} \right)_o^2 . \quad (17)$$

To find the bunching time, we integrate equation (16). With $\left(\frac{d\Delta\phi}{dt}\right)_o = 0$, Eq. 16 may be written

$$\frac{d\Delta\phi}{dt} = \frac{\Omega}{\Delta\phi} \left[-(\Delta\phi)^4 + C(\Delta\phi)^2 - 2\left(\frac{Q}{\Omega}\right)^2 \Delta\phi - \left(\frac{\epsilon}{\Omega}\right)^2 \right]^{1/2} \quad (18)$$

where

$$C = \Delta\phi_o^2 + \frac{2}{\Delta\phi_o}\left(\frac{Q}{\Omega}\right)^2 + \left(\frac{\epsilon}{\Delta\phi_o \Omega}\right)^2 .$$

Integration of equation (18) gives

$$\Omega t_b = \frac{2\alpha_3 K(k)}{\left[\left(\alpha_1 - \alpha_3\right)\left(\alpha_2 - \alpha_4\right)\right]^{1/2}} + 2\left(\frac{\alpha_1 - \alpha_3}{\alpha_1 - \alpha_2}\right)^{1/2} \left[\left[E(k) - K(k) \right] F(\phi, k') + K(k)\, E(\phi, k') \right] \quad (19)$$

where α_1, α_2, α_3 and α_4 are the roots of the equation

$$\Delta\phi^4 - C\Delta\phi^2 + 2\left(\frac{Q}{\Omega}\right)^2 \Delta\phi + \left(\frac{\epsilon}{\Omega}\right)^2 = 0$$

and

$$\alpha_1 > \alpha_2 > \alpha_3 > \alpha_4$$

K (k), E (k), F (ϕ, k') and E (ϕ, k') are elliptic functions where

$$k^2 = \frac{\left(\alpha_1 - \alpha_2\right)\left(\alpha_3 - \alpha_4\right)}{\left(\alpha_1 - \alpha_3\right)\left(\alpha_2 - \alpha_4\right)}, \quad (k')^2 = 1 - k^2 , \quad \phi = \sin^{-1}\sqrt{\frac{\alpha_1 - \alpha_3}{\alpha_1 - \alpha_4}} .$$

For an example, we take

A = 238, γ = 1.6766, β = 0.803, q = 1, R = 318.3 m, $|\eta|$ = 0.35, h = 20, N = 2×10^{13}, $\Delta\phi_{min}$ = 0.0784, $\Delta\phi_o$ = 0.224 and $\left(\frac{\Delta p}{p}\right)_o = 1.56 \times 10^{-4}$.

These give

$$\frac{\epsilon U}{2\pi\gamma A m c^2} = 3.916 \times 10^{-5} + 1.785 \times 10^{-5} = 5.7 \times 10^{-5}$$

or

$$U = 133 \text{ M V}$$

To calculate the bunching time, we have

$\alpha_1 = \Delta\phi_o = 0.224$, $\alpha_2 = \Delta\phi_{min} = 0.0784$, $\alpha_3 = -0.0195$, $\alpha_4 = -0.283$, $k^2 = 0.436$, $\sin^{-1} k = 41.3^o$, $\sin^{-1} k' = 48.7^o$, $\phi = 43.9^o$, $\Omega = 1.88 \times 10^4$, K (k) = 1.803, E (k) = 1.382, F (ϕ, k') = 0.81 and E (ϕ, k') = 0.727.

These give

$\Omega t_b = 2.2$ or $t_b = 117\ \mu$ sec ($\approx$14 turns).

2. BEAM BUNCHING IN A FINAL STORAGE RING

Glen R. Lambertson

In this note, we consider the possibility of carrying out the final bunching of a particle beam for heavy ion fusion in a storage ring or synchrotron using parameteres as follows:

Total kinetic energy	Q = 1 Megajoule
Kinetic energy per particle	= 35 GeV
Burst duration on target	Δt = 6 nanosec(a)
Particle mass (Bismuth)	$Am_p = 209\ M_p$ = 196 GeV/c^2
Particle charge	qe = 1 e
Ring radius	R = 400 meters

From these we calculate for later use

$\beta = v/c = 0.529$

$\gamma = (1-\beta^2)^{-1/2} = 1.18$

$N = 1.78 \times 10^{14}$ total particles

For the bunching calculation, we shall use the approach of D. Judd[1] in which the length L of a beam particles acted on by an electric field with linear gradient $dE/d\ell = 2E_{max}/L$ evolves according to the equation [MKSA units]

$$\frac{d^2L}{dt^2} + \frac{2qe}{Am_p\gamma^3}\left[E_{max} - \frac{6gqeN}{(4\pi\epsilon_o)\gamma^2L^2}\right] - \left(\frac{4c\epsilon_\ell}{\gamma^3}\right)^2\frac{1}{L^3} = 0 \qquad (1)$$

where the geometrical factor $g \approx 1.5$,

$$\frac{1}{4\pi\epsilon_o} = 9 \times 10^9 \text{ meter/farad},$$

and $\pi\epsilon_\ell$ = longitudinal emittance area in $(z,\Delta\beta\gamma)$ space. This equation may be adapted to motion in a ring under the action of a sinusoidal voltage V sin hθ per turn with N/h particles per bunch by setting

$$E_{max} = \frac{hVL}{4\pi R^2}, \text{ (with } \frac{2hL}{\pi R} < 1 \text{ for linearity)},$$

and replacing γ^{-3} by $(-\eta/\gamma)=(\gamma^{-2} - \gamma_{tr}^{-2})\gamma^{-1}$;

N by N/h, and ϵ_ℓ by ϵ_ℓ/h.

Following Judd's definition of dimensionless variable, the equation becomes

$$\frac{d^2\rho}{d\tau^2} + \frac{1}{2}(\rho - P\rho^{-2} - \frac{1}{2}S\rho^{-3}) = 0 \qquad (2)$$

in which

$\rho = L/L_o$

$\tau = t/T$

L_o = L at t = o

$$P = \frac{6\ gq\ eN\ 4\pi R^2}{(4\pi\epsilon_o)\gamma^2h^2V\ L_o^3}$$

$$S = \frac{16\ Am_pc^2(-\eta)\epsilon_\ell^2 4\pi R^2}{qe\gamma h^3\ V\ L_o^4}$$

$$T^2 = \frac{Am_p\gamma\ 4\pi R^2}{4qe(-\eta)hV}$$

For our case, assume S << P to allow dropping the emittance term and let $d\rho/d\tau = 0$ at T = 0. A first integral is then

$$\left(\frac{d\rho}{d\tau}\right)^2 = (1-\rho)\left(\frac{1+\rho}{2} - \frac{P}{\rho}\right). \qquad (3)$$

If most of the bunching takes place while circulating in the ring and a large compression is obtained, as needed, then P << 1 and the final minimum bunch length is approximately (as found by Judd)

$$\rho_{min} \approx 2P. \qquad (4)$$

From this result and the definitions of P and ρ we can calculate the voltage per turn, V, needed to produce a 6 nanosecond bunch of length

$$L_{min} = \beta c\Delta t = (0.529)(3\times10^8)(6\times10^{-9}) = 0.9525 \text{ meter}.$$

The beam must initially have a bunching factor B_f of about 1/4 to assure linearity of the bunching field used. This initial length is

$$L_o = \frac{2\pi RB_f}{h} \text{ with } B_f \simeq 1/4.$$

Substituting in Equation 4 we obtain

$$V = \frac{12\ g\ q\ e\ N}{(4\pi\epsilon_o)\gamma^2L_{min}\ \pi(B_f)^2}$$

$$= \frac{(12)(1.5)(1.6\times10^{-19})(1.783\times10^{14})(9\times10^9)}{(1.39)(0.9525)\ \pi(1/16)}$$

$$= 17.78 \text{ MV/turn}.$$

To supply this bunching voltage with r.f. cavities, assume that 20% of the circumference can be filled with cavities that could provide an average voltage gradient at frequency f of $50(f/10^6)^{\frac{1}{2}}$ kV/m. In a full turn, then, bunching voltage would be

(a) Beam power during the six nanosecond portion of the pulse should be 100 terawatts. The use here of 1 magajoule, or 170 terawatts may be regarded as an over-specification affording some degree of safety factor.

$$V = (0.2)(2\pi R)(5\times10^4)(h\beta c/2\pi R\ 10^6)^{\frac{1}{2}}$$

$$= 6.31\ h^{1/2}\ \text{MV turn}$$

In this case, h = 8 would be needed to give 17.85 MV/turn at a frequency of 0.505 MHz.

Before adopting a harmonic number, we must examine the transverse space charge conditions during the bunching in the ring. We shall propose that some final bunching shall occur after leaving the ring in $\pi 200 = 628$ meters of transport to the target. While still in the ring, one could hope to bunch to the point where the space charge fields shift ν^2 to one-half its normal value, i.e. $\Delta\nu^2/\nu^2 = -0.5$. This limit, if permissible, would allow a maximum bunching factor while in the ring given by:*

$$\frac{1}{B_f} \approx \pi(\pi\beta\gamma\epsilon)\frac{A\beta\gamma^2\nu}{q^2Nr_p}\frac{\Delta\nu^2}{\nu^2} \qquad (5)$$

Use $\beta\gamma\epsilon = 10^{-5}$ radian meters emittance

$\nu \approx 10$

$r_p = 1.53 \times 10^{-18}$ meter

Then $\frac{1}{B_f} = \pi 10^{-5}\frac{(209)(0.529)(1.39)(10)}{(1.78\times10^{14})(1.53\times10^{-18})(2)}$

$= 88.64$

(For comparison, the value for $\Delta\nu = 1/4$ is $1/B_f = 8.86$, smaller by just the factor $\nu = 10$). At the target we must have a final bunching that would correspond to

$$\frac{1}{B_f} = \frac{2\pi R}{hL_{min}} = \frac{800\ \pi}{0.9525\ h} = \frac{2639}{h}$$

A detailed and correct treatment of the bunching process will not be attempted here, but it will be useful to note that over the major part of the process in the ring, the bunch length is given by the approximate integral of equation (3)

$$\rho \approx \cos\tau/\sqrt{2} \qquad (6)$$

This expression gives the approximate bunching time as $\tau \simeq 2.22$ T. An evaluation of T gives

$$T = \frac{317}{h} \times 10^{-6}\ \text{sec.}$$

Hence the bunching time is about

$$t = (2.22)\frac{317}{h} \times 10^{-6} = \frac{704}{h}\ \text{microseconds.}$$

In terms of turns in the ring this is

$$\frac{\beta ct}{800\pi} = \frac{44.47}{h}\ \text{turns.}$$

A drift distance to the target equal to one quarter turn occurs outside the ring and we may ask what value of h would permit the bunching to be less than 88.6 at extraction. Using the approximate equation (6), we find that the harmonic number must be greater that 5.1. The correct bunching formula will require a larger number, so the space charge condition as well as the need to raise the r.f. cavity frequency indicate a value of $h \simeq 8$, which we shall adopt.

The parameters of the bunching process are then:

h = 8, frequency = 0.5053 MHz

V = 17.85 MV/turn, e.g. 503 m (20% of circumference) of cavities at 35.5 kV/m

Bunching at start = 4.0

at extraction = 56.6

at target = 329.9

Bunching period in ring = 5.53 turns

Distance to target = 0.25 turn = 628 meters

The foregoing has explored only bunching by r.f. cavities in the ring. Stronger fields could be generated by pulsed cavities, but no examination of the use of pulsed cavities in a storage ring has been made. Pulsed cavities could, of course, be used in the external transport lines to augment and complete the bunching initiated in a ring.

Reference

1. D. Judd, paper IV-C-3 in this publication.

* This formula neglects the substantial change in ν when $\Delta\nu^2$ is large. Hence it underestimates the allowed limit by a factor $\left(1 + \frac{\Delta\nu^2}{\nu_o^2}\right)^{-1/2} = (1-0.5)^{-1/2} = \sqrt{2}$. Alternatively, one could say that the numerical results above corresponds more correctly to a change of ν from 10 to 7.81.

H. VACUUM CONSIDERATIONS

1. SUMMARY

D. Blechschmidt and H. J. Halama

INTRODUCTION

The vacuum system for Heavy Ion Fusion machines can be divided according to pressure into 4 parts:

a) Ion Sources
b) Linear Accelerators
c) Circular Accelerators, Accumulators and Storage Rings
d) Reactors

Since ion sources will need rather conventional pumping arrangements and reactors will operate with greater pressures, depending on their mode of operation, only items b and c will be treated in this report. In particular, the vacuum system design will be suggested for the machines proposed by various scenarios arrived at during the workshop. High mass numbers will be assumed.

From the vacuum point of view, the selection between the linear and circular machines will be determined by the beam loss and hence by the magnitude of cross sections for various beam-beam and gas-beam interactions. Since these cross sections are known to within an order of magnitude, the vacuum design is accordingly only approximate Very high cross sections at small ion velocities will, however, impose a lower limit on the operating energy of circular machines, i.e. E > 1 GeV. Higher charge state (electrons in first shell completely stripped) should be favored.

Since, in linear accelerators the ions travel in straight lines, these machines have a significant advantage over circular machines.

CROSS SECTIONS AND LIFETIMES

The lifetime and quality of an ion beam is governed by the interactions of ions with the residual gas and with each other. To date the relevant cross sections are not well known. Only a few experimental results exist and theoretical data are not abundant. Nevertheless the assessment of vacuum requirements is based on the knowledge of these cross sections. Predictions of beam lifetimes for a given vacuum system to better than one order of magnitude are practically impossible under present conditions

We have therefore attempted to set up some useful and simple relations allowing a reasonable guess of cross sections for vacuum purposes. They have been established from experimental[1][2] and theoretical [1] [3-6] results. Besides the above references the discussions with Y. K. Kim during the course of the workshop were very useful. To a theoretician they might look like a brute force approach, yet they give figures which rarely differ from cross sections published elsewhere by more than a factor of ten.

a) Multiple Scattering

Multiple scattering leads to emittance blow-up. This is usually more deleterious than the subsequent particle loss to the vacuum chamber, in particular if the chamber diameter is large compared to the rms beam size: the beam loss rate may be small and the pressure rise due to wall desorption not excessive, but the beam size might grow to beyond a tolerable limit.

The time during which the rms amplitude of the beam in nitrogen gas grows from zero to $\hat{x}^2$ (cm^2) is given by [7]

$$\tau_{MS} = \frac{4\,\hat{x}^2\,E^2}{\langle\beta\rangle^2\,pq^2} \quad \text{sec.}$$

The ion energy and charge state are denoted by E(GeV) and q, the structure function is given in cm and the residual gas pressure in Torr N_2 - equivalent. The blow-up rise time is proportional to the square of the residual gas atomic number, i.e. $\propto Z_T^2$.

b) Nuclear Scattering

Ions involved in a scattering event are immediately lost from the beam, either by being scattered into a large angle or by losing a large fraction of their kinetic energy. There is, for nuclear scattering, an energy threshold (which can be derived from $\lambda_{ion} \leq$ target nucleus) of the order of a few MeV/amu. Beyond the threshold, cross sections vary strongly over the energy range and can be considerably higher. For relativistic ions the cross section in nitrogen gas is approximately

$$\sigma_{NS} \approx 4 \times 10^{-25}\, A^{2/3}\, \beta^{-2}\ cm^2$$

where A denotes the ion mass number. The nuclear scattering cross section scales approximately with $A_T^{2/3}$ where the target mass number is A_T.

The beam lifetime τ is then obtained from the relation $\tau\beta c\sigma n = 1$, with n = number of gas nuclei/cm^3, hence

$$\tau_{NS} \approx 1 \times 10^{-3} \frac{\beta}{A^{2/3} p} \text{ sec}$$

for nitrogen.

c) Residual Gas Ionization

Ionization of the residual gas does not directly lead to beam loss because of the small energy loss involved. However, the electrons produced in these events tend to accumulate in the positive space charge of a dc beam and hence may lead to destructive plasma resonances. In bunched beams they give rise to multipactoring or similar effects since under certain conditions they can never escape to the wall before they are pulled back by the next bunch. An effective clearing system must, therefore, be provided. A second, even more dangerous mechanism is the bombardment of the vacuum pipe wall by positive ions created and accelerated by the beam. These ions are highly efficient in desorbing gas from the wall, enhancing the ion production rate further and eventually leading to vacuum breakdown (pressure bump) as observed at the CERN-ISR.

Theoretical cross sections are available and can be used to extrapolate from low-energy data. For protons up to 28 GeV the agreement is very good. For nitrogen we have very approximately (8)

$$\sigma_I \simeq 8 \times 10^{-19} \beta^{-2} Z^{2/3} \text{ cm}^2.$$

The cross section varies about with $Z_T^{2/3}$ where Z_T is the target atomic number. Hence the ion production rate

$$1/\tau_I = 1 \times 10^{9} p Z^{2/3} \beta^{-1} \text{ sec}^{-1}.$$

For U^{1+} for example at 1 GeV and at a pressure of 10^{-11} Torr, $1/\tau = 2$ sec^{-1} which is as serious as operating the CERN-ISR at 2×10^{-9} Torr. Assuming a maximum acceptable momentum spread of $\Delta P/P = 10^{-4}$ and an average energy loss of 10 eV per ionization the beam lifetim is $\simeq 1\frac{1}{2}$ hours.

d) Charge exchange with the residual gas

This is from the vacuum point of view the most serious limitation to beam lifetime. In a guiding field the change in the ions' charge state entails its immediate loss from the beam and consequent bombardment of the beam chamber. Little is known about the effect of such a high energy bombardment except that most of the energy is transferred to the bulk of the chamber material where it enhances the outgassing rate(9). The surface desorption yield may not be much larger than that caused by the ions accelerated in the beam space charge field (11). The increase in bulk outgassing may be considerable and it is doubtful whether the vacuum can be kept stable over a sufficiently long time. Other problems are induced radioactivity, metal sputtering and ablation of the chamber material.

Stripping and capture cross sections are not well known. A review of experimental data is given by Betz(1), together with some semi-empirical formulae. More recent theoretical investigations have given additional information (4) but experimental results are scarce.

The available data can be obtained using "brute force" relation for the stripping cross section for nitrogen gas

$$\sigma_S \simeq 9 \times 10^{-19} q^{-2/5} \beta^{-2} \text{ cm}^2,$$

and for capture cross section

$$\sigma_C \simeq 3 \times 10^{-28} q^{5/2} \beta^{-7} \text{ cm}^2.$$

The formulae have been checked with both experimental and theoretical results and were found to agree to within roughly one order of magnitude for $\beta > 0.01$, $q < 30$.

The corresponding lifetimes are

$$\tau_S \simeq 6 \times 10^{-10} \beta q^{2/5} p^{-1} \text{ sec}$$

and

$$\tau_C \simeq 2\beta^6 q^{-5/2} p^{-1} \text{ sec}.$$

e) Intra-beam charge exchange

This process is not directly a vacuum problem, since the beam loss is not influenced by background pressure. However, its occurrence very seriously affects vacuum performance due to the wall bombardment by the high energy ions lost from the beam and hence reduces the beam lifetime via the other mechanisms. The corresponding cross section is relevant in the low energy range, typically at a few keV/amu is almost geometrical and can be estimated from

$$\sigma_E \approx \frac{8\pi}{3} a_o^2 \frac{n^2}{Z} = 2 \times 10^{-16} \frac{n^2}{Z} \text{ cm}^2$$

where n is the number of the outermost shell occupied by an electron. The beam lifetime using the relations of Barton or Mills (10) is then

$$\tau_E \simeq 4\left(\frac{qe}{I}\right) \frac{\sqrt{\langle\beta\rangle^3}\,\varepsilon}{\sigma\gamma} \approx 3 \times 10^{-3} \frac{qZ\sqrt{\langle\beta\rangle^3}\,\varepsilon}{I\gamma n^2} \text{ sec}.$$

LINEAR ACCELERATORS

Even though various types of linacs could provide the total acceleration required for heavy ion fusion, they are most essential at low energies. The reason is that ions lost from the beam do not end up on the walls of linear accelerators as they do in circular machines. These losses can be quite substantial as various cross-sections for ion-ion and ion-residual gas interactions are very high especially at low energies. For the design of vacuum systems we will, therefore, consider the energy range from 1 MeV to 1 GeV which corresponds to U^+ beta from 3×10^{-3} to 0.1. At higher energies and higher charge states the cross-sections get smaller which results in a smaller loss.

It is obvious from the previous chapter (d) that the loss of ions having low velocity is determined mainly by stripping at low charge state and by electron capture at high charge state. The pressure independent loss due to charge exchange, will be influenced by ion density and other characteristics of the bunched beam and is, therefore, the hardest to estimate. It has to be added to the loss computed below, but its magnitude will be small in the linacs under consideration.

Let us set a limit on the permissible ion loss inside the linacs $\frac{n}{B} = 1\%$ and calculate the required pressure. The charge exchange might make this loss slightly higher, but since the cross-sections are only known within an order of magnitude, large uncertainties are to be expected in the numbers obtained. This fact makes the cross-section measurements mandatory before a realistic vacuum system can be designed or priced. For a 1% loss:

$$\frac{n}{B} = 10^{-2} = 3.3 \times 10^{16} \; L \; P \; \sigma,$$

where L is the length of the machine in cm, P is the pressure in Torr and σ is the cross-section in cm^2.

If we take $\sigma = 3 \times 10^{-15}$ cm^2 (Ref. 12) and L = 200 m,

$$P = 5 \times 10^{-9} \text{ Torr.}$$

Assuming realistic apertures in the drift tubes, the ions which slip out of phase with the rest of the beam will most likely pass through the length of 200 m without hitting the drift tubes. Their effect on blow-up, etc. should, however, be studied. At the end of a 200 m long section, the unwanted ions can be removed by using 3 bending magnets and a slit. To achieve an operating pressure of $< 1 \times 10^{-8}$ Torr will require that only metals and ceramics be used inside the tanks.

A possiblity of a minimum in situ bake-out of 130° C should be provided when designing rf structures. Since the final pressure in this range is determined mainly by the surface phase, rather than the bulk condition of the materials used, aluminum, copper and stainless steel would be good. Aluminum should be sputtered with titanium nitrate to avoid multipactoring.[13] Sputter ion, titanium sublimation and cryopumping with large capacity would be suitable.

Assuming linac tanks of 1 m diameter, the required pumping speed $S = \frac{AQ}{P}$. A = total area and Q = outgassing rate. For a 10 m long tank, P = 3×10^{-9} Torr and Q = 1×10^{-11} T ℓ/s cm^2,

$$S \approx 1000 \; \ell/s \; .$$

The outgassing is likely to increase during the rf operation due to beam loss and possible multipactoring. However, a pump with a pumping speed of 1000 to 3000 ℓ/s should be adequate, for each 10 m long tank.

CIRCULAR MACHINES

Three scenarios have been presented at this workshop, one by the Low-β Linac, one by the Induction Linac and one by the Synchrotron working group. The data relevant to vacuum design are compiled and compared with ISR figures in Table I, assuming P = 10^{-10} Torr.

a) Average Static Pressure

The table shows that all scenarios seem feasible from the vacuum point of view, if it is possible to maintain a pressure of 10^{-10} Torr at maximum energy deposition by the ions lost from the beam. Even though this could be as high as 140 W/m, it is not unreasonable to believe that 10^{-10} Torr <u>static</u> pressure can be maintained, if sufficient cooling is provided. The average pressure is

$$\langle P \rangle \simeq P_o + 50 \; Q \; (L/r)^2 \text{ Torr}$$

with the outgassing rates Q (Torr ℓ/s cm^2), the distance between lumped pumps L (m) and the circular beam pipe aperture radius r (cm). Assuming $P_o = 3.10^{-12}$ Torr, Q = 2×10^{-11} Torr ℓ/s cm^2 would be needed which seems possible under the given conditions.

b) Vacuum stability

The pressure rises exponentially when a bunch passes along the beam pipe, if the net number of gas molecules desorbed by ions generated from the residual gas is greater than unity or if particles are lost from the beam. The number of particles lost from the beam per unit length of vacuum pipe and per unit time is

$$N_B = \frac{I}{e\beta c \tau_{tot}}$$

whereas the number of low energy ions bombarding the wall is

$$N_I = \frac{I}{c\beta c \tau_I}$$

Table

Scenario	Low-β Linac				Induction Linac	Synchrotron	IRS
Type of Ring	Accumulator				Accumulator	Synchrotron	Storage ring
Energy (GeV)	7.4	20	20	2.2	1	2 → 35	26
Beam Current (A)	4			1	20	2	40
Ion	Xe^{+3}	Hg^{+1}	Hg^{+3}	Xe^{+3}	U^{+1}	Hg^{+1}	H^{+1}
β = v/c	0.34	0.46		0.19	0.093	0.14 → 0.6	1
Ring radius (m)	50	300	100	50	20	400	160
Vacuum aperture r (cm)	6 [a]				6	6 [a]	4.3
Emittances (πcmmrad)	0.2				2	3	3
<β> (m) [a]	20				20	20	20
pump distance (m) [a]	2				2	2	2.4
1 mm - blow-up time (min)	600	700	70	0.9	1.7	> 7	1100
Nucl. Scatt. lifetime (min)	2200			1200	400	> 700	1.6×10^5
Gas-ion Production rate (sec^{-1})	40	4	35	65	22	13	0.1
Stripping lifetime (sec)	3	3	4	2	0.6	> 0.8	-
Capture lifetime (hours)	550	∞	3400	17	3½	41	∞
Charge-exchange lifetime (s)	10	4	12	43	2	30	-
Total lifetime (sec) [b]	2.3	1.7	2.9	1.9	0.5	> 0.8	1×10^6
Accumulation time (ms)	320	1.3	16	110	0.35 - 5	15 [c]	10^8
$Q/\eta(10^{-7}$ Torr ℓ/sm)	3	0.2	2	2	30	1.2	0.02

[a] assumed values

[b] $\tau_{tot} = \left[\Sigma 1/\tau_i \right]^{-1}$ without gas-ion production

[c] assuming ΔE/turn = 50 MeV.

The beam induced outgassing "switched on" by the bunch is therefore

$$Q = \eta(N_B + N_I) = 6 \times 10^{-10}\, \eta \frac{I}{B}\left[\frac{1}{\tau_{tot}} + \frac{1}{\tau_I}\right] \text{Torr } \ell/\text{sm},$$

assuming a global desorption yield η(mol/ion). Vacuum stability is only possible if sufficient pumping speed is provided by distributed or lumped pumps, i.e. if

$$Q < \left(S_{lin} + \frac{C\pi^2}{2} \right) P$$

where C is the beam pipe conductance per unit length. It is realistic to assume a lumped pump system $C\pi^2/L^2 \simeq 500$ ℓ/sm and $S_{lin} \simeq 1000$ ℓ/sm, hence $Q_{max} = 1.5 \times 10^{-7}$ Torr ℓ/sm to maintain vacuum stability. The Q-values expected are given in Table I.

For the machines where the accumulation time is short compared to the repetition time, it may be possible to let the vacuum break down and to wait for recovery after the bunch has been ejected. The pressure rise time, which must be long compared with the accumulation time, is

$$\tau = F/\left[\frac{Q}{P} - \left(S_{lin} + \frac{C\pi^2}{L^2}\right)\right]$$

with F being the beam pipe cross-section. With a rise time of about 1 s, i.e. larger than the accumulation time, and

$$S_{lin} + \frac{C\pi^2}{L^2} = 1500 \text{ } \ell/\text{sm} \quad (15000 \text{ cm}^2/\text{s})$$

$$Q_{max} < 10^{-6} \text{ Torr } \ell/\text{sm}$$

could be possibly tolerated.

It seems that vacuum stability could be achieved in all scenarios except for one of the three accumulators in Induction Linac group, provided $\eta < 1$ can be maintained.

CONCLUSIONS

1. The inadequate knowledge of cross-sections prevents us from making a more concrete vacuum system design. Experiments leading to trustworthy numbers for charge exchange, stripping and capture cross-sections are badly needed and should start as soon as possible.

2. In linacs, beam loss will be almost directly proportional to the pressure inside the tanks. The tanks should, therefore, be built in such a way that they can be baked-out in situ to improve their vacuum, especially if the cross-sections turn out to be higher than anticipated. Using standard UHV techniques and existing pumps, an even lower pressure than arrived at in this report can be achieved.

3. The vacuum system design for circular machines will be very difficult, and in some cases, beyond the present state-of-the-art. Investigations in the following areas should be started as soon as possible.

a) Strong linear pumping
b) Desorption and sputtering coefficients of high energy, heavy ions when bombarding metals.
c) Radiation damage and other changes in the properties of vacuum chamber materials

The ions should stay in the ring for short times only and their energy should be high.

References

1. H. D. Betz, Rev. Mod. Phys. 44, 465 (1972).
2. F. F. Rieke and W. Prepejchal, ANL Intern. Phy. Rev. Q, Vol. 6, p. 1507.
3. M, Inokuti, Y. K. Kim and R. L. Platzman, Phys. Rev., 164, 55 (1967).
4. G. H. Gillespie, Y. K. Kim and K. T. Cheng, paper submitted to Phys. Rev. A., ( ).
5. G. L. Saksagansky, I. A. Shukeilo and T. S. Dimitriev, Proceedings of the 7th Int. Vac. Congress, Vienna, 1977, p. A-2679.
6. B. Rossi. H. E. Particles, Prentice Hall (1952).
7. E. Fischer, CERN Internal, Rep., ISR-VAC/67-16 (1967).
8. Y. K. Kim, ERDA Summer Study of Heavy Ions for Fusion, LBL-5543 (1976), p. 11, and references given therein.
9. R. Dobrozemsky, J. Vac. Sci. Technol., 13, 467 (1976).
10. M. Q. Barton, ERDA Summer Study of Heavy Ions for Fusion, LBL-5543 (1976), p. 18.
11. McCracken, Rep. Prog. Phys. 38, 241, (1975).
12. Y. K. Kim, private communication in form of a letter.
13. E. W. Hoyt and W. P. Schulz, SLAC Report, SLAC-TN-75-3 (1975).

I. SYSTEMS/COST

1. SUMMARY

P. Grand, G. Danby, J. Keane, J. Spiro, D. Sutter, F. Cole, E. Hoyer, K. Freytag, and R. Burke

INTRODUCTION

The purpose of the meeting was to discuss and develop cost-estimating methods for heavy-ion fusion accelerator systems. The group did not consider that its purpose was to make technical judgements on proposed systems, but to develop methods for making reasonable cost estimates of these systems. Such estimates will, it is hoped, provide material for systems studies, will help in guiding research and development efforts by identifying "high-leverage" subsystems (areas that account for a significant part of total system cost and that might be reduced in cost by further technical development) and to begin to provide data to aid in an eventual decision on the optimum type of accelerator for heavy-ion fusion.

Prior to the meeting, Committee members had carried out work on cost estimates at their own laboratories, in some cases by scaling from recent construction and in others by detailed itemization of components. A number of accelerator examples were provided for this work by the Chairman. At the meeting, the results were combined to derive unit costs for several different types of accelerator systems. This report gives the results of these considerations.

The systems considered as examples are:

1.	Injection System	2 MV
2.	Wideröe linac	2 MV to 1 GeV
3.	Alvarez linac	1 to 20 GeV
4.	Induction linac	1 to 20 CeV
5.	Superconducting accumulator ring	1 GeV
6.	Synchrotron	1 to 35 GeV
7.	Final rf bunching	
8.	Final beam transport to target	

These systems all accelerate ions of A = 200^{1+}.

COSTING GROUND RULES

For the exercise the following constraints were assumed:

Costs are in 1977 $ only.

2. It is assumed that previous R&D effort has solved all the problems.
3. These costs make no provision for costs of real estate, site preparation, long-distance water and power procurement, or costs of EDIA (engineering, design, inspection and administration). Site development costs will be included in building and installation costs will be included in components.
4. To make things easier for further reference, the total cost are broken down into obvious packages such as: Accelerator structure, rf power, magnets and vacuum system (for circular machines), tunnels, service buildings, etc.
5. The costs are also being prepared so as to make it convenient to change system parameters, therefore, one should be able to derive a cost per meter of machine, or MW of rf power, etc. This should allow cost extrapolation for different systems.
6. It is obviously impossible to cover all the options talked about during the workshop. The concepts described for costing are all based on A ≃ 200^{1+}. Although some may argue that other masses and charge states should be considered, it is quite clear that if we have good unit costs, the machine parameters can be changed and the costs adjusted readily to reflect the changes. So at this point in time for the sake of simplicity, we stick to the case of singly charged ion.
7. In order to provide a common basis for the approach to cost estimating, we assume that we are building one facility only and that it will be built at a national laboratory following standard national laboratory design and procurement procedures.
8. The cost of "boilers" is not to be part of this exercise, we are concerned only with the accelerator system and beam transport.

INJECTION SYSTEM

These estimated costs are derived from quoted prices of equipment. It is assumed that the power supply is SF6 insulated.

WIDERÖE LINAC

The low-beta linac is assumed to be a Wideröe linac in three sections, doubling in frequency at appropriate energies. The linac will be in the form of a "tree" with four sections filling all the buckets of two second sections,

which fill all the buckets of one third section. Parameters of the sections are given below.

Table V-I-1/1. Injector Estimated Costs.

Item	Estimated Cost (K$)
2-MV power supply	1500
2-MV accelerating column	600
Ion source (50 mA of 200^{1+} ions)	300
Beam Transport (including bunching and diagnostics)	600
Building (5000 ft^2) and services	500
Total	3500

Table V-I-1/2. Wideröe Linac Parameters.

Section	1	2	3	
No. of tank trees	4	2	1	
Tank length	30	100	600	m
Frequency	7.5	15	30	MHz
Current	25	50	100	mA
RF power				
Excitation power	0.5	8.5	56	MW
Beam power	0.4	6	90	MW
Total power	0.9	14.5	146	MW
Average electrical gradient	0.5	1.5	1.5	MV/m
Final kinetic energy T_{out}	15	140	1000	MeV

Costs for the Wideröe linac were estimated as follows:

(i) Structure (tanks, drift tubes, quardupoles, vacuum, support and alignment, etc.) costs were scaled from updated Brookhaven and Fermilab costs (including installation) and compared with a detailed estimate. The two methods are in reasonable agreement.

(ii) RF costs are taken from quotations supplied by private industry. Quotes as low as $0.10/W were received, but a figure of $0.15/W was used.

(iii) Beam transport costs were derived from a LBL layout of the systems.

(iv) Controls costs are taken as 10% of the other technical components.

(v) Costs of conventional facilities are estimated as follows (with costs in thousands of dollars per meter of building length):

(a)	Site preparation and excavation	1	k$/m
(b)	Structure (35 ft wide)	6	
(c)	Shielding	3	
(d)	Mechanical services and Cooling	4	
(e)	Electrical services	3	
	Total	17	k$/m

From Table V-I-1/3, we can find the total estimated cost of a Wideröe "tree" to be $122.6 million, without site, EDIA or contingency.

Table V-I-1/3. Wideröe Linac Estimated Costs.

Section	1	2	3	
1. Structure				
per unit length	120	90	80	k$/m
per tank	3.6	7	36	M$
2. RF				
per unit length	5	22	36	k$/m
per tank	0.15	2.2	22	M$
3. Beam Transport				
per tank	1	1.7	1.7	M$
4. Controls				
per unit length	12	7	6	k$/m
per tank	0.36	0.7	3.6	M$
5. Conventional facilities				
per unit length	17	17	17	k$/m
per tank	0.51	1.7	10.2	M$
Totals				
per unit length*	154	136	139	k$/m
per tank tree	5.62	13.3	73.3	M$

*The total cost per unit length includes no beam transport, because this item is added as a unit.

ALVAREZ LINAC

The design assumed here has only one branch; parameters are given in Table V-I-1/4.

There is no beam-transport item in the cost estimate, because there is no tree and the small costs of transport between sections are absorbed into the section costs.

Table V-I-1/4. Alvarez Linac Parameters.

Section	1	2	
Tank length	7000	3500	m
Frequency	60	120	MHz
Current	100	100	mA
RF power			
Excitation	450	400	MW
Beam	1200	700	MW
Total	1650	1100	MW
Average gradient	2	2	MV/m
Final Kinetic energy T_{out}	13	20	GeV

Table V-I-1/5. Alvarez Linac Estimated Costs.

Section	1	2	
1. Structure			
per unit length	100	70	k$/m
per tank	700	245	M$
2. RF			
per tank	247.5	165	M$
per unit length	35	47	k$/m
3. Controls			
per unit length	14	12	M$
per tank	94.5	41	k$/m
4. Conventional facilities			
per unit length	17	17	k$/m
per tank	119	60	M$
Totals			
per unit length	166	146	k$/m
per tank	1161	511	M$

Thus the total estimated cost of the Alvarez linac to carry beam from 1 to 20 GeV is $1.67 billion, without site, EDIA or contingency.

1-GeV ACCUMULATOR RING

This ring is assumed to use superconducting magnets. Some parameters are given in Table V-I-1/6. These make use of a tight lattice design sketched out by C. Leemann of LBL.

Table V-I-1/6. 1-GeV Accumulator Parameters.

Energy	1	GeV
Magnetic field		
dipoles	5	T
quadrupoles	4	T (poletip = 39T/m)
Average radius	22	m
Circumference	137	m
Aperture diameter	14	cm
Revolution frequency	238	kHz

An estimate of individual components was prepared by E. Hoyer. There is a problem in that we do not know what the components of the multi-turn injection system will look like and therefore find it difficult to estimate costs. To a smaller extent, this problem also exists for the extraction system. Hoyer has extrapolated from existing systems to estimate a cost of $2.7M for the injection system and $0.9M for the extraction system. The costs of the remaining "more certain" subsystems are given in Table V-I-1/7.

Table V-I-1/7. Accumulator Ring Estimated Costs.

Item	Cost (K$)
1. Magnets	6400*
2. RF	100
3. Vacuum	400*
4. Support and Alignment	200*
5. Controls	
Computer	800
Control room	200
Beam monitoring	100*
6. Conventional facilities	1700*
Total	9900

*Scales with circumference

Thus, with injection, extraction, and the extra rf needed to form one bunch for injection into a linear induction accelerator, we might estimate the total cost of an accumulator to be $14M, without site, EDIA, or contingency.

These estimated costs give a unit cost of $72 thousand per meter of circumference. As an exercise, we may scale this to the case of a 20-GeV superconducting accumulator ring, with radius 120 m. If we scale simply by the ratio of radii, we find an estimated cost of $54M. If we scale the starred items in Table V-I-1/7, we find a total estimated cost of $49M. The committee believes that these estimates should be considered upper limits, because the unit costs will surely decrease as the ring circumference increases. It should be noted that these estimates do not include injection, extraction, final bunching rf, site, EDIA, or contingency.

35 GeV SYNCHROTRON

The design chosen here is one that would fit one of the HIDE scenarios proposed at the workshop. The cost estimate, based on the design parameters given in Table V-I-1/8, are extrapolated costs of existing facilities adjusted for escalation to the present.

Table V-I-1/8. 35 GeV synchrotron with room Temp temperature magnets.

ρ = 237 m	R = 400 m
B_{max} = 1.7 Tesla	
Aperture = 15 x 30 cm	
ε_{in} = 2 mr. cm	ε_{out} = 13.6 mr. cm
Bending magnet Width = 1.26 m	
Length = 5.8 m	
No bending magnets = 256	
B_{min} = 0.4 T	B_{max} = 1.7 T
Injection energy = 2 GeV	
No Turns = 5 (@ 100 mA)	
Accel Time = 1 sec	
Accel Rate = 2 MV/turn	
Power at 1 pps = 70 MW	
Vacuum 10^{-11} Torr	

Table V-I-1/9. Synchrotron Costs.

Power Supply ($0.1/watt)	M$ 7
Magnet Steel ($1.17/#)	21
Coils	7
RF and Accel Cavities	12
Quads.	7
Vacuum (k$4/m)	10
Controls (10% of hardware)	2
Injection	1
Bldgs.	20
Miscell.	3
	M$ 90

As with the accumulator ring these costs can be extrapolated to different machine energies. In this case, with a 400 m radius, the cost becomes about k$36/meter of circumference. It should be noted, however, that changes in the design parameters (such as: aperture, repetition rate, etc...) will have an effect on unit costs.

The cost estimate of the above system was prepared by R. Burke of ANL. As with the accumulator ring the extraction systems are difficult to estimate, they have been left aside in this case. This also pertains to the pulse compression (rf bunching) system. We have tried to address ourselves to these special systems, but lack of design parameters information made it impossible to arrive at reliable numbers. After some discussion it was felt that these items might cost the following amounts:

1. M$ 1.5/extraction channel
2. M$ 0.1/m of beam transport channel
3. M$ 5/pulse compression system (additional work indicates that this cost might go up to M$50)

These items do not appear in Table V-I-1/9 which lists the costs for a conventional A. G. Synchrotron with a typical lattice only.

Table V-I-1/10. Induction Linac Parameters.

Volts (MV)	Incremental Volts (MV)	Pulse Duration (nsec)	Core Type	Packing Fraction	Length of Acc. Section (m)	Length of Transport Section (m)	Average Gradient (MV/m)
200-500	300	800-400	Iron	.25	375	94	0.64
500-2000	1500	400-200	Iron	.11	1500	170	0.90
2000-5500	3500	200-75	Ferrite	.17	2333	467	1.25
5500**-6500	1000	75	Ferrite	.22	667	188	1.17

** Included bunching in this section.

INDUCTION LINAC

The design parameters for the induction linac assumed are given in Table V-I-1/10. Here the linac consists of accelerating modules of either iron or ferrite, depending on the pulse duration, and quadrupole sections for the required packing fraction.* The parameters given are typical for a 26 GeV, uranium $^{+4}$, 155μC beam capable of 100 TW on target with two beams.

Estimated costs per unit length for induction modules are given in Table V-I-1/11. The iron module estimate is based on a 500 nsec pulse duration; the ferrite core module on a 100 nsec pulse duration.

Table V-I-1/11. Induction Linac Estimated Costs.

Structure Type	Iron Core 500 nsec Pulse Duration	Ferrite Core 100 nsec Pulse Duration	
Structure	23	39	K$/m
Modulator	18	7	K$/m
Control	4	4	K$/m
Conventional Facilities	13	10	K$/m
Totals	58	60	K$/m

Estimated quadrupole transport cost per unit length is given in Table V-I-1/12.

*Fractional space required for beam transport magnets.

Table V-I-1/12. Quadrupole Transport Estimated Cost.

Magnet System		
Vacuum	39	K$/m
Support & Alignment		
Control	4	K$/m
Conventional Facilities	13	K$/m
Total	56	K$/m

Interpolating from the above cost figures, an induction linac from 1 GeV to 20 GeV, Uranium +4, is $262 million without site, EDIA, or contingency.

Note

The estimate for the induction linac is based on a 238^{+4} ion instead of the 200^{+1} ion used in the other estimates. This will have a substantial effect on some of the unit costs as well as the cost of the system (e.g., the length of the machine will quadruple for a given energy). Therefore, we should not make direct comparisons between the induction linac costs presented here and the costs of the other systems described in this section.

VI. PARTICIPANTS

Arnold, Richard C.	(ANL)
Bangerter, Roger O.	(LLL)
Barnett, Clarence F.	(ORNL)
Barton, Mark Q.	(BNL)
Berley, David	(DOE)
Bernstein, Ira B.	(Yale U., CT)
Beuhler, Robert	(BNL)
Blechschmidt, Dieter	
Boehne, Dieter	(GSI, Darmstadt)
Boris, Jay P.	(NRL)
Botts, Thomas	(BNL)
Bruck, Henri D.	(Saclay, France)
Burke, Robert J.	(ANL)
Carey, David C.	(FNAL)
Clark, David J.	(LBL)
Cole, Francis T.	(FNAL)
Cooper, Richard K.	(LASL)
Curtis, Cyril	(FNAL)
Danby, Gordon T.	(BNL)
Faltens, Andris	(LBL)
Fenster, Stanley	(ANL)
Foss, Martyn H.	(ANL)
Freidman, Lewis	(BNL)
Freytag, E. Karl	(LLL)
Gillespie, George H.	(Physical Dynamics, Inc., CA)
Glenn, Joseph W.	(BNL)
Gluckstern, Robert L.	(U. Maryland, MD)
Godlove, Terry F.	(DOE)
Grand, Pierre	(BNL)
Grunder, Hermann A.	(LBL)
Haber, Irving	(NRL)
Halama, Henry	(BNL)
Hammer, D.A.	(Cornell U., NY)
Herrmannsfeldt, William B.	(SLAC)
Hofmann, Ingo	(Max Planck Institut für Plasmaphysik, Germany)
Hoyer, Egon H.	(LBL)
Irani, Ardeshir	(BNL)
Johnsen, Kjell	(CERN, Switzerland)
Johnson, Brant	(BNL)
Jones, Keith	(BNL)
Judd, David	(LBL)
Kaspar, Klaus R.	(GSI, Darmstadt)
Keane, John T.	(BNL)
Keefe, Dennis	(LBL)
Khoe, Tat K.	(ANL)
Kim, Yong-Ki	(ANL)
King, Marshall N.	(RHEL)
Kustom, Robert L.	(ANL)
Lambertson, Glen R.	(LBL)
Laslett, L. Jackson	(LBL)
Lawson, John D.	(RHEL)
Leemann, Christoph C.	(LBL)
Leiss, James E.	(NBS)
LeMaire, Jean-Louis	(Saclay, France)
Levine, Les	(DOE)
Lindl, John D.	(LLL)
Lofgren, Edward J.	(LBL)
Lysenko, Walter P.	(LASL)
Macek, Joseph H.	(U. Nebraska, Neb.)
Makowitz, Henry	(BNL)
Maniscalco, James A.	(LLL)
Martin, Ronald L.	(ANL)
Maschke, Alfred W.	(BNL)
Meeker, Donald J.	(LLL)
Mills, Frederick E.	(FNAL)
Mobley, Richard	(BNL)
Moretti, Alfred	(ANL)
Mosher, David	(NRL)
Neil, V. Kelvin	(LLL)
Nuckolls, John H.	(LLL)
Parker, Everette F.	(ANL)
Penner, Samuel	(NBS)
Poe, Robert T.	(U. Calif. Riverside, CA)
Raffenetti, Richard C.	(ANL)
Reiser, Martin	(U. Maryland, MD)
Resmini, F.	(U. Milano, Italy)
Richter, Burton	(SLAC)
Rubinson, William	(DOE)
Ruggiero, Alessandro G.	(FNAL)
Sandweiss, Jack	(Yale U., CT)
Seliger, Robert L.	(Hughes Res. Lab., CA)
Silberberg, Rein	(NRL)
Smith, Lloyd	(LBL)
Spiro, Julius	(BNL)
Staples, John W.	(LBL)
Stovall, James E.	(LASL)
Sudan, Raui	(Cornell U., NY)
Sutter, David F.	(DOE)
Swenson, Donald	(LASL)
Takahashi, Hiroshi	(BNL)
Tang, K.T.	(Pacific-Lutheran U., Wash.)
Thompson, William B.	(U. Calif. San Diego, CA)
Tidman, Derek, A.	(U. Maryland, MD)
Watson, Jerry M.	(ANL)
Young, Donald E.	(FNAL)
Yu, Simon	(LLL)

ABBREVIATIONS

ANL	Argonne National Laboratory (IL)
BNL	Brookhaven National Laboratory (NY)
DOE	U.S. Department of Energy (DC)
FNAL	Fermi National Accelerator Laboratory (IL)
LBL	Lawrence Berkeley Laboratory (CA)
LLL	Lawrence Livermore Laboratory (CA)
LASL	Los Alamos Scientific Laboratory (NM)
NBS	National Bureau of Standards (DC)
NRL	Naval Research Laboratory (DC)
ORNL	Oak Ridge National Laboratory (TN)
RHEL	Rutherford High Energy Laboratory (England)
SLAC	Stanford Linear Accelerator Center (CA)